

***Chemical and Analytical Aspects of Radioligand  
Development For Quantitative Neuroimaging***

***A THESIS***

Submitted for  
the degree of

***DOCTOR OF PHILOSOPHY***

University College London

***By***

***Rachel Suzanne Mulligan***  
BSc, MSc

May 2001

ProQuest Number: U642366

All rights reserved

INFORMATION TO ALL USERS

The quality of this reproduction is dependent upon the quality of the copy submitted.

In the unlikely event that the author did not send a complete manuscript and there are missing pages, these will be noted. Also, if material had to be removed, a note will indicate the deletion.



ProQuest U642366

Published by ProQuest LLC(2015). Copyright of the Dissertation is held by the Author.

All rights reserved.

This work is protected against unauthorized copying under Title 17, United States Code.  
Microform Edition © ProQuest LLC.

ProQuest LLC  
789 East Eisenhower Parkway  
P.O. Box 1346  
Ann Arbor, MI 48106-1346

## Abstract

Recently, SPET neuroimaging has progressed from simple empirical methods of analysis to more sophisticated quantitative methods for determining receptor-radioligand binding parameters, such as binding potential. In this thesis, different aspects of radioligand development were investigated in support of *quantitative* SPET neuroimaging; these include the preparation of precursors for new improved radioligands, optimisation of radiolabelling and radiochemical purity, evaluation and control of radiochemical stability and accurate measurement of radioactive metabolites in plasma (to provide an accurate input function for biomathematical modelling).

It was shown that the 5-HT<sub>2A</sub> receptor radioligand, [<sup>123</sup>I]5-iodo-R91150 ([<sup>123</sup>I]5-iodo-4-amino-*N*-[1-3-(4-fluorophenoxy)propyl]-4-methyl-4-piperidinyl]-2-methoxybenzamide), was cleared rapidly from blood and plasma in humans. Very low peripheral metabolism was observed. All four detected radioactive metabolites were more polar than 5-iodo-R91150. However, the radiochemical purity of the dose had a significant impact on the measurement of the fraction of radioactivity representing unchanged radioligand in plasma.

The synthesis of precursors for potentially new radioligands for the 5-HT<sub>2A</sub> receptor, based on R91150 as a lead compound, was attempted. The synthesis of a key intermediate, 1-[3-(4-fluorophenoxy)propyl]-4-methyl-4-piperidinamine, was significantly improved. Its coupling to 4-amino salicylic acid failed to give one target precursor, 4-amino-*N*-[1-3-(4-fluorophenoxy)propyl]-4-methyl-4-piperidinyl]-2-hydroxybenzamide. Model coupling reactions, using 1-methyl cyclohexylamine and various analogues of 4-amino salicylic acid, were performed. These indicated the need to protect the phenol and amino groups in 4-amino salicylic acid. The presence and position of these groups, in addition to the carboxyl group, prevented easy protection.

The D<sub>2</sub> receptor radioligand, [<sup>123</sup>I]epidepride ([<sup>123</sup>I](*S*)-*N*-((ethyl-2-pyrrolidinyl)methyl)-5-iodo-2,3-dimethoxybenzamide), was prepared from (*S*)-5-(*tri-n*-butyltin)-*N*-[(1-ethyl-2-pyrrolidinyl)methyl]-2,3-dimethoxybenzamide or its *tri*-methyltin analogue. The *tri*-butylstannyl precursor gave a high percentage of an unidentified and difficult to separate radioactive impurity. However, *tri*-methylstannyl precursor gave radiochemically pure [<sup>123</sup>I]epidepride. This radioligand was rapidly metabolised to 5 radioactive compounds *in vivo*. A high degree of inter-individual variation in results was observed, especially with respect to the level of a radioactive lipophilic metabolite.

## ***Table of Contents***

<b><i>Abstract</i></b> .....	<b>2</b>
<b><i>Table of Contents</i></b> .....	<b>3</b>
<b><i>List of Figures</i></b> .....	<b>9</b>
<b><i>List of Tables</i></b> .....	<b>13</b>
<b><i>Abbreviations</i></b> .....	<b>14</b>
<b><i>Acknowledgment</i></b> .....	<b>17</b>

### ***Chapter 1 Introduction to Radioligand Chemistry and Biology***

<b><i>1.1 Neurotransmission and Psychiatric Disorders 1</i></b> .....	<b>20</b>
1.1.1 Functional Anatomy of the Brain.....	20
1.1.2 Functional Anatomy of Neurotransmission .....	23
1.1.3 Hypotheses of the Involvement of Neurotransmission in Psychiatric Disorders.....	26
<b><i>1.2 Methods for Studying Brain Neurotransmission and Neurotransmitter Receptors</i></b> .....	<b>28</b>
1.2.1 In Vitro Methods .....	28
1.2.1.1 In Vitro Receptor Binding Studies	
1.2.1.2 In Vitro Autoradiography	
1.2.1.3 In Situ Hybridization	
1.2.2 In Vivo Methods .....	30
1.2.2.1 Microdialysis	
1.2.2.2 Ex Vivo Dissection/Autoradiography Studies	
1.2.3 Non-invasive In Vivo Imaging .....	30
1.2.3.1 X-ray and CT	
1.2.3.2 Magnetic Resonance Imaging	
1.2.3.3 SPET	
1.2.3.4 PET	
<b><i>1.3 Radioligands for Neuroimaging In Vivo</i></b> .....	<b>35</b>
1.3.1 Receptor-Radioligand Interactions.....	35
1.3.1.1 Determination of Ligand-Receptor Interaction	
1.3.1.2 Receptor Kinetics in SPET and PET	
1.3.1.3 Data Analysis	
1.3.2 Selection of Candidate Radioligands.....	39
1.3.3 Labelling and Evaluation of Radioligands .....	41
1.3.4 Radioligands for the Investigation of Neuropsychiatric Disorders – Status .....	44
1.3.4.1 D <sub>1</sub> -Receptors	
1.3.4.2 D <sub>2</sub> -Receptors	
1.3.4.3 5-HT <sub>1A</sub> Receptors	



1.3.4.4 5-HT <sub>2A</sub> Receptors	
1.3.4.5 Other Receptor Populations	
<b>1.4 Functional Imaging in Psychiatry and Psychopharmacology</b>	<b>48</b>
<b>1.5 Radioiodines and Neuroimaging</b>	<b>50</b>
1.5.1 Modes of Decay	50
1.5.1.1 $\alpha$ -Decay	
1.5.1.2 $\beta$ -Decay	
1.5.1.3 $\gamma$ -Decay	
1.5.1.4 Electron Capture	
1.5.2 The Isotopes of Iodine	51
1.5.2.1 $\gamma$ -Emitting Iodines	
1.5.2.2 Positron-emitting iodines	
1.5.3 Relevant Application of the Radioiodines for Psychiatric Research	54
<b>1.6 Radioiodination Chemistry</b>	<b>56</b>
1.6.1 Electrophilic Substitution in Arenes – General Considerations	56
1.6.2 Aliphatic Electrophilic Substitution – General Considerations	58
1.6.3 Aliphatic Nucleophilic Substitution – General Considerations	58
1.6.4 Aromatic Nucleophilic Substitution – General Considerations	60
1.6.5 Radioiodinating Agents	60
1.6.6 Direct Iodination of Arenes	62
1.6.7 Iodination by Group Replacement Reactions	63
1.6.7.1 Direct Exchange of Iodine	
1.6.7.2 Labelling by Nucleophilic Substitution	
1.6.7.3 Dediazotization	
1.6.7.4 Iododemetallation	
1.6.8 Effect of iodination on molecular, biochemical and pharmacological properties	69
1.6.9 Characterisation of Radioiodinated Compounds	71
1.6.10 Metabolism of Radioiodinated Compounds	72
<b>1.7 Quantitative Neuroimaging in SPET/PET</b>	<b>75</b>
<b>1.8 Aims of This Thesis</b>	<b>77</b>
<b>1.8 References</b>	<b>78</b>

## **Chapter 2 General Methods**

2.1.1 Detection and measurement of $^{123}\text{I}$ .....	89
2.1.2 Radio HPLC.....	89
2.1.3 Preparative TLC .....	89
2.1.4 Melting Point .....	90
2.1.5 Mass Spectrometry.....	90
2.1.6 Nuclear Magnetic Resonance ( NMR).....	90
2.1.7 Elemental Analysis.....	90
2.1.8 Ultraviolet Spectroscopy.....	90

## **Chapter 3: [ $^{123}\text{I}$ ]5-I-R91150 a radioligand for 5-HT<sub>2A</sub> receptors – Chemical stability and metabolism**

<b>3.1 Introduction.....</b>	<b>92</b>
3.1.1 5-HT <sub>2</sub> Receptors.....	93
3.1.2 5-HT <sub>2A</sub> Receptors and Psychiatry .....	93
3.1.3 5-HT <sub>2A</sub> Antagonists .....	94
<b>3.2 Discussion .....</b>	<b>96</b>
3.2.1 Radioiodination.....	96
3.2.2 Stability and Radiochemical Purity .....	97
3.2.3 Pharmacokinetics.....	99
3.2.3.1 Plasma clearance	
3.2.3.2 Metabolism	
3.2.5 Future Work.....	102
3.2.6 Summary .....	103
<b>3.3 Methods .....</b>	<b>103</b>
3.3.1 Materials and Methods .....	103
3.3.2 Preparation of [ $^{123}\text{I}$ ]5-iodo-R91150 .....	103
3.3.3 Analysis of Radiochemical Purity.....	103
3.3.4 Pharmacokinetics.....	104
3.3.4.1 Plasma clearance	
3.3.4.2 Metabolite Analysis	
3.3.4.3 Plasma Protein Binding	
<b>3.4 Results .....</b>	<b>105</b>

3.4.1 Analysis of Radiochemical Purity.....	105
3.4.2 Pharmacokinetics.....	106
3.4.2.1 Plasma clearance	
3.4.2.2 Metabolism	
3.5 References .....	109

## **Chapter 4 : Synthesis of precursors for prospective imaging agents for 5-HT<sub>2A</sub> receptors**

4.1 Introduction.....	114
4.2 Results and Discussion .....	117
4.2.1 Lipophilicity of potential radioligands .....	117
4.2.2 Synthesis and strategy.....	117
4.2.3 Results from attempted organic synthesis.....	122
4.2.3.1 Formation of 4-methyl-1-benzyl-4-piperidinol <b>8</b> from 1-benzyl-4-piperidone <b>23</b>	
4.2.3.2 N-[1-(Benzyl)-4-methyl-4-piperidinyl]acetamide hydrochloride <b>9</b>	
4.2.3.3 N-[4-Methyl-4-piperidinyl]acetamide hydrochloride <b>10</b>	
4.2.3.4 1-(3-chloropropoxy)-4-fluorobenzene <b>11</b>	
4.2.3.5 N-[1-[3-(4-fluorophenoxy)propyl]-4-methyl-4-piperidinyl]acetamide <b>12</b>	
4.2.3.6 1-[3-(4-Fluorophenoxy)propyl]-4-methyl-4-piperidinamine <b>13</b>	
4.2.3.7 Model Coupling Reactions	
4.2.3.8 Interpretation of NMR Experiments	
4.2.3.9 Protection of 4-amino salicylic acid	
4.2.3.10 Palladium-Catalysed carbonylation and coupling of aromatic halides and amines	
4.3 Conclusions .....	142
4.4 Experimental .....	143
4.5 References .....	152

## **Chapter 5: Radiolabelling of [<sup>123</sup>I]epidepride with alkyl-stannyl precursors**

5.1 Introduction.....	156
5.1.1 Dopamine role in the brain.....	156
5.1.2 Dopamine receptors.....	156
5.1.3 Relevance of the dopaminergic system to psychiatry.....	157

5.1.4 Radioligand for imaging D <sub>2</sub> receptors.....	158
<b>Discussion .....</b>	<b>160</b>
5.2.1 Synthesis of the tri-butyltin precursor 1.....	160
5.2.2 Radioiododestannylation of tri-butylstannyl precursor 1 .....	161
5.2.3 Radioiododestannylation of tri-methylstannyl precursor .....	161
5.2.4 Analysis of the tri-butylstannyl precursor.....	162
5.2.5 Radioiododestannylation of purified tributyltin precursor 1 .....	163
5.2.6 Organic reactions with tri-butylstannyl precursor .....	164
5.2.7 Pharmacokinetics.....	167
5.2.6.1 Plasma clearance	
5.2.6.2 Metabolism	
<b>5.3 Methods .....</b>	<b>171</b>
5.3.1 Materials and Methods .....	171
5.3.2 Standard procedure for radioiododestannylation of tri-alkylstannyl precursors.....	171
5.3.3 Determination of radiochemical purity.....	171
5.3.4 Analysis and purification of the tri-butylstannyl precursor.....	172
5.3.5 Cold reactions with tri-butylstannyl precursor.....	172
5.3.6 Pharmacokinetics of pure [ <sup>123</sup> I]epidepride .....	172
5.3.6.1 Plasma clearance	
5.3.6.2 Metabolite Analysis	
5.3.6.3 Plasma protein binding	
<b>5.4 Results .....</b>	<b>173</b>
5.4.1 Radioiododestannylation of trialkylstannyl precursors.....	173
5.4.2 Assessment of radiochemical purity.....	174
5.4.3 Analysis of the tri-butylstannyl precursor.....	176
5.4.4 Cold reactions with tri-butylstannyl precursor.....	179
5.4.5 Pharmacokinetics.....	179
5.4.5.1 Plasma clearance	
5.4.5.2 Metabolism	
<b>5.5 References .....</b>	<b>183</b>

## ***Chapter 6: General Overview***

<b>6.1 Radioligand Development .....</b>	<b>188</b>
6.1.1 Selection of a lead compound .....	188
6.1.2 Precursor synthesis.....	189
6.1.3 Radiolabelling.....	189
6.1.4 Radioligand analysis.....	190
6.1.5 Metabolite analysis in plasma .....	191
<b>6.2 Conclusion.....</b>	<b>192</b>
<b>6.3 References .....</b>	<b>193</b>
<b>Appendix .....</b>	<b>194</b>

## *List of Figures*

### *Chapter 1: Introduction to Radioligand Chemistry and Biology*

- 1.1 Gross functional anatomy of the human brain.
- 1.2 The proposed neuronal circuit for movement.
- 1.3 The proposed neuronal circuit for emotion.
- 1.4 A “model” nerve cell showing the different structures and the flow of information.
- 1.5 The basic event of fast and slow synaptic transmission.
- 1.6 The three compartment, four parameter kinetic model of the uptake and washout of radioligand in the brain.
- 1.7 Illustration of positron decay of  $^{11}\text{C}$ .
- 1.8 A simplified decay chart for common iodine isotopes.
- 1.9 Electrophilic substitution in arenes.
- 1.10 Potential canonical forms resulting from electrophilic attack on a arene with electron-withdrawing substituents.
- 1.11 Canonical forms present following electrophilic attack on an alky-substituted arene that leads to preferential attack at an *ortho*- or *para*-position.
- 1.12 Canonical forms supporting preferential *ortho*- and *para*- electrophilic attack of an arene with electron-withdrawing substituents plus a lone pair of electrons.
- 1.13 Electrophilic substitution of aliphatic compounds.
- 1.14 Aliphatic nucleophilic substitution by the unimolecular mechanism.
- 1.15 Aliphatic nucleophilic substitution by the bimolecular mechanistic pathway.
- 1.16 Aromatic nucleophilic substitution.
- 1.17 Formation of radioactive molecular iodine from  $[^{123}\text{I}]\text{NaI}$  in the presence of an oxidising agent.
- 1.18 Oxidising and iodinating reagents believed to be generated in reactions employing chloramine-T.
- 1.19 Structure of iodogen and iodobeads.
- 1.20 Peracetic acid as an oxidising agent for iodinations.
- 1.21 Direct iodination of activated arenes by electrophilic substitution.
- 1.22 Synthesis of  $[^{123}\text{I}]\text{IBZM}$  by electrophilic radioiodination.
- 1.23 Synthesis of  $[2\text{-(4-chlorophenyl)(4-[iodophenyl]methoxyethyl)-1-piperidine-3-carboxylic acid}]$ .
- 1.24 Synthesis of  $[^{123/125}\text{I}]\text{IPH}$ .
- 1.25 Labelling of arenes via a diazonium salt.
- 1.26 Synthesis and iododestannylation of aryl tin compounds.
- 1.27 Synthesis and iododestannylation of vinyl tin compound.

- 1.28 Aromatic lithiation via possible halogen-metal interchange as a pathway to stannylation and iododestannylation of arenes.
- 1.29 The stannylation and subsequent destannylation of the tri-butylstannyl derivative of IDAM.
- 1.30 Iodination of alkyl compounds via organoboranes.
- 1.31 Iodination of vinyl compounds via organoboranes.
- 1.32 Synthesis of organoboronic precursor of iodocognex via the palladium(0) catalysed cross-coupling reaction.
- 1.33 Synthesis [ $^{123}\text{I}$ ] IDDE via radioiododemercuration.
- 1.34 Synthesis of aryl-thallium trifluoroacetates as intermediates for iodination.

### ***Chapter 3: [ $^{123}\text{I}$ ]5-I-R91150 a radioligand for 5-HT<sub>2A</sub> receptors – Chemical stability and metabolism***

- 3.1 Chemical structure and affinity of 5-HT<sub>2A</sub> antagonists developed as radioligands for *in vivo* imaging.
- 3.2 SPET images of [ $^{123}\text{I}$ ]5-iodo-R91150 binding in a healthy subject.
- 3.3 Radiosynthesis of [ $^{123}\text{I}$ ]5-iodo-R91150.
- 3.4 [ $^{123}\text{I}$ ]5-iodo-R9115 and sites that may be susceptible to enzymatic attack *in vivo*.
- 3.5 A representative trace of [ $^{123}\text{I}$ ]5-iodo-R91150 on delivery at the INM analysed 20 h after product release.
- 3.6 Typical plasma clearance of radioactivity after administration of [ $^{123}\text{I}$ ]5-iodo-R9115.
- 3.7 Representative HPLC profiles from plasma taken at 180min after injection of [ $^{123}\text{I}$ ]5-iodo-R9115 with a radiochemical purity of > 98% (A) and 93% (B).
- 3.8 The percentage of radioactivity in plasma represented by [ $^{123}\text{I}$ ]5-iodo-R9115, the void volume peak and 3 less polar metabolites after injection of a high radiochemical purity radioligand (>98%) or a lower radiochemically pure radioligand (93%) in normal volunteers.

### ***Chapter 4: Synthesis of precursors for prospective imaging agents for 5-HT<sub>2A</sub> receptors***

- 4.1 Precursors for potential 5-HT<sub>2A</sub> radioligands.
- 4.2 Structure of 5-iodo-R91150.
- 4.3 Possible strategy for the radiolabelling of the phenol derivative of R91150 by direct iodination .
- 4.4 Structure of MDL 100907.
- 4.5 Possible labelling strategies for the synthesis of potential PET radioligands for the 5-HT<sub>2A</sub> receptor.
- 4.6 Pathway for the synthesis of a PET radioligand for imaging the 5-HT<sub>2A</sub> receptor using R91150 as a precursor.
- 4.7 Synthetic strategy for R91150 as reported by Leysen and van Daele.

- 4.8 Reported synthesis of 5-iodo-R91150.
- 4.9 Proposed synthesis of precursors **1** and **2** by direct coupling with amine **13**.
- 4.10 Proposed mechanism for coupling of 4-amino salicylic acid **18** with amine **13** to form the desired precursor **2**.
- 4.11 Possible pathway for the synthesis of R91150 **1** and the phenol analogue **2**.
- 4.12 Palladium-catalysed carbonylation as an alternative pathway for the synthesis of precursors **1** and **2**.
- 4.13 Proposed reaction conditions for alkylation of ketone **23**.
- 4.14 Alternative pathway for acetamide deprotection using basic conditions.
- 4.15 Alternative reaction conditions for deprotection of *N*-acetyl derivatives.
- 4.16 Proposed mechanisms behind adol condensation and alkylation of ketone **23** in the presence of 1.2 equivalents of Grignard reagent.
- 4.17 NMR spectra obtained from a  $^1\text{H}$ - $^{13}\text{C}$  COSY experiment on pure **12**.
- 4.18 NMR spectra obtained from a  $^1\text{H}$ - $^{13}\text{C}$  COSY experiment on pure **12**.
- 4.19 Possible mechanism leading to the production of the side product **26** from the coupling of acid **18** with model amine **25**.
- 4.20 Products formed following the coupling of benzoic acid with the key intermediate, amine **13**.
- 4.21  $^1\text{H}$ -NMR spectra of *N*-(1-methyl-cyclohexyl)-benzamide **27** run at 300 K (A) and 330 K (B).
- 4.22 NMR spectrum obtained from the  $^1\text{H}$ - $^{13}\text{C}$  COSY experiment performed on benzamide **27** at ambient temperature.
- 4.23 Enlargement of cyclohexyl ring region of the NMR spectrum obtained from the  $^1\text{H}$ - $^{13}\text{C}$  COSY experiment performed on benzamide **27**.
- 4.24 Ambient (300K, A) and high temperature (355 K, B)  $^1\text{H}$ -NMR spectra of 2-hydroxy-*N*-(1-methyl-cyclohexyl)-benzamide **30**.
- 4.25  $^1\text{H}$ -NMR spectra obtained for 4-amino-*N*-(1-methyl-cyclohexyl)-benzamide **31** run at 300 K (A) and 355 K (B).
- 4.26 The two canonical forms present for *N*-(1-(methyl(cyclohexyl))-benzamide **27** that account for the partial delocalisation of the  $\text{C}_{\text{CO}}$ -N bond.
- 4.27 The two canonical forms of the coupled product **27** detected by NMR.
- 4.28 Products identified following protection of the amino, phenol and acid groups of 4-amino salicylic acid.
- 4.29 Isolated products following benylation and deprotection of the crude Boc protected acid.
- 4.30 The published scheme for the synthesis of [ $^{13}\text{C}$ ] labelled amides.
- 4.31 Analogues of R91150 that could be formed via palladium-mediated carbonylation.



## Chapter 5: Radiolabelling of [ $^{123}$ I]epidepride with alkyl-stannyl precursors

- 5.1 Structure and affinity of two classes of dopamine D<sub>2</sub> antagonists developed for *in vivo* visualisation of D<sub>2</sub> receptors in human brain.
- 5.2 Human SPET images following injection of [ $^{123}$ I]epidepride illustrating the differentiation that is possible between the cerebellum, temporal cortex and striatum with a high affinity radioligand.
- 5.3 Radioiododestannylation of *tri*-butylstannyl precursor **1**.
- 5.4 Assignment of proton NMR spectrum for the *tri*-butylstannyl precursor **1** from Clanton *et al.*<sup>35</sup>
- 5.5 Proposed metabolic routes of remoxipride in humans.
- 5.6 HPLC profile of crude radioiodination reactions employing the *tri*-butyl or *tri*-methylstannyl precursor.
- 5.7 HPLC analysis (System B) of the main radioactive product from the radioiodination of the *tri*-butylstannyl precursor in the presence of chloramine-T.
- 5.8 HPLC chromatograms following re-injection of the two radioactive products identified during analysis of [ $^{123}$ I]epidepride prepared from *tri*-butyl tin precursor when co-injected with reference epidepride (System B).
- 5.9 HPLC analysis (System B) of the main radioactive product from the radioiodination of the *tri*-methylstannyl precursor with reference epidepride added.
- 5.10 HPLC analysis (System C) of the crude supply of *tri*-butylstannyl precursor.
- 5.11 Electrospray MS of the crude *tri*-butylstannyl precursor.
- 5.12 <sup>1</sup>H-NMR spectrum of purified *tri*-butylstannyl precursor.
- 5.13 Enlargement of the aliphatic region of the <sup>1</sup>H-NMR spectra.
- 5.14 <sup>13</sup>C-NMR spectrum of purified *tri*-butylstannyl precursor.
- 5.15 Analysis of the crude reaction of *tri*-butylstannyl precursor with sodium iodide in the presence of chloramine-T using HPLC System B.
- 5.16 Clearance of total radioactivity and unchanged parent compound from venous plasma for one subject.
- 5.17 HPLC chromatogram of a 60 min plasma sample.
- 5.18 Panel A is the chromatogram from a plasma sample 30 min after injection of [ $^{123}$ I]epidepride analysed in the absence and presence of epidepride. The same sample analysed in the presence of reference epidepride is shown in Panel B.
- 5.19 The time course of radioactive metabolites observed in human plasma after injection of [ $^{123}$ I]epidepride.

## *List of Tables*

- 1.1 Possible nuclear reactions for routine production of  $^{123}\text{I}$ .
- 1.2 Comparison of the physiochemical properties of hydrogen and iodine atoms.
  
- 3.1 Summary of the present clasification of serotonin-modulated receptor subtypes.
- 3.2 Radiochemical purity of delivered doses of [ $^{123}\text{I}$ ]-5-iodo-R91150.
  
- 4.1 Reaction conditions investigated for Grignard reaction.
- 4.2 Experiments investigating possible bases for the coupling to form **12**.
- 4.3 The main products formed from model coupling reactions with a series of benzoic acid analogues and 1-methyl cyclohexylamine.
- 4.4 Spectroscopic data of benzamide **27** as reported by Koziara *et al.*

## *List of Abbreviations*

5-HT	5-hydroxytryptamine, serotonin, 5-hydroxytryptamine, serotonin
3D	3-Dimensional
2D	2-Dimensional
Å	Measure of distance (Ångström)
Ac	Acetyl
ANOVA	Analysis of variance
Bu	Butyl
Boc	Butoxycarbonyl group
Bom	Benzyloxymethyl group
B <sub>max</sub>	Concentration of receptors per unit tissue
BP	Binding potential
c.	Concentrated
Ca <sup>2+</sup>	Calcium ion
CA	Carrier added – term referred to radiolabelling reaction where a non-radioactive counterpart to the radioactive reactant is added.
calcd	Calculated
cAMP	Cyclic adenosine 5'-monophosphate ; a second messenger generated from ??? by the neurotransmitter activated adenylate cyclase
CF	Carrier-free reaction conditions
cGMP	Cyclic guanosine 5'-monophosphate
Ci	Curie (3.7 x 10 <sup>4</sup> MBq)
CIMS	Chemical Ionisation Mass Spectroscopy
COSY	Correlation spectroscopy
cps	Counts per second
CNS	Central nervous system
CT	Computer tomography
d	Day
DEPT	Distortion Enhancement by Polarisation Transfer NMR
DMF	<i>N, N</i> ,-Dimethylformamide
DNA	Deoxyribonucleic acid
ED <sub>50</sub>	Effective dose of cold ligand that leads to 50% displacement of a radioligand
Et	Ethyl
<i>f</i> <sub>2</sub>	“Free fraction” of unbound radioligand in tissue
FUA	Free University of Amsterdam
GBq	Gigabequerel (1 x 10 <sup>9</sup> disintegrations/sec)

G-protein	Guanine protein in the synaptic membran that couples the neurotransmitter receptor to proteins or enzymes on the inner membrane.
h	Hour
HPLC	High performance liquid chromatography
HRMS	High resolution mass spectroscopy
INM	Institute of Nuclear Medicine
IR	Infra red
$J$	Coupling constant
K	Kelvin
$k_f$	Association constant; the rate at which a ligand binds to a target site
$k_d$	Dissociation constant; the rate at which a ligand dissociates from its binding site
KCL	Kings College London
keV	Kilo-electron volts
$K_d$	Equilibrium dissociation constant in concentration units
$K_I$	Displacement potency of a cold competitor with a particular radioligand
kJ	KiloJoule
[L]	Ligand concentration
[LR]	Ligand-receptor complex concentration
LGC	Ligand-gated channel
logP	Logarithm of P, the octanol-water partition co-efficient
LOR	Line of response linking two detectors of a PET camera
$m$	<i>Meta</i> -position
MBq	MegaBequerel ( $1 \times 10^6$ disintegrations/sec)
mCi	Millicurie (37 MBq)
MeV	Milli-electron volts
min	Minutes
mmol	A millimole of substance
mp	Melting point
MRI	Magnetic Resonance Imaging; a non-invasive imaging technique
mRNA	Messenger ribonucleic acid
MS	Mass spectroscopy
mSv	MilliSieverts
NCA	No-carrier added reaction conditions for radiolabelling
nmol	A nanomole of substance
NMR	Nuclear magnetic resonance.
$o$	<i>Ortho</i> -position
obsd.	Observed
o/n	Overnight

<i>p</i>	<i>Para</i> -position
PET	Positron emission tomography
Ph	Phenyl
PI	Intracellular second messenger inositol 1,4,5- <i>tri</i> phosphate
pmol	A picomole of substance
[R]	Receptor concentration
RNA	Ribonucleic acid
rpm	Revolutions per minute
r.t.	Retention time
RT	Room temperature
SD	Standard deviation
SPET	Single photon emission tomography
THF	Tetrahydrofuran
T.L.C.	Thin layer chromatography
TMS	Tetramethylsilyl
TTFA	Thallium(III) trifluoroacetate
$t_{1/2}$	Half life
$\nu$	Neutrino
UCL	University College London
$V_d$	Volume of distribution
y	Year
$\mu$ s	Microsecond

## *Acknowledgements*

“A single bracelet doesn’t jingle”

Zaire proverb



This thesis would not have been possible without the help of a number of people. Thank you for the parts you played in making this bracelet laugh and smile over the years.

Firstly, I’d like to thank the people that made all this happen:

Professor Victor Pike for sharing his knowledge and enthusiasm for radiochemistry, for his amazingly meticulous corrections of the many drafts I sent his way and for keeping faith in my ability even when I asked the simplest questions.

Professor Peter Ell for funding support and dealing with the paperwork and bureaucracy associated with an overseas student, for mastering yet another language (Kiwi English) and at crucial times, providing the momentum that got me to the end.

Dr Lyn Pilowsky, who inspired the whole project, obtained the funding and in addition to providing endless support and encouragement, has been a great friend and boss.

This work would not have been completed without the help of colleagues and friends at both the MRC Cyclotron Unit and the Institute of Nuclear Medicine. They have each played some role in helping me hold it all together and I hope their work hasn’t suffered as a result of my social and work related visits. I’d especially like to thank:

Dr Jaqui Walley for her superb introductory, and advanced, organic chemistry training program, and for understanding my accent and my cravings for certain luxuries from home.

To the past and present students at the Cyclotron Unit, who made lunchtimes an enjoyable part of the day. They also made me understand that the roller coaster of emotions I went through was just part of a PhD student’s life. Without their help this would have been the highest, longest and scariest roller coaster ride ever. Of these people I particularly want to thank Nazreen Khanum who has become a great friend. Over the past years she has willingly given practical, social and emotional support and cooked healthy and delicious meals whenever my diet required a boost.

Drs Mike Travis and Valeria Bigliani who recruited subjects and then bled them so I could have samples to analyse. In addition to this task, Valeria also made work a place where laughter and smiles were the norm and not the exception. Thanks a million for being a great friend and letting me share your London experience.

Dominic, Jenny, Rudra and Mark for allowing me to invade the radiopharmacy, and for not complaining too loudly about the transient trail of destruction that inevitably followed me.

Dr Ian Cullum for fixing numerous computer, detector and HPLC related problems and providing an interesting critique on the play he went and saw each day called "Life at INM".

Safiye Osman for sharing her knowledge of metabolite analysis.

Jane Hawkes at Kings College and John Crowder at the University of North London for invaluable input on NMR analysis

Drs Steve Waters and Mike Carroll (Imperial College London) for running mass spectra.

On a personal note I'd like to thank:

New Zealand telecom and First telecom for enabling me to stay in contact with family and friends all around the world without breaking bank balances.

To my friends spread around the world who will probably never know how valuable it has been to have them on the end of the phone or on email. I apologise now for any times that I have woken them in the middle of the night. Also to those who have been a part of my travels, thanks for the memories and for making it so easy to forget about London.

To Mum and Dad, Andrea, Mike and Simon for their endless support and encouragement at every step of this journey, and for providing brilliant holiday memories and a supply of New Zealand junk food in my times of need.

## ***Chapter 1:***

### ***Introduction to Radioligand Chemistry and Biology***



## **1.1 Neurotransmission and Psychiatric Disorders**

### **1.1.1 Functional Anatomy of the Brain**

In humans, the central nervous system (CNS) includes the spinal cord and the brain. Its functional unit is the nerve cell or neuron. The 100 to 180 billion neurons in the brain are heterogeneously distributed with distinct types clustered into functionally and anatomically distinct areas known as nuclei. Functionally related nuclei are organised into specialised circuits that interact with other circuits to modulate complex patterns of activities. For example, the thalamus, cerebellum and basal ganglia are subsystems that, in humans, interact to control motor activity. The functional anatomy of the brain allows it to sub-serve three main processes: 1) the gathering of external information (*i.e.* sensory function), 2) storing and processing information (integration) and 3) triggering an adaptation or response (*i.e.* motor or secretory function).<sup>1</sup> Anatomically the brain can be divided into three main areas, namely the brain stem, cerebellum and cerebrum (cerebral hemisphere) (Figure 1.1).

The cerebellum contains half of the neurons in the CNS, organised into three functional regions responsible for the planning and initiation of movement (cerebrocerebellum), the coordination of voluntary movements (spinocerebellum) and the maintenance of body equilibrium and head and eye movement coordination (vestibulocerebellum). The pons, medulla oblongata and midbrain of the brain stem constitute the primary centres for the coordination of vital functions (respiratory and cardiovascular functions) and reflexes (such as vomiting and swallowing). The reticular formation is an extension of the interneuronal networks in the spinal cord providing a high level of sensorimotor control. Sensory inputs are channeled to alert and focus attention according to individual needs. This includes the regulation of alertness, the modulation of extensor muscle tone, heart and blood pressure and pain perception.<sup>2</sup>

The functional organisation of the forebrain is more complex. The diencephalon of the brain includes the thalamus and the hypothalamus. In the thalamus, nuclei are classified into two functional groups, the sensory relay nuclei, which receive specific inputs of sensory modalities and projects them to specific areas of the sensory cortex, and the diffuse projection nuclei, which influence a larger area of the cerebral cortex via a widespread connection network. All sensory information, with the exclusion of olfactory inputs, is processed in thalamic nuclei before it reaches the cerebral cortex. Therefore, the role of the thalamus is to integrate motor, general and special sensory, and visceral information. The hypothalamus receives important ascending input from the spinal cord and brainstem, in addition to input from cortical regions (primarily from the limbic system) and the thalamus.

The interaction between the hypothalamus and the limbic system maintains homeostasis of the internal environment by controlling the autonomic nervous system and endocrine glands. The sensors in the hypothalamus that respond to the properties of the circulating blood (*e.g.* temperature,

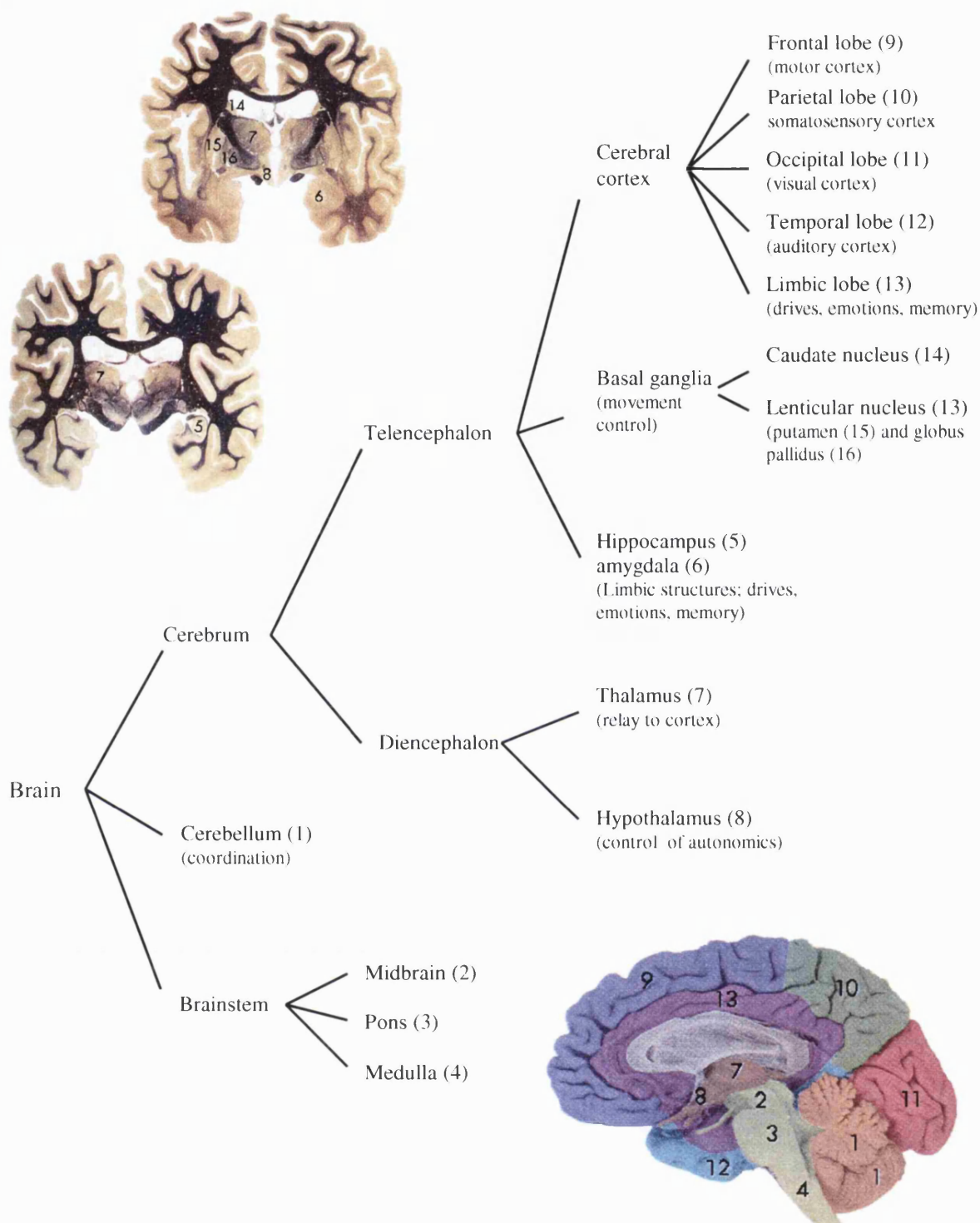


**Figure 1.1:** Gross functional anatomy of the human brain (modified from Nolte<sup>3</sup>)

osmolarity and metabolite and hormone concentration) make it the centre responsible for the crucial integration of neural and endocrine functions. In the telencephalon the final processing and integration of information takes place. The cerebral hemispheres, the basal ganglia, the hippocampus and the amygdala are all part of the telencephalon. The cerebral cortex, the convoluted surface layer of the cerebral hemispheres, is divided into five different lobes delimited by well-defined grooves, the sulci. Each region of the cerebral cortex can be classified according to their anatomical location (*e.g.*

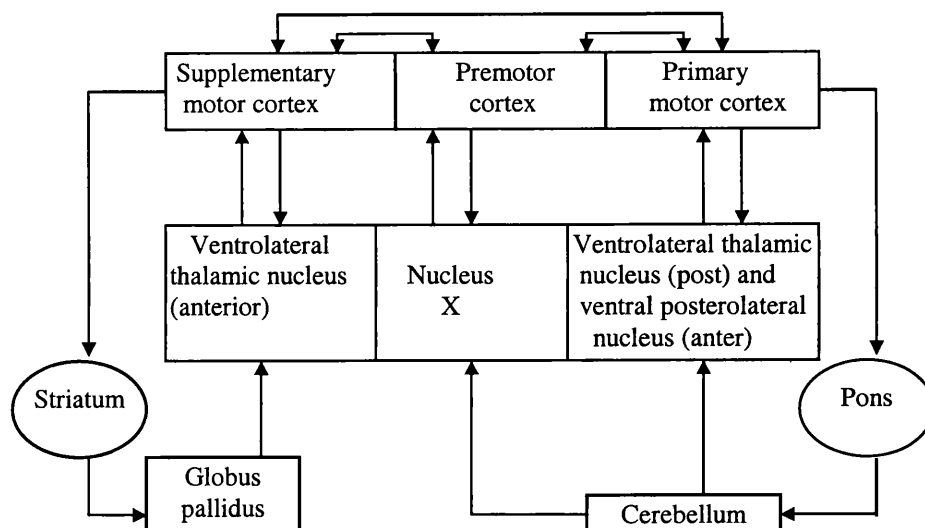


**Figure 1.2:** The proposed neuronal circuit for movement (from Fieldman *et al.*<sup>2</sup>).

frontal, parietal, temporal, occipital or limbic lobes) or the type of information processed (motor, somatosensory, auditory or visual) (Figure 1.1). All anatomical lobes of the cerebral cortex participate in the integration of sensory information for conscious awareness.

The components of the basal ganglia are the caudate nucleus and the putamen (together known as the corpus striatum) and the globus pallidus. The basal ganglia receives input from the cerebral cortex and outputs information via the thalamus. The specificity of the motor, sensory, sensory association and limbic cortex is maintained within the basal ganglia, down to the thalamus as shown in the proposed interconnections mediating voluntary movement (Figure 1.2). The specific role of the basal ganglia in this circuit is the initiation, control and modulation of complex movement sequences that have originated in the cortex. A role in cognition has also been implicated for the basal ganglia.

The limbic lobe is composed of the cingulate and parahippocampal gyri. In conjunction with the thalamus, the hypothalamus, and limbic structures such as the hippocampus, the nucleus accumbens, the amygdala, and limbic cortex form the limbic system. The limbic system is involved in the mechanisms of motivation, emotional responses and basic behaviours involving survival of the individual and species (Figure 1.3). A possible role in learning and recent memory has also been

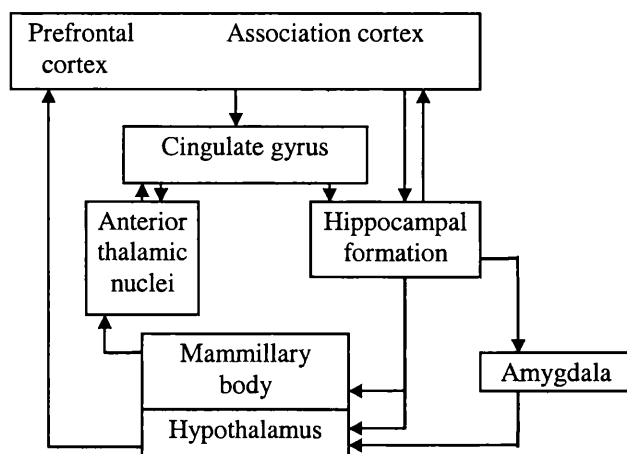


**Figure 1.3:** The proposed neuronal circuit for emotion.

attributed to the hippocampus and the septum, while the amygdala is involved in the integration of autonomic and endocrine functions

### 1.1.2 Functional Anatomy of Neurotransmission

The vertebrate nervous system is characterised by a wide variety of neurons, each with certain specialisations. Neurons can vary with respect to the number, length and mode of branching on the cell body. Neuronal classification often groups nerve cells by these morphological aspects. Every neuron has four major characteristic features namely, the cell body, dendrites, axon, and presynaptic terminals. A “model” nerve cell is illustrated in Figure 1.4. The cell body contains the cell’s nucleus and is the nerve cell’s energy centre. The principal activities attributed to the cell body include energy producing metabolism, and the synthesis of macromolecules that support the execution of cellular functions and structural maintenance.<sup>2</sup> The branches that extend from the cell body, the dendrites, are responsible for receiving input messages from other nerves. These messages will lead to either an increase or decrease in neuronal response. Most of the nerve cells in the CNS have a high degree of dendritic branching resulting in multiple messages being received from a number of juxtaposed neurons at any one time. Any cellular response is a summation of these input signals. The structure of the axon, another branch off the cell body, supports the rapid transfer of messages received from the dendrites to the axon terminals. If an input message is sufficient for a response, the voltage difference between the inside and outside of the neuronal membrane at rest, is transiently modified. If this change in membrane potential reaches a pre-set threshold, an action potential is generated and propagated along the length of the axon to the presynaptic terminal. Nerve cells are not directly connected to their target cells but have a 100 Å gap, known as the synapse, which prevents the direct propagation of an action potential from one nerve cell to another. The electrical signal of the action potential is translated into a chemical message in the form of a neurotransmitter, stored and concentrated within vesicles in the synaptic terminal. Stimulated neurotransmitter release occurs via  $\text{Ca}^{2+}$ -dependent excitation-secretion coupling which allows synaptic vesicles to dissociate from the network of filaments in the pre-synaptic terminal. They are then free to fuse with the plasma membrane and participate in exocytosis. Once released into the synaptic cleft, the neurotransmitter can diffuse across the synapse and transmit a stimulatory or inhibitory message to the target cell.

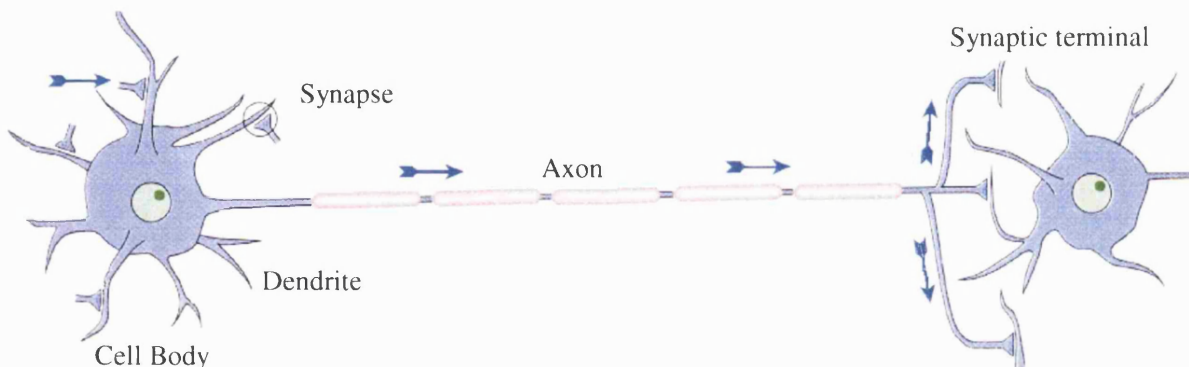


**Figure 1.4:** A “model nerve cell showing the different structures and the flow of information.

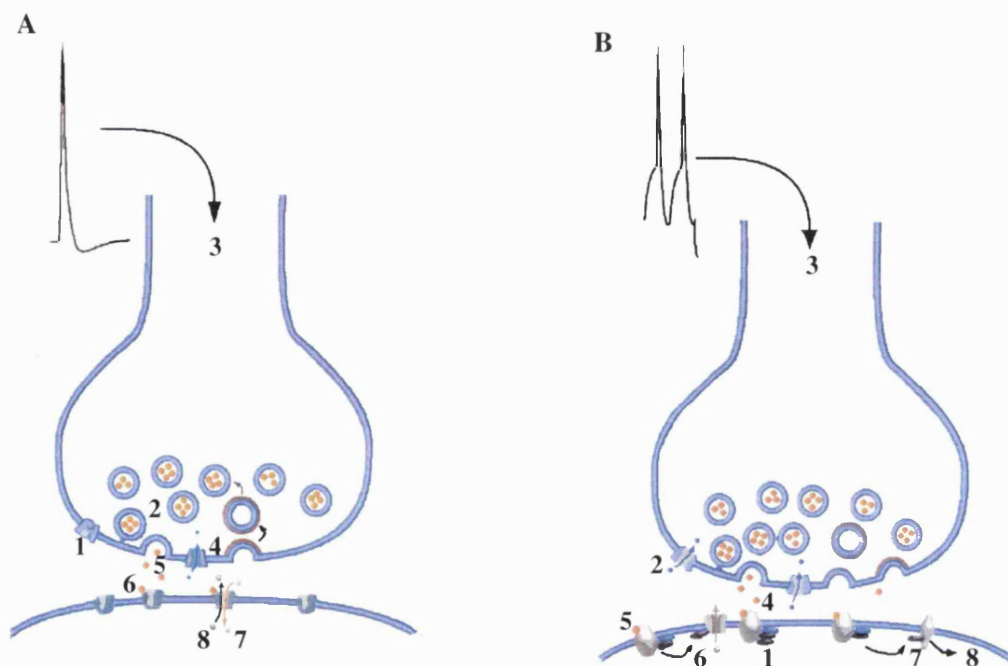


**Figure 1.5:** The basic event of fast (**A**) and slow (**B**) synaptic transmission. **A.** At rest ligand-gated ion channels in the presynaptic terminal are closed (1) and neurotransmitter vesicles are concentrated in the presynaptic terminal (2). Depolarisation of the terminal (3) causes  $\text{Ca}^{2+}$  influx (4), transmitter vesicle exocytosis (5) and the binding of the neurotransmitter to the postsynaptic ion channel (6). The channel is opened allowing, for example,  $\text{Na}^+$  influx (7) and  $\text{K}^+$  efflux (8). In this situation depolarisation and stimulation of the postsynaptic membrane will result. **B.** Slower synaptic transmission involves the G-protein coupled, post-synaptic receptors (1).  $\text{Ca}^{2+}$  influx in the presynaptic terminal (2) as a result of prolonged and rapid membrane depolarization (3) leads to exocytosis (4) and neurotransmitter binding to G-protein coupled receptor (5). Effectors influenced by G proteins can include ion channels (6) or enzymes (7) that mediate the production of various intracellular messenger systems (8).

Generally a nerve cell releases only one type of neurotransmitter *e.g.* dopamine, serotonin or a specific neuropeptide. The process of synaptic transmission is illustrated in Figure 1.5.

Neurotransmitters communicate with the post synaptic target cell by interacting with a specific receptor protein embedded in the cell membrane. Binding of the neurotransmitter to the receptor leads to a series of intracellular events, culminating in a biological response. Therefore, the interaction between the neurotransmitter and receptor is the basis of synaptic transmission. A key feature of the receptor is an extracellular site that is able to accept the incoming message (the neurotransmitter). The interaction between the neurotransmitter and the binding domain of the receptor is transient with the neurotransmitter leaving unchanged, once the message has been passed on to the postsynaptic cell. Since all neurotransmitters, except the neuropeptides, are generally small water-soluble molecules with an amino or carboxyl group, they are able to participate in several types of weak non-covalent interactions (for example, ionic, hydrogen and van der Waals bonding) with specific amino acid sites

in the receptor. The formation of such bonds brings about a conformational change in the receptor and triggers consequential intracellular events.

Neurotransmitter receptors fall into two distinct superfamilies, separated by their structure and mode of action. The first, ligand-gated channels (LGC) are large proteins that contain a ligand binding site and an intrinsic ion channel gated by the neurotransmitter (Figure 1.5A).<sup>2</sup> Receptor binding results in a conformational change in the receptor and the opening of the ion channel. The ionic permeability of the channel will determine if the response is hyperpolarisation or depolarisation of the postsynaptic membrane. Signaling via LGCs has very short latency; there is rapid closing of the channel following neurotransmitter dissociation from the receptor. This is often referred to as fast synaptic transmission. The second group of receptors generally have 7 transmembrane helices, which are coupled to proteins or enzymes situated at the inner surface of the synaptic membrane via one of a number of G-proteins. Activation of a G-protein-coupled receptor can lead to activation or inhibition of the effector depending on the particular G-protein involved. The effectors can be ion channels or enzymes involved in the synthesis or degradation of second messengers, which are physiologically active compounds within the target cell. Identified second messenger systems include cAMP, cGMP, calcium ion,  $\text{Ca}^{2+}$ -binding protein calmodulin, and phosphoinositide derived inositol 1,4,5-*tri* phosphate and diacylglycerol. Triggering of the second messenger system is the beginning of a cascade of intracellular events which act by protein phosphorylation. These events can produce rapid mediatory effects (such as the activation or inhibition of ion channels), short-term modulatory effects (general metabolism, neurotransmitter synthesis and release) or long-term modulatory effects (the regulation of gene expression).

Neurotransmitters need to be quickly removed from the synapse so that their actions can be short-lived and the postsynaptic membrane made available for further stimulation. This is achieved by a number of mechanisms with different kinds of neurotransmitters having a preferred route. Simple diffusion away from the synaptic cleft does occur but is too slow to be the principal mechanism. Free neurotransmitter can be catabolised by enzymes in the synaptic cleft or reabsorbed by the presynaptic terminal, glial cells or postsynaptic processes.<sup>3</sup>

High diversity in particular neurotransmitter receptor types can be observed at multiple levels. Closely related receptor types can be coded by distinct genes or following alternative RNA splicing. The involvement of different receptor subtypes for a given neurotransmitter has important implications in message transduction. If each receptor subtype is associated with a distinct transduction mechanism then the one neurotransmitter can evoke a number of inhibitory or excitatory responses in its target cell.

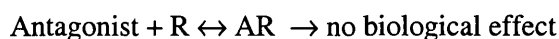
The unique structures of the different subtypes can be exploited for therapy in different neuropsychiatric disorders using pharmacological agents (ligands and drugs) that have high selectivity for one subtype over the others. Selectivity can be extended to the transduction pathway and biological response activated by that particular subtype. Synthetic compounds that bind and activate a



receptor, thereby mimicking the action associated with endogenous neurotransmitter are termed agonists.



Other ligands or drugs that bind to the receptor site but prevent receptor activation and the resulting biological response are called receptor antagonists. They fail to activate the receptor because of either over distortion of the receptor, or conversely a lack of effect on the receptors conformation.



Antagonist binding has the added effect of blocking receptor stimulation by the natural neurotransmitter.<sup>4</sup> However, antagonist binding may also be reversible at a particular rate.

The synapse is responsible for the unidirectional flow of information, the delay, and the control of message transfer from one nerve to another. These loci are a key feature of the nervous system that leads to its specificity, plasticity and variability. Communication and integration of responses is clearly essential for the normal working of the human body. Faulty communication can lead to physiological, neurological and psychiatric disorders such as depression and schizophrenia.<sup>4</sup> The possible basis for such disorders could include either over-stimulation or under-stimulation of target cells as a result of an excess or deficiency in neurotransmitter release. Alteration in the mechanisms involved in neurotransmitter degradation and hence termination of synaptic transmission could also lead to the same outcome. These errors could be corrected by drug treatment. Agents that increase neurotransmitter synthesis or release, or reduce their removal or degradation could enhance transmission. Agonists could affect both G-protein coupled receptors and the gating of neurotransmitter-gated ion channels to increase the magnitude of the postsynaptic signal.<sup>3</sup> In contrast, agents that reduce or block synthesis and release of neurotransmitter could treat over-stimulation. Antagonists could affect neurotransmitter-gated ion channels and G-protein-coupled receptors, as described above to reduce the magnitude of the response to a given stimuli.<sup>3</sup>

### ***1.1.3 Hypotheses of the Involvement of Neurotransmission in Psychiatric Disorders***

Psychotic illness may be characterised by one of two broad categories of symptoms.<sup>5</sup> Positive symptoms (*e.g.* delusions and hallucinations as discussed below) result from an aberration or distortion of normal neuronal function. By comparison, negative symptoms (*e.g.* flattened affect, self-neglect, apathy as discussed below) are associated with a loss of normal function. Perturbations of the normal neural activity in the brain has long been thought to be the basis of mental illness. However, the identification of the underlying mechanisms that leads to psychotic symptoms is difficult. A psychotic syndrome or disease is not characterised by a single symptom but a clustering of symptoms that can vary greatly between individuals. To complicate the situation further, it is possible that both negative and positive symptoms present together in the same syndrome for example, schizophrenia. Any theoretical mechanism needs to account for the constellations of symptoms in addition to the individual symptoms.

Functional psychoses can be divided into two classes, the affective (mood) disorders and schizophrenia. The affective disorders are associated with a persistent disturbance of mood beyond normal every day fluctuations. In depression, normal mood is lowered while the elevation in mood observed with mania is less common, and often interspersed with depressive episodes as in bipolar, manic depression. Schizophrenia is a thought disorder characterised by both a disturbed form and content of thought. The symptoms associated with this psychosis can be classified as either positive or negative. Positive schizophrenia has an acute onset linked to delusions, hallucinations, disorganised speech and bizarre or disorganised behaviour. Negative symptoms show a long course of progressive deterioration and loss of functions such as poverty of speech, self-neglect and loss of social skills.

The major organic psychiatric disorders, such as dementia and delirium, demonstrate pathological lesions or arise from a medical disorder.<sup>6</sup> The primary symptom of dementia is a preferential impairment of short-term memory in the presence of normal consciousness. Alzheimer's disease is the cause of sixty percent of all cases of dementia. Neurodegenerative diseases such as Parkinson's are of interest since the behavioural deficits observed are the result of neuronal damage and therefore provide some insight into the normal function of structures in the CNS.

Psychiatric research can investigate the aetiology of a particular disorder from a number of different perspectives.<sup>6</sup> These can include epidemiology, sociology, psychology and biology. Each of these factors combine in a unique manner, contributing significantly to the progression of the disorder. There are further factors that are distinguished within the biological approach. A definite but moderate genetic predisposition is associated with most disorders. However, the potential complexity of psychiatric disorders has made it difficult to locate specific chromosomal loci or causative genes. Most psychiatric disorders do not have a known neuropathological basis. This approach is normally associated with the neurodegenerative disorders, such as Parkinson's and Alzheimer's. However, the application of more sensitive brain imaging and molecular techniques to the study of psychoses may reveal some neuropathological basis to the disorder. Biochemical theories propose that psychiatric disorders are associated with disturbances in the level of activity of an enzyme, neurotransmitter or receptor. This is true for a number of psychoses. Correction of abnormalities in the neurotransmitter-receptor mechanism is often the aim of therapeutic drug development. Measurements in the brain are used to support claims of a biochemical involvement in a particular psychosis. Any information that increases our knowledge of the involvement of neurotransmission and specific brain receptors in the aetiology of psychiatric disorders can lead to an increased understanding of the basis of some psychiatric disorders. This, in turn, can aid the development of new and more effective therapies.<sup>7</sup>

The major pathological features of Alzheimer's disease are neurofibrillary tangles and senile ( $\beta$ -amyloid) plaques in the hippocampus and cerebral cortex. Degeneration of cholinergic neurons in the basal forebrain is associated with a deficit of acetylcholine. The severity of the dementia is directly proportional to the acetylcholine deficiency and synaptic loss.<sup>6</sup>

In contrast to disorders thought to arise from degeneration in adults, schizophrenia has been posited as a neurodevelopmental disorder. The evidence suggests brain alterations in schizophrenia are



nonprogressive, and may result from genetic abnormalities, or antenatal damage to the developing fetus (usually in the second trimester).<sup>8</sup>

The pre-eminent dopamine hypothesis of schizophrenia proposes that schizophrenia is a result of excess dopaminergic function in the limbic system. Excess dopamine transmission could occur at any point in the series of steps in neuronal transmission. The bulk of the evidence suggests an abnormality in the receptor neuron, and not hyper-activation by an excess of dopamine production in the neuron, limited metabolism or diminished uptake.<sup>5</sup> Although dopaminergic abnormality contributes significantly to the clinical features of schizophrenia, a causal role seems unlikely since no consistent abnormalities in radioligand binding to dopamine-type 2 receptors have been observed in first-episode patients and the dopamine receptor gene has not been linked with schizophrenia.<sup>6</sup> Nevertheless, recent <sup>123</sup>I-IBZM SPET studies by Laruelle *et al.*,<sup>9</sup> suggest there are derangements in dopamine flux in patients with schizophrenia, and this work has revitalized the dopamine hypothesis. Two polymorphisms of the serotonin-type 2A receptor have been found to vary with clinical response to clozapine.<sup>10</sup> This kind of information has led to recent modifications of the dopamine hypothesis of schizophrenia to include serotonin-type 2 blockade as a prerequisite for efficient antipsychotic treatment. The neurochemical basis of psychosis is not well understood, and many candidates await full evaluation.

## ***1.2 Methods for Studying Brain Neurotransmission and Neurotransmitter Receptors***

### ***1.2.1 In Vitro Methods***

#### ***1.2.1.1 In Vitro Receptor Binding Studies***

Receptor-radioligand binding studies *in vitro* provide a direct approach to the investigation of receptor-ligand interactions. The information obtained from such studies can answer questions about the receptor, such as its molecular pharmacology, the mechanism of ligand binding and the nature of receptor-effector interactions. Alternatively, more applied questions about a neuroreceptor's cell biology and anatomical distribution can be investigated.<sup>11</sup> A receptor binding assay entails incubating the receptor, prepared from the tissue of interest, with a suitable radioligand under predetermined conditions (*e.g.* temperature, time and concentration). At the end of the incubation period, the free and bound radioligand are separated and measured. These steps can be repeated in the presence of a number of different agents in order to test different hypothesis. Quantitative estimates of rate constants and/or affinity constants are extracted from the data by curve-fitting and other statistical techniques.

The receptor preparation can have different levels of enrichment ranging from the unenriched whole animal to a purified receptor preparation. In whole animal studies, radioligand injection is usually followed by tissue isolation and assay. This will be discussed further in Section 1.2.2.2.

Receptor binding studies, that employ membrane preparations, reduce the non-specific or carrier-mediated uptake of the radioligand that is often observed with whole tissue preparations. Preparations of solubilised receptors chemically dissect the receptor protein from the cell surface membrane. Receptor-effector connections are often well preserved in these preparations allowing the characterisation of the general properties and physiochemical characteristics of the receptor.

Interpretation of count rates for bound versus free radioligand can become mathematically complex. A large number of variables result from the open-ended nature of binding experiments.<sup>11</sup> Many artifacts may be present that need to be minimised or controlled. These can be attributed to the intrinsic property of the radioligand or receptor preparation, or the result of radioligand-receptor interactions. Inadequacies in the procedures can include incomplete separation of the bound from the free, dissociation of the bound radioligand during separation, loss of the activated receptor-radioligand complex or non-specific binding during the assay. Radioligand depletion and states of non-equilibrium will also produce artifacts in the data that violate the assumptions behind the statistical procedures used during analysis.

#### 1.2.1.2 *In Vitro* Autoradiography

Autoradiography is a technique used for mapping cellular components in thin slices of whole tissue where the cell surface membrane remains locally and globally intact.<sup>12</sup> The radioligand is incorporated into the tissue by incubation *in vitro*. The thickness of the slice is usually set to maximise diffusion and is of the order of micrometres. Cyrosectioned slices are adhered to gelatin-coated or poly-L-lysine-coated glass slides which allows the receptor-bound radioligand to be physically removed from the free radioligand at the end of the incubation. The tissue with bound radioligand is exposed to  $\beta^-$ - or  $\gamma$ -sensitive film. The radiation emitted from the radioligand interacts and darkens the silver halide grains in the film to form the autoradiogram. The duration of film exposure depends on the radionuclide in the radioligand. The most commonly used radionuclides are  $^3\text{H}$  ( $\beta^-$ -emitter  $t_{1/2} = 12.43$  y) and  $^{125}\text{I}$  ( $\gamma$ -emitter,  $t_{1/2} = 60$  d), which require film development for 3–4 weeks and 3–4 days respectively.

Autoradiography using these radionuclides permits radioligand-binding characteristics, such as receptor affinity and selectivity to be determined. This technique can also reveal species specific or disease specific variations in receptor subtypes and ligand interactions. Autoradiography is often the first step in radioligand and drug development.

#### 1.2.1.3 *In Situ* Hybridization

*In situ* hybridization is an *in vitro* technique that enables the localisation of cells containing specific nucleic acid sequences and therefore of specific mRNA molecules responsible for the manufacture of certain proteins essential for neuronal function.<sup>2</sup> The application of molecular biology to the study of synaptic transmission has identified gene products that encode a number of receptor subtypes. Single strands of DNA or RNA, with base pair sequences that complement the nucleic acid for a particular receptor, can be labelled with  $^{32}\text{P}$ ,  $^{35}\text{S}$ ,  $^3\text{H}$  or  $^{125}\text{I}$ . These can be used as probes to determine the

probable sites of receptor protein synthesis and their localisation in different cell types. A simple approach to understanding the genetic basis of neuropsychiatric disorders is to look for allelic variations in genes encoding certain receptor types. A large multi-centre study found a significant association between a serotonin-type 2A receptor gene polymorphism and schizophrenia.<sup>13</sup> *In situ* hybridization can also be used to quantify the impact of drug treatment on receptor and neurotransmitter mRNA levels, thereby providing more information on their specific modes of action. This method is exceptionally specific but is slow and labour intensive.<sup>2</sup>

### 1.2.2 *In Vivo* Methods

The next progression in the study of neurotransmission and neurotransmitter receptors is the study of live animals. This is because of the difficulty in simulating the *in vivo* biological environment *in vitro*. For example, the protein binding of the radioligand to components of the extracellular fluid and plasma proteins, metabolism and the obstacle to CNS neuroreceptor binding *in vivo* (the blood-brain barrier) cannot be mimicked in a test tube.

#### 1.2.2.1 Microdialysis

Microdialysis is a technique developed for brain sampling in free moving animals that allows for either administration or collection of substances at discrete brain regions with a high degree of accuracy. Microdialysis uses the principle of dialysis, the diffusion of substances across a semipermeable membrane from an area of high to low concentration. By continuously flushing the probe with a solution devoid of the substances of interest, a concentration gradient is maintained, promoting diffusion across the membrane for collection and analysis. The concentration gradient is reversed when administering a substance of interest to a particular area of the brain. Flushing a probe with a high concentration of the substance will promote diffusion into the probed region of the brain. An advantage of microdialysis over other brain sampling techniques is the continuous nature of the sampling. In addition to obtaining data on the biochemical response to administration of a particular compound, microdialysis also allows correlations between behavioural and biochemical indices to be investigated.

Microelectrode implants can be used in a similar manner to microdialysis to investigate the concentration of electroactive compounds, for example the oxidisable monoamine neurotransmitters (*e.g.* dopamine), in a particular region of the brain.<sup>14</sup> This technique can be combined with microdialysis to study the electrochemical response following drug administration or behavioural stimulation.

#### 1.2.2.2 *Ex Vivo* Dissection/Autoradiography Studies

Receptor binding studies in whole animals provides information on the kinetic behaviour of a particular radioligand in addition to anatomical distribution obtained with *in vitro* autoradiography. Some period after intravenous injection of a radioligand, scintillation counting or autoradiography of isolated tissue determines the distribution of radioactivity. In addition to analogous kinetic data, an

input function can be obtained from arterial blood measurement. Blood can be analysed for labelled and unlabelled constituents to give some indication of metabolism and the biological half-life of the radioligand. The radioligand's ability to penetrate the blood-brain barrier, its neuroanatomical localisation and kinetics can also be quantified by taking readings from animals sacrificed at set times after radioligand injection. Each animal will provide one point for radioligand binding on the kinetic binding curve. The effect of different, intravenously administered agents on radioligand kinetics can also be assessed. For increased anatomical detail, autoradiography of the brain is preferred over tissue dissection and counting.

### 1.2.3 Non-invasive In Vivo Imaging

While information from animal studies is important in investigating normal synaptic transmission and the binding characteristics of certain radioligands, its relevance to the study of brain neurotransmission in humans is limited. The human frontal cortex is highly developed. Therefore, the investigation of distinctly human functions associated with this region, such as language or complex social interactions, is impossible in animals. *In vitro* and *in vivo* animal models for psychiatric disorders are few, and when available, are restricted by the degree to which the results can be extrapolated to humans.<sup>15</sup> Animal models, especially for the negative symptoms of schizophrenia, are rare or non-existent.<sup>5,10</sup> Animal studies are therefore limited to the investigation of single symptoms or neurotransmitter pathways rather than symptom clusters or interactions between different neurotransmitters. Post mortem autoradiography studies on psychiatric disorders generally use brain tissue from old individuals. Aging and death can be associated with prolonged institutionalisation or drug treatment in addition to other illnesses, thereby confounding any results obtained.<sup>5</sup> The *in vivo* imaging of the CNS in young people has revolutionised the study of radioligand: receptor interactions in normal and diseased states.

#### 1.2.3.1 X-ray and CT

*In vivo* imaging techniques can be divided into structural and functional imaging. The first imaging of the brain was by conventional skull X-ray. A static structural picture of the brain is obtained, determined by the differences in absorbance of X-rays.<sup>2</sup> From a structural viewpoint this technique has very low resolution since different soft tissue parts of the brain show only small density variation making them poorly distinguishable. Another disadvantage is that all the X-ray densities between the source and the film are superimposed into a single plane.<sup>3</sup>

Computerised tomography (CT) is an advanced modification of the standard X-ray. It has comparable spatial resolution but provides three-dimensional images of the brain. CT uses a series of narrow parallel beams of radiation aimed through the tissue, which are detected by sensitive scintillation crystals on the other side of the head. The radiation source is rotated through 180-degrees around the head to give a series of radiation transmission readings. The computerised three dimensional image is the summation of all of the information gathered. Like the conventional X-ray

these images are purely structural giving no information on brain function. However, administration of contrast dyes can be used to enhance the signal to noise ratio between tissues.

#### 1.2.3.2 Magnetic Resonance Imaging

Magnetic Resonance imaging (MRI) is exquisitely sensitive to spatial variations in the concentration and physiochemical situation of particular atomic nuclei.<sup>3</sup> MRI is based on the principle that certain atomic nuclei resonate and emit distinct radiofrequency signals when placed in strong magnetic field. The same atomic nucleus will emit a different frequency dependent on its chemical or physical environment.<sup>2</sup> Since hydrogen in the form of water makes up 75% of the body it is the nucleus of choice for most MRI scans. Differentiation of the grey and white matter is improved over CT scans since grey matter has a higher water content. MRI can be employed to investigate anatomy, metabolism and biochemistry at a micromolar level.<sup>16,17</sup> It is also a very important technique for investigating the pathology of neurodegenerative disorders since cell death and disease frequently alter the water content.

Perfusion MRI produces high resolution images of a series of cerebral perfusion parameters which can be applied to any brain disease where regional abnormalities of cerebral blood flow or autoregulation are suspected.<sup>18</sup> The strong interrelationship between cerebral activity, neuronal activity and blood flow means that local changes in blood flow can be used as an indication of brain function and energy metabolism. Activation of neuronal energy metabolism in response to a particular task would normally result in an increase in local blood flow. Reduced local blood flow could be the result of neuronal damage or death. Therefore, the measurement of cerebral blood flow is important in determining the pathological basis of neurodegenerative and psychiatric disorders.

There are two possible approaches for the quantification of cerebral blood flow by MRI. The first is to magnetically tag either the brain or the blood.<sup>19</sup> The second involves a bolus injection of contrast media in conjunction with rapid MRI to trace its movement through the brain.<sup>20</sup> The latter provides high resolution images from a simple, safe technique. However, absolute quantification is not possible and no reference to normal values can be made at present.

#### 1.2.3.3 SPET

Single photon emission computerized tomography (SPET) is a non-invasive imaging technique that detects single photons from administered radiopharmaceuticals labelled with  $\gamma$ -emitting radioisotopes. The radiopharmaceutical is often a labelled compound that will preferentially localise at a given site of interest allowing the investigation of biochemical, physiological and pharmacological processes in the living brain. The picomolar sensitivity of SPET permits the imaging of structures such as neurotransmitter receptors.

Functional imaging with SPET involves the administration of a  $\gamma$ -emitting radiopharmaceutical to the subject, usually by intravenous injection, followed by tomographic imaging of the distribution of radioactivity with time.  $\gamma$ -Emissions from a particular location in the patient reach the detectors of the gamma camera after passage through the perforations in a lead collimator.

Photomultiplier tubes convert the detected light signals into electrical signals that are then processed to give values for the position and magnitude of the emitted signal.  $\gamma$ -Rays can scatter away from their source or be attenuated by tissue between the site of emission and the detector. These two factors influence the correct localisation of the gamma emitter. The use of collimators in front of the detectors prevents photons outside the line of a particular plane from impacting on the detectors. Any photon that reaches the detector is assumed to originate from a particular plane in the patient directly beneath and parallel to the holes in the collimator. The need for collimation to correct for scatter is a limiting factor for the count sensitivity of SPET. Attenuation is usually addressed with varying degrees of success by post-processing of the image. The most accurate methods for attenuation correction are based on transmission data.<sup>21</sup> With this information, algorithms now exist that include attenuation and scatter correction to produce SPET data with a high degree of accuracy.<sup>22</sup>

The overall resolution of a SPET image is governed by the photon energy emitted by the radionuclide, the collimator and the distance of the detector from the source.<sup>23</sup> The optimum energy range (50–300 keV) for  $\gamma$ -ray detection by a gamma camera is determined by detector thickness.  $^{99m}\text{Tc}$  and  $^{123}\text{I}$  are ideal radionuclides for SPET, since they emit principal  $\gamma$ -rays in this range (140 and 159 keV, respectively).  $^{99m}\text{Tc}$  is the  $\gamma$ -emitting radionuclide most commonly used in the clinical environment and decays with a 6 h half-life.  $^{123}\text{I}$  is the radionuclide commonly used for labelling ligands for neuroreceptor investigations and has a 13.2 h half-life. Other radionuclides that have a use in SPET are  $^{131}\text{I}$ ,  $^{201}\text{Tl}$  and  $^{111}\text{In}$  ( $t_{1/2}$  = 8.04 d, 73.1 h and 2.83 d, respectively).

Advantages associated with SPET for psychiatric research include its relatively low cost and accessibility compared with PET (see below) allowing large studies with increased flexibility. The commercial availability of radiopharmaceuticals and the half-life of the radionuclides simplify the logistics of SPET scanning procedures and can increase the rate of patient recruitment. Patient acceptance of the scanning procedure is especially important when studying psychotic patients. The long half-life of  $^{123}\text{I}$  can also be exploited for imaging certain radioligands with slow kinetics.<sup>24</sup> Possible scanning up to 24 h after injection of such radioligands can be exploited to improve the signal to noise ratios.

The accuracy of the parameters obtained from quantitative methods of analysis is a reflection of the input data. Expressing radioactivity in absolute terms requires accurate recovery of photons, including attenuation and scatter correction. SPET is limited by its poor selectivity for recording high spatial resolution, kinetic tomographic data. This has meant that information is generally obtained from functional SPET via relative or semi-quantitative measures that exploit the time-dependent nature of the radioligand-receptor binding relationship.<sup>25</sup> However, there is an increased trend towards more quantitative approaches in SPET.

#### 1.2.3.4 PET

Positron emission tomography (PET) is a non-invasive imaging technique that uses radiopharmaceuticals labelled with positron-emitting radioisotopes to investigate biochemical,

physiological and pharmacological processes in the living brain. The sensitivity and resolution achieved with PET enables the detection of picomolar concentrations of intravenously administered radiopharmaceuticals and the imaging of molecular processes occurring at low concentrations.<sup>16</sup>

The basis for the detection and localisation of the radiopharmaceutical in PET is the detection of coincident  $\gamma$ -rays resulting from  $\beta^+$ -decay (see Section 1.6.1.1). A  $\beta^+$ -particle emitted during the decay of a neutron-deficient nuclide, loses kinetic energy by interaction with matter, and pairs with an electron to form a transient entity called positronium. The annihilation of positronium results in the simultaneous release of two photons with equal energy (511 keV), travelling in opposite directions. A PET camera is composed of multiple scintillation detectors, linked to photomultipliers placed on opposite sides of the radiation source. Incident  $\gamma$ -rays, registered by the detectors, are amplified and fed into energy discrimination circuits that identify two detection events 180° apart, unambiguously occurring within a certain, brief time window (~ a nanosecond). These coincidence events are assumed to have come from the same annihilation event with the positron emitter located somewhere along a line of response (LOR) linking the two detectors. The coincidence events are stored as two-dimensional matrices and reconstructed using standard tomographic techniques.

The detection of coincident pairs of  $\gamma$ -rays can provide positional information in PET without the need for physical collimation. Most PET cameras use block-detectors in a series around the patient. Lead or tungsten septa can be employed as physical collimators so that the registration of coincident  $\gamma$ -rays is limited to opposing detectors or closely neighbouring detectors within the ring. Alternatively, removal of the septa and running of the camera in 3D mode increases the number of LORs. This increases the sensitivity to true coincidence events.<sup>26</sup> Scatter of photons can lead to detection of coincidences that do not originate from the same annihilation. Scatter coincidences lead to an overestimation of isotope concentrations and increases statistical noise. Approximately 15% of the detected coincidence events will result from scatter when a camera is operated in 2D mode (*i.e.* with septa present). In 3D mode a much greater range of scatter angles will be detected leading to a significant increase in the number of scatter coincidences (40–45% of the total coincidence events).<sup>26</sup> For 3D PET accurate correction for scatter is required. Scatter correction in brain imaging may be successfully implemented because the radioactivity and scatter medium is quite uniformly distributed and concentrated in the centre of the field of view. Therefore, 3D operation is preferred for brain studies because of the associated increase in sensitivity to true coincidences.

In PET the correction for  $\gamma$ -ray attenuation in tissue is applied to the LOR with the attenuation factor being the same for annihilations at any position along that line. Accurate attenuation correction with PET makes it possible to directly relate count rates from rapid sequential images to the absolute concentration of radioligand. The overall result is truly quantitative information that can be applied to kinetic models of radioligand-receptor binding to obtain values for receptor binding potential and density.

The positron-emitters most commonly used in PET are  $^{11}\text{C}$ ,  $^{15}\text{O}$  and  $^{18}\text{F}$ . These isotopes have a number of characteristics that make them attractive candidates for medical imaging. The average

distance that a positron travels before annihilation is an intrinsic property of each radioisotope and ultimately determines the intrinsic spatial resolution that can be achieved. The higher the energy of the  $\beta^+$ -particle the greater the distance between positron emission and annihilation. For the routine PET isotopes, positron energies less than 2 MeV result in an intrinsic loss of spacial resolution of less than 2 mm.<sup>27</sup> Carbon-11 and oxygen-15 have half-lives of 20.3 min and 2 min, respectively and decay to non-radioactive daughters. Therefore, they can be administered in relatively large doses to increase count statistics without exposing patients to high radiation doses. However, the short half-life also leads to a very tight time frame for radionuclide production through to the time of injection.<sup>17</sup> The presence of an on-site cyclotron and radiochemistry facilities and expertise is essential for “on demand” preparations of PET radiopharmaceuticals. While this has resulted in extensive development of the radiochemistry associated with positron-emitters, it has also increased the cost.

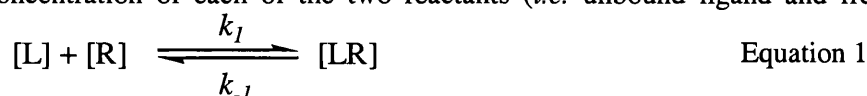
### 1.3 Radioligands for Neuroimaging In Vivo

#### 1.3.1 Receptor-Radioligand Interactions

Radioligands are developed for the selective imaging of high affinity binding sites. The sites of interest include neurotransmitter receptors, antigens or enzymes. Functional imaging techniques such as SPET and PET allows measurement of receptor parameters *in vivo*.

##### 1.3.1.1 Determination of Ligand-Receptor Interactions

The law of mass action is universally applied to describe the relationship of radioligand-receptor interactions. According to this law the reversible binding of free ligand to free receptor will occur at a rate proportional to the concentration of each of the two reactants (*i.e.* unbound ligand and free



receptor sites, Equation 1).

Similarly, the rate at which the ligand dissociates from the resulting complex will be proportional to the concentration of the complex. When the rate of association is equal to the rate of dissociation, a state of equilibrium is reached. In 1933, Clarke<sup>28</sup> applied this law to pharmacological systems, leading to the introduction of the simple bimolecular association reaction to describe receptor-ligand interactions, and the rate constants for association and dissociation,  $k_1$  and  $k_{-1}$ , respectively.

The relative concentrations of receptor, ligand and complex can be used to calculate the rate of association ( $k_1[L][R]$ ) and dissociation ( $k_{-1}[LR]$ ). At equilibrium Equation 2 is true.

$$k_1[L][R] = k_{-1}[LR] \quad \text{Equation 2}$$

This can be rearranged to give the equilibrium dissociation constant ( $K_d$ ) in concentration units (Equation 3):

$$K_d = k_{-1} / k_1 = [L][R] / [LR] \quad \text{Equation 3}$$



The  $K_d$  is an indication of the relative affinity of radioligands for the receptor, with a low  $K_d$  denoting a high affinity.

There are a number of assumptions implicit to these equations. The interaction is assumed to be always completely reversible. The reactants are assumed to be present only in a totally free or totally bound state. The measured products are assumed to include only species that are available for binding (*i.e.* no degraded ligand). Lastly, it is assumed that the receptor sites act independently and exhibit uniform affinity. These assumptions can be met during *in vitro* receptor-radioligand experiments. Such experiments produce graphical representations of receptor occupancy parameters, such as the  $K_d$ , receptor concentration per unit tissue ( $B_{max}$ ) and the displacement potency of a cold competitor ( $K_I$ ). Kinetic binding assays are a means of investigating the rate of formation or breakdown of the receptor-ligand complex. Equilibrium binding assays use the steady state condition where  $k_{-1}/k_1 = K_d$  to determine kinetic parameters. This is achieved by following the formation of receptor-ligand complex over varying concentrations of ligand. A saturation plot ( $[LR]$  against  $[L]$ ) for specific binding can be determined by dividing the total binding by the estimated non-specific binding (calculated following radioligand displacement *in vitro* with cold ligand). The  $B_{max}$  is given as the point of saturation of specific binding whilst the  $K_d$  is the drug concentration under equilibrium conditions, that leads to half receptor saturation. The relationship between  $B_{max}$ ,  $K_D$  and free radioligand concentration is given by Equation 4

Equation 4

$$B = \frac{B_{max} [L]}{K_D + [L]}$$

The non-linear fit of this relationship to experimental data is used to determine the values of  $B_{max}$  and  $K_D$ .

### 1.3.1.2 Receptor Kinetics in SPET and PET

The dynamic imaging of receptor radioligands *in vivo* generally shows one of two patterns of distribution.<sup>24</sup> Lipophilic radioligands show high and roughly uniform extraction across the blood-brain barrier which means that the initial uptake resembles blood flow. The rate of washout from the brain may be influenced by the presence of targeted receptors in certain tissues resulting in areas with high receptor densities exhibiting different time radioactivity curves to areas devoid of receptors. If the pattern of radioactivity distribution changes over time, as the blood concentration falls and the radioligand washes out of the brain, images of radioligand-receptor interactions may be obtained. These images contain the relevant information for determining receptor parameters *in vivo*. However, the situation *in vivo* is more complex due to the following reasons:<sup>29</sup>

- 1) The activity and quantity of radioligand injected into the subject is low in order to reduce the radiation dose and the pharmacological effects of the ligand. Quantification of both  $K_d$  and  $B_{max}$  from SPET and PET data is not possible from tracer alone experiments.

- 2) *In vivo* receptor populations are not in isolation. Radioligands are required to exhibit high selectivity since binding to alternative sites will influence the calculation of  $K_d$  and  $B_{max}$ .
- 3) The rate of washout from regions is influenced by receptor concentration. Radioligand clearance from regions devoid of receptors will be faster than from receptor-rich regions due to rebinding. Metabolism and peripheral clearance may also have some influence on the rate of washout. The resulting non-linearity in the measurements can influence the values obtained for  $B_{max}$ .
- 4) The fact that radioligands need to cross the blood-brain barrier to enter the brain and reach the target site prevents free access to the receptor and influences its ability to reach a state of equilibrium.
- 5) Very few foreign compounds such as radioligands are stable *in vivo*. Many radioligands show substantial distribution in the metabolic organs (kidney, liver and lungs) which can reduce radioligand concentrations in the brain. Any labelled metabolites formed during the scanning period, that have the capability of entering the brain, can enter into different equilibria with the receptor of interest or some other binding site. This will have a major impact on quantification of receptor parameters since imaging techniques record only radioactivity and do not discriminate on the chemical composition of the radioactive species.
- 6) It is possible that the kinetics of non-specific binding may differ in grey and white matter. If there is a variation in the proportion of grey and white matter across the brain, then the levels of non-specific binding in receptor-devoid areas may not be representative of non-specific binding in regions with varying concentrations of receptors.
- 7) The presence of endogenous neurotransmitter will compete with the radioligand *in vivo*. The formation of endogenous neurotransmitter: receptor complexes will complicate the state of equilibrium.

Improved radioligand characteristics can reduce the impact these factors have on functional imaging. For SPET and PET the receptor parameter of interest is usually the binding potential (BP), the product of the density and affinity of the receptors for a given radioligand. Information on the regional binding kinetics of a radioligand can be determined by a number of approaches. The quantitative nature of the method and the data requirements can vary for each.

### 1.3.1.3 Data Analysis

#### Kinetic method

Kinetic modelling of *in vivo* imaging data uses a compartment model (Figure 1.6) to describe the transfer of radioactivity from one compartment to another by a series of differential equations.<sup>30</sup> The equations represent the concentration of parent radioligand in the different compartments as a function of time. The standard model includes three compartments: two tissue compartments and a single arterial input function. This approach to kinetic analysis requires serial brain images of compartments that are representative of non-specific and specific radioligand binding, and an input function derived

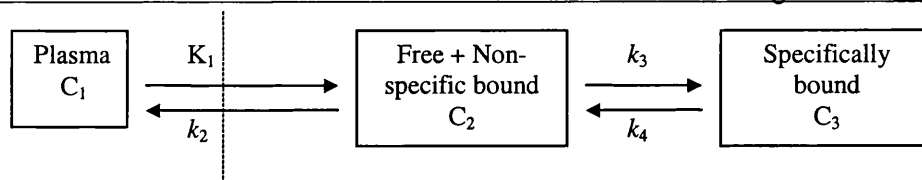


**Figure 1.6:** The three-compartment, four-parameter kinetic model of the uptake and washout of radioligand in the brain where  $C_1$  = concentration of parent compound in the plasma (nM),  $C_2$  = concentration of free radioligand plus that bound to non-specific sites in the brain and  $C_3$  = the concentration of specifically bound radioligand. The  $k$  values are the rate constants.

from the concentration of parent radioligand in arterial plasma. The computer fits the model to the data using an iterative least squared minimization procedure and provides the kinetic transfer from the concentration of parent radioligand in arterial plasma. The computer fits the model to the data using an iterative least squared minimization procedure and provides the kinetic transfer coefficients  $K_1$ ,  $k_2$ ,  $k_3$  and  $k_4$ . The separate measurement of  $B_{\max}$  and  $K_d$  is not possible with *in vivo* receptor imaging unless the specific activity of the radioligand is varied (*i.e.* cold ligand is added). However, the binding potential can be derived from Equation 5.

$$BP = \frac{k_3}{f_2 k_4} = \frac{B_{\max}}{K_d} \quad \text{Equation 5}$$

where  $f_2$  is the “free fraction” of unbound radioligand in the tissue. This constant can only be measured indirectly so it is assumed to be identical in all individuals.

The use of kinetic modelling provides a measure of receptor binding potential that is linearly related to receptor density. However, there is a need for arterial sampling to obtain an input function. For some radioligands, the simplified reference tissue model can be used where a region in the brain devoid of receptors can be used to provide an input function, thereby eliminating the need for arterial sampling.<sup>31</sup> This approach requires an appropriate reference region in the brain and should be validated against the full kinetic model.

The kinetic model can be simplified by the use of the constant infusion protocol (a single bolus followed by a prolonged constant infusion). With constant radioligand concentrations in the plasma a constant count rate is seen in different brain regions. This means that the rate of change of radioactivity between compartments is zero. Therefore, Equation 6 can be used to obtain a value for the volume of distribution ( $V_d$ ) for the receptor being studied.

$$V_d = \left[ \frac{C_{\text{brain}}}{C_{\text{plasma}}} \right]_{\text{equilibrium}} \quad \text{Equation 6}$$

### Graphical method

Graphical analysis of regional time radioactivity curves is another method for calculating binding potential. Linear regression lines can be applied to the time radioactivity curves for regions of interest. The difference between the slope of the regression line for regions of specific binding and non-specific binding will provide a value for the binding potential without assuming a particular compartmental

configuration. Graphical generation of binding potentials for [<sup>123</sup>I]iodobenzofuran SPET data showed good agreement with those obtained from a more complex three compartment modelling technique.<sup>32</sup>

#### *Empirical Equilibrium Method*

When an equilibrium is achieved between the concentration of radioligand specifically bound to receptors and that in the non-displaceable compartment (C<sub>2</sub>), the kinetic model can be simplified as shown in Equation 7.

$$\frac{k_3}{k_4} = \frac{C_3}{C_2} \quad \text{Equation 7}$$

This means that under conditions of equilibrium or transient equilibrium, the ratio of radioactivity in regions where specific binding occurs to regions of nonspecific binding (receptor-devoid areas) is an indication of receptor density. This method is easy to execute. However, its dependence on the identification of the point of equilibrium means that there is a potential for error when a predetermined and limited scanning period is used. A comparison of receptor densities obtained from [<sup>123</sup>I]iodobenzofuran SPET, and the target to reference ratio method versus more complex modelling approaches indicated an average difference of 10%.<sup>32</sup> This error results from the fact that the specific-to-nonspecific ratio is only linear with receptor density at equilibrium and that this can be influenced by individual variations in peripheral clearance of the radioligand. The formation of a labelled lipophilic metabolite complicates the equilibrium conditions and potentially increases the error associated with target to reference ratios. With a single bolus injection of radioligand, equilibrium is established for a short time. Equilibrium conditions can be maintained for a prolonged period if the initial bolus injection is followed by a prolonged constant infusion.<sup>33</sup>

The accuracy of the parameters obtained from kinetic modelling is a reflection of the input data. Expressing the radioactivity in absolute terms requires accurate recovery of photons, including scatter and attenuation correction. It is this requirement that has, until recently, limited the application of kinetic modelling to radioligand studies with SPET.

### **1.3.2 Selection of Candidate Radioligands**

Candidates for radioligand development must have the potential to provide the information required by the investigator. As mentioned previously (section 1.4.1.2), the characteristics of a radioligand can minimise the problems associated with measurements of receptor-ligand interactions *in vivo*. For neurotransmitter receptor studies radioligands need to exhibit high selectivity and affinity for the binding site of interest. Other factors that can influence the quality of the PET or SPET data include the ability of the compound to reach its target site, its pharmacokinetics, lipophilicity and metabolism. Radioligands are administered at tracer amounts. However, a need for non-toxicity and a lack of pharmacological effects also need to be considered when selecting new candidates.

High selectivity of the radioligand for one particular receptor population means that only one equilibrium state is present simplifying the interpretation of *in vivo* binding parameters. The affinity of the radioligand for the binding site of interest should generally be greater than one order of

magnitude higher than any other potential binding site (Pike<sup>34</sup> and references therein). In some instances, anatomically distinct distributions allows a single radioligand to be used to evaluate multiple receptor sites by semi-quantitative methods. [<sup>11</sup>C]N-methyl spiperone is one example, showing high affinity for both 5-HT<sub>2</sub> and D<sub>2</sub> receptors.<sup>35,36</sup> Since D<sub>2</sub> receptors are mainly localised in the basal ganglia and 5-HT<sub>2</sub> receptors mainly in the neocortex there is very little anatomical overlap in their distribution. As a result, selective binding is observed in the respective regions. However, this is not an ideal situation.

When studying neurotransmitter receptors in diseased states the magnitude of the effect can vary greatly. In order to visualise small changes in radioligand binding the ratio of specific to non-specific binding in the normal state should provide a sufficient signal to allow for quantification of these changes. The magnitude of the signal can be influenced by a number of factors, the most significant being the affinity of the radioligand for the receptor. If *in vivo* binding follows the theoretical basis of ligand-receptor interactions, the maximum specific binding signal (binding potential) is the ratio of the receptor concentration ( $B_{\max}$ ) to the equilibrium dissociation constant ( $K_d$ ). Since many receptors are present in the brain at nanomolar concentrations, a  $K_d$  value of nanomolar or sub-nanomolar magnitude is associated with successful PET or SPET signals.<sup>34</sup> For investigation of receptor populations of lower density for example extrastriatal dopamine D<sub>2</sub> receptors, a higher affinity radioligand is required.

All radioligands show some level of binding to non-specific sites such as plasma proteins, enzymes and blood cells. Albumin is often responsible for the majority of the binding in plasma. Sequestration of the radioligand in tissue lipids can also contribute to non-specific binding. Potential radioligands should exhibit minimal non-specific binding and a rapid rate of clearance from these sites. The lipophilicity of a compound is a general indicator of potential non-specific binding.<sup>34,37</sup> The logP is a measured constant commonly used as an indication of lipophilicity for a compound (see section 1.7.8). Binding to albumin increases with lipophilicity in a parabolic relationship with a maximum biological activity at logP 3.8.<sup>4</sup> It is also the more lipophilic compounds that are entrapped in fatty deposits. Therefore, high levels of non-specific binding are often associated with high lipophilicity. However, low lipophilicity is not conducive to penetration of the highly selective blood-brain barrier. Radioligands are usually unable to utilise carrier-mediated entry into the brain and so rely on diffusion to cross the blood-brain barrier. Dischinois *et al.*<sup>38</sup> found an inverted parabolic relationship between lipophilicity and first-pass extraction of carbon-11 labelled compounds to the brain. This can be explained by low brain extraction associated with low logP, and strong binding to plasma proteins and cell membranes at high logP. The lipophilicity of a potential radioligand should be compatible with good brain uptake and minimal non-specific binding. A logP value near 2.5 may fulfill both of these requirements.<sup>34</sup> A comparison of striatal uptake for a number of benzamide derivatives indicates that a useful signal is associated with a  $K_d$  of 0.1 nM or less and an apparent lipophilicity of between 1.7 and 2.5.<sup>39</sup> In conclusion, the magnitude of the PET or SPET signal generated from neurotransmitter radioligands is dependent on both lipophilicity and affinity.

The pharmacokinetics of a particular radioligand will influence the method of analysis that can be employed. A state of equilibrium needs to occur within the scanning period for meaningful information to be obtained about receptor density. Radioligands that show reversible binding with rapid brain uptake and washout phases during the scanning session are more amenable to quantification by kinetic models<sup>30</sup> (See section 1.4.1).

SPET and PET cameras detect radioactivity and give no information on the chemical entities in which the radionuclide is incorporated. The presence of radioactive entities which are able to cross the blood-brain barrier and possibly enter into equilibria with the same receptor as the parent compound or some other non-specific site is one of the major problems associated with the *in vivo* imaging of radioligand-receptor interactions. Therefore, metabolic stability *in vivo* during the scanning period is desirable for a clear, interpretable signal. Any metabolites should not accumulate at the site of interest. For neuroimaging this means that metabolism should be limited to the periphery, ideally giving polar compounds that have no affinity for the target binding site and are unable to enter the brain.

### 1.3.3 Labelling and Evaluation of Radioligands

Labelling and evaluation of a potential candidate ligand involves a number of steps:

1. Radionuclide production
2. Production of a labelling agent
3. Labelling chemistry
4. Purification
5. Formulation
6. Automation of production
7. Quality control/ assurance
8. Biological testing for efficacy *in vivo*
9. Metabolite analysis

The choice of radionuclide depends on the imaging technique (SPET or PET) and the compound to be labelled. The most frequently used radionuclides are carbon-11 and fluorine-18 in PET and iodine-123 or technetium-99m in SPET. Chemical synthesis can be devised to place carbon-11 at a particular site in a candidate radioligand. This is known as isotopic labelling, where the chemical structure of the ligand and the derived radioligand are the same. Several drugs or receptor antagonists already possess a fluorine atom and some an iodine atom. These allow isotopic labelling with fluorine-18 or iodine-123. However, labelling with fluorine-18 and iodine-123 is often non-isotopic. A new structure is produced that may show modified biological activity. Addition of fluorine-18 to a molecule can in some instances lead to more favourable behaviour *in vivo*.<sup>37</sup> Fluorine-18 is often substituted for a hydrogen atom or a hydroxyl group. The fluorine atom is considered to be isosteric with the hydrogen atom and isoelectronic with the hydroxyl group. In addition, it is highly electronegative and has the ability to influence the acidity of neighbouring groups. By comparison, an

iodine atom is large, occupying the space equivalent to a benzene ring. As a result, non-isotopic introduction of iodine for a hydrogen atom or a hydroxyl group may have a substantial effect on the functional properties of the molecule.

Feasible labelling procedures that are simple and efficient are important. A range of labelling agents and possible precursors can be exploited for this purpose. For the positron-emitters, fluorine-18 and carbon-11, short half-lives demand rapid radiochemistry that involves only a few chemical steps and operations. The production of positron-emitting ligands (from radionuclide production to intravenous injection into the subject) is generally limited to 2–3 half-lives. These limitations have led to the development of a mature and versatile discipline that is capable of labelling a high proportion of potential radioligands in a particular position. The half-life of iodine-123 (13.2 h) allows more flexibility in the radiochemistry. However, the above demands still hold true to maximise yield and minimise radioligand degradation and radiation dose to the radiochemist.

The percentage of radioactivity in the labelling agent incorporated into the product is the radiochemical yield. A number of factors can influence radiochemical yield, such as precursor concentration, temperature, pressure and pH. Labelling procedures very rarely have a radiochemical yield of 100%. Therefore, purification to high radiochemical purity is achieved by high performance liquid chromatography (HPLC) of the reaction mixture, generally on a 'semi-preparative' size column. This procedure separates the desired radioligand from other undesirable radioactive and non-radioactive products formed during the labelling procedure. The eluate corresponding to the desired labelled product can be collected and formulated for intravenous injection.

A particular labelling agent and reaction conditions will not only influence the speed and efficiency of the reaction but will have some impact on the final radioligand preparation. The specific radioactivity of a radiopharmaceutical preparation is defined as the ratio of the radioactive, relative to the non-radioactive, or carrier, version of the compound. The maximum theoretical specific radioactivity (Bq/ mol) for a given radionuclide is a function of its half-life and is attained in the absence of carrier dilution. The theoretical specific activity is expressed by the following equation:

$$A = \frac{\ln 2 \cdot N}{t_{\frac{1}{2}}}$$

where  $N$  = Avogadro's number,  $A$  = radioactivity (Bq) and  $t_{\frac{1}{2}}$  = half-life (in sec).

A radioligand is defined as "carrier free" (CF) when no carrier is present. In reality, the CF state seldom exists. The term "no-carrier added" (NCA) is used to describe radiopharmaceutical preparations in which no source of carrier has been deliberately added during labelling. In some cases a source of stable carrier is added during radiosynthesis. This may be required, for example to encourage the labelling reaction. Radiopharmaceuticals prepared by such methods are termed "carrier added" (CA).

In most PET radiopharmaceuticals there is some degree of carrier dilution. This is often due to the starting reagent or the precursor acting as a source of carrier. With fluorine-18 two chemical forms can be produced, [ $^{18}\text{F}$ ]fluoride and molecular [ $^{18}\text{F}$ ]fluorine.<sup>37</sup> Reactions that use [ $^{18}\text{F}$ ]fluorine to directly label organic molecules are CA. This is due to a requirement for fluorine (carrier) addition during the recovery of the radioactivity from the target following irradiation. By comparison [ $^{18}\text{F}$ ]fluoride is NCA, having a very high (near theoretical) specific radioactivity. Carbon-11 is generally produced with a cyclotron as [ $^{11}\text{C}$ ]carbon dioxide or [ $^{11}\text{C}$ ]methane. Due to the ubiquity of carbon materials in the environment, the specific radioactivity of  $^{11}\text{C}$  is always lower than in the CF state.  $^{11}\text{C}$ -Labelled radioligands are therefore, described as NCA. The reaction conditions in iodine-123 chemistry are generally considered to be NCA, since [ $^{123}\text{I}$ ] is commercially available as [ $^{123}\text{I}$ ]NaI with very high specific radioactivity. There are a few exceptions to this rule. Stable iodine atoms in a compound can be exchanged for  $^{123}\text{I}$  to produce the radioiodinated ligand. Since this reaction does not proceed to completion some of the stable ligand is present in the final preparation. Reactions that involved use of iodine monochloride (ICl) as the iodinating species are also considered to be CA procedures. The radioiodinating agent,  $^{123}\text{ICl}$ , is prepared by treating ICl with radioactive sodium iodide. In these reactions, the iodinating species is the source of carrier. In some radioiodinations carrier [ $^{127}\text{I}$ ]NaI is added to the reaction to increase the radiochemical yield to acceptable levels. In these CA reactions the increase in yield is associated with a reduction in specific activity of the final dose.

Quality control procedures should be performed on all radioligand batches before their release for human injection. Radio-HPLC is used to determine the radiochemical and chemical purity of a particular dose. The stability of the radioligand also needs to be established. This has more relevance for ligands labelled with longer half-life radionuclides. SPET radioligands labelled with  $^{123}\text{I}$  are available commercially, and are often produced the day before injection to allow for transportation to the scanning centre. As mentioned previously, the SPET camera cannot discriminate between different radiolabelled molecules. Any radioactive impurity in the injected dose has the potential to impact on the emitted signal and data interpretation, so stability *in vitro* should be high. Quality assurance procedures are tests that cannot be performed within the life of the radiopharmaceutical but are intended to ensure its safety and efficacy. Analytical techniques can be used to characterise thoroughly the quality of reactants and products. Mass spectroscopy and nuclear magnetic resonance have limited use in routine quality control but are important in determining the chemical purity of both the precursor and any reference compounds. Toxicological studies are required to provide information on the safety of the radiopharmaceutical for intravenous injection.

Following intravenous injection of the radioligand, an input function for the brain can be obtained from measured radioactivity in arterial blood samples. The arterial input of unchanged radioligand into the brain, is an important factor which determines the accumulation of radioactivity in all regions. This information is needed on a quantitative basis for the implementation of certain biomathematical models. Rapid washout of radioactivity from the blood will promote rapid washout



from brain regions devoid of the targeted receptor. This is therefore a desirable characteristic for radioligands.

Radioligands, like drugs, are foreign molecules and the human body has a number of metabolic processes to eliminate them.<sup>4</sup> Phase I metabolic processes include oxidation, reduction and hydrolysis. *N*-methyl groups, aromatic rings and terminal positions of alkyl chains are susceptible to oxidation while nitro and carbonyl groups will be reduced by the enzyme, reductase. Amides and esters are prone to hydrolysis by esterases.<sup>4</sup> The proportion of the radioactivity in blood attributed to the unchanged radioligand can be determined by a number of methods. Though thin layer chromatography (TLC) is common, HPLC is now preferred. Separation by HPLC can give some indication of the polarity of the radiolabelled metabolites, but usually not their identity. Polar, radioactive metabolites of brain receptor radioligands will tend not to interfere with the SPET or PET signal since their ability to cross the blood-brain barrier is limited. Lipophilic metabolites can usually cross the blood-brain-barrier, and confound imaging studies. At best, radioactive metabolites in the CNS will contribute to nonspecific binding and the unbound or free compartments. The worst scenario is one where the radioactive metabolites bind specifically to either the site targeted by the parent radioligand or to other specific sites.

Once non-polar radioactive metabolites have been identified, it may be possible to label them in the laboratory to determine their biodistribution *in vivo*. Thus, [<sup>11</sup>C] (*N*-2-(4-(2-methoxyphenyl)-1-piperazinyl)ethyl)-*N*-2-pyridyl)cyclohexane carboxamide (WAY-100635) was the first PET radioligand employed to investigate human 5-HT<sub>1A</sub> receptors *in vivo*.<sup>40</sup> It was shown that [<sup>11</sup>C]WAY-100635 is deacylated *in vivo* to [*O*-methyl-<sup>11</sup>C]WAY-100634. When labelled and injected into rats and primates, this radioligand crosses the blood-brain barrier and contributes to both specific and non-specific binding.<sup>41</sup> The metabolism of [<sup>11</sup>C]WAY-100635 to [*O*-methyl-<sup>11</sup>C]WAY-100634 is species-dependent. It is observed in primates but not in rats. Modification of the radioligand may be possible to prevent metabolism to lipophilic, radioactive molecules that have the potential to bind specifically in the CNS. Labelling WAY-100634 with <sup>11</sup>C in the acyl moiety avoided metabolism to [*O*-methyl-<sup>11</sup>C]WAY-100634 and led to a radioligand with far superior efficacy.<sup>41</sup>

### 1.3.4 Radioligands for the Investigation of Neuropsychiatric Disorders – Status

#### 1.3.4.1 D<sub>1</sub>-Receptors

The D<sub>1</sub> receptor subtype is present at a high concentration in the basal ganglia and to a lower extent in the substantia nigra and cerebral cortex. The benzazepine, SCH 23390 [(*R*)-(+)-8-chloro-2,3,4,5-tetrahydro-3-methyl-5-phenyl-1*H*-3-benzazepin-7-ol)] was the first potent (K<sub>D</sub> = 0.3 nM) ligand to show selectivity for D<sub>1</sub> receptors over the D<sub>2</sub> subtype. [*N*-methyl-<sup>11</sup>C]SCH 23390 has been used in PET to image D<sub>1</sub> receptors *in vivo*, producing a striatum to cerebellum signal ratio of 3 in humans.<sup>42</sup> The lower densities in extrastriatal regions are not detectable with [<sup>11</sup>C]SCH 23390. A number of other benzazepines have been labelled as potential candidates for imaging extrastriatal D<sub>1</sub> receptors. In healthy human subjects at 60 min after intravenous injection of [<sup>11</sup>C](+)- NNC 112 [(+)-8-chloro-

5-(7-benzofuranyl)-7-hydroxy-3-methyl-2,3,4,5-tetrahydro-1H-3-benzazepine)], the ratio of radioactivity in striatum to that in cerebellum was 8–12.<sup>43</sup> In addition a neocortex/cerebellum ratio of 2.5–4 was observed. These qualities make (+)-[<sup>11</sup>C] NNC 112 a useful radioligand for studying both striatal and extrastriatal D<sub>1</sub> receptors in normal and diseased states.

Labelling benzazepines with iodine-123 has not produced many successful SPET radioligands for imaging D<sub>1</sub> receptors. Placing iodine-123 in the phenyl ring of SCH 23982 limits *in vivo* deiodination. 7-Chloro-8-hydroxy-1-(3'-iodophenyl)-3-methyl-2,3,4,5-tetrahydro-1H-3-benzazepine (TISCH) is formed when the iodine is introduced at the 3'-position. [<sup>125</sup>I]-R(+) TISCH has a K<sub>D</sub> of 0.2 nM for D<sub>1</sub> receptors, shows good brain uptake and selective regional distribution in rat, primate and human brain *in vivo*.<sup>44</sup>

#### 1.3.4.2 D<sub>2</sub>-Receptors

The D<sub>2</sub> receptor subtype has a similar distribution to the D<sub>1</sub> subtype, with high densities in striatal brain regions and lower densities in extrastriatal regions. Due to the large amount of interest in D<sub>2</sub> receptor involvement in psychiatric disorders, especially schizophrenia, no fewer than eleven radioligands have been investigated for their potential use in humans with SPET and PET, respectively.<sup>45</sup> Most of the radioligands available for D<sub>2</sub> receptors also have some affinity for the D<sub>3</sub> receptor. As yet no radioligand has shown selectivity for either D<sub>2</sub> or D<sub>3</sub> receptor subtypes. Therefore, radioligands are described as having affinity and selectivity for D<sub>2</sub>-like dopamine receptors.

Initially, radioligands were developed for the D<sub>2</sub> receptor from analogues of butyrophenone neuroleptics, especially spiperone. However, these compounds showed irreversible binding and a lack of selectivity for D<sub>2</sub> versus 5-HT<sub>2</sub> receptors (reviewed by Mazière *et al.*<sup>46</sup>). The most routinely used radioligands for SPET and PET are the substituted benzamides, <sup>123</sup>I-IBZM ([<sup>123</sup>I]-(S)-2-hydroxy-3-iodo-6-methoxy-N-[(1-ethyl-2-pyrrolidinyl)methyl]benzamide) and [<sup>11</sup>C]-raclopride ([<sup>11</sup>C](-)-(S)-3,5-dichloro-N-[(1-ethyl-2-pyrrolidinyl)methyl]-6-methoxysalicylamide). Both radioligands have nanomolar affinity and high selectivity for the D<sub>2</sub>-like dopamine receptor.<sup>47,48</sup> However, their low signal to noise ratios limits their use in imaging extrastriatal receptor populations. FLB 457 and epidepride are two substituted benzamides that show higher affinity and selectivity for D<sub>2</sub>-like dopamine receptors and have been developed to visualise extrastriatal receptors with PET and SPET, respectively. Epidepride [(S)-3-iodo-N-[(ethyl-2-pyrrolidinyl)methyl]-5,6-dimethoxy-benzamide] has an affinity (K<sub>D</sub> = 0.025 nM) two magnitudes higher than IBZM, and is routinely labelled with <sup>123</sup>I for SPET.<sup>49</sup> Four hours after an intravenous injection of [<sup>123</sup>I]epidepride to a healthy volunteer, ratios of radioactivity in striatal, and extrastriatal regions to that in the cerebellum (a region devoid of D<sub>2</sub>/D<sub>2</sub>-like dopamine receptors) of 7.8 and 2.4, respectively, were seen.<sup>49</sup> [<sup>123</sup>I]Epidepride has been used to determine receptor blockade in schizophrenic patients treated with a variety of neuroleptic drugs.<sup>50,51</sup> FLB 457 [(S)-N-[(1-ethyl-2-pyrrolidinyl)methyl]-5-bromo-2,3-dimethoxy-benzamide] is another substituted benzamide which has an affinity for D<sub>2</sub> receptors of the same order as epidepride (K<sub>i</sub> = 0.018 nM<sup>42</sup>). The presence of both a N-methyl group and a bromine atom allows alternative labelling

for PET with either carbon-11 or bromine-76.<sup>52-54</sup> PET examinations in healthy human subjects after injection of [<sup>11</sup>C]FLB 457 showed accumulation of radioactivity in neocortical areas in addition to striatal regions of the brain.<sup>52</sup> Uptake in extrastriatal regions was 2–5 times higher than in cerebellum<sup>54</sup> with a ratio of the integrated area of specific binding curves (33 min to 60 min after injection) in the temporal cortex relative to the cerebellum of  $1.2 \pm 0.3$ .<sup>52</sup> The pharmacokinetics of [<sup>11</sup>C]FLB457 is slower in striatal regions compared with extrastriatal regions. Specific binding is maximal within 60 min in extrastriatal regions, but is still increasing in the basal ganglia, preventing quantitation of binding in this region within the duration of the PET scan.<sup>55</sup> The longer half-life of <sup>76</sup>Br (16.6 h) is advantageous for radioligands with slow kinetics *in vivo* as it allows scanning over a longer duration. Labelling FLB 457 with <sup>76</sup>Br has provided a PET radioligand that can assess receptor binding in both striatal and extrastriatal regions of the brain.<sup>53,56,57</sup>

#### 1.3.4.3 5-HT<sub>1A</sub> Receptors

Pre-synaptic 5-HT<sub>1A</sub> receptors in the raphe nuclei are believed to mediate the inhibition of 5-hydroxytryptamine (5-HT, serotonin) release.<sup>58</sup> Since 5-HT has a major role in normal brain function, especially the control of mood and behaviour, this receptor subtype is implicated in a number of psychotic illnesses. WAY-100635 (*N*-2-(4-(2-methoxyphenyl)-1-piperazinyl)ethyl)-*N*-2-pyridyl)cyclohexane carboxamide) was the first potent, selective 5-HT<sub>1A</sub> antagonist, and was labelled with <sup>11</sup>C for *in vivo* studies.<sup>40</sup> In human brain, the ratio of radioactivity accumulated in the receptor-rich medial temporal cortex to that in the cerebellum, between 20 min to 90 min after injection of [*O*-methyl-<sup>11</sup>C]WAY-100635 was 3.1.<sup>40</sup> The *in vivo* metabolism of [*O*-methyl-<sup>11</sup>C]WAY-100635 was found to be species-dependent, with humans producing the radioactive metabolite [*O*-methyl-<sup>11</sup>C]WAY-100634, which could contribute to the non-specific and specific binding in the brain during the PET study.<sup>59</sup> Labelling WAY-100635 in the carbonyl position ([*carbonyl*-<sup>11</sup>C]WAY-100635) resulted in metabolism only to very polar radioactive compounds and a specific PET signal of 25 for the medial temporal cortex relative to the cerebellum at 60 min after injection. This continues to be the preferred radioligand for PET investigations of the 5-HT<sub>1A</sub> receptor.<sup>59</sup> At present no SPET ligands are available for the *in vivo* imaging of 5-HT<sub>1A</sub> receptors in humans.<sup>45</sup>

#### 1.3.4.4 5-HT<sub>2A</sub> Receptors

Radioligands developed for imaging 5-HT<sub>2A</sub> receptors were initially based on spiperone (see Fletcher *et al.*,<sup>7</sup> for a review). However, [<sup>11</sup>C]*N*-methybspiperone, [<sup>18</sup>F]*N*-methybspiperone and [<sup>76</sup>Br]bromospiperone all suffered from a high degree of non-specific binding and low ratios of specific to non-specific binding. Despite these drawbacks [<sup>11</sup>C]*N*-methybspiperone has been routinely used with PET to evaluate 5-HT<sub>2A</sub> receptors *in vivo*.<sup>35,36</sup> Ketanserin is a potent 5-HT<sub>2A</sub> antagonist that shows increased selectivity over D<sub>2</sub> receptors. Labelling ketanserin with either <sup>11</sup>C or <sup>123</sup>I was not useful with respect to obtaining a sensitive brain signal. However, [<sup>18</sup>F]altanserin and [<sup>18</sup>F]setoperone give frontal cortex to cerebellum radioactivity ratios of 3 and 2.5 respectively. [<sup>18</sup>F]Altanserin is the more selective since [<sup>18</sup>F]setoperone, like [<sup>11</sup>C]*N*-methybspiperone, binds specifically to D<sub>2</sub> receptors in

the basal ganglia.<sup>7</sup> The most useful PET radioligand, [<sup>11</sup>C](R)-(+)-4-[1-hydroxy-(2,3-dimethoxyphenyl)methyl]-N-2-(4-fluoro-phenylethyl)piperidine ([<sup>11</sup>C]MDL 100907), has high selectivity and affinity ( $K_i = 0.2 \text{ nM}^{60}$ ) for the 5-HT<sub>2A</sub> receptor. While a useful brain signal is observed in receptor-rich regions, [<sup>11</sup>C]MDL 100907 is rapidly metabolised *in vivo* with unchanged radioligand representing only 40% of the total radioactivity in human plasma 50 min after injection.<sup>61</sup> [<sup>123</sup>I]-5-iodo-R91150 [4-amino-N-[1-3-(4-fluorophenoxy)propyl]-4-methyl-4-piperidinyl]-2-methoxybenzamide] is a SPET radioligand that has high affinity for the 5-HT<sub>2A</sub> receptor ( $K_d = 0.1 \text{ nM}$ ).<sup>62</sup> Unlike ketanserin, R91150 has selectivity that is at least 50-fold higher for 5-HT<sub>2A</sub> receptors than for 5-HT<sub>1A</sub>, 5-HT<sub>1B</sub>, 5-HT<sub>1D</sub>, 5-HT<sub>3</sub>,  $\alpha_1$ ,  $\alpha_2$ , adrenergic, histamine-H<sub>1</sub> and D<sub>2</sub> receptors.<sup>62,63</sup> Intravenous injection of [<sup>123</sup>I]-5-iodo-R91150 into man produces ratios of radioactivity in the frontal cortex to cerebellum of 1.4.<sup>64</sup> The radioactivity in the frontal cortex is displaceable ketanserin<sup>65</sup> and by antipsychotic drugs that have an affinity for the 5-HT<sub>2A</sub> receptor.<sup>64,66</sup>

#### 1.3.4.5 Other Receptor Populations

Several other receptor populations seem to be implicated in psychiatric illnesses. However, a lack of selective and effective PET or SPET radioligands has limited the possibilities for psychopharmacological and neurochemical investigations. A hypothesis for disruption of glutamate function in schizophrenia and movement disorders has strong support.<sup>45</sup> However, *in vivo* imaging of the neuroreceptors mediated by glutamate is only just being made possible with the NMDA antagonist N-(1-naphthyl)-N'-(3-[<sup>125</sup>I]-iodophenyl)-N'-methylguanidine.<sup>67,68</sup> Psychiatric interest in schizophrenia now centres around the role of D<sub>3</sub> versus D<sub>2</sub> receptors. Again a lack of selective D<sub>3</sub> receptor radioligands has prevented the elucidation of the respective roles of these two receptors in mediating the neuronal response to dopamine in normal and diseased individuals.

Selective antagonists for the 5-HT<sub>1B</sub>, 5-HT<sub>1D</sub>, 5-HT<sub>1E</sub>, 5-HT<sub>1F</sub>, 5-HT<sub>2B</sub>, 5-HT<sub>2C</sub>, 5-HT<sub>3</sub>, 5-HT<sub>4</sub>, 5-HT<sub>5</sub>, 5-HT<sub>6</sub> and 5-HT<sub>7</sub> receptors, when available, are only just starting to be developed as radioligands. This is the result of an increased understanding of the distribution and possible roles attributed to the different receptor subtypes.

Imaging of the acetylcholinergic system has a role in the study of dementia progression and the effectiveness of acetylcholinesterase inhibitors in balancing nicotinic cholinergic deficits in Alzheimer's patients. The muscarinic acetylcholine receptors can be imaged *in vivo* using a number of radioligands including <sup>123</sup>I-quinuclidinyl benzylate (<sup>123</sup>I-QNB),<sup>69</sup> <sup>123</sup>I-iododexetimide<sup>70</sup> [<sup>11</sup>C]benztropine,<sup>71</sup> [<sup>11</sup>C]N-methylpiperidinyl benzilate,<sup>72</sup> and [<sup>11</sup>C]dexetimide.<sup>73</sup> These radioligands were developed to measure receptor numbers in the human brain. Recently, radiotracer development has moved towards trying to measure changes in endogenous acetylcholine. N-(2-[<sup>18</sup>F]fluoroethyl)-4-piperidyl benzilate ( $K_i = 1.7 \text{ nM}$ )<sup>74</sup> and (R)-N-[<sup>11</sup>C]methyl-3-pyrrolidyl benzilate ( $K_i = 0.71 \text{ nM}$ )<sup>75</sup> are two PET radioligands that have the potential to be acetylcholine-sensitive ligands for the muscarinic acetylcholine receptor system in humans. The nicotinic acetylcholine receptor is a ligand-gated ion channel that was first imaged in humans with [<sup>11</sup>C]-nicotine. Radiolabelled derivatives of

epibatidine and 3-(2(S)-azetidinylmethoxy)pyridine (A-85380) have been used for *in vivo* imaging of this ion channel in animal brain. 5-[<sup>123</sup>I]Iodo-A85380 and 2-[<sup>18</sup>F]fluoro-A-85380 both show promise for use in humans. However, they exhibit slow kinetics. Brown *et al*<sup>76</sup> has recently reported a series of 5-(2-(4-pyridinyl)vinyl)-6-chloro-3-(1-[<sup>11</sup>CH<sub>3</sub>]methyl-2-(S)-pyrrolidinylmethoxy)pyridine analogues which exhibit substantially faster accumulation in nicotinic receptor rich regions in the mouse and monkey brain.

## 1.4 Functional Imaging in Psychiatry and Psychopharmacology

PET and SPET allow visualisation and quantification of selective radioligand-receptor interactions in the living human brain. This permits the study of neurochemistry and neuropharmacology *in vivo*. In psychiatric research, both neurochemical and pharmacology based questions can be addressed with functional imaging. Neurochemical investigations employing neuroimaging include studying the regional abnormalities of receptor density (as a marker of neuronal integrity), receptor distribution, receptor binding and clinical variable relationships and neurotransmitter concentrations in a particular psychosis.<sup>25</sup> With respect to pharmacology, neuroimaging can contribute information on receptor binding profile of drugs, the duration of occupancy, the potency of psychotropic drugs (displacement studies), dose: receptor occupancy relationships and the correlation between receptor occupancy, clinical response, plasma concentration and side effects of psychotropic drugs.<sup>77</sup>

Neurochemistry of diseased states can be investigated by comparing selective radioligand binding to certain receptors between untreated patients and healthy normal individuals. The competition between endogenous neurotransmitter and radioligands can provide a noninvasive method to measure endogenous neurotransmitter release *in vivo*. Dynamic changes in endogenous neurotransmitter can be achieved during the scanning period by the performance of particular tasks known to stimulate synaptic release of a neurotransmitter or by challenge studies. The former requires a radiopharmaceutical that can be displaced by small changes in the synaptic concentration of endogenous neurotransmitter as a result of a particular task, while still providing a meaningful specific signal to noise image. Challenge studies are normally associated with larger changes in neurotransmitter concentration. Laruelle *et al.*<sup>78</sup> used the relationship between amphetamine-induced dopamine release and [<sup>123</sup>I]IBZM binding potential in drug free schizophrenics versus healthy volunteers to gain information on the levels of endogenous dopamine available for binding to D<sub>2</sub> dopamine receptors.

Pharmacological questions in drug development can be approached from two angles, both providing a noninvasive technique for measuring drug concentrations in the human brain. The first is to radiolabel the potential drug and trace its anatomical distribution and binding throughout the brain.<sup>15</sup> With this method it is possible to determine the ability of the drug to cross the blood-brain-barrier, and in favourable circumstances, the degree of specific binding to brain receptors. An added benefit is that an intravenous injection of only a trace of the drug need be given. This approach can be exploited with PET where isotopic labelling of a molecule with <sup>11</sup>C results in a radioligand with identical

pharmacokinetic properties to the unlabelled drug. However, for this design to be possible the drug of interest must have high binding affinities, and a chemical structure that allows rapid labelling.<sup>15</sup>

When a molecule does not fulfill these requirements, then its action at a particular receptor can be indirectly studied via inhibition of specific radioligand binding by the unlabelled drug. With this second approach, the level of drug-induced receptor occupancy can be quantified and related to clinical effects and plasma concentrations.<sup>15</sup> This method is commonly used with both SPET and PET to increase the bank of information available on the mode of action for psychopharmaceuticals that have a uniquely high clinical efficacy for application in future drug development.

Two strategies can be used to achieve a measure of drug-induced receptor occupancy without the requirement for absolute quantification.<sup>25</sup> The “chaser method” which involves an intravenous bolus or infusion of a test or challenge drug during a dynamic sequence of SPET images.<sup>25</sup> This method can be used to calculate the *in vivo* potency of the drug for displacing the radioligand from its binding site. In this instance the psychotic drug must be available in an injectable form and the affinity and kinetics of the drug versus the radioligand must be conducive to displacement. The “pre-dose method” involves performing two scans in the same subject, firstly in an unmedicated state (baseline scan) and then later, after a period of treatment with the drug. Any reduction in the specific, radioligand binding in the drug treated scan is expressed as a percentage of the baseline binding giving a relative value of the number of receptors blocked by the psychotic drug. The short half-life of carbon-11 is an advantage with this protocol, as it allows the baseline and treatment scan to be performed on the same day, following two radioligand injections. This technique can be used in healthy volunteers to determine the degree of receptor occupancy that is associated with a certain dose of drug after a certain period of time. Ideally, baseline and post-treatment scans should be from the same individual. However, access to untreated psychotic patients can be limited. Receptor occupancy by neuroleptics can be determined by comparing the levels of radioligand binding in treated patients relative to a normal population.<sup>35,50,51,79-83</sup> A major assumption behind this method is that the receptor population in the patient and control group is the same. In some psychotic illnesses this is not the case so care must be taken during data interpretation.

Psychopharmacology studies with SPET and PET are limited by the number of selective and effective radioligands for the receptor populations that are perceived as being important factors in the symptoms and aetiology of psychiatric disorders. The classification of further receptor subtypes whose actions are mediated by a certain neurotransmitter increases the complexity of this task. Neuroimaging has enlarged our knowledge of the neurochemical, structural and metabolic abnormalities in a wide range of mental disorders. Any future radioligand development can only increase our understanding of the changes in neurotransmitter mediated, synaptic transmission during the onset, progression and treatment of affective and neurodegenerative disorders.

## 1.5 Radioiodines and Neuroimaging

A major part of this work was concerned with radioiodinated ligands for neuroreceptor imaging. The fundamental property of radionuclides is instability due to an imbalance in the ratio of protons to neutrons in the nucleus. Such unstable nuclei emit one or more forms of radiation to achieve stability. The form of radioactive decay depends on whether the unstable nucleus is neutron- or proton-deficient. The main types of radioactive decay are described below.

### 1.5.1 Modes of Decay

#### 1.5.1.1 $\alpha$ -Decay

$\alpha$ -Decay occurs in heavy nuclei ( $Z > 51$ ) when an alpha particle (helium nucleus) consisting of two protons and two neutrons is emitted from the parent nucleus. Alpha-emitters are of no use for nuclear medicine imaging as the particles have only a short range and are highly damaging in tissue.

#### 1.5.1.2 $\beta$ -Decay

$\beta$ -Decay can be of two kinds depending on the balance of neutrons to protons in the nucleus. Neutron-rich nuclei can stabilise by transformation of a surplus neutron into a proton plus an electron ( $\beta^-$  particle) and a neutrino ( $\nu$ ).  $\beta^-$ -Decay can be represented by Equation 8.



Positron ( $\beta^+$ )-decay occurs in proton-rich nuclei. A proton is converted into a neutron by emission of a positron ( $\beta^+$  particle; the antimatter equivalent of an electron), and a neutrino.  $\beta^+$ -Decay can be represented by Equation 9.



A key feature of positron emission is the resultant annihilation radiation (Figure 1.7). After

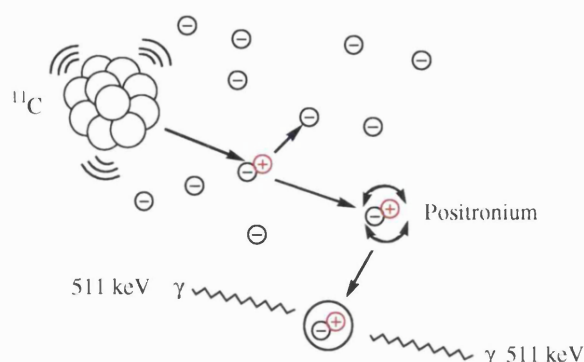


**Figure 1.7:** Illustration of positron decay of  $^{11}\text{C}$ . During decay  $^{11}\text{C}$  emits a positron ( $\beta^+$  particle) which travels a short distance in tissue colliding with electrons until it forms a positronium. Almost instantaneously the positronium annihilates, forming two  $\gamma$ -rays of equal energy (511 keV), emitted in opposite directions. The  $\gamma$ -ray coincidences are detected by the PET camera.

travelling a few millimeters in human tissue the emitted positron has usually lost most of its kinetic energy and combines with a nearby electron to form a short-lived entity called a positronium. During its annihilation the mass of the positronium is converted into energy in the form of two photons. Each of the two photons has an energy of 511 keV (equal to the energy at rest of an electron or positron). They are emitted in opposite directions to conserve near zero energy and momentum.

### 1.5.1.3 $\gamma$ -Decay

$\gamma$ -Decay occurs when a nucleus is in a high energy, or excited, state. The excited state is generally the result of a nuclear reaction or some decay process. An excited nucleus will generally decay to a lower energy state and in the process emit a gamma photon at an energy representative of the loss of energy during the transition from one state to the other. Decay may proceed to another excited state so further decay can occur leading to the release of other gamma photons of different energy. In some instances a nucleus will decay to an excitatory state that has a slow rate of decay (greater than microseconds). These nuclei are said to be metastable.

### 1.5.1.4 Electron capture

In addition to  $\beta^+$ -decay, neutron-deficient radionuclides can also decay by electron capture. During electron capture a proton rich nucleus 'captures' one of the atomic electrons and a proton is transformed into a neutron plus a neutrino (Equation 10). The vacancy in the orbital electron shell is filled with an electron from a higher energy orbital and a characteristic X-ray is emitted. The nucleus that is produced following electron capture is often in an excited state which can decay further by gamma photon emission, to a stable ground state.  $\beta^+$ -Decay competes with electron capture unless there is insufficient energy for positron emission. The energy available is dependent on the energy levels of the parent and daughter of the decay process. Nuclei where the parent and daughter are separated by less than 1.022 MeV decay solely via electron capture.



## 1.5.2 The Isotopes of Iodine

Figure 1.8 shows part of the chart of nuclides of iodine and the main decay paths for the mentioned radioisotopes. The stable naturally abundant isotope of iodine is  $^{127}\text{I}$ .

### 1.5.2.1 $\gamma$ -Emitting Iodines

$\gamma$ -Emitting nuclides have a number of practical advantages for both *in vivo* and *in vitro* research. The greatest is probably the ease of detecting small quantities.

$^{125}\text{I}$  has a relatively long half-life (60.1 d). Its mechanism of decay is via electron capture and the emission of a  $\gamma$ -ray to give the  $^{125}\text{Te}$  daughter nucleus. All of the  $\gamma$ -emissions have an energy of 35 keV.



Z		54											
			$^{120}\text{Xe}$	$^{121}\text{Xe}$		$^{122}\text{Xe}$	$^{123}\text{Xe}$	$^{124}\text{Xe}$	$^{125}\text{Xe}$	$^{126}\text{Xe}$	$^{127}\text{Xe}$	$^{128}\text{Xe}$	$^{132}\text{Xe}$
			$^{119}\text{I}$	$^{120\text{g}}\text{I}$	$^{120\text{m}}\text{I}$	$^{121}\text{I}$	$^{122}\text{I}$	$^{123}\text{I}$	$^{124}\text{I}$	$^{125}\text{I}$	$^{126}\text{I}$	$^{127}\text{I}$	$^{131}\text{I}$
			19 min	1.35 h	53 min	2.12 h	3.6 min	13.2 h	4.18 d	60.1 d			8.04 d
			EC $\beta^+$	EC	EC	$\beta^+$	EC	EC	EC	EC			$\beta^-$
				$\beta^+$	$\beta^+ \searrow$	$\gamma$	$\gamma$	$\gamma \searrow$	$\beta^+ \searrow$	$\gamma \searrow$			$\gamma$
		52	Te	$^{118}\text{Te}$	$^{119}\text{Te}$		$^{121}\text{Te}$	$^{122}\text{Te}$	$^{123}\text{Te}$	$^{124}\text{Te}$	$^{125}\text{Te}$	$^{126}\text{Te}$	$^{130}\text{Te}$
				66	67	68	69	70	71	72	73	74	78
				N									

EC electron capture       $\beta^-$ ,  $\beta^+$ , electron, positron decay       $\gamma$  gamma rays

Stable  
nuclides

**Figure 1.8:** A simplified decay chart for common iodine isotopes.  $^{128}\text{I}$  -  $^{130}\text{I}$  have been excluded since they have limited relevance to this discussion.

$^{123}\text{I}$  is widely applied in functional brain SPET and decays by electron capture to 7 different excited states of the radioactive  $^{123}\text{Te}$  daughter nucleus with a physical half life of 13.2 h. The most prominent  $\gamma$ -ray, with an energy of 159 keV, contributes 83% of the  $\gamma$ -emissions.  $^{123}\text{I}$  can be produced via a number of direct or indirect methods (Table 1.1). The possible radionuclidic impurities are  $^{124}\text{I}$  (frequently),  $^{125}\text{I}$  and  $^{126}\text{I}$  (rarely).<sup>84</sup> The favoured method for  $^{123}\text{I}$  production is based on the  $^{124}\text{Te}$  (p,2n) $^{123}\text{I}$  nuclear reaction in a small compact cyclotron.<sup>84-86</sup> The level of  $^{124}\text{I}$  impurity can be controlled in this method by using a thick target with high  $^{124}\text{Te}$  enrichment. Following target irradiation,  $^{123}\text{I}$  is separated by dry distillation in a carrier gas (*e.g.* nitrogen). The distilled iodine fraction is collected in sodium hydroxide solution (pH < 9.6) where it is converted to iodide.<sup>85</sup>

The only other iodine isotope that is in routine use is iodine-131, which decays by  $\beta^-$  emission and electron capture to different excited states of  $^{131}\text{Xe}$ , with an 8.04 d half-life. The principal  $\gamma$ -ray energy is 364 keV occurring with an abundance of 83%, while the  $\beta^-$  particles have an associated energy of 608 keV and occur in 91% of the nuclear transitions.  $^{131}\text{I}$  is used in SPET but, like  $^{124}\text{I}$  (see below), the high effective doses at long biological half-lives, has limited its application in nuclear medicine to oncology therapies.

Nuclear reaction	Energy of incident beam, MeV	Target material (enrichment)	Yields (mCi/μAh)	Impurities
<b>Direct Methods</b>				
$^{122}\text{Te}(\text{d}, \text{n})^{123}\text{I}$	11	$^{123}\text{Te}$ metal (95%)	< 1	< 1% $^{124}\text{I}$
$^{124}\text{Te}(\text{p}, 2\text{n})^{123}\text{I}$	27–30	$^{124}\text{Te}$ (91.9–99.9%)	8–45	0.62–0.88%
	24–26	$^{124}\text{TeO}_2$ (91.9–96%)	20	$^{124}\text{I}$
	22	$^{124}\text{Te}$ -Al alloy (96%)	1.3	0.7% $^{124}\text{I}$ 0.7% $^{124}\text{I}$
<b>Indirect Methods</b>				
$^{127}\text{I}(\text{p}, 5\text{n})^{123}\text{Xe}$	70	NaI crystal	...	0.1% $^{125}\text{I}$
$\xrightarrow{\beta^+, \text{EC}} ^{123}\text{I}$	58–60	NaI solution	4.5–6	0.13–0.2%
	65	KI	14	$^{125}\text{I}$
				< 0.1% $^{125}\text{I}$
$^{139}\text{La}(\text{p}, 4\text{p}13\text{n})^{123}\text{Xe}$	590	La-Cu alloys	6–10	Unknown
$\xrightarrow{\beta^+, \text{EC}} ^{123}\text{I}$				

**Table 1.1:** Possible nuclear reactions for routine production of  $^{123}\text{I}$ .

#### 1.5.2.2 Positron-emitting iodines

Iodine-124 decays via a complex scheme to  $^{124}\text{Te}$  (stable) with a 4.2 d half life. The decay can proceed by electron capture to 16 excited states of  $^{124}\text{Te}$  or by positron emission. Only 23% of its decay leads to emission of  $\beta^+$  particles, most of which are of relatively high energy (1550 keV (11%), 2150 keV (11%)).<sup>84</sup> In addition, the principal  $\gamma$ -emissions have an energy of 602 (61%) and 511 keV (46%).  $^{124}\text{I}$  can be produced directly by the  $^{125}\text{Te}(\text{p}, 2\text{n})^{124}\text{I}$  nuclear reaction using enriched tellurium (II) oxide ( $[\text{Te}]^{125}\text{O}$ ) as the target.

An alternative positron-emitting iodine is  $^{120\text{g}}\text{I}$ . However, the decay scheme is difficult to elucidate due to the presence of the metastable, isomeric impurity,  $^{120\text{m}}\text{I}$  ( $t_{1/2} = 53$  min). A certain, undetermined proportion, of  $^{120\text{m}}\text{I}$  may decay through the  $^{120\text{g}}\text{I}$  ground state. Decay of the ground state isomer to  $^{120}\text{Te}$  proceeds with a half life of 81 min. Because of these considerations any decay scheme for  $^{120}\text{I}$  should be interpreted with caution. Both the ground and metastable state isomers emit positrons with an associated energy of 4.9 MeV and 3.75 MeV, respectively. However, the percentage of the total decay energy attributed to each positron emission is difficult to quantify.

There are a number of reactions that lead to the production of  $^{120}\text{I}$ . Unfortunately it is not possible to produce the ground state isomer in isolation from the metastable or vice versa. The  $^{122}\text{Te}(\text{p}, 3\text{n})^{120}\text{I}$  reaction over the energy range of 37 to 32 MeV produces the highest yield of  $^{120}\text{I}$  but the  $^{120\text{m}}\text{I}$  content is around 25% with an additional 6% in the form of  $^{119}\text{I}$  at the end of bombardment.

By comparison the  $^{120}\text{Te}(\text{p},\text{n})^{120}\text{I}$  reaction over an energy range 16–9 MeV, has a lower yield but the percentage of  $^{120\text{m}}\text{I}$  and  $^{119}\text{I}$  impurities for this reaction, are lower, 4.8 and 4.4% respectively.<sup>87</sup> The favoured route with respect to restricting impurities is the  $^{120}\text{Te}(\text{p},\text{n})^{120}\text{I}$  reaction. Unfortunately the  $^{120}\text{Te}$ -enriched target is three times the cost of  $^{122}\text{Te}$  and produces a lower yield.

$^{119}\text{I}$  is another positron-emitting iodine that has a less complicated decay scheme. Fifty one percent of the decay is by  $\beta^+$  particles with an energy of 235 keV, and the  $\gamma$ -rays have a lower energy (258 keV, 86.7%). The half-life is short at 19 min.

### 1.5.3 Relevant Application of the Radioiodines for Psychiatric Research

Each radioisotope of iodine has characteristics that can be exploited in psychiatric research. New radioligands are continually being developed for the study of receptors *in vivo*. A labelling procedure developed for one isotope of iodine is applicable to the others, once certain factors such as production time, chemical form and half-life are taken into consideration. This should also be true for the behaviour of the radioiodinated compound with respect to its receptor interactions.

The  $\gamma$ -ray emitted by  $^{125}\text{I}$  has too low an energy to penetrate tissue and therefore cannot be detected outside the human body after intravenous injection. Therefore, iodine-125 is of little use for medical imaging. However, the long half-life of iodine-125 makes it a useful isotope for the development of potential radiopharmaceuticals. Receptor ligand studies and autoradiography *in vitro* can be used to determine the affinity and selectivity of  $^{125}\text{I}$ -labelled radioligands for different receptor types. The high specific radioactivity of  $^{125}\text{I}$  means brain slices need only be exposed to film for 3–4 d (c.f. 3–4 weeks required for  $^3\text{H}$ -labelled ligands). *Ex vivo* autoradiography, following injection of the  $^{125}\text{I}$ -labelled ligand in small animals, can also provide information on the ability of the compound to cross the blood-brain barrier and the kinetics of subsequent receptor binding.

$^{123}\text{I}$  is most closely associated with functional brain SPET.  $^{125}\text{I}$  labelled radioligands that have shown potential in small animal work are then labelled with  $^{123}\text{I}$  and evaluated for SPET imaging. The optimum energy for  $\gamma$ -ray detection with a gamma camera is determined by the thickness of the crystal used. Radionuclides that decay by emitting single  $\gamma$ -ray in the 50–300 keV range are favoured for SPET. The 159 keV  $\gamma$ -ray emitted from  $^{123}\text{I}$  can be detected from deep inside tissue and is not so high in energy as to reduce the resolution of the image. The half-life of  $^{123}\text{I}$  and the low energy of its decay by  $\gamma$ -emission means that the radiation dose to a human during a SPET scan for functional brain imaging is well within acceptable limits (about 6 mSv for a 180 MBq dose).

An advantage of PET over SPET is the truly quantitative nature of the information obtained, where the count rates are directly related to the absolute radioligand concentration. This information can be used to obtain quantitative kinetic information about the radioligand such as binding potentials. The introduction of positron-emitting iodines to receptor radioligand development could lead to the integration of SPET and PET. More quantitative validation of the kinetic behaviour of radioiodinated ligands *in vivo* could be determined with PET as a preface to less costly, large-scale studies being performed with  $^{123}\text{I}$  in SPET.

The half lives of the positron-emitting radioiodines,  $^{120g}\text{I}$  and  $^{124}\text{I}$ , would allow radiotracer kinetics to be recorded for longer compared with the most popular positron-emitter, carbon-11 ( $t_{1/2} = 20.4$  min). This is particularly relevant for ligands that are slow at reaching an equilibrium state with its target site. Two factors that need to be considered with  $^{120g}\text{I}$  is the level of  $^{120m}\text{I}$  impurity and the high  $\beta^+$  end-point energy.<sup>88</sup> The difficulties associated with  $^{120}\text{I}$  production have been mentioned above. The favoured  $^{120}\text{Te}(p,n)^{120}\text{I}$  reaction gives 5%  $^{120m}\text{I}$  at the end of bombardment which will decay during the radioligand production. If the labelling procedure took 1.5 h then the level of  $^{120m}\text{I}$  at the time of scanning will be only 3%. Unfortunately production costs favour the  $^{122}\text{Te}(p,3n)^{120}\text{I}$  reaction. For the same labelling procedure, using  $^{120}\text{I}$  produced from this reaction, the projected level of  $^{120m}\text{I}$  at the time of scanning would be 17%. Because of the half-life of  $^{119}\text{I}$  (19 min), contamination by this impurity would be negligible. Scans with  $^{120}\text{I}$ -labelled radioligands will always have a mixture of both  $^{120m}\text{I}$  and  $^{120g}\text{I}$ . As a result of their different half-lives, the ratio of one to the other will change during the study and this needs to be identified for each step in the data collection. The accuracy normally associated with PET could be strongly compromised by the need for such corrections.

There are a number of disadvantages associated with the positron emitting iodines for use in human studies.<sup>88</sup> The low level of positron emission (23%) means that the count rate from a given dose will be low. In addition the significant emissions of high energy  $\gamma$ -rays and the relatively long half-life means that the effective radiation dose to the patient per unit of radioactivity will be high. These limitations on the potential for the use of  $^{124}\text{I}$  and  $^{120g}\text{I}$  in routine human investigations are exacerbated for radioligands with a long biological half-life. Pagani *et al.*<sup>27</sup> calculated the effective dose per MBq for a number of alternative PET radionuclides at biological half-lives of 1 h, 10 h and 100 h assuming complete uniform distribution in man. With a 1 h biological half-life the effective dose for  $^{124}\text{I}$  was equivalent to  $^{18}\text{F}$ . A disparity between the effective doses for  $^{124}\text{I}$  and  $^{18}\text{F}$  labelled radioligands is seen with a longer biological half-life. The dose associated with  $^{124}\text{I}$  is four and eighteen times higher than  $^{18}\text{F}$  with a 10 and 100 h biological half-life, respectively. To date, applications with  $^{124}\text{I}$  have centred around studies in cancer patients, for example in the determination of the time course of monoclonal antibody uptake in solid tumours and the prediction of the dosimetry associated with therapies involving  $^{131}\text{I}$ -labelled agents.<sup>27</sup> A comparison of the gamma rays emitted during  $^{120}\text{I}$  and  $^{124}\text{I}$  decay suggests that the dose associated with  $^{120}\text{I}$  could be at least the same as  $^{124}\text{I}$ , if not worse. The positron-emitting radioiodines could be used in small animal and primate work to provide valuable information on radioligands, the investigation of animal models of disease and psychopharmacological investigation. Here radiation dose is not a major consideration. The use of small-animal dedicated PET cameras extends the information obtained from rat studies by allowing imaging of the brain *in vivo* following injection of the radioligand. Validation of the kinetic behaviour could also be investigated in primates with this radioisotope before studies in humans.

The primary advantage associated with positron-emitting iodines would be to validate a radioligand using an imaging technique where accurate recovery of photons is not a limiting factor or a possible source of error. However, the benefits associated with PET validation using  $^{124}\text{I}$  do not

justify the high effective dose to the subject. In addition to the high effective dose associated with  $^{120}\text{I}$  labelling compounds, the level of accuracy in measures is significantly compromised by the radionuclide purity. It may be possible that radioligands labelled with  $^{123}\text{I}$  could be cross-validated with positron-emitting iodine and PET in non-human primates or small animals where radiation dose is not such a limiting factor.

## 1.6 Radioiodination Chemistry

### 1.6.1 Electrophilic Substitution in Arenes – General Considerations

Carbon atoms in multiple bonds, benzene and other arenes are susceptible to attack by electrophilic (electron-deficient) reagents. In benzene, and related molecules six electrons are accommodated in two delocalised  $\pi$  orbitals. This is the most accessible feature of an arene and generally the key to its reactivity.

Electrophilic substitution in arenes involve an initial addition of an electrophile (*e.g.*  $\text{E}^{\oplus}$ ) to a carbon atom in the ring (Figure 1.9a). The positive charge is distributed among the *ortho* and *para* positions in the ring by resonance (Figure 1.9b). Elimination of the proton eliminates the positive charge and allows the delocalised  $\pi$  orbitals to reform. Aromaticity and stability are re-established.

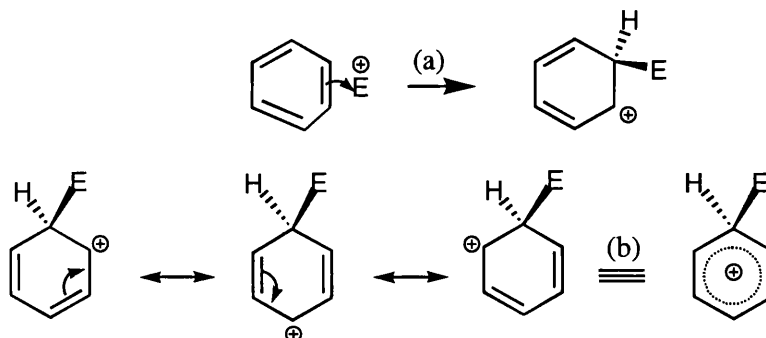


**Figure 1.9:** Electrophilic substitution in arenes.

The overall result is substitution of the hydrogen by the electrophile. The site and rate of electrophilic substitution is greatly influenced by any substituents, as a result of their electronic and steric effects.

Electrophilic substitution of a mono-substituted benzene may occur in *ortho*-, *meta*- or *para*-position to a substituent  $\text{Y}$ , at a rate that is faster or slower than in benzene. While all three isomers are usually formed, there is generally a preference for either the *m*-isomer or a mixture of the *p*- and *o*-isomers, a feature which is dependent on the nature of the substituent.

Substituents that are electron-withdrawing with respect to the aryl ring, for example  $^{\oplus}\text{NR}_3$ ,  $\text{CCl}_3$ ,  $\text{CF}_3$ ,  $\text{CN}$ ,  $\text{NO}_2$ ,  $\text{CHO}$  and  $\text{CO}_2\text{H}$ , all place a positively charged or positively polarised atom adjacent to an aryl ring carbon. For illustration, the potential intermediates following electrophilic attack by  $\text{E}^{\oplus}$  on an  $^{\oplus}\text{NR}_3$  substituted benzene are shown in Figure 1.10. There are two canonical forms (*o*-c, and *p*-b) that increase the free energy of activation for *o*- and *p*- attack respectively due to the close proximity of the two positive charges. This destabilising effect cannot occur with *meta*-

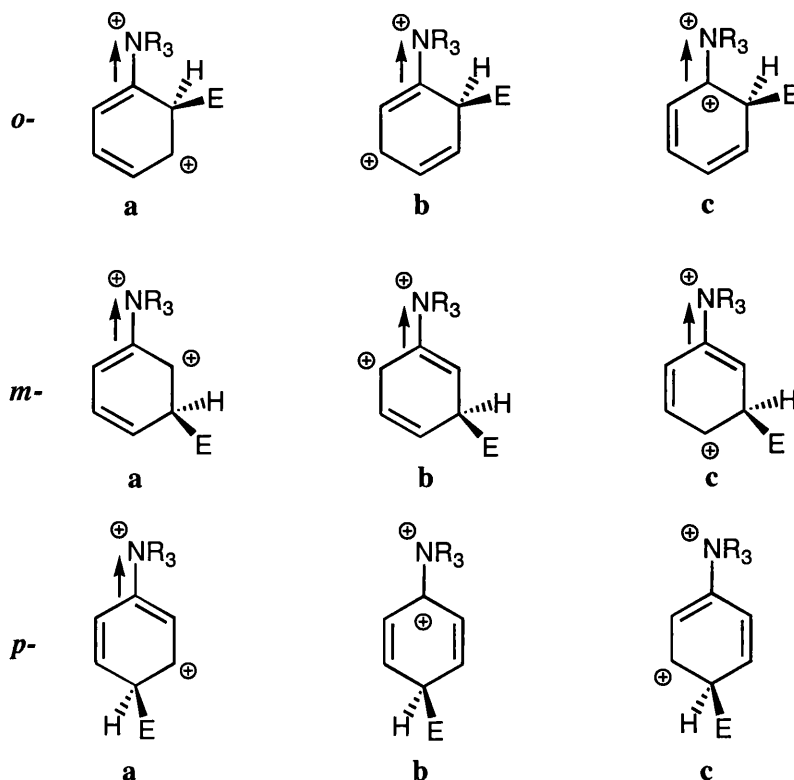


**Figure 1.10:** Potential canonical forms resulting from electrophilic attack on an arene with electron-withdrawing substituents.

substitution, which is therefore preferred. This group of substituents is not only *meta*-directing but also *deactivating* since their electron-withdrawing nature polarises and destabilises all three positively-charged isomeric intermediates making attack at any position slower than in benzene.

Alkyl substituents (R) increase the reactivity of arenes towards electrophiles because of their electron-donating inductive effects. Electrophilic attack on an alkyl-substituted arene is preferentially at the *para*- and *ortho*-positions. This is due to the stabilisation of the ring from the contribution of the canonical forms in Figure 1.11, where the positive charge is located adjacent to the electron donating substituent. This charge stabilisation is not present in the canonical forms following attack in the *meta*- position.



**Figure 1.11:** Canonical forms present following electrophilic attack on an alkyl-substituted arene that leads to preferential attack at an *ortho*- or *para*-position.

The third group of substituents have a lone pair of electrons in addition to an electron-withdrawing inductive effect. Examples include OCOR, NHCOR, OR, OH, NH<sub>2</sub> and NR<sub>2</sub>. The canonical forms for electrophilic attack are similar to those in arenes containing electron-withdrawing

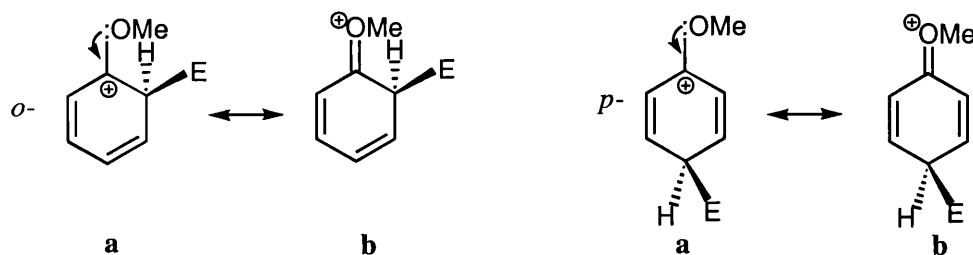


**Figure 1.12:** Canonical forms supporting preferential *ortho*- and *para*- electrophilic attack of an arene with electron-withdrawing substituents plus a lone pair of electrons.

substituents (Figure 1.12), except that the lone pair of electrons introduces a fourth form for the *o*- and *p*-complexes (*o*-b and *p*-b) alone. Having the positive charge on the oxygen atom makes the structure inherently more stable and far exceeds the electron-withdrawing effect of the group in the other canonical forms. This makes them almost completely *o*- and *p*-directing and activates the molecule towards electrophilic attack.

In molecules where electrophilic attack is *o*- and *p*-directed, the ratios of one isomer to the other depends to some extent on steric factors (an increase in the size of the substituent limits access to the *ortho* position of the molecule) and the electronegativity of the substituted group in the ring. A highly electronegative group will have a stronger impact on the *ortho* position so that attack preferentially occurs at the more electron-rich *para* position.

The important leaving groups in electrophilic substitution are those that can best exist with an outer shell deficient in a pair of electrons. The proton is the most common leaving group in electrophilic aromatic substitution reactions. Some organometal groups can also be used as effective leaving groups in electrophilic substitutions since they can easily bear a positive charge.

### 1.6.2 Aliphatic Electrophilic Substitution – General Considerations

As with electrophilic substitution in arenes, the most common leaving group for aliphatic electrophilic substitution is the proton. However, the reactivity depends on the acidity of the proton environment. Protons in saturated aliphatic compounds are very unreactive towards electrophilic substitution. In some cases, it is possible for deprotonation to occur following attack by an electrophile at positions that are more acidic (Figure 1.13). The introduction of an arylmetallic substituent into an aliphatic compound will increase its susceptibility to attack by an electrophile (Figure 1.13).

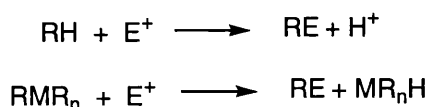


**Figure 1.13:** Electrophilic substitution of aliphatic compounds.

### 1.6.3 Aliphatic Nucleophilic Substitution – General Considerations

Nucleophilic substitution at a saturated carbon atom can occur following attack by an electron-rich reagent that carries an electron pair. The nucleophile may be neutral or negatively charged and the aliphatic substrate, neutral or positively charged. The substrate, nucleophile, leaving group and the

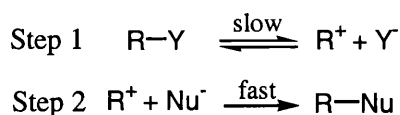


**Figure 1.14:** Aliphatic nucleophilic substitution by the unimolecular mechanism.

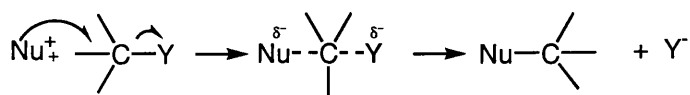


**Figure 1.15:** Aliphatic nucleophilic substitution by the bimolecular mechanistic pathway.

reaction conditions can all have some influence on the mechanistic pathway. The two extreme, but common pathways are by the unimolecular,  $\text{S}_{\text{N}}1$  (Figure 1.14), and bimolecular,  $\text{S}_{\text{N}}2$  (Figure 1.15), mechanisms. The  $\text{S}_{\text{N}}1$  mechanism is a two-step reaction involving the formation of a positively charged carbonium ion intermediate at a rate independent of the nucleophile concentration. By contrast, the bimolecular  $\text{S}_{\text{N}}2$  mechanism involves the formation of a transitional state that includes both the leaving and attacking groups at a rate proportional to both reactant concentrations.

The rate of nucleophilic substitution is dependent on two factors, the intrinsic nucleophilicity and polarisation of the attacking nucleophile and the relative ability of the leaving group. Any species with an unshared pair of electrons can act as a nucleophile. For  $\text{S}_{\text{N}}1$  reactions the rate is independent of the nucleophile. However, for the  $\text{S}_{\text{N}}2$  reactions there are four main factors with respect to the nucleophile that govern the reaction rate.<sup>89</sup> Namely, i) a negatively charged nucleophile is more effective than its conjugate acid, ii) nucleophilicity increases for a series of atoms in the same row of the periodic table, approximately in order of basicity, iii) free nucleophiles react faster than those in unsolvated forms, iv) going down the periodic table, nucleophilicity increases due to an increased concentration of negative charges in small nucleophiles. For the halides, the order of increasing nucleophilicity is chloride, bromide and iodide. Both size and electronegativity govern the ability of a nucleophile to become polarised in a particular solvent. The fact that  $\text{I}^-$  is readily converted into a large, highly polarised, weakly solvated ion makes it an effective nucleophile with a nucleophilicity value (n) of 5.0 compared with 2.0 for  $\text{F}^-$ .<sup>89</sup>

The ability of the leaving group (Y) is dependent on a) the strength of the R-Y bond, b) the polarisability of the bond, and to a lesser extent c) the stability of  $\text{Y}^-$  as a free entity. Within the alkyl halides a leaving groups ability increases from the alkyl fluorides to the alkyl iodides. The structure of the substrate undergoing nucleophilic attack will have some influence on the reactivity of the reaction, depending on the speculated mechanism. Branching, unsaturation and substitution at the  $\alpha$  and  $\beta$  carbons can increase or decrease reactivity due to increased resonance in the carbocation and steric hindrance and/or electronegative effects, respectively.



### 1.6.4 Aromatic Nucleophilic Substitution – General Considerations

Attack by electron-rich nucleophiles on benzene is hindered by the two delocalised  $\pi$  orbitals which are a) likely to repel the attacking nucleophile and b) make it difficult to delocalise and therefore stabilise the negatively charged intermediate. Arene substitution by powerful electron-withdrawing groups (*e.g.*  $\text{NO}_2$ ,  $\text{CF}_3$ ,  $\text{CN}$  and  $\text{CO}$ ) reduces the reactivity of the ring to electrophilic attack and reduces the impact of both factors a) and b) for nucleophilic attack. As a result nucleophilic attack may be possible. A good leaving group such as  $\text{I}^-$ ,  $\text{NO}_2^-$ ,  $\text{N}^+\text{Me}_3$  is required. The position of the electronegative substituent needs to be *ortho*- or *para*- to the leaving group for successful nucleophilic substitution (Figure 1.16).

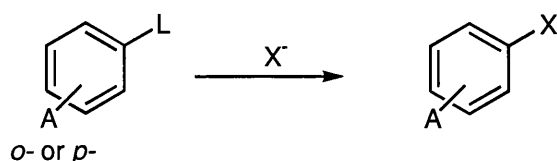


**Figure 1.16:** Aromatic nucleophilic substitution.

### 1.6.5 Radioiodinating Agents

Iodine-123 is commercially available as  $^{123}\text{I}$ sodium iodide. This can be used in direct nucleophilic substitution for halide substituents in aliphatic compounds and arenes, for  $-\text{N}^+\text{X}^-$  in diazonium salts and for metal groups in arenes.<sup>84</sup>

Since radioiodinations generally need to be performed at a NCA rather than a macro level, oxidising agents have been employed to a) convert  $^{123}\text{I}$ sodium iodide into molecular radioiodine, effective electrophiles such as  $\text{I}^\oplus$ , or complexes that contain a positively polarised form of radioiodine that can participate in electrophilic substitution reactions and b) develop reactions that can be classified as NCA. The use of oxidising agents is not common in macro reactions. However, their use in radioiodination is equivalent to the addition of iodine in larger scale reactions. While oxidation of iodide is widely used in radiochemistry, the exact nature of the radioiodinating agent generated is often only a matter of speculation.

Ammonium persulphate, hydrogen peroxide and ferric sulphate were the first oxidising agents used to produce radioactive molecular iodine (Figure 1.17).<sup>84</sup> The molecular iodine was then used to label small organic molecules by addition to double bonds or substitution for hydrogen or a halogen.

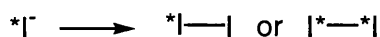
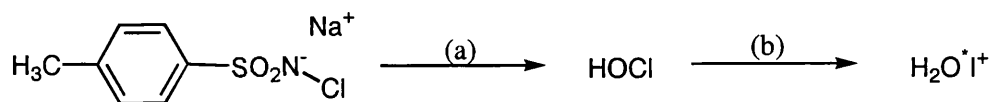


**Figure 1.17:** Formation of radioactive molecular iodine from  $^{123}\text{I}$ NaI in the presence of an oxidising agent.

These methods have a number of disadvantages, namely the volatility of the molecular iodine and the low radiochemical yield. Since half of the molecular iodine is unable to participate in radioiodination a maximum radiochemical yield of only fifty percent is possible.



Conditions: (a)  $\text{H}_2\text{O}$ , (b)  $\text{Na}^+\text{I}^-$

**Figure 1.18:** Oxidising and iodinating reagents believed to be generated in reactions employing chloramine-T.

Iodine monochloride was also used to produce positively charged radioactive iodine species from sodium iodide.<sup>90</sup> This is a carrier-added procedure. It has been proposed that the nature of the generated electrophilic iodinating species is pH-dependent with active iodonium ions ( $\text{H}_2\text{O}^+\text{I}^+$ ) or radioactive iodine monochloride ( $^*\text{ICl}$ ) being formed at low, or high pH, respectively. Theoretically, a 100% radiochemical yield is obtainable by this method.

The most widely used oxidising agent for rapid and simple iodinations, yielding products with high specific radioactivity is chloramine-T, the sodium salt of the *N*-monochloro derivative of *p*-toluene-sulfonamide (Figure 1.18).<sup>90</sup> In aqueous solution chloramine-T releases hypochlorous acid ( $\text{HOCl}$ ), the species that oxidises radioiodide. The oxidised iodine species generated from this interaction is thought to be the active iodonium ion ( $\text{H}_2\text{O}^+\text{I}^+$ ).

Reactions that involve oxidation by chloramine-T expose the substrate to harsh oxidising conditions. Undesirable side reactions are possible and can include chlorination, cleavage of peptide bonds and oxidation of thiols.<sup>90</sup> The reaction is terminated by the addition of a reducing agent which deactivates the chloramine-T and iodinating species. Reducing agents such as sodium metabisulfite can also interact with the radioiodinated product and influence its biological function. Despite its many disadvantages chloramine-T is still one of the most commonly used oxidising agent for radioiodinations and has been used in the radiolabelling of [ $^{123}\text{I}$ ]epidepride,<sup>39</sup> *N,N*-dimethyl- $[\beta$ -(3,4-diacetoxy-6- $^{123}\text{I}$ -iodophenyl)]-ethylamine (IDDE),<sup>91</sup> [ $^{123}\text{I}$ ]I-L-DOPA,<sup>92</sup> [ $^{125}\text{I}$ ]IPWAY<sup>93</sup> and [ $^{123}\text{I}$ ]SB 207710,<sup>94</sup> to name a few.

Two phase oxidising agents, based on chloramine-T-like compounds, have been developed with the aim of reducing oxidative damage of the substrate and product. The oxidising agent iodogen (1,3,4,6-tetrachloro-3 $\alpha$ ,6 $\alpha$ -diphenylglycouril) resembles a 4-fold chloramine-T (Figure 1.19a). Because it is water insoluble iodogen can be plated onto glass or plastic reaction vials to form a two phase radiolabelling system. Contact between the oxidising agent and the solubilised substrate is limited and no reducing agent is required since removal of the product from the reaction vial and the oxidising agent terminates the reaction. Chemically, iodogen produces slightly lower radiochemical yields, in a slightly long time (generally 10–15 min) than seen with the conventional chloramine-T method but with less oxidative damage.<sup>95</sup> The plating technique can have a major impact on the iodination. Non-uniform application of iodogen to the vessel can cause the oxidising agent to remain with the protein solution and prolong protein oxidation. Iodogen has been used as the oxidising agent in the synthesis of the benzodiazapene imaging agent [ $^{123}\text{I}$ ]iomazenil, resulting in an overall yield of  $54 \pm 22\%$ .<sup>96</sup>

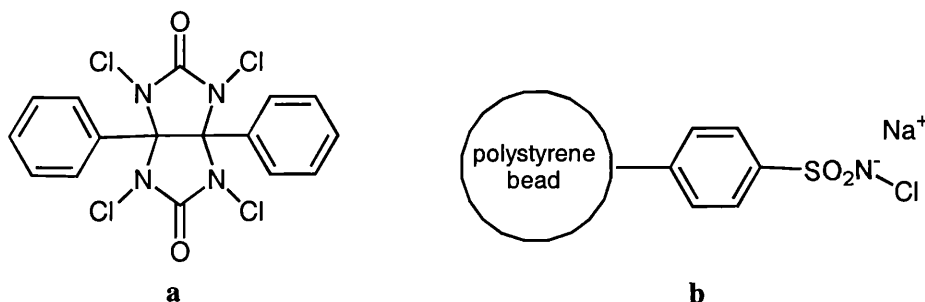


**Figure 1.19:** Structure of iodogen (a) and iodobeads (b).

Iodobeads eliminate the problems associated with iodogen plating. Iodobeads are a ready to use alternative where *N*-chloro-benzenesulfonamide is immobilized on uniform, non-porous polystyrene beads (Figure 1.19b). The reaction conditions are milder, slower (generally 2–15 min) and more easily controlled than for chloramine-T.

Peracetic acid is a monosubstituted analogue of hydrogen peroxide which can be used as an alternative to the chlorine-based oxidising agents, especially in situations where the presence of chlorinated side products would pose a potential problem during purification.<sup>97</sup> To obtain concentrations optimal for iodination, peracetic acid can be generated *in situ* from aqueous hydrogen peroxide and glacial acetic acid (Figure 1.20). Hypoiodous acid is the generated iodinating agent.

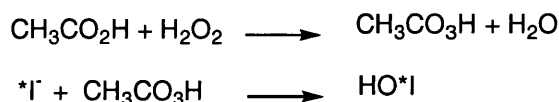


**Figure 1.20:** Peracetic acid as an oxidising agent for iodinations.

Peracetic acid has been used as the oxidising agent for the radioiodination of 5-iodo-R91150<sup>62</sup> (see Chapter 3), [<sup>123</sup>I]IBZM,<sup>98</sup> [<sup>123</sup>I]epidepride,<sup>99</sup> the monoamine uptake site ligand [<sup>123</sup>I]methyl 3β-(4-iodophenyl)-tropane-2β-carboxylate ([<sup>123</sup>I]β-CIT),<sup>100</sup> the dopamine D<sub>2</sub> receptor antagonist [<sup>123</sup>I]iodobenzofuran (IBF),<sup>101</sup> and the NMDA ion-channel blocker [<sup>123</sup>I]CNS1261.<sup>67</sup>

An alternative oxidative radioiodination method is to use oxidising agents that are capable of directly oxidising labelled sodium iodide *in situ*. The iodide formed as a result of iodination is then reoxidised to iodine. The theoretical radiochemical from such reactions is 100%.<sup>90</sup> Hydrogen peroxide is one such oxidising agent that has used to radioiodinate the serotonin transporter imaging agents 5-iodo-2-((2-((dimethylamino)methyl)-phenyl)thio)benzyl alcohol (IDAM)<sup>102</sup> and 2-((2-((dimethylamino)methyl)-phenyl)thio)-5-iodophenylamine (ADAM).<sup>103</sup>

### 1.6.6 Direct Iodination of Arenes

The direct iodination of an arene by electrophilic substitution occurs only on an activated nucleus. The reaction with iodine is reversible with the rate-limiting step being proton elimination (Figure 1.21). Direct iodination by this mechanism is assisted by bases or oxidising agents which remove the proton and shift the equilibrium towards iodination of the arene. Oxidising agents also tend to produce more effective electrophilic forms of iodine to participate in the substitution reaction.

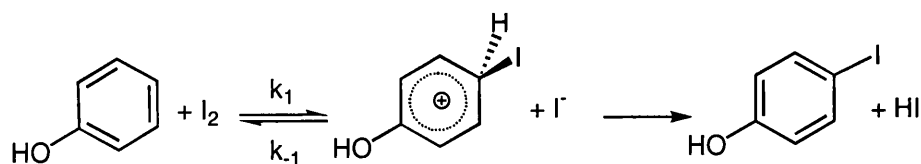
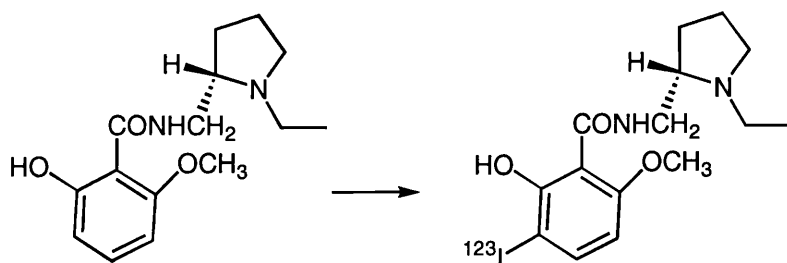


**Figure 1.21:** Direct iodination of activated arenes by electrophilic substitution.



**Conditions:** Na[<sup>123</sup>I]I, 3.2% CH<sub>3</sub>CO<sub>3</sub>H, 65°C, 14 min

**Figure 1.22:** Synthesis of [<sup>123</sup>I]IBZM by electrophilic radioiodination.<sup>98</sup>

The resonance and inductive effects of an activating substituent means that direct electrophilic iodination will occur in the *ortho* and *para* positions (see Figures 1.11 and 1.12). The formation of difficult to separate isomers and/or diiodinated species is always a possibility. This can be problematic for radioiodinated ligand development. Different behavioural characteristics may be associated with different positional isomers, especially with respect to ligand-receptor interactions. This problem is eliminated in compounds where steric factors influence the position of direct electrophilic iodination leading to only one radioactive product. This is true for [<sup>123</sup>I]5-iodo-R91150, where iodination of R91150 in the presence of peracetic acid occurs only at the 5-position<sup>104</sup> in radiochemical yields of >90%<sup>105</sup> (see Chapter 3). Electrophilic iodination has also been developed by Zea-Ponce & Laruelle<sup>98</sup> as a reliable method for the routine synthesis of [<sup>123</sup>I]IBZM from BZM (Figure 1.22). Radiochemical yields of between 56% and 69% are obtained depending on the volume of Na[<sup>123</sup>I]I solution.

A number of procedures have been developed to increase the efficiency, versatility and regiospecificity of radioiodinations. These include methods that permit iodination of a wider number of compounds, even those with substituents that are electron-withdrawing with respect to the aryl ring (see Figure 1.10).

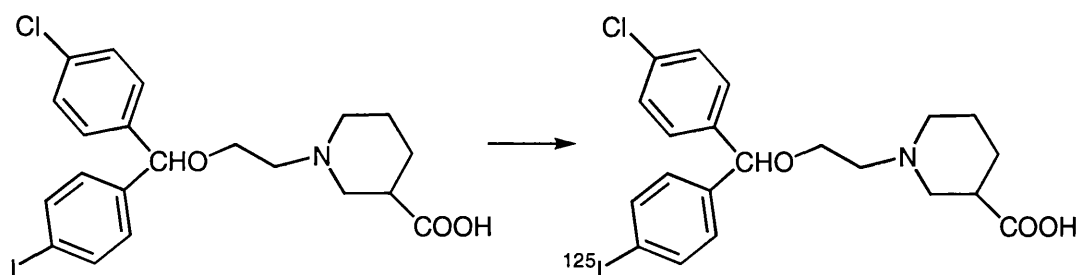
### 1.6.7 Iodination by Group Replacement Reactions

Iodination by group replacement reactions may occur in molecules bearing an appropriate leaving group. During the reaction the iodine atom substitutes the leaving group. The leaving groups can be bromo, diazo group or organometallic groups, such as *tri*-alkylboron, *tri*-alkyltin, *tri*-alkylsilicon, *tri*-alkylmercury *etc.* For radioiodinations, stable iodine can also be used as a leaving group in direct exchange with radioiodine. However, this is necessarily a carrier-added process.

## 1.6.7.1 Direct Exchange of Iodine

Isotopic radiolabelling by substitution of radioiodide for stable iodine can be achieved by exchange in either a solvent or a melt. Heating an iodo-compound to a melt with radioiodide in, for example, water or acetone, is sufficient for radioiodination. The rate of exchange depends on the substrate to be labelled. An increased rate is observed in the presence of electron-withdrawing substituents. The most widely used radioiodinated pharmaceutical for imaging neuroendocrine tumors *meta*-iodobenzylguanidine (MIBG) can be prepared under these reaction conditions.<sup>106</sup> Improved labelling efficiency and reduced reaction times for exchange reactions on iodo substrates can be achieved with catalysts such as cuprous(I) chloride, silica gel and polymer-supported phosphonates. Copper (I) assisted nucleophilic exchange was employed to radiolabel the muscarinic receptor antagonist (R)-(-)-1-azabicyclo[2.2.2]oct-3-yl-(R)-(+)- $\alpha$ -hydroxy- $\alpha$ -(4-iodophenyl)- $\alpha$ -phenyl acetate ((R,R)I-QNB) to high specific radioactivity with iodine-123 (radiochemical yield 36%).<sup>69</sup>

For compounds that do not undergo direct exchange in solvent under reflux conditions, exchange in a melt is a possible alternative. Three procedures can be employed for radioiodinations in a melt. The first involves performing the reaction in a melt of the nonradioactive compound (*i.e.* the nonradioactive compound is heated to its melting point). The substrate has to be stable at its melting point and have a high enough dielectric constant to dissolve the radioiodide. Another two procedures have been developed for situations where one or both of these requirements are not met. For compounds that have low dielectric constants, a melt of acetamide can be used. Ammonium sulphate melts can be used to avoid high temperatures. Heating the substrate in ammonium sulphate with radioactive iodide at a temperature below its melting point (120–160°C) for 1–4 h is an effective method for radioiodination. This method was used to synthesise the radioiodinated analog of [2-[(4-chlorophenyl)(4-[iodophenyl])methoxyethyl]-1-piperidine-3-carboxylic acid, a potential radioligand for the GABA uptake site (Figure 1.23).<sup>107</sup> The moderately high specific activity (118 Ci/mmol) was adequate for *in vivo* animal studies. However, a non-carrier added synthesis is preferred for the synthesis of the <sup>123</sup>I analog. While isotopic exchange is a simple method for the iodination of a wide range of compounds, it is a carrier-added reaction, giving a low specific radioactivity. As mentioned above this situation is not always ideal for human studies.

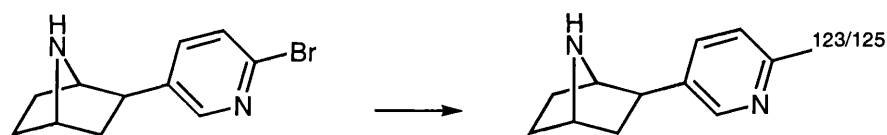


**Conditions:** Na[<sup>125</sup>I]I, (NH<sub>4</sub>)<sub>2</sub>SO<sub>4</sub>, 145°C, 25 min

**Figure 1.23:** Synthesis of [2-[(4-chlorophenyl)(4-[iodophenyl])methoxyethyl]-1-piperidine-3-carboxylic acid.<sup>107</sup>

### 1.6.7.2 Labelling by Nucleophilic Substitution

The use of bromine as a leaving group permits the NCA radioiodination of aliphatic compounds by nucleophilic substitution. Reflux in acetone is sufficient for the labelling of many compounds. For radioligand production it is important to note that the bromo precursor might have similar receptor-binding characteristics to the radioiodinated product, as may any impurity in the precursor preparation. Rigorous purification of the radioiodinated product by, for example, HPLC is therefore an important consideration. As with iodo substrates, catalysts can be used to increase labelling efficiency and reduce reaction times. Synthesis of the radioiodinated epibatidine analogue, ( $\pm$ )-*exo*-2-(2-iodo-5-pyridyl)-7-azabicyclo[2.2.1]heptane (IPH) was prepared by nucleophilic non-isotopic exchange of the 2-bromo pyridyl precursor under reducing conditions (Figure 1.24).<sup>108</sup> The radiochemical yield was 37% and 20% for  $^{125}\text{I}$  and  $^{123}\text{I}$  respectively. Both [ $^{125}\text{I}$ ]IPH and [ $^{123}\text{I}$ ]IPH were produced with high specific radioactivity, 1540 mCi/ $\mu\text{mol}$  (57 GBq/ $\mu\text{mol}$ ) and >1750 mCi/ $\mu\text{mol}$  (65 GBq/ $\mu\text{mol}$ ). A similar method has been used for the radiolabelling of analogues of the non-peptide  $\delta$ -receptor antagonist naltrindole and N1'-methynaltrindole.<sup>109</sup> Contamination of these radioiodinated products with the bromo precursor was avoided by two different strategies. Purification of [ $^{123}\text{I}$ ]IPH and [ $^{125}\text{I}$ ]IPH required a two-phase reverse phase HPLC method,<sup>108</sup> while Kinter & Lever found that a precursor concentration less than 0.5mg was required to prevent bromo precursor contamination resulting from HPLC trailing.<sup>109</sup>



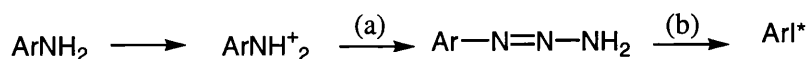
**Conditions:** Na[ $^{123/125}\text{I}$ ]I,  $\text{CuSO}_4$ ,  $\text{Na}_2\text{S}_2\text{O}_5$ , HOAc, 200-220°C

**Figure 1.24:** Radiosynthesis of [ $^{123/125}\text{I}$ ]IPH.<sup>108</sup>

### 1.6.7.3 Dediazotization

Another method for labelling arenes with radioactive iodide is by dediazotization reactions. The reaction involves treating an appropriate aniline with nitrous acid or alkyl nitrate to form the diazonium salt. The diazo group is subsequently replaced with radioiodide (Figure 1.25). Since 1960, related Wallach-type reactions have been employed where the diazotized amine is reacted with a secondary amine to form a stable aryltriazene which can be isolated and reacted with radioiodides under acidic conditions to form the labelled compound (Figure 1.25). A point to note with this procedure is that other functional groups in the aniline need to be stable or protected from reaction with the nitrous acid or alkyl nitrate.

A search of recent literature found only one situation where radioiodination was performed via a diazonium salt intermediate *i.e.* the labelling of the delta opioid receptor ligand [D-Ala2, 4'- $^{125}\text{I}$ -Phe3, Glu]deltorphin from [D-Ala2, 4'-NH<sub>2</sub>-Phe3, Glu]deltorphin.<sup>110</sup>



**Conditions:** (a)  $\text{NHR}_2\text{Na}_2\text{CO}_3$ , (b)  $\text{H}^+$ ,  $^*\text{I}^-$

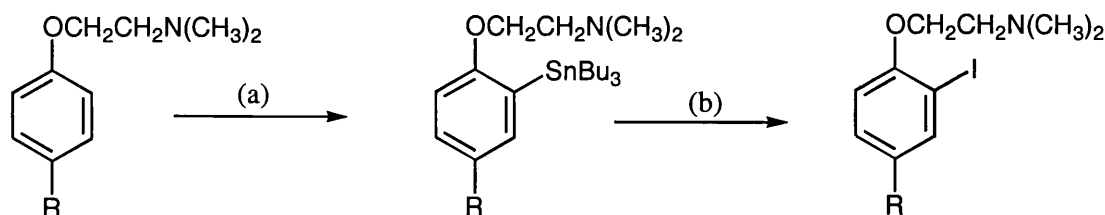
**Figure 1.25:** Labelling of arenes via a diazonium salt.

#### 1.6.7.4 Iododemallation

The most widely used technique for regiospecific introduction of radioiodide is the iododemallation process. Organometallic intermediates of arenes and alkenes have high reactivity towards electrophilic iodine species such that the labile metal moiety is displaced. These reactions give high chemical and radiochemical yields, even for non-activated arenes. Choosing the appropriate and pure organometallic precursor also permits regiospecificity in the placement of the radioiodine atom.

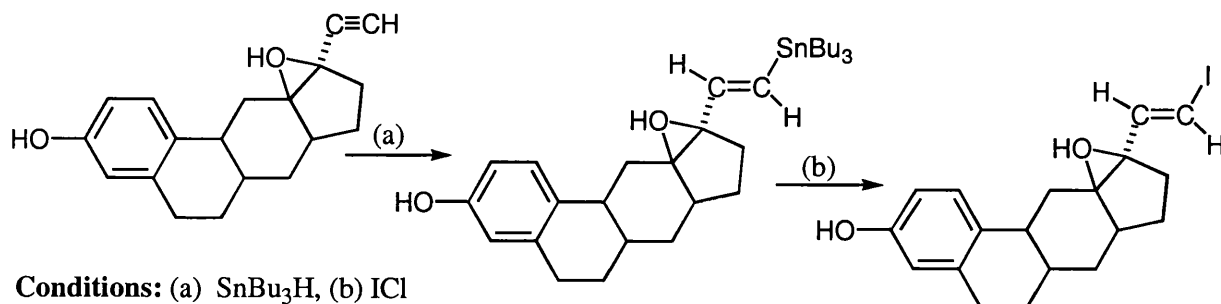
#### Iododestannylation

Organostannanes are among the most reactive and most useful organometallic reagents for radioiodination. They are often chosen over other reagents because of their ease of production, chemical stability and high reactivity towards radioiodine.<sup>111</sup> The aryl carbon-tin bond can be cleaved selectively and efficiently by iodine irrespective of whether the arene is activated or deactivated towards electrophilic substitution. This process also occurs at vinyl carbon-tin bonds but not at the stronger alkyl carbon-tin bond. Specific examples of the reactions for aryl (Figure 1.26) and vinyl (Figure 1.27) tin compounds are shown. Hydrostannylation is a route to vinylstannanes. Tri-*n*-butyltin hydride is added to the corresponding alkyne to produce the *trans*-vinyl-*tri-n*-butyltin compound (Figure 1.27). For arenes, the organotin intermediates can be prepared by either



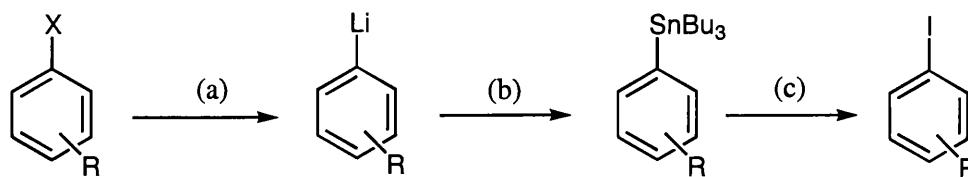
**Conditions:** (a)  $\text{Sn}_2\text{Bu}_6/\text{PdO}$  or i) *sec*-BuLi  $-78^\circ$  ii) *n*-Bu<sub>3</sub>SnCl, (b) ICl or NaI/chloramine-T

**Figure 1.26:** Synthesis and iododestannylation of aryl tin compounds.



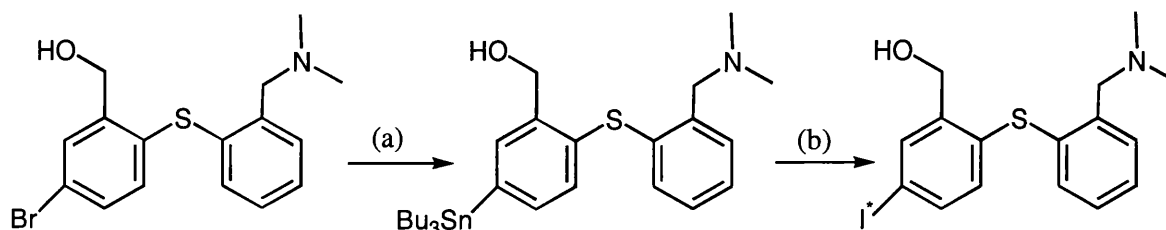
**Conditions:** (a)  $\text{SnBu}_3\text{H}$ , (b) ICl

**Figure 1.27:** Synthesis and iododestannylation of vinyl tin compounds.



**Conditions:** (a) BuLi, (b) SnBu<sub>3</sub>Cl, (c) ICl or NaI/chloramine-T

**Figure 1.28:** Aromatic lithiation via possible halogen-metal interchange as a pathway to stannylation and iododestannylation of arenes.



**Conditions:** (a) (*n*-Bu<sub>3</sub>Sn)<sub>2</sub>, Pd(0) (b) Na[<sup>123/125</sup>I] I, H<sub>2</sub>O<sub>2</sub>, HCl

**Figure 1.29:** The stannylation and subsequent destannylation of the *tri*-butylstannyl derivative of IDAM.<sup>102</sup> \* indicates the site of labelling.

transmetallation reactions with lithium or magnesium metallated arenes or via nucleophilic displacement using the *tri*-alkyltin anion (Figure 1.26).<sup>112</sup> Features of the molecule can be used to direct arene lithiation and produce a single positional isomer.<sup>84,90</sup> *Ortho*-directing metallation is possible in many biologically active compounds, for example, amines, ethers, amides and sulfonamides. A single, *ortho*-positional isomer of the stannylated precursor can be obtained with high yields, under mild reaction conditions. Therefore, iododestannylation will produce a regiospecifically radioiodinated compound. Aromatic lithiation is also possible via halogen-metal interchange (Figure 1.28).<sup>90</sup> This type of reaction is important in radioiodination since the aromatic iodide is the starting material and the regiospecific radioiodinated product can be produced rapidly, with high yield, by stannylation followed by iododestannylation. Two SPET imaging agents for the serotonin transporters, IDAM<sup>102</sup> and ADAM,<sup>103</sup> are prepared by no-carrier added radioiododestannylation of the *tri-n*-butyltin derivatives. The organostannyl precursors of both IDAM (Figure 4.29)<sup>102</sup> and ADAM<sup>103</sup> are synthesised by bromo-metal interchange.

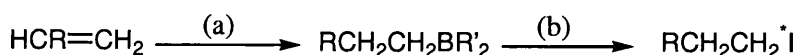
For iododestannylation reactions oxidising agents are required to produce electrophilic iodine species to participate in the substitution. Chloramine-T is commonly used. However, radioiodination of stannylated aromatic rings in the presence of peracetic acid has been shown to proceed rapidly and generate high chemical yields. The list of radioligands prepared by radioiododestannylation reactions includes [<sup>123</sup>I]epidepride,<sup>49</sup> [<sup>125</sup>I]-R(+) TISCH,<sup>44</sup> [<sup>125</sup>I]6IPWAY,<sup>93</sup> [<sup>123</sup>I]SB 207710,<sup>94</sup> [<sup>123</sup>I]CNS1261,<sup>67</sup> [<sup>123</sup>I]IDAM,<sup>102</sup> and [<sup>123</sup>I]ADAM.<sup>103</sup>



## Iodoboronation

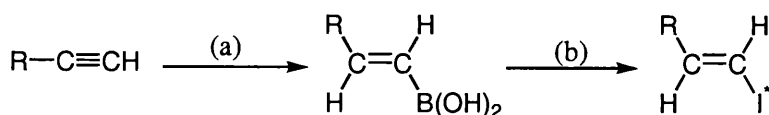
Organoboranes react with molecular iodine under basic conditions to produce alkyl or vinyl iodides. Iodoboronation has been modified for radioiodination by use of oxidising agents and [ $^{123}\text{I}$ ]sodium iodide to produce electrophilic species of iodine, thereby preventing the requirement for molecular iodine. This method is useful for the labelling of alkyl compounds from the corresponding alkene derivative (Figure 1.30), while vinyl iodides can be formed from alkynes via vinylboronic acid intermediates (Figure 1.31).

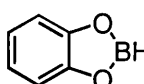
While iodination of organoboranes is rapid, proceeds under mild conditions, and tolerates a variety of functional groups,<sup>113</sup> its application has been limited by the difficulties associated with synthesising arylboronic acids.<sup>114</sup> Recently, a convenient strategy has been published where arylboronic esters are synthesised by a palladium(0) catalysed cross-coupling reaction of alkoxydiboron with haloarenes.<sup>115</sup> The arylboronic ester can then be hydrolysed to the boronic acid. This approach has been applied to the synthesis of the boronic acid precursor of iodocognex, a potent agent for mapping acetylcholinesterase (Figure 1.32).<sup>114</sup> Radioiododeboronation occurred in 66% radiochemical yield following a 15 min reaction with  $\text{Na}^{123}\text{I}$  and chloramine T at room temperature.<sup>114</sup>



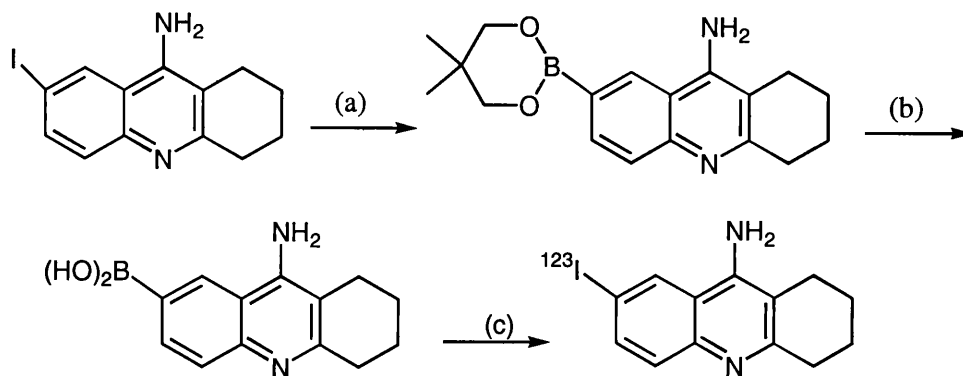
**Conditions:** (a)  $\text{RBR}'_2$ , (b)  $\text{I}^*\text{Cl}$  or  $\text{Na}^*\text{I}$ /chloramine-T

**Figure 1.30:** Radioiodination of alkyl compounds via organoboranes.



**Conditions:** (a) i)  ii)  $\text{H}_2\text{O}$ , (b)  $\text{I}^*\text{Cl}$

**Figure 1.31:** Radioiodination of vinyl compounds via organoboranes.



**Conditions:** (a)   $\text{PdCl}_2(\text{dppf})$ ,  $\text{KOAc}$ ,  $\text{DMSO}$  (b)  $6\text{ M HCl}$ ,  $\Delta$  (c)  $\text{Na}^{123}\text{I}$  I, chloramine-T, 50% aq THF

**Figure 1.32:** Synthesis of organoboronic precursor of iodocognex via the palladium(0) catalysed cross-coupling reaction.<sup>114</sup>

*Iododesilanation*

The carbon-silicon bond shows a number of similarities to the carbon-tin bond, which can be exploited for radioiodination. Organosilanes are quite stable, non-toxic and can be synthesised from inexpensive starting products. Aryltrimethylsilyl intermediates are readily accessible and highly reactive towards electrophilic species of radioiodine, even for highly deactivated arenes (e.g. nitrosubstituted). Iododesilanation is an alternative procedure to iododestannylation for introducing radioiodine into unreactive aromatic rings. The use of organosilanes is not a common strategy for the synthesis of neuroreceptor radioligands. However, they have been employed in the preparation of tumor imaging agents such as 2'-substituted analogues of (R)-5-(2-[<sup>125</sup>I]iodovinyl)-2'-deoxyuridine<sup>116</sup> and MIBG. [<sup>123</sup>I]MIBG is routinely prepared by isotopic exchange. However, radioiododesilanation has been employed to obtain no-carrier added MIBG with both iodine-131 and iodine-123 (radiochemical yield of 80–90%, with an estimated specific radioactivity of 3700 Ci/mmol).<sup>117</sup>

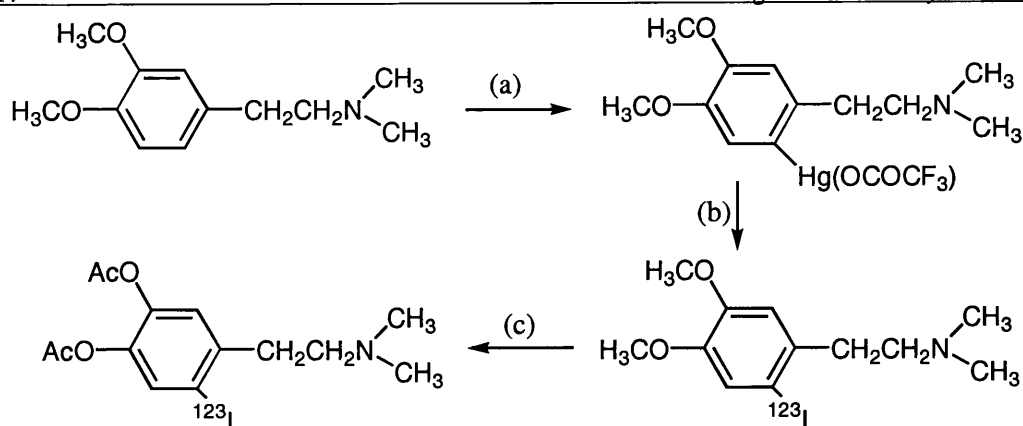
*Iododegermanation*

Germanium has a similar electronegativity to silicon and tin. However, its bond energy, covalent radius and lability to proton displacement are intermediate.<sup>111</sup> The use of aryltrimethylgermanium compounds as reagents for rapid, high yielding, radioiodination reactions is comparable to organosilicon and organotin substrates. In terms of reactivity with respect to iodinating species, trimethylgermanium compounds are between silicon and tin intermediates. However, their use in radioiodinations is not common.

*Iododemercuration*

Organomercury compounds are stable, easily accessible and show high reactivity towards iodination. Aliphatic, vinylic and aromatic mercury reagents can be used in radioiodinations. Crystalline organomercuric acetates can be synthesised by treating the appropriate vinylboronic acid with mercuric acetate in tetrahydrofuran. Chloromercury intermediates can be obtained via transmetallation or direct electrophilic substitution of arene rings or mercuration of alkenes.

IDDE, a potential imaging agent for the dopaminergic system has been prepared by iododemercuration of a fully protected mercury dopamine derivative in a 43% radiochemical yield (Figure 1.33).<sup>91</sup> This method was chosen over an exchange method to obtain the product in high specific activity, measured as >30 000 Ci/mmol at end of synthesis. Radioiododemercuration has also been used to instantaneously label [<sup>123</sup>I/<sup>125</sup>I]5-iodo-2'-deoxyuridine from its chloromercuric precursor.<sup>118</sup> For this radiotracer demercuration was favoured over destannylation since the mercuric precursor was stable for up to 3 months in aqueous solution aliquoted in vials pre-coated with the oxidation agent, iodogen and could therefore be developed for kit formulation.



**Conditions:** (a)  $\text{Hg}(\text{OCICF}_3)_2$ , MeOH, RT, 5 days (b)  $\text{Na}[^{123}\text{I}]\text{I}$ , chloramine-T, phosphate buffer, pH 7, RT, 20 min (c) i.  $\text{BBr}_3$ ,  $\text{CH}_2\text{Cl}_2$ , ii. Pyridine,  $\text{Ac}_2\text{O}$ , iii. HPLC purification

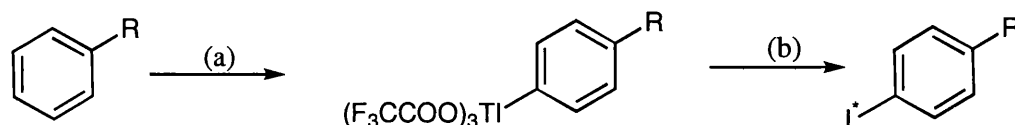
**Figure 1.33:** Synthesis  $[^{123}\text{I}]$  IDDE via radioiododemercuration.<sup>91</sup>

#### Iododethallation

The thallation of arenes, by thallium(III) trifluoroacetate (TTFA) in the presence of trifluoroacetic acid, produces aryl-thallium trifluoroacetates (Figure 1.34). The position of the organothallium substituent can be controlled by varying the kinetic and thermodynamic conditions.<sup>119</sup> Treatment of the preformed thallium derivative with iodide results in direct, instantaneous production of the corresponding aryl iodide. The iodine substitution occurs regioselectively as determined by the thallation reaction.<sup>119</sup> TTFA can also be used as an oxidant to introduce one to four iodine atoms into an arene ring.<sup>119</sup> Each of these two methods has been applied for the NCA regioselective radioiodination of toluene. Mennicke *et al.*<sup>120</sup> found that reacting NCA radioiodide with thallium substituted toluene produces radioiodotoluene with a 40% radiochemical yield and a preference for the *para* isomer (*o/p* = 4). The addition of carrier increased the radiochemical yield for this reaction. Using TTFA as an oxidant, resulted in, carrier-independent, radiochemical yields of greater than 70%, but with low regioselectivity (*o/p* = 1.2).

Alkylvinylthallium trifluoroacetate intermediates can be synthesised *in situ* by reacting the relevant vinylboronic acid with TTFA. These intermediates provide another pathway for the production of vinyl iodides as they react with radioiodide.

To date iododethallation has only been applied to model systems. However, with optimization it could provide an alternative strategy to iododestannylation for the radioiodination of substrates that are sensitive to acidic conditions and oxidising agents or are only weakly activated to electrophilic substitution.



**Conditions:** (a)  $\text{Tl}(\text{OCOCF}_3)_3$ , (b)  $\text{CF}_3\text{COOH}$ ,  $\text{Na}^+\text{I}^-$

**Figure 1.34:** Synthesis of aryl-thallium trifluoroacetates as intermediates for iodination.

### 1.6.8 Effect of iodination on molecular, biochemical and pharmacological properties

Generally, the introduction of iodine into a potential receptor ligand is non-isotopic. This means that a new compound is formed that may have different physicochemical properties from the lead ligand. For radioligands, alterations in these properties can have either a positive or negative influence on receptor affinity and selectivity, biological half-life and permeability to the blood-brain barrier.

A number of constants have been introduced to quantify the physiochemical effects of the introduction of a new substituent into a molecule. The octanol-water partition co-efficient (P) is derived from a simple test that determines the ability of the compound to distribute between a two-phase system of octanol and water. The logarithm of P (logP) is commonly used as an indication of the lipophilicity (hydrophobicity) for a given molecule. The hydrophobicity constant is an empirically derived value assigned to a specific substituent relative to hydrogen. This constant can be used to calculate the impact of a substituent on the overall hydrophobicity (logP) of a neutral molecule. The Pauling electronegativity scale can be used to indicate electron distribution in a covalent bond between two different atoms. This scale is derived from bond energies in diatomic molecules.<sup>89</sup> The electron affinity is the energy (in kJ/g atom) required for a cation to accept an electron ( $X^+ + e^- \rightarrow X$ ), while conversely, the ionisation energy is the energy (in kJ/g atom) required for the atom to release an electron ( $X \rightarrow X^+ + e^-$ ). The molar refractivity of a substituted group is an indication of the volume occupied by the group, corrected for polarity.

In the majority of lead compounds radioiodination is achieved by replacing a hydrogen atom with iodine. This may cause large changes in lipophilicity, electronic, steric and bonding properties (Table 1.2).

	H	I
<b>Lipophilicity</b>		
Hydrophobicity constant –aromatic		0.59
Hydrophobicity constant –aliphatic		1.35
<b>Electronic properties</b>		
Electronic configuration	1s <sup>1</sup>	5s <sup>2</sup> 5p <sup>5</sup>
Electronegativity (Pauling)	2.1	2.5
Electron affinity (kJ/mol)	72	282
Ionisation energy (kJ/g atom)	1260	964
<b>Steric properties</b>		
Atomic radius (Å)	0.55	1.33
Molar refractivity	0.1	1.39
<b>Bonding properties</b>		
Bond		
lengths		
sp <sup>3</sup> –X	1.09	2.16
(Å) sp <sup>2</sup> –X	1.08	2.10
sp–X	1.08	1.99

**Table 1.2:** Comparison of the physiochemical properties of hydrogen and iodine atom

The biological behaviour of a compound may depend on several physicochemical factors. With respect to radioligands for imaging brain receptors lipophilicity is important in determining blood-brain barrier permeability. An inverted parabolic relationship between logP and biological activity has often been observed in several series of compounds.<sup>4,38,121</sup> This is because high logP values promote entrapment in fatty deposits and an increased susceptibility to metabolism. Radioligand binding to non-specific sites such as plasma proteins and cell membranes during a PET or SPET scan will reduce the specific signal to noise ratios. The relationship between serum albumin binding and lipophilicity also follows an inverted parabolic shape. However, the optimal logP value for this biological activity is approximately 3.8. For a majority of radioligands, logP values between 1.6 and 2.5 are often associated with optimal radioactivity signals.<sup>39</sup> For values between 2.5 and 3.8 the level of non-specific binding to plasma proteins will increase while specific binding may decrease. The overall effect will be a reduction in the receptor-specific signal. The hydrophobicity constants for iodine attached to aromatic and aliphatic carbons are 0.59 and 1.35, respectively.<sup>122</sup> This indicates an increase in lipophilicity following iodine for hydrogen substitution. Therefore, radioiodination of a lead compound might have positive or negative effects on radioligand behaviour depending on whether lipophilicity is changed towards or away from the optimal value. While the logP is the most commonly quoted value for lipophilicity the logP at physiological pH (logD) is more relevant to a compound's behaviour *in vivo* since it corrects logP for the pKa of the compound.

Electronic alterations of a compound following iodine substitution will greatly influence its electron distribution, ionization or polarity, and even the conformation of the compound. This, in turn, could alter the interactions between radioligand and receptor. The increase in electron number and a reduced electron affinity are important determinants of the charge surface and conformation of radioligands. The electron-withdrawing effect of the iodine atom will create dipoles. The strength of the dipole will depend on the electronic effects associated with other substituents on the arene ring. In a mono-iodinated arene ring the positive end of the dipole is on the nucleus. This will influence the ability of the aromatic ring to interact with hydrophobic regions of the binding site. The magnitude and direction of the electronic effects of iodination will depend on the atom or groups that participate, and the position of iodine substitution. If atoms or groups that participate in ionic binding with sites on the receptor become more positive as the result of iodination then their binding will be more effective. This is also true if groups involved in hydrogen bonding become more electronegative following iodination. However, if the opposite is true then the binding of the radioligand will be reduced.

Receptor-ligand binding involves interactions between complementary sites. Therefore, the structure and conformation of a molecule can have a major impact on the relative ease with which relevant groups can interact. The volume occupied by iodine is over ten times greater than hydrogen (1.39 versus 0.1 respectively)<sup>4</sup> and comparable to that of a benzene ring. Bond lengths in carbon tetraiodide are also greater than in methane. Consequently, substitution of iodine for hydrogen in a ligand will influence both the shape and size of the radioligand, and greatly increase the steric demands for binding to a receptor. While the correct binding groups may be present in the iodinated

ligand, the conformation of the molecule may prevent binding to appropriate sites on the receptor. This could be due to a reduction in the number of binding sites or the strength of the interactions. For these reasons radioiodination is preferred in areas of the molecule that are not directly involved in receptor interactions. Radioligands also interact with enzymes which can hydrolyse, oxidise or reduce certain sites. This can reduce or eliminate their receptor binding potential. The steric influence of iodine could act to either shield or expose potential sites to enzyme attack. This will either increase or reduce the biological half-life of the compound.

#### 1.6.9 Characterisation of Radioiodinated Compounds

The low mass of iodine associated with NCA radioiodinations limits the characterisation techniques that can be applied to the radioactive product. Performing an equivalent non-radioactive reaction with [ $^{127}\text{I}$ ]iodine or iodide on a macroscale will enable molecular characterisation by all the conventional methods. However, the products from a non-radioactive macro reaction may not always match identically with those from a NCA radioiodination. This needs to be taken into consideration during the characterisation process.

The direct analysis of a NCA radioiodinated compound involves the use of radiochromatographic techniques that detect radioactive components. Radio-TLC and radio-HPLC are the two common techniques. HPLC is becoming the preferred method due to the resolution that can be achieved. Both of these methods provide information on the relative affinity of compounds for either the mobile or stationary phase. One method for obtaining more information about the nature of the different components is by comparison with fully characterised 'cold' standards, detected by uv absorption. This is often the first step in radioligand identification. HPLC analysis of formulated doses can be used to determine radiochemical purity and specific radioactivity. Specific radioactivity calculations require a calibration curve of uv absorbance verses ligand concentration so that the associated mass of carrier observed for the dose can be calculated. When no detectable mass is associated with a dose the lowest detectable concentration of carrier is used in the calculation and the minimum specific activity is quoted.

Radioiodinations are often performed using NCA [ $^{123}\text{I}$ ]sodium iodide and an oxidising agent on a particular precursor. Treatment of the same precursor with molecular iodine on a macro-scale can produce a sufficient mass of iodinated product for structure determination by chromatographic (HPLC, TLC *etc.*) or spectroscopic techniques (MS, IR,  $^1\text{H}$  NMR,  $^{13}\text{C}$  NMR *etc.*). This indirectly provides information about the radiolabelled compound.

#### 1.6.10 Metabolism of Radioiodinated Compounds

Few radioligands are stable *in vivo*. As foreign structures, most drugs are metabolised in the liver, and to some extent in the kidneys, intestines and lungs. Brain involvement in drug elimination is generally low.<sup>123</sup> Phase I metabolic processes involve a simple change in chemical structure following attack by a single enzyme (*e.g.* oxidation, reduction and hydrolysis). *N*-Methyl groups, aromatic rings and terminal positions of alkyl chains will be susceptible to oxidation. Direct hydroxylation is the primary

metabolic route for aromatic compounds compared with  $\omega$ -hydroxylation of aliphatic compounds to form the relevant alcohol. Nitro and carbonyl groups may be attacked by reductase. Aliphatic and aromatic nitro-compounds or ketones may be reduced to primary amines or alcohols. Carbon-carbon double bonds may be reduced to saturated alkyl structures. Hydrolysis of esters and, to a lesser extent, amides by specific and non-specific esterases will produce the corresponding carboxylic acids or amines. In addition to these primary pathways there are a series of secondary metabolic routes where the foreign compound undergoes conjugation reactions. The effect of conjugation is to make the compound more polar and, therefore, more easily excreted in urine or bile. The most important types of conjugation in humans involves reactions with glucuronic acid, glutathione, sulphuric acid and ethanoic acid. Any one compound can be converted by a number of these reactions depending on the affinity of the molecule for the mediating enzymes.

In addition to these metabolic pathways many radioiodinated ligands are prone to deiodination, especially aliphatic ligands. This is due to the weakness of the C-I bond. The ability of the iodine atom to exist as a free entity increases the chance of deiodination of saturated aliphatic carbons. The overall effect of radiolytic decomposition *in vivo* will be to reduce the radioligand concentration during the scanning period.

Metabolic stability *in vivo* maintains radioligand concentration and simplifies the kinetics of receptor interactions. Although prediction of metabolic pathways is almost impossible, the identification of potentially susceptible metabolic groups in radioligands is important to the development process. Preferential labelling at a particular site in the molecule, replacement of susceptible groups with stable substituents, or sterically hindering enzyme attack may prevent the formation of lipophilic, radioactive metabolites that are capable of crossing the blood-brain barrier and confounding receptor-ligand equilibrium.

Measuring the proportion of the radioactivity in blood or tissue attributed to the unchanged parent compound is an initial requirement for the validation of kinetic models employed to determine *in vivo* receptor binding parameters. It can also provide information on the possible metabolic pathway involved. This requires the separation of the radioligand from the associated endogenous material followed by sample analysis. For a review of the techniques available refer to Mazière *et al.*<sup>123</sup>

Procedures employed in the preparation of samples from solid biological samples include 'mortar and pestle', blade or sonication techniques. Protein filtration, precipitation with acidic reagents or a single organic solvent are quick and effective methods of eliminating the large amount of proteins in plasma samples. Chromatography on internal-surface reverse phase columns<sup>124</sup> combines both sample preparation and analysis.

For SPET and PET analysis, interest in determining radioligand metabolism centres, firstly on the fraction of unchanged parent and secondly on the lipophilicity of any radioactive metabolites. The method used needs to be simple, quick and have the capacity to separate the parent compound from other radioactive metabolites. Techniques that have been successfully used for this purpose include HPLC, TLC, overpressure-TLC and solid phase extraction. Radio-HPLC of plasma samples

throughout the scanning period is the method generally used for routine metabolite analysis of radioligands. HPLC is a rapid process with high resolution and sensitivity. From HPLC, information on the polarity of any radiolabelled metabolites can be obtained. This has relevance in determining if a metabolite is able to penetrate the blood-brain barrier. No mass is associated with the radioactive peaks separated by HPLC so molecular structures can only be determined by further analysis. This requires the synthesis of potential metabolites as standards for co-injection with plasma samples.

Irrespective of the techniques employed for the metabolite analysis of biological samples the radioligand should remain stable throughout. A number of sources of errors can occur that need to be limited or controlled. Possible areas for concern include the degradation of radioligand during sample preparation, the degree of recovery of the unchanged radioligand, and separation from metabolites and low levels of radioactivity introducing statistical errors.

Radioligand metabolism can vary from one individual to another. Inter-individual variation could be the result of polymorphism, the presence of other drugs in the body such as enzyme inhibitors or physiopathological conditions. For unstable radioligands metabolite analysis may need to be performed on all individuals undertaking a scan, to enable radioligand-receptor binding parameters to be truly quantitative.

## 1.7 Quantitative Neuroimaging in SPET/PET

SPET has historically been relatively cheaper and, in particular, more accessible as an *in vivo* imaging technique than PET. Hence, only SPET has been widely used as a routine clinical tool. The commercial availability of radiopharmaceuticals and the half-life of single photon-emitting radionuclides increases the flexibility, and simplifies the logistics of the SPET scanning procedure. In comparison, PET started out in a research domain where there was great emphasis on accurate quantitative measurements. Scatter and attenuation correction in SPET and PET are accepted as vital components for the production of artifact-free, quantitative data. A PET camera can be run in either 2D or 3D mode. The percentage of detected coincidence events that result from scatter increases from 15% to 40-45% with a shift to 3D PET.<sup>26</sup> Therefore, 3D mode is used when conditions allow successful implementation of scatter correction *i.e.* the radioactivity and scatter medium is quite uniformly distributed and concentrated in the centre of the field of view. Measurements in PET have traditionally been corrected for attenuation using transmission data.<sup>125</sup> Since attenuation of positron emitting radionuclides is independent of the origin of the annihilation along a line of response, correction is exact making it possible to directly relate count rates from rapid sequential images to the absolute concentration of radioligand. Combined with superior count statistics and the high resolution intrinsic to positron-emitting radionuclides such as carbon-11 and fluorine-18, PET provides truly quantitative information. This type of data can be applied to kinetic models of radioligand-receptor binding to obtain measurements of receptor binding potential and density. The accuracy of the parameters obtained from kinetic modelling is a reflection of the input data. Expressing the radioactivity in absolute terms requires accurate recovery of photons, corrected for scatter and



attenuation. In the past it has been this requirement that has limited the application of kinetic modelling to radioligand studies in SPET.

The use of single photon-emitting radionuclides in SPET necessitates the need for collimation, which significantly reduces the sensitivity of this imaging technique. The degradative physical process of scatter and attenuation is even more inherent for SPET. As much as 60% of emitted photons can be lost as a result of attenuation, while scatter constitutes approximately 30% of the detected photons for a typical  $^{99m}\text{Tc}$  brain scan.<sup>126</sup> Therefore, without scatter and attenuation correction artefactual misrepresentation of physiological parameters can occur. A number of scatter compensation methods are available in order to reduce the degradation of image contrast and loss of quantitation resulting from photon scatter.<sup>127</sup> Unlike PET, the attenuation correction factor for SPET measurements cannot be separated from the radioactivity distribution, making all SPET methods for attenuation correction approximations at best.<sup>125</sup> However, the most accurate correction methods are based on transmission data obtained before, during or after emission scans.<sup>125</sup> With this information, algorithms which include attenuation and scatter correction now exist that produce SPET data with a high degree of accuracy.<sup>125,128</sup> The increased availability of SPET cameras that can perform both transmissions scans and rapid emission scans of the whole brain has lead to improved brain SPET quantification and the application of kinetic models for measuring radioligand-receptor binding. A study comparing the radioactive concentrations obtained from [ $^{123}\text{I}$ ]epidepride with SPET and [ $^{11}\text{C}$ ]epidepride (PET) in baboons illustrates the accuracy of SPET measurements after correction.<sup>129</sup> For the striatum the percentage error of SPET measures relative to PET data dropped from a mean of 53% for uncorrected SPET images to 3% after correction for scatter, collimator blurring and attenuation. This type of study adds significant support to the notion that SPET can provide accurate, quantitative data.

The precise nature of the important positron-emitters in imaging has meant that PET radiochemistry is a dynamic field that has undergone extensive development over the years. The emphasis on accurate, quantitative measurements in PET imaging is also at the forefront of PET radiochemistry. In order to achieve this a list of general criteria has been generated that ideally should be satisfied for a radioligand to quantitatively measure its target binding site *in vivo*. In SPET, the shift to improved quantification and the application of quantitative analysis techniques has a number of implications for SPET radiochemistry. Some of these will be addressed in this thesis.

## 1.8 Aims of This Thesis

The aim of this thesis was to investigate the many facets of radioligand development with an emphasis on the implication of the desire to quantify SPET data. More specifically, rigorous methods of analysis were applied to the investigation of relevant labelling techniques for SPET radioligands with  $^{123}\text{I}$ , precursor purity, radioligand purity and stability, and quantitatively true measures of metabolism *in vivo*.

Initial work with one SPET radioligand, [ $^{123}\text{I}$ ]5-iodo-R91150 has lead to an attempt to synthesise potential precursors for SPET and PET imaging agents. The aim was to obtain radioligands that have improved characteristics *in vivo*, compared with those already available for the imaging of the 5-HT<sub>2A</sub> receptor system.

## 1.9 References

1. Lança AJ. Functional Organization of the Central Nervous System In *Principles of Medical Pharmacology* Ed Kalant H & Roschlau WHE. Oxford University Press, Oxford. 1998: 217-240.
2. Feldman RS, Meyer JS, Quenzer LF. *Principles of Neuropsychopharmacology*. Sinauer Associates, Inc. Publishers, Sunderland Massachusetts. 1998
3. Nolte J. *The Human Brain. An introduction to its functional anatomy*. 4<sup>th</sup> Ed. Mosby, St Louis. 1999;365-367.
4. Patrick GL. *An Introduction to Medicinal Chemistry*. Oxford University Press, Oxford. 1995.
5. Andreasen N. Brain Imaging: Applications in Psychiatry. *Science*. 1988; **239**: 1381-1387
6. Harrison P, Geeddes J, Sharpe M. *Lecture Notes on Psychiatry* 8<sup>th</sup> edition Blackwell Science. 1998.
7. Fletcher A, Pike VW, Cliffe IA. Visualization and characterization of 5-HT receptors and transporters *in vivo* and in Man. *Semin Neur Sci*. 1995; **7**: 421-231.
8. Pilowsky LS, Kerwin RW, Murray RM. Schizophrenia - a Neurodevelopmental Perspective *Neuropsychopharmacology* 1993; **9**: 83-91
9. Laruelle M, Abi-Dargham A, Gil R, Kegeles L, Innis R. Increased dopamine transmission in schizophrenia: relationship to illness phases. *Biol Psychiatry*. 1999; **46**: 56-72.
10. Busatto GF & Kerwin RW. Perspectives on the role of serotonergic mechanisms in the pharmacology of schizophrenia. *J Psychopharmacol*. 1997; **11**: 3-12.
11. Hulme & Birdsall. Strategy and tactics in receptor-binding studies. In *Receptor-Ligand Interactions. A practical approach*. Ed Hulme EC. Oxford University Press, Oxford. 1992; 63-175.
12. Hulme & Buckely. Receptor preparations for binding studies. In *Receptor-Ligand Interactions. A practical approach*. Ed Hulme EC. Oxford University Press, Oxford. 1992; 177-212
13. Williams J, Spurlock G, McGuffin P, Mallet J, Nothen MM, Gill M, Aschauer H, Nylander P-O, Macciardi F, Owen MJ for the European Multicentre Association Study of Schizophrenia. Association between schizophrenia and T102C polymorphism of the 5-hydroxytryptamine type 2A-receptor gene. *Lancet*. 1996; **347**: 1294-1296.
14. Garguilo MG & Michael AC. An enzyme-modified microelectrode that detects choline injected locally into brain-tissue. *J Amer Chem Soc*. 1993; **115**: 12218-12219.
15. Farde L. The advantage of using positron emission tomography in drug research. *Trends Neurosci*. 1997; **19**: 211-214.
16. Jones, T. The role of positron emission tomography within the spectrum of medical imaging. *Eur J Nucl Med*. 1996; **23**: 207-211.
17. Halldin, C & Högberg T. Radiotracers: Synthesis and use in imaging. In *A Textbook of Drug Design and Development*. Eds. Krogsgaard-Larsen P, Liljefors T, Madsen U. Harwood Academic Publishers. 1996: 78-205.

18. Jackson A. Perfusion MRI evolves in imaging brain disease. *Diagnostic Imaging Europe* 1999; **March/April**: 25-32.
19. Alsop DC & Detre JA. Reduced transit-time sensitivity in noninvasive magnetic resonance imaging of human cerebral blood flow. *J Cereb Blood Flow Metab.* 1996; **16**: 1236-1249.
20. Rosen BR, Belliveau JW, Buchbinder BR, McKinstry RC, Porkka LM, Kennedy DN, Neuder MS, Fiser CR, Aronen HJ, Kwong KK, Weisskoff RM, Cohen MS, Brady TJ. Contrast agents and cerebral hemodynamics. *Magn Reson Med.* 1991; **19** : 285.
21. Bailey DL. Transmission scanning in emission tomography. *Eur J Nucl Med.* 1998; **25**: 774-785.
22. Stodilka RZ, Kemp BJ, Msaku P, Prato FS, Nicholson RL. The relative contributions of scatter and attenuation correction toward improved brain SPECT quantification. *Phys Med Biol.* 1998; **43**: 2991-3008.
23. Baily DL & Parker JA. Single photon emission computerized tomography. In *Nuclear Medicine in Clinical Diagnosis and Treatment*. Eds Murray IP and Ell PJ. Churchill Livingstone, Edinburgh. 1994: 109.1-109.12
24. Lassen NA. A reappraisal of the relative merits of SPET and PET in the quantitation of neuroreceptors: the advantage of a longer half-life! *Eur J Nucl Med.* 1996; **23**: 1-4.
25. Bigliani V & Pilowsky LS. The in vivo neuropharmacology of schizophrenia. *Brit J Psychiatry.* 1999; **174** (Suppl 38): 23-34.
26. Cherry SR, Dahlbom M, Hoffman EJ. 3D PET using a conventional multislice tomograph without septa. *J Comput Assist Tomogr.* 1991; **15**: 655-668.
27. Pagani M, Stone-Elander S, Larsson SA. Alternative positron emission tomography with non-conventional positron emitters: effects of their physical properties on image quality and potential clinical application. *Eur J Nucl Med.* 1997; **24**: 1301-1327.
28. Clark AJ. *The mode of action of drugs in cells*. Edward Arnold, London. 1933
29. Kerwin RW & Pilowsky LS. Traditional receptor theory and its application to neuroreceptor measurements in functional imaging. *Eur J Nucl Med.* 1995; **22**: 699-710.
30. Seibyl JP. Development of SPET as a tool for neuropsychopharmacological research. In *Neuroimaging Vol3*. Ed Kerwin R. Cambridge University Press, Cambridge. 1995: 59-79.
31. Lammertsma AA & Hume SP. Simplified reference tissue model for PET receptor studies. *NeuroImage.* 1996; **4**: L153-158.
32. Laruelle M, van Dyck C, Abi-Dargham A, Zea-Ponce Y, Zoghbi SS, Charney DS, Baldwin RM, Hoffer PB, Kung HF, Innis RB. Compartmental modeling of iodine-123 iodobenzofuran binding to dopamine D2 receptors in healthy subjects. *J Nucl Med.* 1994; **35**: 743-754.
33. Laruelle M, Abi-Dargham A, Al-Tiliriti MS, Baldwin RM, Zea-Ponce Y, Zoghbi SS, Charney DS, Hoffer PB, Innis RB. SPECT quantification of [<sup>123</sup>I]iomazenil binding to benzodiazepin

- receptors in nonhuman primates. II. Equilibrium analysis of constant infusion experiments and correlation with *in vitro* parameters. *J Cereb Blood Flow Metab.* 1994; **14**: 453-465.
34. Pike VW. Positron-emitting radioligands for studies *in vivo* – probes for human psychopharmacology. *J Psychopharmacol.* 1993; **37**: 139-158.
35. Nördstrom A-L, Farde L, Halldin C. High 5-HT<sub>2</sub>-receptor occupancy in clozapine treated patients demonstrated by PET. *Psychopharmacology.* 1993; **110**: 365-367.
36. Wong DF, Wagner HN, Dannals RF, Links JM, Frost JJ, Ravert HT, Wilson AA, Rosenbaum AE, Gjedde A, Douglass KH, Petronis JD, Folsterin MF, Toung JK, Burns HD, Kuhar MJ. Effects of age on dopamine and serotonin receptors measured by positron emission tomography in the living brain. *Science.* 1984; **226**: 1393-1396.
37. Pike VW. The status of PET radiochemistry for drug development and evaluation. *Drug Info J.* 1997; **31**: 997-1013.
38. Dischinnio DD, Welch MJ, Kilbourn MR, Raichle ME. Relationship between lipophilicity and brain extraction of C-11-labelled radiopharmaceuticals. *J Nucl Med.* 1983; **24**: 1030-1038.
39. Kessler RM, Ansari MS, de Paulis T, Schmidt DE, Clanton JA, Smith HE, Manning RG, Gillespie D, Ebert MH. High affinity dopamine D2 receptor radioligands. 1. Regional rat brain distribution of iodinated benzamides. *J Nucl Med.* 1991; **32**: 1593-1600.
40. Pike VW, McCarron JA, Lammertsma AA, Hume SP, Poole KG, Grasby, PM, Malizia A, Cliffe IA, Fletcher A, Bench CJ. First delineation of pre-clinical development of a radioligand for studies of 5-HT<sub>1A</sub> receptors in human brain with PET and [<sup>11</sup>C]WAY-100635. *Eur J Pharmacol.* 1995; **283**: R1-R3.
41. Pike VW, McCarron JA, Hume SP, Ashworth S, Opacka-Juffry J, Osman S, Lammertsma AA, Poole KG, Fletcher A, White AC, Cliffe IA. Pre-clinical development of a radioligand for studies of central 5-HT<sub>1A</sub> receptors *in vivo*. *Med Chem Res.* 1995; **5**: 208-227.
42. Halldin C. Dopamine receptor radioligands. *Med Chem Res.* 1994; **4**: 217-249.
43. Karlsson P, Farde L, Halldin C, Swahn C-G, Sedvall G, Foged C, Hansen K, Skrumsager B. PET examination of [C-11] NNC 687 and [C-11] NNC 756 as a new radioligand for the D-1-dopamine receptor. *Psychopharmacology.* 1993; **113**: 149-156.
44. Chumpradit S, Kung MP, Billings J, Kung HF. Synthesis and resolution of (+/-)-7-chloro-8-hydroxy-1-(3'-iodophenyl)-3-methyl-2,3,4,5-tetrahydro-1h-3-benzazepine (TISCH) - a high-affinity and selective iodinated ligand for CNS D1 dopamine receptor. *J Med Chem.* 1991; **34**: 877-883.
45. Verhoeff NPLG. Ligands for neuroreceptor imaging by single photon emission tomography (SPET) or positron emission tomography (PET). In *Nuclear Medicine in Clinical Diagnosis and Treatment*. Eds Murray IP and Ell PJ. Churchill Livingstone, Edinburgh. 1998; **43**: 1-43.
46. Mazière B, Coenen HH, Halldin C, Nagren K, Pike VW. PET radioligands for dopamine-receptors and reuptake sites – chemistry and biochemistry. *Nucl Med Biol.* 1992; **19**: 497-512.

47. Kung HF, Pan S, Kung MP, Billings J, Kasliwal R, Reilley J, Alavi A. In vitro and in vivo evaluation of [I-123]IBZM – a potential CNS D-2 dopamine receptor imaging agent. *J Nucl Med.* 1989; **30**: 88-92.
48. Köhler C, Hall H, Ogren SO, Gawell L. Specific in vitro binding of H-3 –raclopride – a potent substituted benzamide drug with high-affinity for dopamine D-2 receptors in the rat brain. *Biochem Pharmacol.* 1985; **34**: 2251-2259.
49. Kessler RM, Mason NS, Votaw JR, de Paulis T, Clanton JA, Ansari MS, Schmidt DE, Manning RG, Bell RL. Visualization of extrastriatal dopamine D(2)-receptors in the human brain. *Eur J Pharmacol.* 1992; **223**: 105-107.
50. Pilowsky LS, Mulligan RS, Acton PD, Ell PJ, Costa DC, Kerwin, RW. Limbic selectivity of clozapine. *Lancet.* 1997; **350**: 490-491.
51. Bigliani V, Mulligan RS, Acton PD, Kerwin RW, Ell PJ, Gacinovic S, Stephenson C, Pilowsky LS. In vivo occupancy of striatal and temporal cortical D2/D3 dopamine receptors by different classes of typical antipsychotic drugs – a [123I] epidepride single photon emission tomography (SPET) study. *Brit J Psychiatry.* 1999; **175**: 231-238.
52. Farde L, Suhara T, Nyberg S, Karlsson P, Nakashima Y, Hietala J, Halldin C. A PET study of [C-11]FLB 457 binding to extrastriatal D-2-dopamine receptors in healthy subjects and antipsychotic drug-treated patients. *Psychopharmacology.* 1997; **133**: 396-404.
53. Loc'h C, Halldin C, Borraeander M, Swahn C-G, Moresco RM, Mazière M, Farde L, Mazière B. Preparation of [Br-76]FLB 457 and [Br-76]FLB 463 for examination of striatal and extrastriatal dopamine D-2 receptors with PET. *Nucl Med Biol.* 1996; **23**: 813-819.
54. Halldin C, Farde L, Höglberg T, Mohell N, Hall H, Suhara R, Karlsson P, Nakashima Y, Swahn C-G. Carbon-11-FLB-457 – A radioligand for extrastriatal D2 dopamine-receptors. *J Nucl Med.* 1995; **36**: 1275-1281.
55. Langer O, Halldin C, Dollé F, Swahn C-G, Olsson H, Karlsson P, Hall H, Sandell J, Lundkvist C, Vaufrey F, Loc'h C, Crouzel C, Mazière B, Farde L. Carbon-11 epidepride: a suitable radioligand for PET investigation of striatal and extrastriatal dopamine D<sub>2</sub> receptors. *Nucl Med Biol.* 1999; **26**: 509-518.
56. Loc'h C, Guillem E, Martinot JL, Halldin C, Syrota A, Farde L, Mazière B. Neuroleptic interactions on the in vivo dopamine D2 extrastriatal binding of Br-76 FLB 457 studied by PET in human. *J Nucl Med.* 1997; **38**: S547.
57. Mazière B, Halldin C, Loch C, Moresco RM, Delforge J, Bottlaender M, Fuseau C, Syrota A, Farde L, Mazière M. Evaluation in baboon and human of Br-76 FLB-457, a high-affinity PET ligand for studying dopamine D-2 receptors. *J Nucl Med.* 1993; **34**: P102.
58. Sharp T, Bramwell SR, Hjorth S, Grahame Smith DG. Pharmacological characterization of 8-OH-DPAT-induced inhibition of hippocampal 5-HT release *in vivo* as measured by microdialysis. *Br J Pharmacol.* 1989; **98**: 989-997.

59. Pike VW, McCarron JA, Lammertsma AA, Osman S, Hume SP, Satrgent PA, Bench CJ, Cliffe IA, Fletcher A, Grasby PM. Exquisite delineation of 5-HT<sub>1A</sub> receptors in human brain with PET and [carbonyl-<sup>11</sup>C]WAY-100635. *Eur J Pharmacol.* 1996; **301**: R5-R7.
60. Lundkvist C, Halldin C, Ginovart N, Nyberg S, Swahn CG, Carr AA, Brunner F, Farde L. [<sup>11</sup>C]-MDL 100907, a radioligand for selective imaging of 5-HT<sub>2A</sub> receptors with positron emission tomography. *Life Sciences* 1996; **58**: PL187-PL192.
61. Ito H, Nyberg S, Halldin C, Lundkvist C, Farde L. PET imaging of central 5-HT<sub>2A</sub> receptors with carbon-11-MDL 100,907. *J Nucl Med.* 1998; **39**: 208-214.
62. Mertens J, Terriere D, Sipido V, Gommeren W, Janssen PMF, Leysen JE. Radiosynthesis of a new radioligand for serotonin-5-HT<sub>2</sub>-receptor, a promising tracer for gamma-emission tomography. *J Label Compd Radiopharm.* 1994; **34**: 795-806.
63. Terriere D, Janssen PMF, Gommeren W, Gysemans M, Mertens JJR, Leysen JE. Evaluation of radioiodo-4-amino-N-[1-[3-(4-fluorophenoxy)-propyl]-4-methyl-4-piperidiny]-5-iodo-2-methoxybenzamide as a potential 5-HT<sub>2</sub> receptor tracer for SPECT. *Nucl Med Biol.* 1995; **22**: 1005-1010.
64. Busatto GF, Pilowsky LS, Costa DC, Mertens J, Terriere D, Ell PJ, Mulligan R, Travis MJ, Leysen JE, Lui D, Gacinovic S, Waddington W, Lingford-Hughes A, Kerwin RW. Initial evaluation of 123-I-5-R91150, a selective 5-HT<sub>2A</sub> ligand for single photon emission tomography (SPET), in healthy human subjects. *Eur J Nucl Med.* 1997; **24**: 119-124.
65. Travis MJ, Visvikis D, Erlandsson K, Mulligan RS, Waddington WA, Matthiasson P, Pilowsky LS, Costa DC, Ell PJ, Kerwin RW. Dynamic displacement of the selective 5-HT<sub>2A</sub> receptor ligand I-123-5-I-R91150 by unlabelled ketanserin. *J Nucl Med.* 2000; **41**: 935.
66. Travis MJ, Busatto GF, Pilowsky LS, Mulligan R, Acton PD, Gacinovic S, Mertens J, Terriere D, Costa DC, Ell PJ, Kerwin RW. 5-HT<sub>2A</sub> receptor blockade in patients with schizophrenia treated with risperidone or clozapine. *Brit J Psychiatry.* 1998; **173**: 236-241.
67. Owens J, Tebbutt AA, McGregor AL, Kodama K, Magar SS, Perlman ME, Robins DJ, Durant GJ, McCulloch J. Synthesis and binding characteristics of N-(1-naphthyl)-N'-(3-[<sup>125</sup>I]-iodophenyl)-N'-methylguanidine ([<sup>125</sup>I]-CNS1261): A potential SPECT agent for imaging NMDA receptor activation. *Nucl Med Biol.* 2000; **27**: 557-564.
68. Muir K, Grosset D, Owens J, McGregor A, Hadley D, Patterson H, McCulloch J. Imaging of NMDA receptor activation in acute stroke. *Cerebrovasc Dis.* 1998; **8** (Supl 4); 9
69. Owens J, Murray T, McCulloch J, Wyper D. Synthesis of (R,R)-<sup>123</sup>I-QNB, a SPECT imaging agent for cerebral muscarinic acetylcholine receptors *in vivo*. *J Label Compd Radiopharm.* 1992; **31**: 45-60.
70. Müller-Gärtner HW, Wilson AA, Dannals RF, Wagner HN, Frost JJ. Imaging muscarinic cholinergic receptors in human brain *in vivo* with SPECT, [<sup>123</sup>I]4-iododexetimide, and [<sup>123</sup>I]4-iodolevetimide. *J Cereb Blood Flow Metab.* 1992; **12**: 562-570.

71. Dewey SL, Volkow ND, Logan J, MacGregor RR, Fowler JS, Schlyer DJ, Bendriem B. Age-related decreases in muscarinic cholinergic receptor binding in the human brain measured with positron emission tomography (PET). *J Neurosci Res.* 1990; **27**:569-575.
72. Mulholland GK, Kilbourn MR, Sherman P, Carey JE, Frey KA, Koeppe RA, Kuhl DE. Synthesis, in vivo biodistribution and dosimetry of [ $^{11}\text{C}$ ]N-methylpiperidiny benzilate([C-11]NMPB), a muscarinic acetylcholinergic-receptor antagonist. *Nucl Med Biol.* 1995; **22**: 13-17.
73. Dannals RF, Langstrom B, Ravert HT, Wilson AA, Wagner HN. Synthesis of radiotracers for studying muscarinic cholinergic receptors in the living human brain using positron emission tomography. *Appl Radiat Isot.* 1988; **39**: 291-295.
74. Skaddam MB, Kilbourn MR, Snyder SE, Sherman PS, Desmond TJ, Frey KA. Synthesis,  $^{18}\text{F}$ -labeling, and biological evaluation of piperidyl and pyrrolidyl benzilates as in vivo ligands for muscarinic acetylcholine receptors. *J Med Chem.* 2000; **43**: 4552-4562.
75. Skaddam MB, Jewett DM, Kilbourne MR, Sherman PS. The synthesis,  $^{11}\text{C}$ -labeling, and biological evaluation of (R)-N-[ $^{11}\text{C}$ ]methyl-3-pyrrolidyl benzilate as an acetylcholine-sensitive ligand for the muscarinic acetylcholine receptor. *J Lab Cpd Radiopharm.* 2001; **44**: S24-S25.
76. Brown LL, Mukhin AG, Chefer SI, Pavlova O, Koren AO, Kimes AS, Horti AG. Radiosynthesis and evaluation of 5-(2-(4-pyridinyl)vinyl)-6-chloro-3-(1-[ $^{11}\text{CH}_3$ ]methyl-2-(S)-pyrrolidinylmethoxy)pyridine and its analogs, high affinity ligands for studying nicotinic acetylcholine receptors by positron emission tomography. *J Label Compd Radiopharm.* 2001; **44**: S9-S11.
77. Busatto G & Pilowsky LS. Neuroreceptor imaging with PET and SPET: research and clinical application. In *Neuroimaging Vol3*. Ed Kerwin R. Cambridge University Press, Cambridge. 1996: 111-124.
78. Laruelle M, Abi-Dargham A, van Dyck C, Gil R, D'Souza CD, Erds J, McCance E, Rosenblatt W, Fingado C, Zoghbi SS, Baldwin RM, Seibyl JP, Krystal JH, Charney DS, Innis RB. Single photon emission computerized tomography imaging of amphetamine-induced dopamine release in drug-free schizophrenic subjects. *Proc Natl Acad Sci USA.* 1996; **93**: 9235-9240.
79. Farde L, Wiesel FA, Nördstrom AL, Sedvall G. D1- and D2-dopamine receptor occupancy during treatment with conventional and atypical neuroleptics. *Psychopharmacology.* 1989; **99**: S28-S31.
80. Farde L, Nördstrom AL, Nyberg S, Halldin C, Sedvall G. D1-receptor, D2-receptor and 5-HT(2) receptor occupancy in clozapine-treated patients. *J Clin Psychiatry.* 1994; **55**: SB67-69.
81. Farde L, Wiesel FA, Halldin C, Sedvall G. Central D2-dopamine receptor occupancy in schizophrenic patients treated with antipsychotic drugs. *Arch Gen Psychiatry.* 1988; **45**: 71-76.



82. Pilowsky LS, Costa DC, Ell PJ, Murray RM, Verhoeff NPLG, Kerwin RW. Clozapine, single photon emission tomography, and the D2 dopamine receptor blockade hypothesis of schizophrenia. *Lancet*. 1992; **340**: 199-202.
83. Nördstrom A-L, Farde L, Nyberg S, Karlsson P, Haldin C, Sedvall G. D1, D2 and 5-HT2 receptor occupancy in relation to clozapine serum concentration. – A PET study of schizophrenic patients. *Am J Psychiatry*. 1995; **152**: 1444-1449.
84. Dewanjee MK. *Radioiodination. Theory, Practice and Biomedical Application*. Kluwer Academic Publishers, Dordrecht. 1991.
85. Acerbi E, Birattari C, Castiglioni M and Resmini F. Production of  $^{123}\text{I}$  for medical purposes at the Milan AVF Cyclotron. *Inter J App Rad Isot*. 1975; **26**: 741-747.
86. Assmus KH, Jäger K, Schütz F, Schulz F, Schweickert H. Routine production of iodine-123 at the Karlsruhe Isochronous Cyclotron. *Int. Conf Cyclotrons and their Applic*. 1978
87. Hohn A, Coenen HH, Qaim SM. Nuclear data relevant to the production of  $^{120}\text{gI}$  via the  $^{120}\text{Te}(\text{p},\text{n})$ -Process at a small-sized cyclotron. *App Radiat Isot*. 1998; **49**:1493-1496.
88. Zweit J, Luthra SK, Brady F, Carnochan P, Ott RJ, T Jones. Iodine 124: A new positron emitting radionuclide for PET radiopharmaceuticals. *Proc Int Worksh Targ*. 1995
89. March J. *Advanced Organic Chemistry. Reactions, mechanisms and structure*. 4<sup>th</sup> Ed. John Wiley & Sons, New York.
90. Seevers RH and Counsell RE. Radioiodination techniques for small organic molecules. *Chem Rev*.1982; **82**:575-590.
91. Adam MJ, Zea Ponce Y, Berry JM, Lu J. Synthesis of *N,N*-dimethyl- $[\beta\text{-(3,4-diacetocy-6-}^{123}\text{I-iodophenyl)}]\text{-ethylamine (IDDE)}$ : A potential radiotracer for the study of the dopaminergic system. *J Labelled Cpd Radiopharm*. 1991; **31**: 3-10.
92. Kawai K, Ohta H Kubodera A, Channing MA, Eckelman WC. Synthesis and evaluation of radioiodinated 6-iodo-L-DOPA as a cerebral L-amino acid transport marker. *Nuc Med Biol*. 1996; **23**: 251-255
93. Sandell J, Pike VW, Hall H, Marchais S, Wilström, Halldin C.  $[\text{}^{125}\text{I}]\text{6IPWAY}$  – A candidate radioligand for the 5-HT<sub>1A</sub> receptor – radiolabeling and preliminary examination with human post mortem autoradiography. *J Lab Cpd Radiopharm*. 2001; **44**:S173-175.
94. Pike VW, Mulligan RS, Halldin C, Nobuhara K, Hiltunen J, Swahn CG, Karlsson P, Pilowsky LS, Ell P, Larsson S, Schnell PO, Farde L.  $[\text{}^{123}\text{I}]\text{SB 207710}$  exhibits 5-HT<sub>4</sub> receptor-selective binding in monkey brain in vivo. *J Nucl Med*. 2000; **41**: 477.
95. Iodo-gen, iodination reagent. In *Pierce protocol*, Pierce Chemical Company, USA.
96. Zoghbi SS, Baldwin RM, Seibyl JP, Al-Tikriti S, Zea-Ponce Y, Laruelle M, Sybirska EH, Woods SW, Goddard AW, Malison RT, Zimmerman R, Charney DS, Smith EO, Hoffer PB, Innis RB. Pharmacokinetics of the SPECT benzodiazepine receptor radioligand  $[\text{}^{123}\text{I}]\text{Iomazenil}$  in human and non-human primates. *Nucl Med Biol*. 1992; **19**: 881-888.

97. Moerlein SM, Beyer W, Stöcklin G. No-carrier-added radiobromination and radioiodination of aromatic rings using *in situ* generated peracetic acid. *J Chem Soc Perkin Trans.* 1988; **I**: 779-786.
98. Zea Ponce Y & Laruelle M. Synthesis of [ $^{123}$ I]IBZM: A reliable procedure for routine clinical studies. *Nucl Med Biol.* 1999; **26**: 661-665.
99. Fujita M, Seibyl JP, Verheff PLG, Ichise M, Baldwin RM, Zoghbi SS, Burger C, Staley JK, Rajeevan N, Charney DS, Innis RB. Kinetic and equilibrium analyses of [ $^{123}$ I]epidepride binding to striatal and extrastriatal dopamine D<sub>2</sub> receptors. *Synapse.* 1999; **34**: 290-304.
100. Baldwin RM, Zea-Ponce Y, Zoghbi SS, Laurelle M, Al-Tikriti MS, Sybirska EH, Malison RT, Neumeyer JL, Milius RA, Wnag S, Stabin M, Smith EO, Charney DS, Hoffer PB, Innis RB. Evaluation of the monoamine uptake site ligand [ $^{123}$ I]methyl 3 $\beta$ -(4-iodophenyl)-tropane-2 $\beta$ -carboxylate ([ $^{123}$ I] $\beta$ -CIT) in non-human primates: pharmacokinetics, biodistribution and SPECT brain imaging coregistered with MRI. *Nucl Med Biol.* 1993; **20**: 597-606.
101. Laurelle M, van Dyck C, Abi-Darghan A, Zea-Ponce Y, Zoghbi SS, Charney DS, Baldwin RM, Hoffer PB, Kung HF, Innis RB. Compartmental modeling of iodine-123-iodobenzofuran binding to dopamine D<sub>2</sub> receptors in healthy subjects. *J Nucl Med.* 1994; **35**: 743-754.
102. Oya S, Kung M-P, Acton PD, Mu M, Hou S, Kung HF. A new single-photon emission computed tomography imaging agent for serotonin transporters: [ $^{123}$ I]IDAM, 5-iodo-2-((2-((dimethylamino)methyl)-phenyl)thio)benzyl alcohol. *J Med Chem.* 1999; **42**: 333-335.
103. Oya S, Choi S-R, Hou S, Mu M, Kung M-P, Acton PD, Siciliano M, Kung HF. 2-((2-((Dimethylamino)methyl)-phenyl)thio)-5-iodophenylamine (ADAM): An improved serotonin transporter ligand. *Nucl Med Biol.* 2000; **27**: 249-254.
104. Mertens J, Terriere D, Sipido V, Gommeren W, Janssen PMF, Leysen JE. Radiosynthesis of a new radioligand for serotonin-5-HT<sub>2</sub>-receptor, a promising tracer for gamma-emission tomography. *J Label Compd Radiopharm.* 1995; **34**: 795-806.
105. Eersels, J.K.H, personal communication, Radionuclide Centre, Vrije Universiteit, De Boelelaan 1085c, 1081 HV Amsterdam, The Netherlands..
106. Manger TJ, Wu J-I, Wieland DW. Solid-phase exchange radioiodination of aryl iodides. Facilitation by ammonium sulfate. *J Org Chem* 1982; **47**: 1484-1488.
107. Van Dort ME, Gildersleeve DL, Wieland DM. Synthesis of [2-[(4-chlorophenyl)(4-[ $^{125}$ I]iodophenyl)]methoxyethyl]-1-piperidine-3-carboxylic acid, [ $^{125}$ I]CIPCA: a potential radiotracer for GABA uptake sites. *J Label Compd Radiopharm.* 1995; **36**: 961-971.
108. Musachio JL, Horti A, London ED, Dannals RF. Synthesis of a radioiodinated analog of epibatidine, ( $\pm$ )-*exo*-2-(2-iodo-5-pyridyl)-7-azabicyclo[2.2.1]heptane for *in vitro* and *in vivo* studies of nicotinic acetylcholine receptors. *J Label Compd Radiopharm.* 1997; **39**: 39-48.
109. Kinter CM & Lever JR. Synthesis of radioiodinated naltrindole analogues: Ligands for studies of delta opioid receptors. *Nucl Med Biol.* 1995; **22**: 599-606.

110. Fang L, Knapp RJ, Matsunaga T, Weber SJ, Davis T, Hurby VJ, Yamamura HI. Synthesis of [D-Ala2, 4'-<sup>125</sup>I-Phe3, Glu]Deltorphin and characterization of its delta-opioid receptor-binding properties. *Life Sciences*. 1992; **51**: PL189-PL193.
111. Kabalka GW & Varma RS. The synthesis of radiolabelled compounds via organometallic intermediates. *Tetrahedron*. 1989; **45**: 6601-6621.
112. Ali H & van Lier JE. Synthesis of Radiopharmaceuticals via Organotin Intermediates. *Synthesis*. 1996; **April**: 423-445.
113. Kabalaka GW, Gooch EE, Smith TL, Sells MA. Rapid incorporation of iodine-123 via the reaction of <sup>123</sup>I-sodium iodide with organoboranes. *J Appl Radiat Isot*. 1982; **33**:223-224.
114. Akula MR, Zhang JH, Kabalka GW. [<sup>123</sup>I]Iodocognex, a potent SPECT agent to map acetyl cholinesterase via a boronic acid precursor. *J Label Compd Radiopharm*. 2001; **44**: S260-S261.
115. Ishiyama I, Murata M, Miyaura N. Palladium(O)-catalyzed cross-coupling reaction of alkoxydiboron with haloarenes – a direct procedure for arylboronic esters. *J Org Chem*. 1995; **60**: 7508-7510.
116. Morin KW, Atrazheva ED, Knaus EE, Wiebe LI. Synthesis and cellular uptake of 2'-substituted analogues of (E)-5-(2-[<sup>125</sup>I]iodovinyl)-2'-deoxyuridine in tumor cells transduced with the herpes simplex type-1 thymidine kinase gene. Evaluation as probes for monitoring gene therapy. *J Med Chem*. 1997; **40**: 2184-2190.
117. Vaidyanathan G & Zalutsky MR. No-carrier-added *meta*-[<sup>123</sup>I]iodobenzylguanidine: Synthesis and preliminary evaluation. *Nucl Med Biol*. 1995; **22**: 61-64.
118. Foulon CF, Adelstein SJ, Kassis AI. Kit formulation for the preparation of radiolabelled iododeoxyuridine by demetallation. *J Nuc. Med*. 1996; **37**: S1-S3.
119. Merkuskey EB. Advances in the Synthesis of Iodoaromatic Compounds. *Synthesis*. 1988; **Dec**: 923-937.
120. Mennicke E, Henneken H, Holschbach M, Coenen HH. Thallium-tris(trifluoroacetate): A powerful reagent for the N.C.A. radioiodination of weakly activated arenes. *J Lab Compd Radiopharm*. 1997; **40**: 107-108.
121. de Paulis T, Kumar Y, Johanssen L, Rämbsy S, Florvall L, Hall H, Ängeby-Möller K, Ögren S-O. Potential neuroleptic agents. 3. Chemistry and antidopaminergic properties of substituted 6-methoxysalicylamides. *J Med Chem*. 1985; **28**:1263-1269.
122. Lyman WJ, Reehi WF, Rosenblatt DH Eds. *Handbook on Chemical Property Estimation Methods. Environmental Behaviour of Organic Compounds*, McGraw Hill Book Co. 1992.
123. Mazière B, Cantineau R, Coenen HH, Guillaume M, Halldin C, Luxen A, Loc'h C, Luthra SK. PET radiopharmaceutical metabolism – plasma metabolite analysis. In *Radiopharmaceuticals for Positron Emission Tomography*. Eds Stöcklin G & Pike VW. Kluwer Academic Publishers, Dordrecht. 1993; 151-178.

124. Westerlund D. Direct injection of plasma into column liquid chromatographic systems. *Chromatographia*. 1987; **24**: 155-164.
125. Bailey DL. Transmission scanning in emission tomography. *Eur J Nucl Med*. 1998; **25**: 774-785.
126. Jaszczyk RJ, Greer KL, Floyd CE, Harris CC, Coleman RE. Estimating SPET count densities, scatter fractions, and statistical noise. *IEEE Trans Nucl Sci*. 1985; **32**: 762-768.
127. Beekman FJ, Kamphuis C, Frey EC. Scatter compensation methods in 3D iterative SPECT reconstruction: A simulation study. *Phys Med Biol*. 1997; **42**: 1619-1632.
128. Stodilka RZ, Kemp BJ, Msaku P, Prato FS, Nicholson RL. The relative contributions of scatter and attenuation correction toward improved brain SPECT quantification. *Phys Med Biol*. 1998; **43**: 2991-3008.
129. Almeida P, Ribeiro MJ, Bottlaender M, Loc'h C, Langer O, Stru D, Hugonnard P, Grangeat P, Mazière B, Bendriem B. Absolute quantitation of iodine-123 epidepride kinetics using single-photon emission tomography: comparison with carbon-11 epidepride and positron emission

## ***Chapter 2:***

### ***General Methods***

### 2.1.1 Detection and measurement of $^{123}\text{I}$

High levels of  $^{123}\text{I}$  in closed sources were measured in a calibrated ionisation chamber (Amersham Radioisotope Calibrator ARC-120, Capintec Inc., New Jersey, USA). The radionuclidic purity of commercially purchased sodium [ $^{123}\text{I}$ ] iodide is >99.65%  $^{123}\text{I}$  on the day of release. The radioculide impurities have been identified as  $^{121}\text{Te}$  and  $^{125}\text{I}$  (MDS Nordion International Ltd., SA, Belgium). Both of these isotopes have long half-lives (16.8 and 60.1 d, respectively) compared with  $^{123}\text{I}$ . Therefore, the radionuclidic purity of the sodium [ $^{123}\text{I}$ ] iodide at the time of radioiodination was at least 98.6%  $^{123}\text{I}$ .

The level of radioactivity in blood and plasma samples were determined using an automatic well gamma counter (LKB 1282 Compugamma, Wallac, UK). Samples were counted for a maximum of 300 sec or 10000 counts per min, background corrected and decay-corrected to the time of injection.

### 2.1.2 Radio HPLC

Preparative radio-HPLC was performed using a gradient HPLC pump (Water 600 Multisolvant Delivery System, Watford, UK) with injector (Rheodyne U6K injector; 1 ml loop). The sample size varied between 100 and 500  $\mu\text{l}$ . The column eluate was measured sequentially for light absorbance and radioactivity with a Waters LC Spectrophotometer (Waters, Watford, UK) and an in-house sodium iodide well detector, respectively. Counts from the radioactivity detector were measured and converted into an analogue output by an in-house scaler rate meter. Light absorbance and radioactivity data were collected on-line by Millenium computer software (Waters, Watford, UK). Radioactive fractions were also collected and measured in a calibrated ionisation chamber. The system was operated under reverse phase conditions with the appropriate column and mobile phase.

Radioactive plasma samples were analysed on an HPLC system consisting of a pump (Kontron T-414), injector (Rheodyne 1761; 1 ml loop) and a reverse-phase column (Waters  $\mu$ -Bondapak C18 column; 300 x 7.8 mm; 10  $\mu\text{m}$  particle size). The HPLC eluate was monitored sequentially for absorbance of light at 254 nm (Thermo Separation Products SpectraSERIES UV150) and an in-house sodium iodide well detector linked to an ACEMate (EG & G Ortec). Data was collected by LabVIEW (National Instruments, USA). Integration of the areas under the radioactive curve corrected for background in Microsoft Excel (Microsoft Office) enabled the percentage of total radioactivity in each fraction to be determined for each plasma sample. The sensitivity of the radioactivity detector was enhanced by having a large volume (2.0 ml) of eluate present in the well at any given time.

### 2.1.3 Preparative TLC

Preparative TLC was performed using Silica gel layers on plastic or aluminium (200–400 mesh, 60 $\text{\AA}$ , Aldrich). TLC plates were visualised for absorbance of light at 254 nm. Where appropriate,

aluminium TLC plates were sprayed with a solution of 0.2% ninhydrin in ethanol (Aldrich, UK) and heated to 80°C.

#### 2.1.4 Melting Point

Melting points were determined on a Stuart Scientific melting point apparatus (Merk).

#### 2.1.5 Mass Spectrometry

Mass Spectrometry (MS) was used to investigate the contents of crude reaction mixtures and the relative purity of purified products. Low resolution electron impact mass spectra and chemical ionisation were recorded at 70eV on either a Nermag R10/10C single quadrupole instrument (Nermag, France), Micromass Platform II or Micromass AUTOSPEC-Q (Micromass Ltd., Manchester, UK). Electrospray mass spectra were recorded on a Micromass Quattro-II tandem quadrupole instrument (Micromass Ltd., Manchester, UK). High resolution mass spectra were obtained from either the Micromass Platform II or Micromass AUTOSPEC-Q instruments using heptacosafuorotributylamine as a reference.

#### 2.1.6 Nuclear Magnetic Resonance (NMR)

NMR spectra were obtained using a Bruker AM400 spectrometer ( $^1\text{H}$ , 400.13 MHz,  $^{13}\text{C}$ , 100.62 MHz) at ambient temperature. Samples were run in deuterated solvents as stated using tetramethylsilane as an internal standard ( $\delta$  0.00 ppm). Data are presented in the following order: chemical shifts (ppm) relative to tetramethylsilane; multiplicity; intensity as to the number of protons; coupling constant  $J$ ; assignment. The following abbreviations have been adopted: s (singlet); d (doublet); t (triplet); m (multiplet); dd (doublet of doublets); dt (doublet of triplets), bs (broad singlet), bd (broad doublet). First order analyses of spectra were attempted when possible, and consequently, chemical shifts and coupling constants for multiplets may only be approximate.  $^{13}\text{C}$  assignments were made by a best-fit approximation so some assignments may be interchangeable. Multiplicities were determined from polarisation transfer techniques (DEPT).  $^1\text{H}$ - $^1\text{H}$  and  $^{13}\text{C}$ - $^1\text{H}$  Correlation Spectroscopy (COSY) experiments were performed on certain compounds to help with assignment.

Variable temperature experiments were performed using a Bruker AM 250 spectrometer.  $^1\text{H}$ - and  $^{13}\text{C}$ -NMR spectra were run in deuterated solvents at 250.13 MHz and 62.90 MHz, respectively.

#### 2.1.7 Elemental Analysis

Elemental analysis (C, H, N, Cl) were determined by Butterworth Laboratories Ltd (Twickenham, UK) and are within 0.5% of theory.

#### 2.1.8 Ultraviolet Spectroscopy

UV Spectral analysis was performed on a Spetronic Unicam spectrophotometer (PU 8720; Philips). Each sample was run over a fixed bandwidth of 200 –600 nm. A background measure for the appropriate solvent was obtained before obtaining the sample spectrum.

### ***Chapter 3***

#### ***[<sup>123</sup>I]5-I-R91150 a Radioligand for 5-HT<sub>2A</sub> Receptors – Chemical Stability and Metabolism***



### 3.1 Introduction

Serotonergic mechanisms are believed to influence a wide range of centrally mediated effects, for example motor behaviour, cognition, appetite, mood, sleep, body temperature and hormonal release.<sup>1</sup> These behavioural and affective states that are characteristically disturbed in psychiatric disorders making the study of serotonin (5-hydroxytryptamine, 5-HT) and its associated receptor subtypes important for psychiatry.

The diverse behavioural effects of 5-HT are the result of its extensive and widespread innervation throughout the brain, arising from 5-HT neuronal cell bodies confined to small raphe nuclei in the brainstem.<sup>2</sup> The dense 5-HT innervation of the cortex and limbic regions of the brain is believed to lead to a high degree of anatomical, morphological and pharmacological specialisation.<sup>2</sup> The complexity of serotonergic systems within the brain extends to the receptor types through which it mediates its actions. Several 5-HT receptor subtypes have been characterised, each differing in molecular structure, transduction mechanisms, brain regional distribution, pre-synaptic or post-synaptic location and the type of response elicited by receptor agonists and antagonists.<sup>3</sup> Molecular biology has greatly increased our knowledge and understanding of the 5-HT receptor family, confirming the existence of multiple 5-HT receptor subtypes, and discovering gene products encoding putative “new” 5-HT receptors.<sup>4</sup> 5-HT Receptor subtypes are now assigned to five, well-defined classes, and a further two putative classes (Table 3.1).<sup>4</sup> The ligand selectivity of serotonin receptor subtypes may depend on only subtle changes in the primary amino acid sequence.<sup>5</sup>

Receptor	5-HT <sub>1A</sub>	5-HT <sub>1B</sub>	5-HT <sub>1D</sub>	5-HT <sub>1E</sub>	5-HT <sub>1F</sub>
2 <sup>nd</sup> messenger	cAMP ↓ K <sup>+</sup> , Ca <sup>2+</sup>	cAMP ↓ PI, K <sup>+</sup> , Ca <sup>2+</sup>	cAMP ↓	cAMP ↓	cAMP ↓
Receptor	5-HT <sub>2A</sub>	5-HT <sub>2B</sub>	5-HT <sub>2C</sub>	5-HT <sub>3</sub>	5-HT <sub>4</sub>
2 <sup>nd</sup> messenger	PI ↓	PI	PI, Ca <sup>2+</sup>	Na <sup>+</sup> , K <sup>+</sup> (ligand gated)	cAMP ↑
Receptor	5-HT <sub>5A</sub>	5-HT <sub>5B</sub> ‡	Putative classes	5-HT <sub>6</sub>	5-HT <sub>7</sub>
2 <sup>nd</sup> messenger	cAMP ↓?			cAMP ↑	cAMP ↑

‡No human equivalent has been identified

**Table 3.1:** Summary of the present classification of serotonin-modulated receptor subtypes. The arrows indicate whether receptor activation leads to an inhibition or stimulation of the intracellular second messenger pathway. cAMP = adenylate cyclase mediated cAMP, PI = phosphoinositide derived inositol 1,4,5-*tri* phosphate.

### 3.1.15-HT<sub>2</sub> Receptors

The 5-HT<sub>2</sub> receptor family comprises the post-synaptic, heptahelical, G-protein linked 5-HT<sub>2A</sub>, 5-HT<sub>2B</sub> and 5-HT<sub>2C</sub> receptors, which activate intracellular calcium influx via the phosphoinositol-derived second messengers. The 5-HT<sub>2A</sub> subtype is the most characterised due to the availability of selective ligands. However, there is evidence of 5-HT<sub>2B</sub> receptor mRNA in human brain making it a possible target for future work in neuroimaging.<sup>6</sup> Within the CNS the 5-HT<sub>2A</sub> receptor is moderately localised in the limbic cortex and basal ganglia in addition to a dense distribution throughout the neocortex,<sup>7</sup> in association with fine serotonergic terminals.<sup>8</sup> The 5-HT<sub>2A</sub> receptor is thought to mediate serotonin-induced neuronal excitation in several brain regions, and functionally modulate other ascending transmitter systems including dopamine.<sup>1</sup>

### 3.1.2 5-HT<sub>2A</sub> Receptors and Psychiatry

The 5-HT<sub>2</sub> receptor subtypes are the 5-HT receptors most frequently implicated in the pharmacology of psychotic states.<sup>9,10</sup> A large number of psychotropic drugs, including atypical antipsychotics, antidepressants, anxiolytics and hallucinogens, mediate their actions, to some extent, via direct or indirect interactions with various 5-HT<sub>2</sub> receptors.<sup>11</sup> Clearly, 5-HT<sub>2</sub> receptors may be important drug targets for many disorders, including depression and anxiety. However, of specific interest to this thesis, arising from the collaboration between the Institute of Nuclear Medicine, UCL and the Institute of Psychiatry, KCL, is the involvement of the 5-HT<sub>2A</sub> receptor in schizophrenia. Interest in the possible role of the 5-HT system in the pharmacology of schizophrenia has increased due to the following findings:

- 1) Allelic variation of 5-HT receptor genes has been implicated in both susceptibility to schizophrenia and clinical response to atypical antipsychotics. The 5-HT<sub>2A</sub> receptor gene polymorphism (T102C) is associated with both the expression of the disease<sup>12</sup> and the observed inter-individual variation in clinical response to clozapine.<sup>13</sup>
- 2) A selective reduction in 5-HT<sub>2A</sub> receptors in the dorsolateral prefrontal cortex is observed in schizophrenic brains *in vitro*<sup>14,15</sup> irrespective of antipsychotic drug treatment.<sup>16</sup>
- 3) Atypical antipsychotics such as risperidone and olanzapine, which potently block 5-HT<sub>2A</sub> receptors, are at least as effective as classical antipsychotics in the treatment of both positive and negative schizophrenic symptoms, with fewer extrapyramidal side effects.<sup>17-19</sup> The archetypal atypical antipsychotic drug, clozapine, shows relatively weak D<sub>2</sub> antagonism<sup>20,21</sup> compared to its affinity for other sites including the 5-HT<sub>2A</sub>, 5-HT<sub>2C</sub>, and 5-HT<sub>3</sub> receptors.<sup>22-24</sup> Evidence suggests that the uniquely high clinical efficacy of clozapine can be attributed, in part, to its 5-HT antagonism.<sup>10</sup> *In vitro* studies suggest that the ratio of 5-HT<sub>2A</sub> to D<sub>2</sub> blockade for a variety of atypical antipsychotic drugs, is the best measure for discriminating atypical drugs from typical neuroleptics.<sup>22</sup>

These findings have led to a modification of the traditional dopamine hypothesis of schizophrenia. It has been proposed that the relative balance of atypical antipsychotics towards greater 5-HT<sub>2</sub> blockade compared to D<sub>2</sub> antagonism is a crucial aspect in the ability of these drugs to

minimalise neuroleptic-induced extrapyramidal side effects and improve antipsychotic efficacy in schizophrenia.<sup>1</sup> The development of selective radiolabelled antagonists for 5-HT<sub>2</sub> receptors and functional imaging techniques allows visualisation and quantitation of these receptors in living human brain of both treated and untreated schizophrenics.

### 3.1.3 5-HT<sub>2A</sub> Antagonists

*In vivo* imaging of these receptors has been limited by the availability of radioligands that show high receptor affinity and selectivity for a particular subtype. Ketanserin [3(2-(4-(4-fluorobenzoyl)piperidinyl)ethyl)-2,4,(1*H*,3*H*) quinazolinedione; (Figure 3.1)] was the first potent antagonist to show increased selectivity for binding to 5-HT<sub>2</sub> over D<sub>2</sub> dopamine receptors. The amino acid residues essential for ketanserin binding to the 5-HT<sub>2A</sub> receptor have been identified,<sup>25</sup> and are thought to involve an interaction with the *p*-fluorobenzoyl moiety. Comparisons between models for dopamine D<sub>2</sub> and 5-HT<sub>2</sub> receptor-ligand interactions suggest that the pharmacophore for these two sites is common. However, steric factors play a role in determining whether a 5-HT<sub>2</sub> receptor antagonist exhibits high selectivity over D<sub>2</sub> receptors.<sup>26</sup>

The labelling of ketanserin with either carbon-11 or iodine-123 achieved limited success in providing a radioligand that could produce a sensitive brain signal in humans.<sup>27</sup> Until recently, the most useful radioligands for imaging 5-HT<sub>2</sub> receptors with PET were structural analogues of ketanserin. In human brain, <sup>18</sup>F-labelled altanserin (Figure 3.1) and setoperone exhibit frontal cortex to cerebellum ratios of 3<sup>28</sup> and 2.5,<sup>29</sup> respectively. [<sup>18</sup>F]Altanserin is the more selective since [<sup>18</sup>F]setoperone also binds to D<sub>2</sub> dopamine receptors in basal ganglia. The last few years have seen the development of a novel PET radioligand for imaging 5-HT<sub>2A</sub> receptors. (*R*)-(+)-4-[1-hydroxyl-(2,3-dimethoxyphenyl)methyl]-*N*-2-(4-fluoro-phenylethyl)piperidine ([<sup>11</sup>C]MDL 100907, Figure 3.1) has high selectivity and an equilibrium dissociation constant in the nanomolar range (*K*<sub>I</sub> = 0.2nM<sup>30</sup>; *i.e.* high affinity) for the 5-HT<sub>2A</sub> receptor. In baboons useful ratios of radioactivity in the receptor-rich neocortex, to receptor-devoid cerebellum (3.5–4.5) have been observed 60–80 min after injection of [<sup>11</sup>C]MDL 100907.<sup>30</sup> However, rapid *in vivo* metabolism has also been observed with unchanged parent radioligand representing only 25–30% of the radioactivity in the plasma 40 min after injection in baboons.<sup>30</sup> In humans, *in vivo* metabolism of [<sup>11</sup>C]MDL 100907 is not as rapid with unchanged radioligand representing 40% of the total radioactivity in plasma samples taken 50 min after injection.<sup>31</sup>

The most suitable radioligand for SPET imaging of the 5-HT<sub>2A</sub> receptor was developed from a new class of antagonists reported by the Janssen Pharmaceutical Company.<sup>32,33</sup> One of these, R91150 [4-amino-*N*-[1-3-(4-fluorophenoxy)propyl]-4-methyl-4-piperidinyl]-2-methoxybenzamide], is a selective and potent 5-HT<sub>2A</sub> antagonist. The [<sup>123</sup>I]5-iodo derivative (5-iodo-R91150, Figure 3.1) can be obtained by direct electrophilic radioiodination of R91150. 5-Iodo-R91150 shows high affinity and selectivity for the 5-HT<sub>2A</sub> receptor in rat forebrains *in vitro* and *in vivo*.<sup>34,35</sup> Unlike ketanserin, 5-iodo-R91150 has a 50-fold higher selectivity for 5-HT<sub>2A</sub> receptors than for 5-HT<sub>1A</sub>, 5-HT<sub>1B</sub>, 5-HT<sub>1D</sub>, 5-HT<sub>3</sub>,

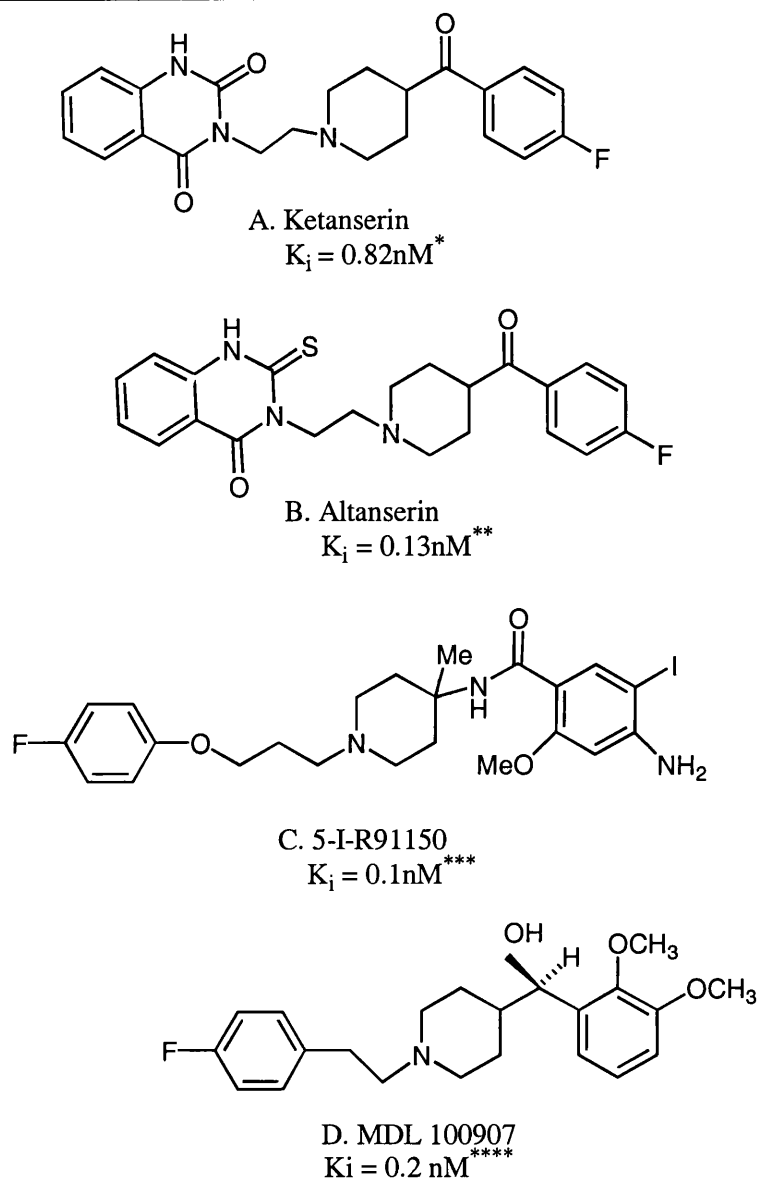


**Figure 3.1:** Chemical structure and affinity of 5-HT<sub>2A</sub> antagonists developed as radioligands for *in vivo* imaging (\*<sup>36</sup>, \*\*<sup>37</sup>, \*\*\*<sup>36</sup>, \*\*\*\*<sup>30</sup>).

$\alpha_1$ ,  $\alpha_2$ , adrenergic, histamine- $H_1$ , and dopamine  $D_2$  receptors. *In vivo* studies have been performed in the rat,<sup>34</sup> baboon<sup>38</sup> and human.<sup>39</sup> One hour after injection of [<sup>123</sup>I]5-iodo-R91150 into the tail vein of rats, a ratio of radioactivity in the 5-HT<sub>2A</sub> receptor-rich frontal cortex to receptor-devoid cerebellum of 10 is observed. This cortical specific binding is displaceable by ketanserin. The percentage of the injected dose per gram of rat frontal cortex tissue is 0.24. Brain uptake and the specific target to background ratios were lower in the baboon compared with the rat, but indicated a potential candidate for human studies.<sup>38</sup> SPET scans in healthy human volunteers injected intravenously with [<sup>123</sup>I]5-iodo-R91150 showed maximal brain radioactivity uptake at two hours after injection (2% of the administered dose).<sup>39</sup> This is associated with a ratio of radioactivity in the frontal cortex to that in the cerebellum of 1.4 (Figure 3.2).<sup>39</sup> The receptor-specific binding has been shown to be displaceable following pretreatment with antipsychotic drugs that exhibit an affinity for the 5-HT<sub>2A</sub> receptor<sup>40</sup> and

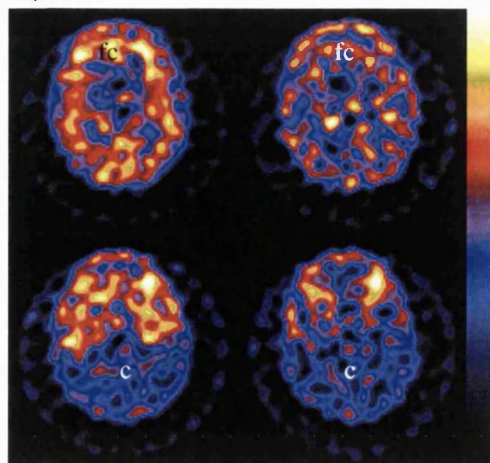


**Figure 3.2:** SPET images of [<sup>123</sup>I]5-iodo-R91150 binding in a healthy subject. The left images were acquired 150 min after radioligand injection, while the right images show the displacement of [<sup>123</sup>I]5-iodo-R91150 binding 210 min later, after a bolus injection of ketanserin (1 mg/kg). Each image is a single slice acquired by the SME Strictman camera. The top images are at the level of the 5-HT<sub>2A</sub> receptor-rich frontal cortex (fc) compared with the receptor-devoid cerebellum (c, bottom images).

by in injection of ketanserin (1 mg/kg, Figure 3. 2).<sup>41</sup> Thus, [<sup>123</sup>I]5-iodo-R91150 is a useful SPECT ligand for studies of the 5-HT<sub>2A</sub> receptor in humans *in vivo*.

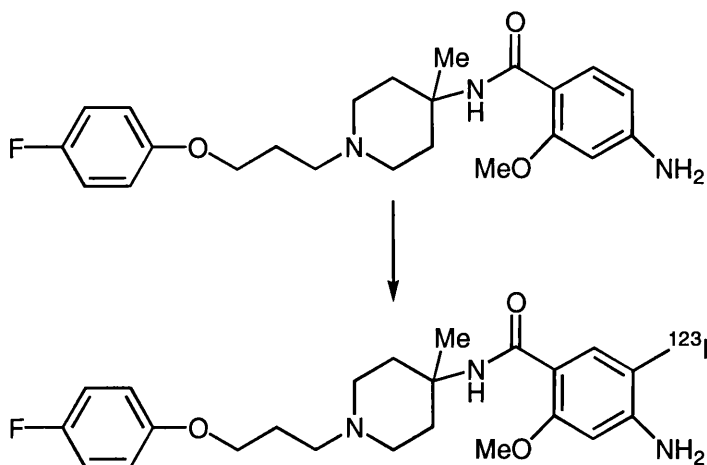
This work will investigate the radiochemical stability and metabolism of [<sup>123</sup>I]5-iodo-R91150 in human plasma. In collaboration with the Free University of Amsterdam (FUA) three university hospitals were provided with [<sup>123</sup>I]5-iodo-R91150 for a multi-centre clinical trial. This meant that doses were prepared, released and imported the day before scanning. Hence there was a long period between production and use. The possibility for radiochemical decomposition during transport and storage had not previously been examined rigorously. Radiochemical instability has the potential to adversely affect the quality of scans or the quantitation of image data.

Metabolite analysis, following intravenous injection of [<sup>123</sup>I]5-iodo-R91150 has been performed in the rat and baboon. To date there is no published data on the metabolism of this radioligand in humans. The specific aims of this study were i) to devise methodology for radiochemical and metabolite analysis, ii) to examine the radiochemical stability of the radioligand and iii) to assess the appearance of radioactive metabolites in plasma after administration of the radioligand to healthy volunteers.

## 3.2 Discussion

### 3.2.1 Radioiodination

[<sup>123</sup>I]5-Iodo-R91150 was synthesised by direct electrophilic substitution of R91150 (Figure 3.3). The radiolabelling yield with iodine-125 was about 95% with no other radiolabelled side product observed.<sup>34</sup> In theory, both the methoxy and amino groups will activate the arene ring towards electrophilic iodination at both positions 3 and 5. In practise, iodination of R91150 with [<sup>127</sup>I]NaI or [<sup>125</sup>I]NaI in the presence of peracetic acid occurs entirely at the 5-position.<sup>34</sup> This is possibly due to steric hindrance imposed by the freely rotating methoxy group on substitution at the 3-position. The radiochemical yield observed with both iodine-125 and iodine-123 is dependent on the volume of NaI solution.<sup>34,42</sup> This effect is more significant with iodine-123 where the yield drops from >90% down to 80% with an increase in the radioactivity from 50 mCi to 200 mCi.<sup>42</sup>



**Conditions:** CH<sub>3</sub>CO<sub>3</sub>H, Na[<sup>123</sup>I]I, 15–20 min, RT

**Figure 3.3:** Radiosynthesis of [<sup>123</sup>I]5-iodo-R91150.

### 3.2.2 Stability and Radiochemical Purity

HPLC System A (see Section 3.3.2) was a duplicate of the analytical system already used at the FUA for quality control of the doses before release. Analysis on System A at the Institute of Nuclear Medicine, London (INM) allowed parallel stability tests at the two sites to be performed. Reverse phase HPLC System B (see Section 3.3.2) was set up to independently determine the radiochemical purity of the delivered doses of [<sup>123</sup>I]5-iodo-R91150. Both methods were rapid (< 20 min). The values obtained for radiochemical purity on the two systems were not significantly different (Table 3.2). Both HPLC methods showed that, on arrival at the INM, undiluted doses of [<sup>123</sup>I]5-iodo-R91150 had a radiochemical purity of 93.16% ± 0.67% (Figure 3.5) and would not meet the general specifications set for radioligand release for human use (>95%). Parallel analysis at the FUA at equivalent times revealed higher radiochemical purity (95.4% ± 0.5%<sup>42</sup>). A radiochemical purity of *ca.* 95% was also observed following transportation of doses to Gent, Brussels and Petten, Holland.<sup>42</sup> For doses that were sent to all three centers, the radiochemical purity was consistently lower in the vials delivered to the INM. This indicated that the conditions, and possibly the duration of transportation influenced the rate of radiolytic decomposition.

Purification of the delivered doses by solid phase extraction proved to be a quick and effective method, enabling recovery of 60–70% of the loaded radioactivity with a radiochemical purity above the specification for release. This technique also provided an alternative, but less effective method compared to HPLC, for determining the radiochemical purity of the delivered doses. The radiochemical purity determined by solid phase extraction tended to be higher than that determined by HPLC, with higher variability, implying less precision.

The radiochemical purity of [<sup>123</sup>I]5-iodo-R91150, determined by HPLC, depended on the degree of dilution of the sample, and the diluent used. The radiochemical purity calculated for [<sup>123</sup>I]5-iodo-R91150 doses at >28 h after release was lower than at ~20 h when no dilution was required. The radioactivity detector used in the later analysis had increased sensitivity, so dilution of the dose was

required to bring the radioactivity injected onto the column, down to a level where dead-time errors were minimised. The calculated radiochemical purity following dilution of the sample in “water for injection” was significantly lower (86.5%) than when mobile phase or citrate/acetate solution were used as the diluent (91% and 90%, respectively). The extent to which the purity of the diluted dose was reduced also depended on the time between dilution in sterile water and injection onto the HPLC column. This effect was not observed following dilution with either mobile phase or citrate/acetate solution. These results showed that aqueous dilution of the citrate/acetate solution used in dose formulation resulted in further radiolytic degradation of [<sup>123</sup>I]5-iodo-R91150. A change in pH following aqueous dilution is a possible explanation for this dramatic drop in radiochemical purity since both the mobile phase and citrate/acetate solution were slightly acidic (pH 6–7).

At the beginning of this work there were questions relating to the radiochemical stability of [<sup>123</sup>I]5-iodo-R91150 and its impact on the relative distribution of radioactivity *in vivo*. It was found that there is a consistent degradation in the radiochemical purity of [<sup>123</sup>I]5-iodo-R91150 during transport from the site of production (Holland) to the INM (Table 3.2). The fact that this level of degradation was not observed when doses were transported over shorter distances to other imaging centres in Holland and Belgium is significant for neuroimaging centres in the United Kingdom since all commercially purchased radioligands are imported from Europe. Radiolytic decomposition during transportation is always going to be a potential problem in the United Kingdom unless the SPET centre has its own radioiodination facilities.

Deterioration in the radiochemical purity of iodine-123 labelled radiopharmaceuticals is often associated with the formation of radical species. The inclusion of radical scavengers such as ascorbic acid or gentisic acid in the formulated dose is one strategy for reducing radioligand radiolysis and maximising radiochemical purity. Unfortunately, these classical radiolysis-scavenging systems degrade during autoclaving, a process that is used in the preparation of [<sup>123</sup>I]5-iodo-R91150.<sup>43</sup> As a result of the work presented in this thesis the radiopharmacy at FUA have investigated a number of different radiolysis-scavenging systems that could minimise or prevent radiolysis while being non-toxic. Irradiation of formulated doses of [<sup>123</sup>I]5-iodo-R91150 with a  $\gamma$ -source was used as a method to rapidly induce the formation of a cascade of radical species thereby allowing the effect of different dose formulations on radiolysis to be quantified.<sup>43</sup> The absence of other radioactive products following irradiation indicated that this process specifically induced deiodination. The addition of either the hydroxyl-scavenger thiourea, or the competitor, *ortho*-iodohippuric acid, to the isotonic citrate/acetate buffer lead to a significant reduction in irradiation induced radiolysis.<sup>43</sup> The non-toxic properties of *ortho*-iodohippuric acid made it the preferred scavenger system. This information was applied to the preparation of [<sup>123</sup>I]5-iodo-R91150 doses. The final dose formulation now includes 1 mg/ml hippuran (*ortho*-iodohippuric acid) as a competitor to deiodination and 0.5 mg ethylenediaminetetraacetic acid, di sodium salt, dihydrate (EDTA) / ml as a complex agent to prevent the formation of degradation-products.<sup>42</sup> With this formulation the radiochemical purity measured at the FUA after autoclaving and the day after production was 98–99% [<sup>123</sup>I]5-iodo-R91150.<sup>42</sup> On

arrival at the INM the purity of equivalent doses had dropped to around 97% (data not shown). This was a significant improvement on the 93% radiochemical purity observed for the original doses delivered to the INM. This change in formulation means that repurification at the INM is no longer required to achieve doses with high radiochemical purity.

### 3.2.3 Pharmacokinetics

#### 3.2.3.1 Plasma clearance

The rapid clearance of radioactivity from the blood and plasma following intravenous injection of [<sup>123</sup>I]5-iodo-R91150 (Figure 3.6) is favourable for the kinetics of radioligand-receptor interactions. The low, and slowly decreasing level of radioactivity in plasma, observed 20 min after radioligand injection, means that the washout of free radioligand in the brain will be rapid. The blood to plasma radioactivity ratio of 0.6 was constant throughout the sampling period showing an absence of an increase in binding to red blood cells. [<sup>123</sup>I]5-Iodo-R91150 showed a high level of binding to plasma proteins. The fact that brain uptake for this radioligand is 2% of the injected dose,<sup>39</sup> despite 92% being bound to plasma proteins, shows that a high level of plasma protein binding does not always prevent a radioligand from crossing the blood-brain barrier and reaching its target site. However, the relatively low receptor-specific signal observed for [<sup>123</sup>I]5-iodo-R91150 in areas of high 5-HT<sub>2A</sub> receptor density is possibly due to a high level of non-specific binding.

#### 3.2.3.2 Metabolism

In order to measure the metabolism of [<sup>123</sup>I]5-iodo-R91150 in plasma, it was necessary to pretreat blood samples to obtain plasma and precipitate proteins. HPLC is the preferred method for analysing the deproteinised plasma,<sup>44</sup> and was used in this work. The use of acetonitrile in this work for the deproteinisation of plasma was shown to be 85–90% effective for [<sup>123</sup>I]5-iodo-R91150. The percentage of radioactivity that precipitated with the proteins was independent of the time that the sample was taken after radioligand injection. There was a consistent loss of 20–25% of the radioactivity following filtration of the sample before injection onto the HPLC. This level of loss also occurred when filtering the radioligand during dose formulation. These losses indicate the “sticky” nature of the compound. The HPLC method was able to separate the radioligand from four radioactive metabolites. 90–100% of the radioactivity injected onto the column was recovered over 15 min. No radioactive metabolites eluted after the parent radioligand. Three individuals, having received labelled R91150 and scanned on two separate days, showed minimal variation in the appearance, and relative percentages of radioactive metabolites in plasma. The recovery of radioactivity at the different steps in the analysis was similar to that obtained when plasma incubated *in vitro* with [<sup>123</sup>I]5-iodo-R91150 was treated in the same manner. The analysis of such samples revealed no other radioactive compounds, showing the absence of metabolism or degradation of [<sup>123</sup>I]5-iodo-R91150 in plasma *in vitro*.

The results presented here (Figure 3.7 and 3.8) show a very low level of peripheral metabolism of [<sup>123</sup>I]5-iodo-R91150 in human venous plasma *in vivo*. Reverse phase HPLC analysis of acetonitrile-



treated plasma revealed four radioactive metabolites that eluted before [<sup>123</sup>I]5-iodo-R91150. These are therefore expected to be more polar than the parent radioligand. The rate and pathway of metabolism was consistent and predictable between individuals and between scans, as shown by the lack of statistically significant intra- and inter-individual variation ( $P = 0.7$  and  $0.6$ , respectively). Of the four radioactive metabolites present, one was more lipophilic than the others, eluting at about 10 min [Figure 3.7, (d)], compared to 3.8 min, 5.2 min and 5.5 min for the more polar radioactive metabolites a, b and c respectively, and 13 min for [<sup>123</sup>I]5-iodo-R91150. This peak at 10 min made up a small percentage of the total radioactivity in later plasma samples ( $< 5\%$ ) and should have minimal impact on the image quality if its lipophilicity enabled it to cross the blood-brain barrier. The level of unchanged radioligand observed in humans ( $86\% \pm 3.5\%$ , 3 h after injection) was significantly higher than that reported in baboons [ $24\% \pm 1.6\%$ , 2 h after injection<sup>38</sup>], but similar to that reported in rats [ $95\%$ , 3 h after injection<sup>34</sup>]. These results show that [<sup>123</sup>I]5-iodo-R91150 has the added advantages for SPET of rapid clearance from the plasma and very slow metabolism *in vivo*. However, care needs to be taken as the radiochemical purity of the injected dose can have a significant impact on the fraction of unchanged parent in plasma (see discussion below).

A direct comparison of the radioactive metabolites observed in human plasma, and those reported by others in the baboon, was limited due to the differences in protocols used. In the baboon study, plasma samples were prepared for HPLC analysis by treatment with ethyl acetate.<sup>38</sup> This removes all polar components, which amounted to  $>50\%$  of the total plasma radioactivity by 60 to 90 min after intravenous injection of [<sup>123</sup>I]5-iodo-R91150. No further analysis of this polar fraction was performed. In the work presented here, the use of acetonitrile to deproteinise human plasma was about 90% effective. There was no observed temporal reduction in the fraction of radioactivity recovered from plasma with this procedure suggesting that any possible explanation for the level of recovery is independent of metabolism. When human plasma samples (60 and 120 min samples) were treated with ethyl acetate and run on HPLC System B, only one radioactive peak ([<sup>123</sup>I]5-iodo-R91150) was observed (data not shown). A parallel reduction in the percentage of radioactivity recovered following extraction with ethyl acetate was found compared to the acetonitrile precipitation method. A lipophilic, radioactive metabolite was shown both here, in humans, and in the baboon study.<sup>38</sup> At present it is difficult to determine whether this metabolite is the same in both species. The fact that only one radioactive peak was present during the HPLC analysis of ethyl acetate-treated human plasma does not preclude identical metabolite processes occurring in both species.

[<sup>123</sup>I]5-Iodo-R91150 has a number of sites that might be susceptible to metabolic transformation (Figure 3.4). Metabolic pathways might include amide hydrolysis to form the corresponding acid (a), demethylation of the terminal amine (b), deiodination (c), dealkylation of the ether link (d), defluorination (e) and *N*-oxide formation (f). Any one of the products from these reactions could be metabolically modified at another site, leading to a wide range of potential radioactive metabolites. A point of interest is whether any lipophilic metabolite could cross the blood-

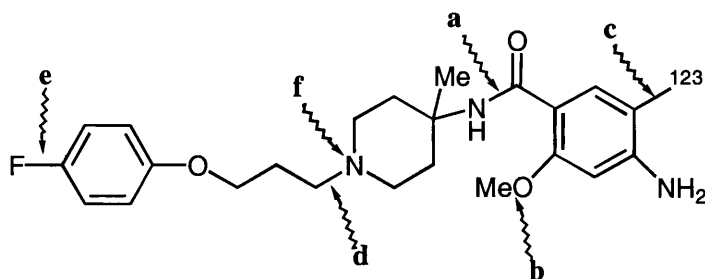


**Figure 3.4:**  $[^{123}\text{I}]5\text{-Iodo-R91150}$  and sites, as indicated by the arrows, that may be susceptible to enzymatic attack *in vivo*.

brain barrier and increase the level of free radioactivity, nonspecific binding or interfere in the specific binding equilibrium.

Of the radioactive products that could be formed by these pathways, a number would be lipophilic enough to cross the blood-brain barrier. The products of demethylation, defluorination and *N*-oxidation of  $[^{123}\text{I}]5\text{-iodo-R91150}$  would all have similar characteristics to the parent radioligand. In addition to their ability to cross the blood-brain barrier, they may also show some affinity for the 5-HT<sub>2A</sub> receptor site. Other possible radioactive metabolites might cross the blood-brain barrier and contribute to the radioactive signal from nonspecific binding. Metabolite analysis of  $[^{18}\text{F}]$ altanserin has reported that  $[^{18}\text{F}]4\text{-(4-fluoro-benzoyl)piperidine}$ , the product of *in vivo* oxidative dealkylation,<sup>45</sup> has the ability to enter the brain and contribute to non-specific binding.<sup>46</sup> A comparison of the structures of  $[^{123}\text{I}]5\text{-iodo-R91150}$  and  $[^{18}\text{F}]$ altanserin suggests that the product of dealkylation of the ether link in  $[^{123}\text{I}]5\text{-iodo-R91150}$  would be radioactive and could behave in a similar manner to the radioactive metabolite of  $[^{18}\text{F}]$ altanserin contributing to non-specific binding in the brain.

In radiolysed  $[^{123}\text{I}]5\text{-iodo-R91150}$  preparations, the polar impurity eluted on HPLC with the polar metabolite observed in plasma samples (Figure 3.7 (a)). However, the temporal and quantitative profile of plasma radioactivity following injection of doses with lower radiochemical purity is disproportionately altered. After intravenous injection of a dose with >98% radiochemical purity, only 2% of the radioactivity is metabolised in the first 5 min of the scanning period. If we assume that all other factors influencing *in vivo* metabolism are equal in the subjects that received  $[^{123}\text{I}]5\text{-iodo-R91150}$  with a radiochemical purity of >98% and 93%, the fraction of unchanged  $[^{123}\text{I}]5\text{-iodo-R91150}$  expected in a 5 min plasma sample following injection of a 93% radiochemically pure dose would be approximately 90–91%. However, the observed fraction of unchanged parent compound was  $76\% \pm 6\%$ . This difference prevailed for the remainder of the scan while the other radioactive metabolites were unaffected by the radiochemical purity of the injected dose.  $[^{123}\text{I}]5\text{-Iodo-R91150}$  is a “sticky” ligand as indicated by the consistent 20–25% loss of radioactivity following filtration of the sample for HPLC. However, a disproportionate retention of  $[^{123}\text{I}]5\text{-iodo-R91150}$  versus the polar fraction on the filter before injection onto the HPLC would not explain the discrepancy observed between the expected and observed levels of  $[^{123}\text{I}]5\text{-iodo-R91150}$  in the plasma. The “sticky” nature of this radioligand was also observed following intravenous injection of the dose. Counting the syringe after injection and a saline flush revealed that 5–10% of the measured dose was retained in the syringe for

all doses, irrespective of the radiochemical purity. With doses of low radiochemically purity, a selective retention of [<sup>123</sup>I]5-iodo-R91150 on the syringe would mean that the radioactivity injected into the patient could be only 83.4–88.35% [<sup>123</sup>I]5-iodo-R91150. However, this level is still higher than that observed in the 5 min plasma sample. It is possible that a combination of these two factors, selective retention of [<sup>123</sup>I]5-iodo-R91150 on the injection syringe and the filter, could be responsible for the observed levels of radioligand in plasma.

While the explanation for the dramatic dependence of the plasma radioactivity profile on the radiochemical purity of the injected radioligand is not exactly clear, the increasingly disproportionate percentage of the radioactivity in the plasma attributed to the radiochemical impurity in the patient dose could potentially risk both scan quality and successful analytical interpretation. These results indicate a real need for doses of [<sup>123</sup>I]5-iodo-R91150 to be of high radiochemical purity in order to obtain accurate measures of the fraction of unchanged radioligand.

### 3.2.4 Future Work

While this work has shown that [<sup>123</sup>I]5-iodo-R91150 has a low level of metabolism there is no evidence to confirm whether or not any of the radioactive metabolites formed during the scanning period have the ability to contribute to brain radioactivity. In order to eliminate this factor a thorough investigation in animals should be carried out. Metabolism in rats has been reported by Mertens *et al.*<sup>34</sup> Unfortunately this work did not include an analysis of brain homogenate to determine the fraction of unchanged parent in the brain. Such a study would answer any questions surrounding the contribution of the radioactive metabolites to data acquired during a [<sup>123</sup>I]5-iodo-R91150 scan.

In addition to identifying the low level of peripheral metabolism of [<sup>123</sup>I]5-iodo-R91150 in human the information presented here could be used to provide a strategy for investigating analogues which could have improved characteristics as radioligands for 5-HT<sub>2A</sub> receptors. One aim is to radioiodinate the phenol derivative of R91150 and test the product as a potential radioligand with possibly greater resistance to metabolism than [<sup>123</sup>I]5-iodo-R91150. Removal of iodine from 5-iodo-R91150 and radiolabelling with carbon-11 in the methoxy group would decrease the lipophilicity of the radioligand product and potentially increase the signal to noise ratio obtained in the brain provided brain penetration could still be achieved. The synthesis of two compounds that could act as precursors for these potential PET radioligands has been attempted and will be discussed in Chapter 4 of this thesis. A third aim is to investigate the possibility of labelling with fluorine-18 as a potential PET radioligand for imaging 5-HT<sub>2A</sub> receptors.

### 3.2.5 Summary

These results indicate that [<sup>123</sup>I]5-iodo-R91150 has favourable pharmacokinetics for SPET in humans with rapid clearance from plasma and very low metabolism *in vivo*. However, there is an issue surrounding the demonstrated radiochemical instability of the radioligand during transportation and storage. This is especially significant for SPET centres in the United Kingdom that receive commercially prepared doses of 123-iodine labelled radioligands from Europe. Care needs to be

taken, since any significant radiochemical impurity from radiolytic decomposition can make up an increasingly disproportionate percentage of the measured radioactivity in the plasma during the course of the SPET scan. This has the potential to adversely affect the quality of the scans or the quantitation of SPET data.

### **3.3 Methods**

#### **3.3.1 Materials and Methods**

For general methods refer to Chapter 2.

Reference 5-iodo-R91150 was a gift from Dr J Mertens, VUB Cyclotron, Belgium.

#### **3.3.2 Preparation of [<sup>123</sup>I]5-iodo-R91150**

Doses of [<sup>123</sup>I]5-iodo-R91150 were prepared at the Free University of Amsterdam (FUA) the day prior to injection using the following procedure. [<sup>123</sup>I]Sodium iodide concentrate was supplied by the VU-Cyclotron B.V. and diluted with 1 sodium hydroxide (1 mM, pH 10.5 –11.5) to obtain a concentration of 1.85 GBq/ml at 18:00 h the following day. To the reaction vial containing the [<sup>123</sup>I]sodium iodide was added an equivalent volume of [<sup>127</sup>I]sodium iodide solution (0.1 mM in 1 mM sodium hydroxide), glacial acetic acid (250 µl) and R91150 (40 µl, 0.05 mg/50 µl acetic acid). A syringe containing active charcoal was inserted through the stopper before the addition of 25 µl hydrogen peroxide. A further 25 µl of hydrogen peroxide was added after 10, 20 and 25min. The reaction was terminated after 30min by transferring the reaction vial onto ice and adding sodium sulphite (0.5 ml. 0.5 M in 4.5 M sodium hydroxide). The crude reaction was purified by HPLC (RP Select B LiChrosphere, Merck, 250 x 4 mm, 10µm particle size eluted with acetic acid buffer (0.1 M, pH 5.2) – ethanol (60–40) at a flow rate of .8 ml/min)). On this system the precursor, R91150, eluted with a retention time of 7–9 min compared with 22–28 min for 5-iodo-R91150. The fraction containing 5-iodo-R91150 was diluted in citrate/acetate buffer (61 mM tri-sodium citrate, 2.4 mM citric acid, 51 mM sodium acetate in 2% EtOH, pH 6–7), filtered through a Millex FG syringe filter and autoclaved. The specific activity of the final dose was about 10000 Ci/mmol 12 h after release. The radiochemical specification for release on the day of synthesis was > 97% [<sup>123</sup>I]5-iodo-R91150 (≤ 2.5% [<sup>123</sup>I], ≤ 0.5% other radioactive peaks). The doses were delivered to the Institute of Nuclear Medicine (London) the day after synthesis at a radioactive concentration of about 180 MBq in 3 ml.

#### **3.3.3 Analysis of Radiochemical Purity**

Investigation of the radiochemical purity of the prepared doses was carried out the day after synthesis at the site of scanning (London). The first analysis was approximately 20 h after product release and then at regular intervals during the day. Analysis was performed on one of two HPLC systems. System A, a RP Select B LiChrospher (Merck) column (125 x 4.5 mm) plus guard column eluted with 0.08M anhydrous sodium phosphate - acetonitrile – methanol (57: 26: 17 by vol.) at 1 ml/min, and System B, a Waters µ-Bondapak C18 column (300 x 7.8 mm, 10 µm particle size) eluted isocratically

with methanol - 0.1M ammonium formate (63: 35 v/v) at 3 ml/min. The major radioactive peak on both Systems A and B eluted with the same retention time as reference I-R91150, at 10 min and 13 min, respectively. The first analysis was performed on both Systems A and B. At 28 h after release a fraction of the prepared stock dose was diluted with i) sterile water for injection, ii) mobile phase or iii) isotonic citrate/acetate solution for analysis with System B.

A simple solid-phase extraction method was developed for the purification of the delivered patient doses so that they would meet radiochemical purity specifications for injection (>95%). This was also used as a simple method for comparing with HPLC values for radiochemical purity. The delivered doses (~750 MBq in 10 ml) were loaded onto a Sep-pak column (Adsorbex RP-18 (100mg), Merk, Germany) that had been activated with ethanol (5 ml) and pre-washed with water (10 ml). The radioactivity not retained on the column was expressed as a percentage of the total radioactivity loaded onto the column and subtracted from 100 to give the radiochemical purity of the delivered dose. The radioactivity retained on the Sep-pak was recovered by eluting with ethanol (0.5 ml) and formulated for injection by dilution with saline for injection.

### **3.3.4 Pharmacokinetics**

#### **3.3.4.1 Plasma clearance**

Venous blood samples (2.5 ml) were collected from healthy volunteers at regular intervals for the first 60 min of the scanning period, followed by 30 min intervals out to 180 min after intravenous injection of [<sup>123</sup>I]5-iodo-R91150 (185 MBq). An aliquot of blood (0.5 ml) was taken for determination of radioactivity while the remainder of the sample was centrifuged at 3000 rpm for 5 min at room temperature and the plasma separated. An equal volume of plasma (0.5 ml) was counted. Clearance was determined by taking equal aliquots of blood and plasma for counting of <sup>123</sup>I radioactivity in an automatic well gamma counter. A standard of known radioactivity was used to convert counts per minute into Bequerels.

#### **3.3.4.2 Metabolite Analysis**

Larger blood samples (5 ml) were also obtained at 5, 30, 60, 90, 120, 150 and 180 min after injection for metabolite analysis of plasma. Plasma proteins were precipitated from plasma (1 ml) with acetonitrile (9 volumes). Following centrifugation (3000 rpm, 10 min, 4°C), the supernatant was taken and the acetonitrile evaporated off. The residue was reconstituted in mobile phase [MeOH-0.1M HCOONH<sub>4</sub> (63: 35 v/v); 1.5 ml]. The reconstituted sample was filtered through a Millipore MV syringe filter and injected (1 ml) onto a Waters μ-Bondapak C18 column (300 x 7.8 mm; 10 μm particle size) and eluted with System B mobile phase for determination of radioactive metabolites. Radioactivity was measured by an on-line, NaI crystal detector. The fraction of unchanged [<sup>123</sup>I]5-iodo-R91150 in plasma was determined by integrating the areas under the radioactive curve for each time point.

Five individuals were injected with doses of [<sup>123</sup>I]5-iodo-R91150 that had been repurified at the INM to give a radiochemical purity >98%. Three of these individuals were taking part in a scan:

rescan protocol so comparisons of metabolism were performed between the first, and the second scan, two weeks later to determine intra-individual variability in metabolism. The mean radiochemical purity of <sup>123</sup>I-5-iodo-R91150 in five other individuals was 93% ± 0.67%.

Intra and inter-individual variations were tested for statistical significance using an analysis of variance (ANOVA) test (Sigmastat, Jandel).

#### 3.3.4.3 Plasma Protein Binding

The binding to plasma proteins *in vitro* was determined by ultrafiltration of human plasma incubated with [<sup>123</sup>I]5-iodo-R91150 (30 min, 34°C). Incubated plasma (1 ml) was centrifuged in ultrafiltration units with YMT membranes that have a 10000 molecular weight cut off (MPS micropartition device No. 4010, Amicon, Beery, MA, USA). *In vitro* incubation of [<sup>123</sup>I]5-iodo-R91150 diluted in 0.9% NaCl was run concurrently to control for non-specific binding to the unit. Aliquots of equal volume were taken from both the ultrafiltrate and total plasma and counted. The degree of plasma protein binding was determined by expressing the radioactivity in the ultrafiltrate as a percentage of the total radioactivity in the plasma, corrected for the degree of non-specific binding.

### 3.4 Results

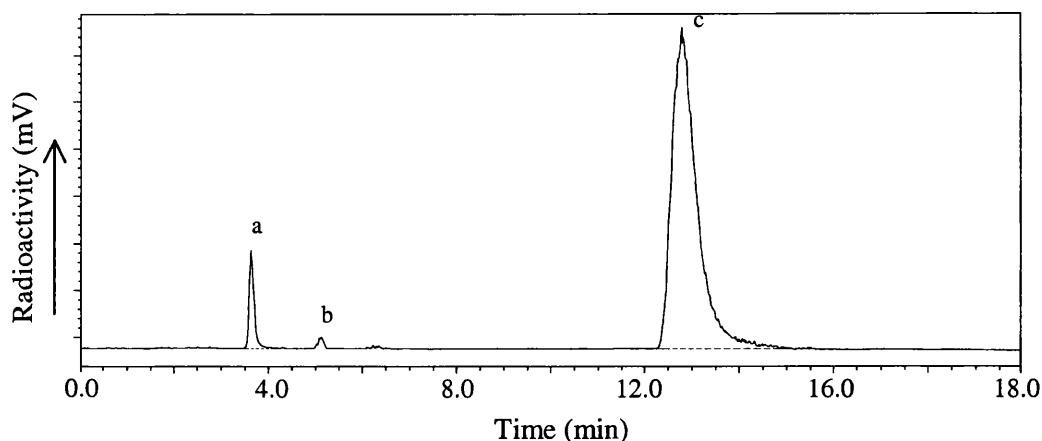
#### 3.4.1 Analysis of Radiochemical Purity

Table 3.2 shows the radiochemical purity of five doses of [<sup>123</sup>I]5-iodo-R91150 that were analysed 20 h after release, by all three methods developed. A total of eight doses were analysed on HPLC System A on site without dilution. The mean radiochemical purity ± standard deviation for these doses was 93.16% ± 0.67%. The major impurity eluted with the column void volume for both HPLC systems (Figure 3.5, peak a). However, two other radioactive peaks were sometimes observed at very low levels (Figure 3.5, peak b), eluting before [<sup>123</sup>I]5-iodo-R91150. Figure 5.4 shows a typical HPLC profile of an unpurified dose on arrival at the INM (20 h after product release).

Analysis of the diluted dose at >28 h after preparation revealed a further reduction in the radiochemical purity. The level of purity calculated was found to be dependent on the diluent. Dilution in either mobile phase or the citrate/acetate solution gave a radiochemical purity of 91% and

	HPLC System A	HPLC System B	Sep pak
Mean RCP	93.25% ± 0.95%	93.30% ± 0.81%	94.00% ± 1.32%
	<i>n</i> = 5	<i>n</i> = 5	<i>n</i> = 5

**Table 3.2:** Radiochemical purity of the delivered doses of [<sup>123</sup>I]5-iodo-R91150 as determined by the three methods. Values equal mean ± standard deviation.



**Figure 3.5:** A representative HPLC trace (System B) of  $[^{123}\text{I}]5\text{-iodo-R91150}$  on delivery at the INM analysed 20 h after product release.  $[^{123}\text{I}]5\text{-Iodo-R91150}$  (peak c) constitutes 93% of the radioactivity above background. The rest of the radioactivity is associated with the peak (a) eluting with the column void volume and peak b (r.t. = 5.2 min) .

90%, respectively. However, the radiochemical purity was 86.5% with dilution in sterile water for injection. This value is from an injection immediately following dilution. One hour later the radiochemical purity of the same sample had dropped to only 37%.

Solid-phase extraction was a quick and effective method for purifying doses with reduced radiochemical purity. Recovery of  $[^{123}\text{I}]5\text{-iodo-R91150}$  off the Sep-pak column was 60-70%. The radiochemical purity of the purified doses was always > 98%  $[^{123}\text{I}]5\text{-iodo-R91150}$ .

### 3.4.2 Pharmacokinetics

#### 3.4.2.1 Plasma clearance

A typical plasma clearance curve after injection of  $[^{123}\text{I}]5\text{-iodo-R91150}$  is shown in Figure 3.6. After intravenous injection of  $[^{123}\text{I}]5\text{-iodo-R91150}$ , the radioactivity in both the venous blood and plasma

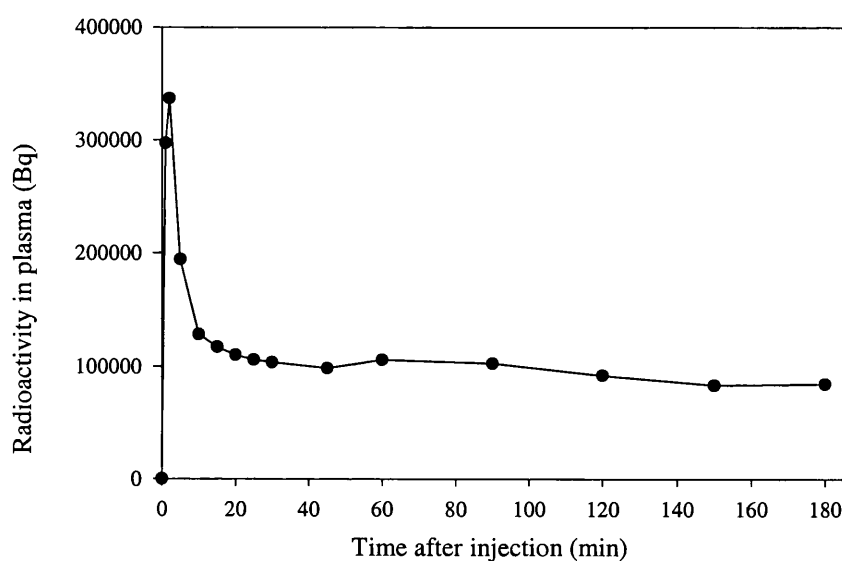


**Figure 3.6:** Typical plasma clearance of radioactivity (decay-corrected) after administration of  $[^{123}\text{I}]5\text{-iodo-R91150}$ .

peaked between 1 and 3 min. Thereafter, there was a rapid clearance of radioactivity to a low plateau level. The blood to plasma ratio was 0.6 for all subjects at all time points. Plasma protein binding of [<sup>123</sup>I]5-iodo-R91150, corrected for non-specific binding to the ultrafiltration unit was 92%.

### 3.4.2.2 Metabolism

The use of 9 volumes of acetonitrile to deproteinate human plasma enabled 85–90% of the total plasma radioactivity to be recovered in the supernatant at all time points. There was a consistent loss of 20–25% of the radioactivity following filtration of the sample before injection onto the HPLC column. Eluting the column for 15 min recovered >90% of the injected radioactivity.

Following injection of a dose of [<sup>123</sup>I]5-iodo-R91150, with a radiochemical purity greater than 98% into healthy volunteers, low metabolism to 4 radioactive compounds was observed (Figure 3.7A, peaks a, b, c and d). All the radioactive metabolites eluted before [<sup>123</sup>I]5-iodo-R91150 and were thus more polar. The major non-parent radioactive peak, (a), eluted with the column void volume. By 180 min after injection 86% ± 3.5% (*n* = 5) of the total radioactivity in the plasma was unchanged radioligand (Figure 3.7A). Inter-individual variation and intra-individual variation (scan: rescan protocol) was not statistically significant (ANOVA *P* = 0.6 and 0.7, respectively).

Following injection of doses of [<sup>123</sup>I]5-iodo-R91150 at a lower radiochemical purity (~93%), as a result of radiochemical decomposition, the percentage of radioactivity in the plasma represented by parent radioligand was lower at all times (Figure 3.7B). By 180 min post injection only 63% ± 4.3% (*n* = 5) of the total radioactivity in the plasma was still parent radioligand (Figure 3.8B). This major difference was due to the increased proportion of the radioactivity in the form eluting at the void volume (27.2% ± 2.75% compared with 8.0% ± 1.4%). By contrast, the time course for the appearance of the more retained radioactive metabolites in plasma were unaffected by the radiochemical purity of the injected dose.

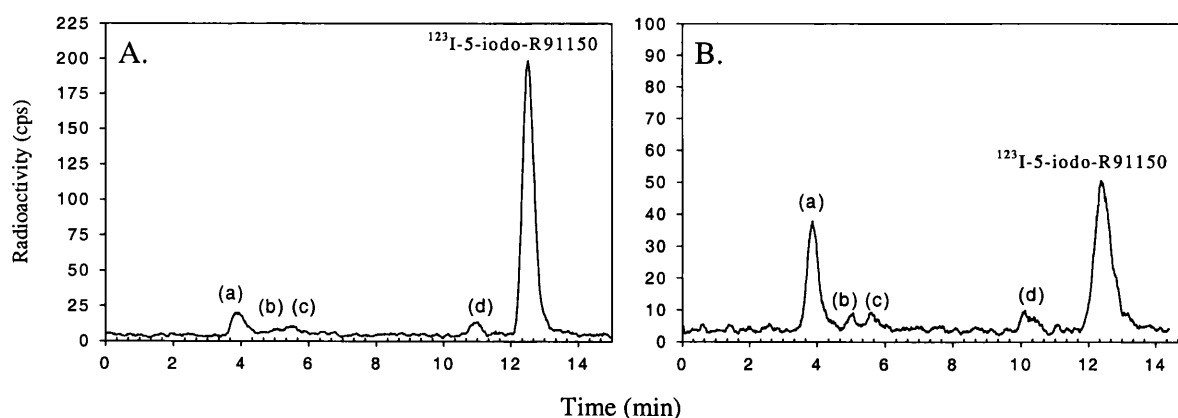


**Figure 3.7:** Representative HPLC profiles from plasma taken 180 min after injection of a dose of [<sup>123</sup>I]5-iodo-R91150 with a radiochemical purity of > 98% (A) and 93% (B) in healthy subjects. The four radioactive metabolites are labelled a, b, c and d.



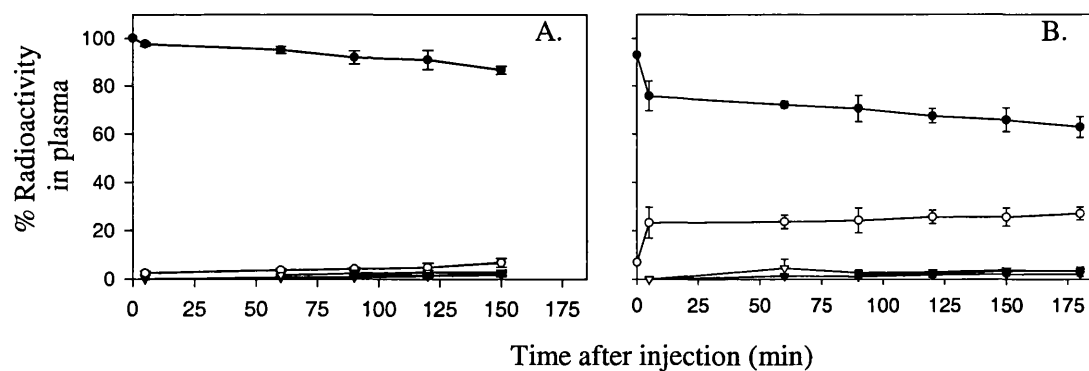


**Figure 3.8:** The percentage of radioactivity in plasma represented by  $[^{123}\text{I}]5\text{-iodo-R91150}$  (●), the void volume peak a (○) and 3 less polar metabolites b, c and d after intravenous injection of a high radiochemical purity radioligand (>98%) (A) or a lower radiochemically pure radioligand (93%) (B) in normal volunteers. Each point equals mean  $\pm$  SD ( $n=5$ ).

### 3.5 References

1. Busatto GF & Kerwin RW. Perspectives on the role of serotonergic mechanisms in the pharmacology of schizophrenia. *J Psychopharmacol.* 1997; **11**: 3-12.
2. Cowen P. Serotonin receptor subtypes: implications for psychopharmacology. *Br J Psychiatry.* 1991; **159 Suppl 12**: 7-14.
3. Hoyer D, Clarke DE, Fozard JR, Hartig PR, Martin GR, Mylecharane EJ, Saxena PR, Humphrey PP. International Union of Pharmacology classification of receptors for 5-hydroxytryptamine (serotonin). *Pharmacol Rev.* 1994; **46**: 157-203.
4. Hoyer D & Martin GR. 5-HT receptor classification and nomenclature: towards a harmonization with the human genome. *Neuropharmacology.* 1997; **36**: 419-428.
5. Kroeze WK & Roth BL. The molecular biology of serotonin receptors. Therapeutic implications for the interface of mood and psychosis. *Biol Psychiatry.* 1998; **44**: 1128-1142.
6. Kursar JD, Nelson DL, Wainscott DB, Baez M. Molecular cloning, functional expression and messenger-RNA tissue distribution of the human 5- hydroxytryptamine(2B) receptor. *Mol Pharmacol.* 1994; **46**: 227-234.
7. Pazos A, Probst A, Palacios JM. Serotonin receptors in the human brain – III. Autoradiographic mapping of serotonin<sub>2</sub> receptors. *Neuroscience.* 1987; **21**: 123-139.
8. Blue ME, Yagalow KA, Mamounas LA, Hartig PR, Molliver ME. Correspondence between 5-HT<sub>2</sub> receptors and serotonergic axons in rat neocortex. *Brain Res.* 1988; **453**: 315-328.
9. Meltzer HY. An overview of the mechanism of action of clozapine. *J Clin Psychiatry.* 1994; **55** (Suppl B): 47-52.
10. Breier A. Serotonin, schizophrenia and antipsychotic drug action. *Schizophr Res.* 1995; **14**: 187-202.
11. Roth BL, Willins DL, Kristiansen K, Kroeze WK. 5-Hydroxytryptamine<sub>2</sub>-family receptors (5-Hydroxytryptamine<sub>2A</sub>, 5-Hydroxytryptamine<sub>2B</sub>, 5-Hydroxytryptamine<sub>2C</sub>): Where structure meets function. *Pharmacol Ther.* 1998; **79**: 231-257.
12. Williams J, Spurlock G, McGuffin P, Mallet J, Nothen MM, Gill M, Aschauer H, Nylander P-O, Macciardi F, Owen MJ for the European Multicentre Association Study of Schizophrenia. Association between schizophrenia and T102C polymorphism of the 5-hydroxytryptamine type 2<sub>A</sub>-receptor gene. *Lancet.* 1996; **347**: 1294-1296.
13. Arranz M, Collier D, Sodhi M, Ball D, Roberts G, Price J, Sham P, Kerwin R. Associations between clozapine response and allelic variation in 5-HT<sub>2A</sub> receptor gene. *Lancet.* 1995; **346**: 281-282.
14. Dean B, Hussain T, Hayes W, Scarr E, Kitsoulis S, Hill C, Opeskin K, Copolov DL. Changes in serotonin (2A) and GABA(A) receptors in schizophrenia: Studies on the human dorsolateral prefrontal cortex. *J Neurochem.* 1999; **72**: 1593-1599.

15. Dean B, Tomaskovic Crook E, Opeskin K, Keks N, Copolov D. No change in the density of the serotonin (1A) receptor, the serotonin (4) receptor or the serotonin transporter in the dorsolateral prefrontal cortex from subjects with schizophrenia. *Neurochem Int.* 1999; **34**: 109-115.
16. Dean B, Hayes W, Hill C, Copolov D. Decreased serotonin (2A) receptors in Brodmann's area 9 from schizophrenic subjects – A pathological or pharmacological phenomenon. *Mol Chem Neuropath.* 1998; **34**: 133-145.
17. Chouinard G, Jones B, Remington G, Bloom D, Addington D, MacEwan GW, Labelle A, Beauclair L, Arnott W. Canadian multicentre placebo-controlled study of fixed doses of risperidone and haloperidol in the treatment of chronic schizophrenic patients. *J Clin Psychopharmacol.* 1993; **13**: 25-40.
18. Marder SR & Meibach RC. Risperidone in the treatment of schizophrenia. *Am J Psychiatry.* 1994; **151**: 825-835.
19. Beasley CM, Tollefson G, Tran P, Satterlee W, Sanger T, Hamilton S and the Olanzapine HGAD Study Group. Olanzapine versus placebo and haloperidol – acute phase results of the North American double-blind olanzapine trial. *Neuropharmacology.* 1996; **14**: 111-123.
20. Pilowsky LS, Costa DC, Ell PJ, Murray RM, Verhoeff NPLG, Kerwin, RW. Clozapine, single photon emission tomography, and the D2 dopamine receptor blockade hypothesis of schizophrenia. *Lancet.* 1992; **340**: 199-202.
21. Farde L, Norstrom AL, Wiesel FA, Pauli S, Halldin C, Sedvall G. Positron emission tomographic analysis of central D<sub>1</sub> and D<sub>2</sub> dopamine receptor occupancy in patients treated with classical neuroleptics and clozapine. Relation to extrapyramidal side effects. *Arch Gen Psychiatry.* 1992; **49**: 538-544.
22. Meltzer HY, Matsubara S, Lee JC. Classification of typical and atypical antipsychotic drugs on the basis of dopamine D<sub>1</sub>, D<sub>2</sub> and serotonin<sub>2</sub> pK<sub>i</sub> values. *J Pharmacol Exp ther.* 1989; **251**: 238-246.
23. Hoyer D, Gozlan H, Bolanos F, Schechter LE, Hamon M. Interaction of psychotropic drugs with central 5-HT<sub>3</sub> recognition sites: fact or artifact? *Eur J Pharmac.* 1989; **171**: 137-139.
24. Deutch AY, Moghaddam B, Innis RB, Krystal JH, Aghajanian GK, Bunney BS, Charney DS. Mechanisms of action of atypical antipsychotic drugs. Implications for novel therapeutic strategies for schizophrenia. *Schizophr Res.* 1991; **4**: 121-156.
25. Kristiansen K & Dahl SG. Molecular modeling of serotonin, ketanserin, ritanserin and their 5-HT<sub>2C</sub> receptor interactions. *Eur J Pharmacol.* 1996; **306**: 195-210.
26. Anderson K, Liljefors T, Gundertofte K, Perregaard J, Bøgesø KP. Development of a receptor-interaction model for serotonin 5-HT<sub>2</sub> receptor antagonists. Predicting selectivity with respect to dopamine D<sub>2</sub> receptors. *J Med Chem.* 1994; **37**: 950-962.
27. Baron JC, Samson Y, Crouzel C, Berridge M, Chretien L, Deniker P, Comar D, Agid Y. Pharmacological studies in man with PET: an investigation using <sup>11</sup>C-labeled ketanserin, a 5-HT<sub>2</sub>

- receptor antagonist. In *Cerebral Blood Flow and Metabolism Measurements*. Eds Hartman A & Hoyer S. Springer, Berlin. 1985; 471-480.
28. Biver F, Goldman S, Luxen A, Monclus M, Forestini M, Mendlewicz J, Loststra F. Multicompartmental study of fluorine-18 altanserin binding to brain 5HT<sub>2</sub> receptors in humans using positron emission tomography. *Eur J Nucl Med*. 1993; **21**: 937-946.
29. Blin J, Pappata S, Kiyosawa M, Crouzel C, Baron JC. [<sup>18</sup>F]Setoperone: a new high affinity ligand for positron emission tomography study of serotonin-2 receptors in baboon brain *in vivo*. *Eur J Pharmacol*. 1988; **147**: 73-82.
30. Lundkvist C, Halldin C, Ginovart N, Nyberg S, Swahn CG, Carr AA, Brunner F, Farde L. [C-11]MDL 100907, a radioligand for selective imaging of 5-HT<sub>2A</sub> receptors with positron emission tomography. *Life Sciences* 1996; **58**: PL187-PL192.
31. Ito H, Nyberg S, Halldin C, Lundkvist C, Farde L. PET imaging of central 5-HT<sub>2A</sub> receptors with carbon-11-MDL 100,907. *J Nucl Med*. 1998; **39**: 208-214.
32. Leysen J & Van Daele G. 4-Amino-N-(4-methyl-4-piperidiny)-2-methoxybenzamide for treating smooth muscle contraction disorders. Patent US-0549818 1996.
33. Leysen J & Van Daele G. 4-Amino-N-(4-methyl-4-piperidiny)-2-methoxybenzamide. Patent WO-09402462 1995.
34. Mertens J, Terriere D, Sipido V, Gommeren W, Janssen PMF, Leysen JE. Radiosynthesis of a new radioligand for serotonin-5-HT<sub>2</sub>-receptor, a promising tracer for gamma-emission tomography. *J Label Compd Radiopharm*. 1995; **34**: 795-806.
35. Terriere D, Janssen PMF, Gommeren W, Gysemans M, Mertens JJR, Leysen JE. Evaluation of radioiodo-4-amino-N-[1-[3-(4-fluorophenoxy)-propyl]-4-methyl-4-piperidiny]-5-iodo-2-methoxybenzamide as a potential 5-HT<sub>2</sub> receptor tracer for SPECT. *Nucl Med Biol*. 1995; **22**: 1005-1010.
36. Mertens J, Gysemans M, Bossuyt-Piron C, Thomas M. High-yield preparation of pure 2-radioiodo-ketanserin of high specific activity. A serotonin S<sub>2</sub> receptor tracer for SPECT. *J Label Compd Radiopharm*. 1990; **28**: 731-738.
37. Leysen JE. Gaps and peculiarities in 5-HT<sub>2</sub> receptor studies. *Neuropsychopharmacology*. 1990; **3**: 361-369.
38. Abi-Dargham A, Zea-Pounce Y, Terriere D, Al-Tikriti M, Baldwin RM, Hoffer P, Charney D, Leyen JE, Laurelle M, Mertens J, Innis RB. Preclinical evaluation of [<sup>123</sup>I]R93274 as a SPET radiotracer for imaging 5-HT<sub>2A</sub> receptors. *Eur J Pharmacol*. 1997; **321**: 285-293.
39. Busatto GF, Pilowsky LS, Costa DC, Mertens J, Terriere D, Ell PJ, Mulligan R, Travis MJ, Leysen JE, Lui D, Gacinovic S, Waddington W, Lingford-Hughes A, Kerwin RW. Initial evaluation of 123-I-5-R91150, a selective 5-HT<sub>2A</sub> ligand for single photon emission tomography (SPET), in healthy human subjects. *Eur J Nucl Med*. 1997; **24**: 119-124.

40. Travis MJ, Busatto GF, Pilowsky LS, Mulligan R, Acton PD, Gacinovic S, Mertens J, Terriere D, Costa DC, Ell PJ, Kerwin RW. 5-HT<sub>2A</sub> receptor blockade in patients with schizophrenia treated with risperidone or clozapine. A SPET study using the novel 5-HT<sub>2A</sub> ligand <sup>123</sup>I-5-I-R-91150. *Br J Psychiatry*. 1998; **173**: 236-241.
41. Travis MJ, Visvikis D, Erlandsson K, Mulligan RS, Waddington WA, Matthiasson P, Pilowsky LS, Costa DC, Ell PJ, Kerwin RW. Dynamic displacement of the selective 5-HT<sub>2A</sub> receptor ligand I-123-5-I-R91150 by unlabelled ketanserin. *J Nucl Med*. 2000; **41**: 935.
42. Eersels J.K.H, personal communication, Radionuclide Centre, Vrije Universiteit, De Boelelaan 1085c, 1081 HV Amsterdam, The Netherlands.
43. Eersels JLH & Herscheid JDM. O-Iodohuppuric acid as stabilizer against deiodination of I-123-radiopharmaceuticals. *J Label Compd Radiopharm*. 2001; **41**: S939-S941.
44. Mazière B, Cantineau R, Coenen HH, Guillaume M, Halldin C, Luxen A, Loc'h C, Luthra SK. PET radiopharmaceutical metabolism – plasma metabolite analysis. In *Radiopharmaceuticals for Positron Emission Tomography*. Eds Stöcklin G & Pike VW. Kluwer Academic Publishers, Dordrecht. 1993; 151-178.
45. Tan P-Z, Baldwin RM, van Dyck CH, Amici L, Al-Tikriti M, Roth B, Khan N, Fowler JS, Shea C, Soufer R, Charney DS, Innis RB. Identity and receptor binding of radiometabolites of the 5-HT<sub>2A/2C</sub> ligand [F-18]altanserin. *J Nucl Med*. 1997; **38**: 287P.
46. Mason NS, Huang Y, Holt DP, Perevuznik JJ, Lopresti BJ, Mathis CA. Synthesis and characterization of [F-18]4-(4-fluorobenzoyl)piperidine, and [F-18]altanserin metabolite. *J Nucl Med*. 1997; **38**: 56P.

## ***Chapter 4***

### ***Synthesis of precursors for prospective imaging agents for 5-HT<sub>2A</sub> receptors***

## 4.1 Introduction

The aim of this work was to synthesise [4-amino-*N*-[1-3-(4-fluorophenoxy)propyl]-4-methyl-4-piperidinyl]-2-methoxybenzamide (R91150) **1** and the phenol analogue **2** (Figure 4.1). Both compounds were intended to be used as precursors for radiolabelling, with carbon-11 and iodine-123 in order to develop new potential PET and SPET radioligands for the imaging of the 5-HT<sub>2A</sub> receptor system in humans.

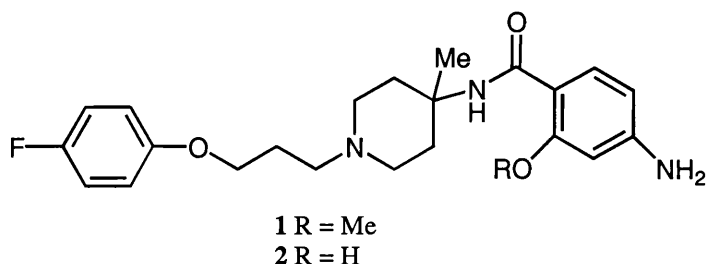


**Figure 4.1:** Precursors for potential 5-HT<sub>2A</sub> radioligands.

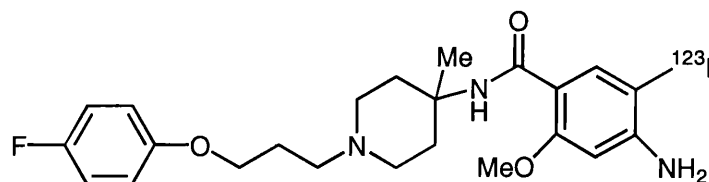


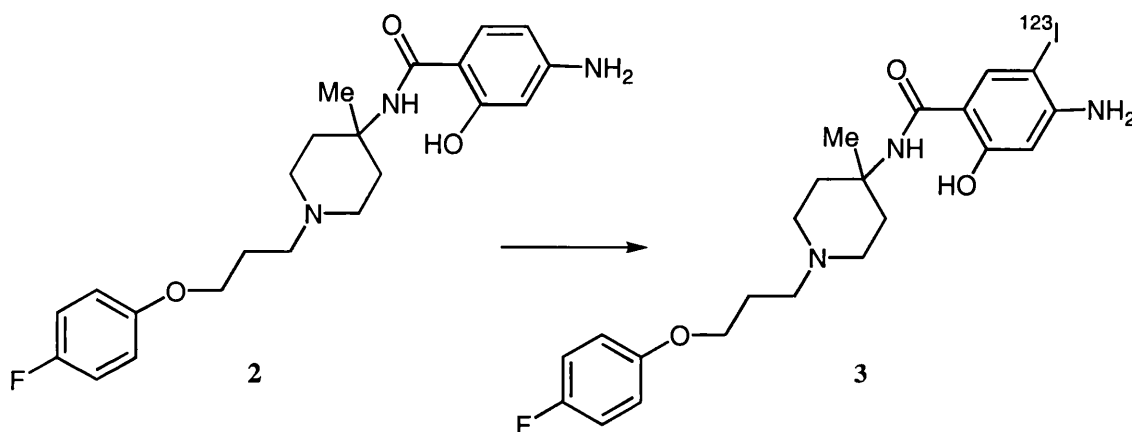
**Figure 4.2:** Structure of 5-iodo-R91150.

Janssen Pharmaceutical Company (Belgium) investigated a series of 5-HT<sub>2A</sub> receptor antagonists as potential radioligands for imaging this population of receptors.<sup>1,2</sup> From this series, the 5-iodo derivative of R91150 (Figure 4.2) has proven to be a potent and selective radioligand for the 5-HT<sub>2A</sub> receptor *in vitro*<sup>1-4</sup> and *in vivo*.<sup>4-6</sup> In living humans, [<sup>123</sup>I]5-iodo-R91150 gives displaceable radioactivity in the 5-HT<sub>2A</sub> receptor-rich frontal cortex that is 1.4 times greater than the level of radioactivity observed in the receptor-devoid cerebellum.<sup>6-8</sup> In addition [<sup>123</sup>I]5-iodo-R91150 has favourable pharmacokinetics for SPET in humans with rapid clearance from plasma and very low metabolism *in vivo*.<sup>9</sup>

One of the characteristics of 5-iodo-R91150 that could be improved is the relatively low receptor-specific signal that it gives in areas with high 5-HT<sub>2A</sub> receptor density. A possible explanation for this low signal is a high level of binding to plasma proteins throughout the brain. Plasma protein binding is related to lipophilicity. For successful neuroimaging agents, lipophilicity has to be high enough to support diffusion across the blood-brain barrier without causing excessive plasma protein binding. A logP between 1.7 and 2.5 is considered conducive to a useful brain signal.<sup>10</sup> A measured logP for 5-iodo-R91150 is not available. However, the calculated logP is 3.70 (Chemdraw Ultra). Any analogues of 5-iodo-R91150 with a lower lipophilicity but similar binding characteristics might give a higher signal to noise ratio and prove to be a more useful imaging agent.

However, it should be noted that only 2% of the injected dose of [ $^{123}\text{I}$ ]5-iodo-R91150 crossing the blood-brain barrier. Therefore, lowering lipophilicity could reduce or even prevent brain penetration.

One potential SPET radioligand that could provide an alternative agent for imaging 5-HT<sub>2A</sub> receptors is the phenol derivative of [ $^{123}\text{I}$ ]-5-iodo-R91150 **3**. A possible strategy for the preparation of this radioligand is illustrated in Figure 4.3. To date, all the antagonists reported by the Janssen Pharmaceutical Company contain a methoxy substituent on the benzamido group.<sup>1,2</sup> However, the nature of the substituents on the benzamido group of R91150 appears to have little effect on affinity or selectivity (J. Mertens, personal communication); radioligand **3** would be expected to have affinity and selectivity for the 5-HT<sub>2A</sub> receptor similar to 5-iodo-R91150. In theory, replacing the methoxy group with the phenol should reduce the lipophilicity, which in turn could increase the specific radioactive signal in receptor-rich regions. However, the phenol group is also susceptible to glucuronidation, which could increase its metabolism *in vivo*. The efficacy of this compound would depend on the balance of all of these factors.



**Conditions:** Na[ $^{123}\text{I}$ ]I, peracetic acid

**Figure 4.3:** Possible strategy for the radiolabelling of the phenol derivative of R91150 by direct iodination.

At present there are a very limited number of PET radioligands for selective imaging of the 5-HT<sub>2A</sub> receptor. The most commonly employed PET radioligand for this purpose is the highly selective (*R*)-(+)-4-[1-hydroxy- (2,3-dimethoxyphenyl) methyl] -N-2- (4-fluorophenylethyl)piperidine ([3-methoxy- $^{11}\text{C}$ ]MDL 100907, Figure 4.4). The affinity of MDL 100907 for the 5-HT<sub>2A</sub> receptor is similar to that of 5-iodo-R91150 ( $K_i = 0.2 \text{ nM}^{11}$  and  $0.1 \text{ nM}^4$ , respectively). In baboons, ratios of radioactivity in the receptor-rich neocortex, to receptor-devoid cerebellum of 3.5–4.5 have been observed 60–80 min after injection of [ $^{11}\text{C}$ ]MDL 100907.<sup>11</sup> However, [ $^{11}\text{C}$ ]MDL 100907 is rapidly

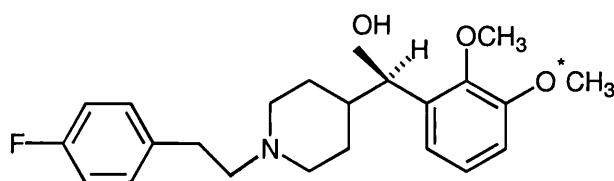


**Figure 4.4:** Structure of MDL 100907. \* indicates the site of radiolabelling



metabolised *in vivo*, with unchanged parent radioligand representing only 25–30% of the radioactivity in the plasma 40 min after injection in baboons.<sup>11</sup> This drops further to only 10% at 90 min after injection.<sup>12</sup> In humans, a slightly lower extent of metabolism has been observed. However, only 40% of the total radioactivity in plasma 50 min after injection was attributed to unchanged parent radioligand.<sup>13</sup> The rapid rate of metabolism of [<sup>11</sup>C]MDL 100907 could prove to be an obstacle in the quantification of receptor binding kinetics for this radioligand.

There are a number of novel carbon-11 labelled ligands that could be prepared for PET from R91150 **1** or the free phenol **2** (Figures 4.5 and 4.6). Removal of the iodine from 5-iodo-R91150 will have no significant effect on 5-HT<sub>2A</sub> affinity and selectivity<sup>1,2</sup> but would have an added benefit of reducing the lipophilicity and perhaps the level of non-specific binding in the brain. In order to test this hypothesis the precursors for these potential radioligands needed to be synthesised.

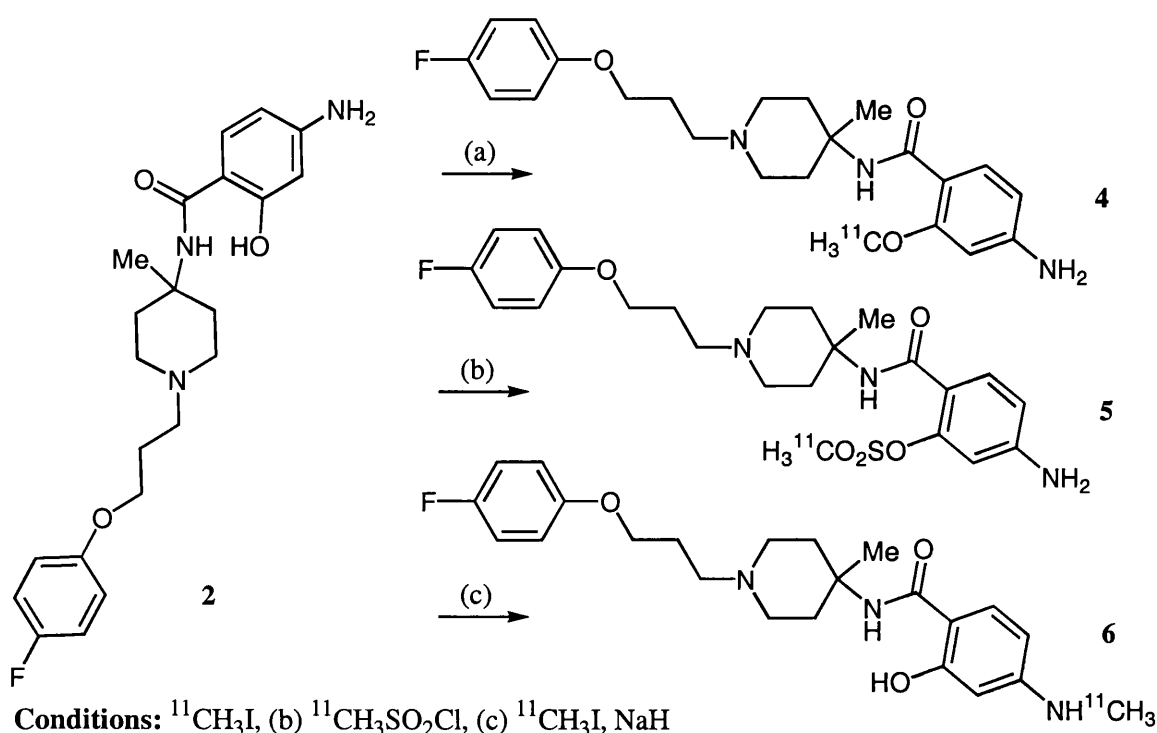


**Figure 4.5:** Possible labelling strategies for the synthesis of potential PET radioligands for the 5-HT<sub>2A</sub> receptor.

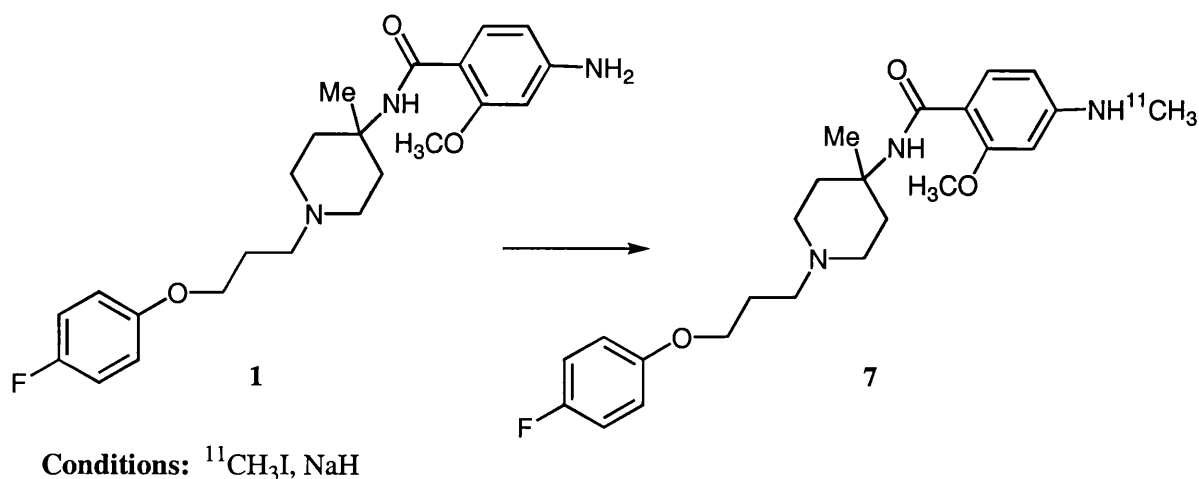


**Figure 4.6:** Pathway for the synthesis of a PET radioligand for imaging the 5-HT<sub>2A</sub> receptor using R91150 as a precursor.

## 4.2 Results and Discussion

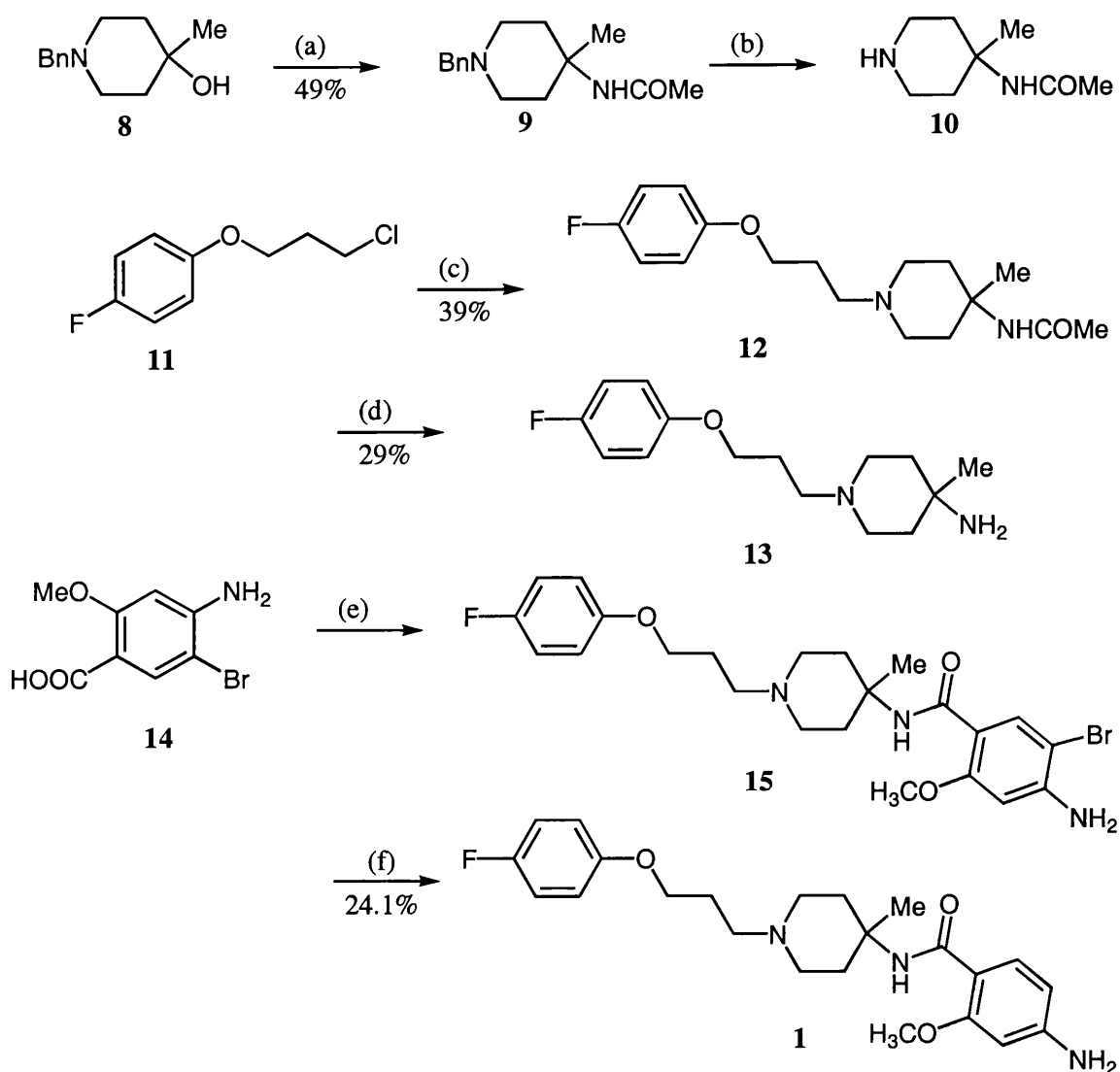
### 4.2.1 Lipophilicity of potential radioligands

The computer calculated logP for 5-iodo-R91150 (3.70) is higher than the corresponding values obtained for the potential radioligands discussed above. Thus, the iodinated free phenol **3**, has a calculated logP value of 3.43. This is slightly lower than 5-iodo-R91150 and would support the ideal compromise between diffusion across the blood-brain barrier and reduced binding to non-specific sites in the brain. The methoxybenzamide **4** and the *N*-methylenamides **6** and **7** have calculated logP values of 2.34, 2.38 and 2.64, respectively. If brain penetration is maintained, these compounds could be useful alternative for imaging 5-HT<sub>2A</sub> receptors with PET. The logP of 1.37 calculated for the mesylated amide **5** would not support brain uptake given that with [<sup>123</sup>I]5-iodo-R91150 only 2% of the injected dose is able to cross the blood-brain barrier. While there are questions surrounding the accuracy of calculated logP values, they do provide useful information that can be used comparatively to determine the most promising candidates.

### 4.2.2 Synthesis and strategy

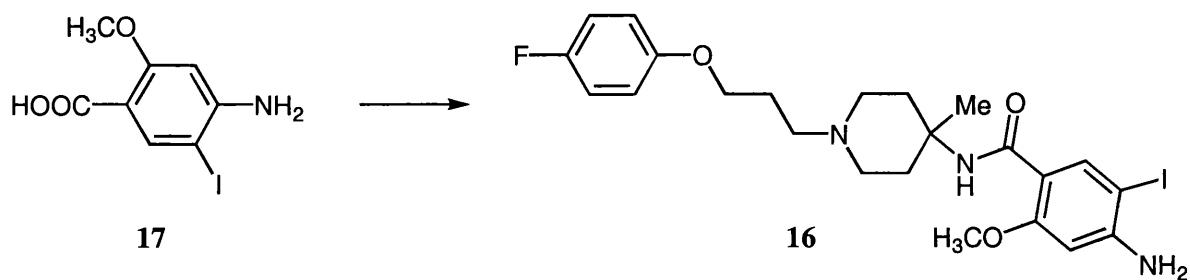
Leysen and Van Daele<sup>1,2</sup> have patented a synthesis of R91150 (Figure 4.7). In this patent a Ritter reaction has been employed to *N*-acetylate the starting material **8** to give the acetamide derivative **9**, which in turn has been hydrogenated in the presence of palladium-on-charcoal catalyst to deprotect the secondary amine. The key intermediate, 1-[3-(4-fluorophenoxy)propyl-4-methyl-4-piperidinamine **13** has been synthesised by coupling acetamide **10** with fluorophenoxypropyl chloride **11** to form acetamide **12**, followed by hydrolysis with concentrated hydrochloric acid. This key amine was coupled with various halogen-substituted analogues of 4-amino-2-methoxybenzoic acid (*e.g.* **14**, Figure 4.7) to prepare a number of potential 5-HT<sub>2A</sub> antagonists (*eg.* **15**, Figure 4.7). R91150 has been synthesised by the coupling of amine **13** with a bromine-substituted benzamide, followed by debromination (Figure 4.7). 5-Iodo-R91150 **16** has been prepared in 38% yield by coupling amine **13** with 4-amino-5-iodo-2-methoxybenzamide **17** (Figure 4.8).<sup>1,2</sup> It was considered that the desired precursors **1** and **2**, might be synthesised similarly from amine, **13**, and the benzoic acid, **19**, or salicylic acid, **18**, respectively (Figure 4.9).

The only reported coupling reactions with amine **13** has used analogues of salicylic acid with the phenol group protected as the methyl ether.<sup>1,2</sup> However, no literature is available on how to prepare these analogues. It was considered that 4-amino-salicylic acid **18**, which is commercially available, might be employed directly in the key coupling reaction for the synthesis of precursor **2**. However, the presence of the free phenol and amino groups may affect the reactivity of **18** and its subsequent ethyl formate derivative **20**, formed *in situ* in the coupling reaction (Figure 4.10). Protection of the phenol and/or the amino groups may be necessary for successful coupling. The choice of protective groups has to take into account the need for selective deprotection in order to afford the optimum number of potential precursors, which could be evaluated for utilisation in the crucial coupling reaction.



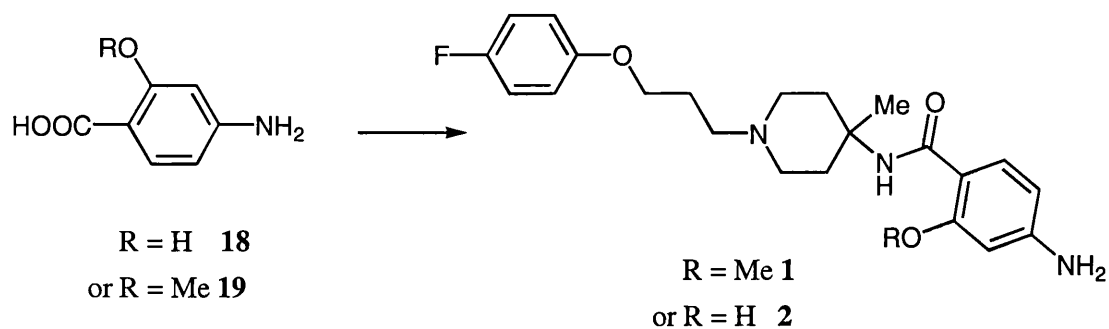
**Conditions:** (a)  $\text{H}_2\text{SO}_4/\text{MeCN}$ , 20 h RT, (b)  $\text{H}_2$  Pd/C, RT (c)  $\text{Et}_3\text{N}$ , DMF, KI, 1.5 h,  $70^\circ\text{C}$ , (d) *conc.* HCl, reflux 24 h (e) i)  $\text{Et}_3\text{N}$ ,  $\text{CH}_2\text{Cl}_2$ ,  $<5^\circ\text{C}$ , 15 min, ii)  $\text{ClCO}_2\text{Et}$ ,  $<5^\circ\text{C}$ , 1 h, iii) amine **13**, RT, o/n (f)  $\text{CaO}$ ,  $\text{H}_2$ , Pd/C

**Figure 4.7:** Synthetic strategy for R91150 as reported by Leysen and van Daele.<sup>1,2</sup>



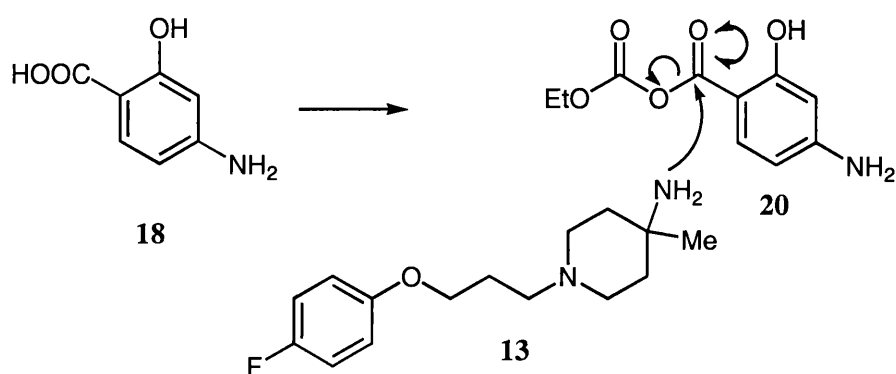
**Conditions:** i)  $\text{Et}_3\text{N}$ ,  $\text{CH}_2\text{Cl}_2$ ,  $<5^\circ\text{C}$ , 15 min, ii)  $\text{ClCO}_2\text{Et}$ ,  $<5^\circ\text{C}$ , 1 h, iii) amine **13**, RT o/n

**Figure 4.8:** Reported synthesis of 5-iodo-R91150.<sup>1,2</sup>



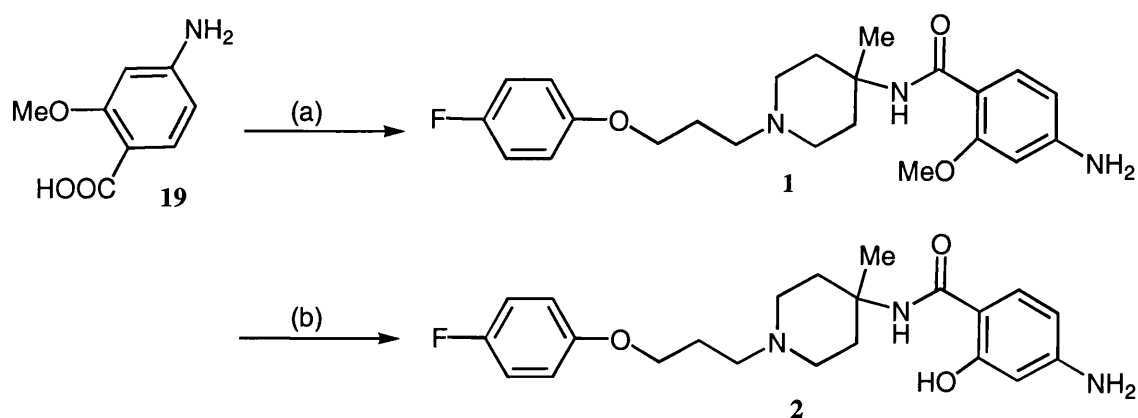
**Conditions:** i)  $\text{Et}_3\text{N}$ , ii)  $\text{ClCO}_2\text{Et}$ , iii) amine **13**

**Figure 4.9:** Proposed synthesis of precursors **1** and **2** by direct coupling with amine **13**



**Conditions:** i)  $\text{Et}_3\text{N}$ , ii)  $\text{ClCO}_2\text{Et}$

**Figure 4.10:** Proposed mechanism for the coupling of 4-amino salicylic acid **18** with amine **13** to form the desired precursor **2**



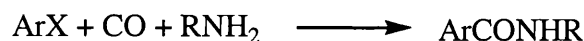
**Conditions:** (a) i)  $\text{Et}_3\text{N}$ , ii)  $\text{ClCO}_2\text{Et}$ , iii) amine **13** (b)  $\text{BBr}_3$

**Figure 4.11:** Possible pathway for the synthesis of R91150 **1** and the phenol analogue **2**

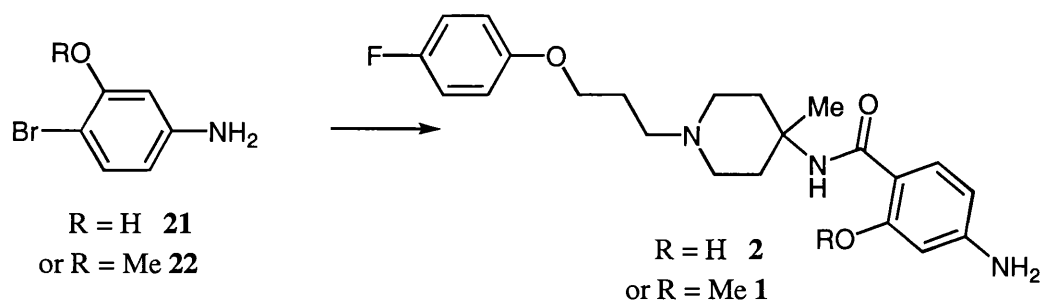
The most direct route would be to selectively methylate the phenol group of **18** to provide the suitable precursor, **19**, for the synthesis of both **1** and **2** (Figure 4.11). Unfortunately, there are inherent problems in using the methyl ether **19** to synthesise **2**, due to the strong acidic conditions (such as the use of boron tribromide)<sup>14</sup> traditionally needed to remove the methyl protective group. Such conditions may also result in the cleavage of the amide and the other ether linkage in the molecule. It may be that protection of the amino group alone is sufficient to ensure a fruitful coupling with amine **13**.

The aim was to protect the amino and phenol groups of 4-aminosalicylic acid thereby forming an intermediate carboxylic acid that could be activated in the presence of ethyl chloroformate and base. It is possible that the relative positions of the three substituents in 4-aminosalicylic acid could cause problems during protection reactions as well as during the crucial coupling with amine **13**.

In addition to investigating the use of analogues of 4-aminosalicylic acid, an alternative strategy was proposed that should eliminate the competition between the amino and phenol substituents with the acid group during protection reactions or the final coupling with amine **13**. Aryl bromides and iodides, when treated with carbon monoxide, an amine, a base and a palladium complex catalyst, give the relevant amide.<sup>15</sup>

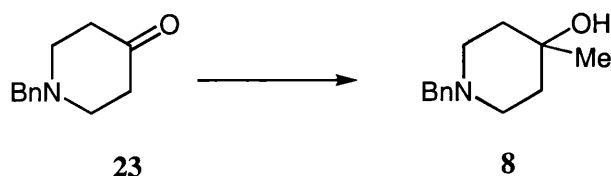


It is possible that amine **13** could be coupled to 2-bromo-5-aminophenol **21** or 2-bromo-5-methoxyaniline **22** to produce the desired precursors **1** and **2** (Figure 4.12). Neither of the aryl bromides were commercially available but might be synthesised by brominating 3-aminophenol and 3-methoxyaniline, respectively. Electron-rich arenes are readily brominated by direct treatment with bromine.<sup>15</sup> However, for active substrates such as aminoarenes, control of the position and number of substitutions under these conditions is difficult leading to undesirable di-, and possibly tri-bromination. A variety of reagents other than bromine have been reported for the bromination of arenes. A literature search revealed that *N*-bromosuccinimide has been used to synthesis 2-bromo-5-aminophenol from 3-aminophenol.<sup>16</sup> Paul *et al.*<sup>16</sup> reported that monobromination occurred in 84% yield when the aminophenol, in carbon tetrachloride was treated with *N*-bromosuccinimide. The



**Conditions:** amine **13**, CO, Pd(0), base

**Figure 4.12:** Palladium-catalysed carbonylation as an alternative pathway for the synthesis of precursors **1** and **2**.



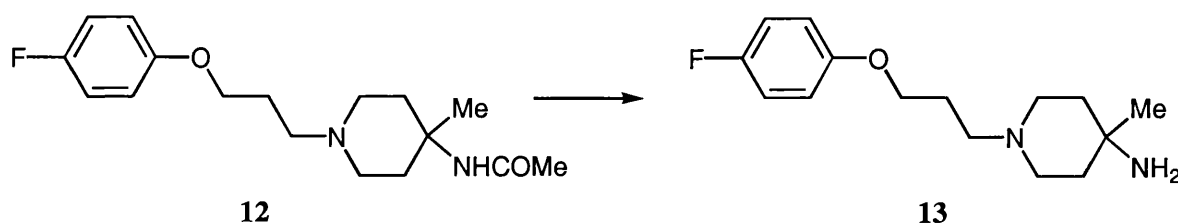
**Conditions:** MeMgBr, Et<sub>2</sub>O

**Figure 4.13:** Proposed reaction conditions for alkylation of ketone **23**.

reported ratio of the desired *para* to the undesired *ortho* substitution was 6 to 1. The regioselectivity for *para* bromination was improved to 30 to 1 by addition of the zeolite catalyst, HZSM-5.<sup>16</sup> This method could be used for the synthesis of the amino phenol **21** and the methoxy aniline **22**, since both the phenol and methoxy groups are *ortho*- and *para*- directing substituents.

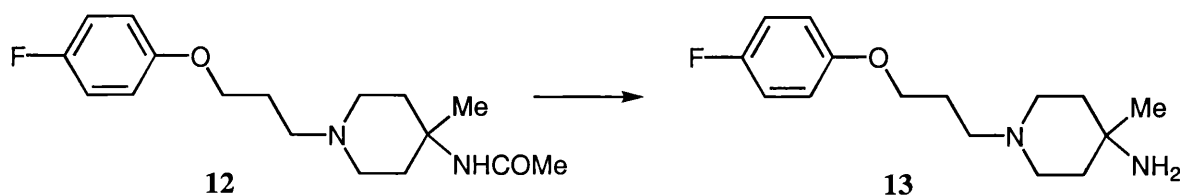
The patented strategy for the synthesis of amine **13** has a number of problems including incomplete details in the experimental section, limited characterisation of key intermediates, lack of starting material and the very low yields reported for a number of the reactions. 4-Methyl-1-(phenylmethyl)-4-piperidinol **8** was not commercially available and development of a method for its synthesis was required. It was decided that **8** might be prepared from the commercially available 1-benzyl-4-piperidone **23** via a Grignard alkylation employing methylmagnesium bromide (Figure 4.13).

One of the key problematic reactions in Leysen and Van Daele's methodology<sup>1,2</sup> was identified as the hydrolysis of acetamide **12** to amine **13** using *conc.* HCl, which had given a yield of only 29% (Figure 4.7d). The low yield may be due to the cleavage of the fluorobenzyl ether of R91150 in the strongly acidic conditions. A literature search identified two alternative reaction conditions for deprotection of acetamides, that might be applied to the deacylation of **12** (Figures 4.14 and 4.15). Keith *et al.*<sup>17</sup> reported that deprotection of an acetamide can be achieved in good yield by treatment with 85% hydrazine hydrate at 70°C for 15 h. Alternatively, Dilbeck *et al.*<sup>18</sup> found that



**Conditions:** 85% H<sub>2</sub>NNH<sub>2</sub>, 70°C, o/n

**Figure 4.14:** Alternative pathway for acetamide deprotection using basic conditions.<sup>16</sup>



**Conditions:** 2 M aqueous HCl, reflux, 48 h

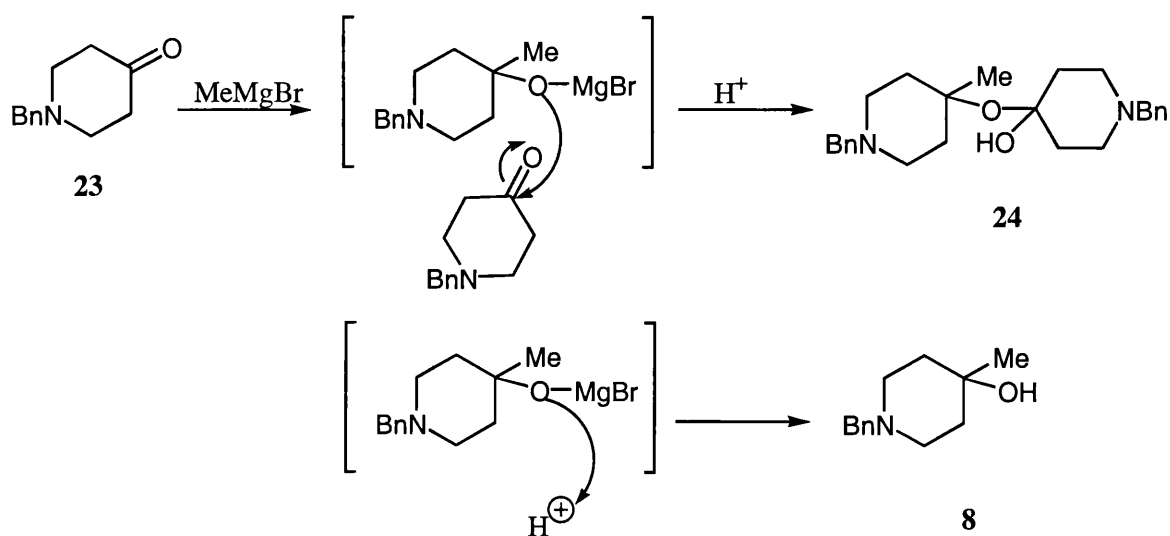
**Figure 4.15:** Alternative reaction conditions for deprotection of *N*-acetyl derivatives.<sup>17</sup>

deprotection occurred in good yield when an *N*-acetyl derivative in 2N hydrochloric acid was heated at reflux for 60 h. A lower concentration of HCl or the use of basic conditions was expected to provide improved yields of amine **13**.

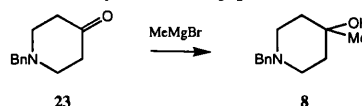
#### 4.2.3 Results from attempted organic synthesis

##### 4.2.3.1 Formation of 4-methyl-1-benzyl-4-piperidinol **8** from 1-benzyl-4-piperidone **23**

The standard procedure for the alkylation of Grignard reagents is to add an ethereal solution of the ketone to one equivalent of Grignard reagent under an inert atmosphere and then heat to reflux.<sup>19</sup> These reactions are generally slow, requiring up to 4 h to reach completion. Initial reactions for the alkylation of ketone **23** were undertaken using these standard conditions. However, aldol condensation gave a significant amount of dimer **24** with the desired product **8** (Figure 4.16). Dimer formation resulted from the reaction of the intermediate, formed in the presence of methylmagnesium bromide, reacting with the starting ketone **23** (Figure 4.16). A series of reactions were undertaken to investigate the effect of solvent, temperature, reaction time and reactant concentration in order to improve the product yield (Table 4.1). In all of the experiments using a 1.2 molar equivalent of Grignard reagent, dimer **24** was formed in addition to the desired product **8**. Changing the solvent from diethyl ether to tetrahydrofuran improved the workup procedure but did not eliminate aldol condensation and the resulting dimer formation. At reflux the reaction did not proceed to completion. Reducing the reaction temperature (20°C) improved the consumption of starting material but not the product vs dimer ratio. A further reduction in temperature to -8°C lead to very low, relative yields of **8** and **24**, and large amounts of unreacted ketone **23**. With 1.2 molar equivalents of Grignard reagent the best product to dimer ratio was obtained from a 5 min reaction at ambient temperature. Half the amount of ketone **23** was converted into the desired product with insignificant aldol condensation. Using the same reaction conditions but increasing the molar equivalents of methylmagnesium bromide



**Figure 4.16:** Proposed mechanisms behind aldol condensation and alkylation of ketone **23** in the presence of 1.2 equivalents of Grignard reagent.

**Table 4.1** Reaction conditions investigated for the Grignard reaction:

Solvent	Molar equivalents of MeMgBr	Temperature (°C)	Reaction time (min)	% Yield of <b>8</b>
Et <sub>2</sub> O	1.2	To reflux	120	7
THF	1.2	RT	240	10
THF	1.2	RT	90	10
THF	1.2	RT	30	10
THF	1.2	RT	15	20
THF	1.2	RT	5	50
THF	1.2	RT	2	40
THF	1.2	RT	1	40
THF	1.2	-8°C	30	10
THF	1.2	-8°C	15	10
THF	1.2	-8°C	5	5
THF	2	RT	5	100

to two, produced the desired alcohol quantitatively and eliminated dimer formation. Increasing the excess of Grignard reagent five-fold appeared to increase the conversion of ketone **23** to the reactive intermediate and reduce the amount of ketone **23** that could participate in aldol condensation and dimer formation.

#### 4.2.3.2 *N*-[1-(Benzyl)-4-methyl-4-piperidinyl]acetamide hydrochloride **9**

Initial attempts to *N*-acetylate piperidinol **8** following the procedure outlined by Leysen and Van Daele<sup>1,2</sup> resulted in highly variable yields (12–30%) of the desired product **9**. Maintaining the reaction temperature at 70°C during sulphuric acid addition resulted in more consistent yields of about 30%. This was closer to the published yield of 49%.<sup>1,2</sup> During the addition of acid the temperature of the reaction increased rapidly causing evaporation of the solvent thereby increasing the reactions medium viscosity, making stirring difficult. The colour of the reaction at the completion of acid addition gave some indication of the success of the reaction with a yellow reaction leading to higher yields of acetamide **9** than a brown reaction mixture.

#### 4.2.3.3 *N*-[4-Methyl-4-piperidinyl]acetamide hydrochloride **10**

Amine deprotection of **9** was obtained with optimal yields using the procedure outlined by Leysen and Van Daele.<sup>1,2</sup> The reaction was monitored by the loss of light absorbance at 254 nm (starting



material), and the appearance of a deep purple spot which developed when acetamide **10** reacted with ninhydrin and heat.

#### 4.2.3.4 1-(3-chloropropoxy)-4-fluorobenzene **11**

Fluorobenzene **11** was commercially obtained at 85% purity. No other commercial source was available. Analytical data obtained with this compound identified the other 15% as the bromo analogue. Both the bromo and chloro compounds should behave in a similar manner during coupling to *N*-[4-methyl-4-piperidinyl]acetamide hydrochloride **10** so this level of purity was believed to be acceptable.

#### 4.2.3.5 *N*-[1-[3-(4-Fluorophenoxy)propyl]-4-methyl-4-piperidinyl]acetamide **12**

The synthesis was first attempted under the conditions established by Leysen and Van Daele.<sup>1,2</sup> The reaction was followed by T.L.C. The desired product was isolated from the crude mixture by flash column chromatography, and structurally identified by <sup>1</sup>H- and <sup>13</sup>C-NMR (Figure 4.17). The integration of the <sup>1</sup>H-NMR revealed the appropriate number of proton signals to indicate coupling was successful. However, the presence of nine proton signals ( $\text{—O—CH}_2\text{CH}_2\text{CH}_2\text{—N(CH}_2)_4\text{C—CH}_3^{\text{NHC(=O)CH}_3}$ ) indicated that each group of protons were magnetically different and therefore resonated with different chemical shifts. The spectra from a <sup>1</sup>H-<sup>1</sup>H COSY experiment (Figure 4.18) allowed the 4 piperidine proton signals at 1.52, 2.05, 2.20 and 2.52 ppm to be distinguished from the methyl and propyl proton signals. While the exact assignment of these 4 piperidine proton signals to the respective proton pairs, C(2), C(5), C(3) and C(4) was not possible, <sup>1</sup>H-<sup>13</sup>C coupling affirmed that the proton signals at 1.52 and 2.05 ppm corresponded to the C(2) and C(5) protons. Similarly, the C(3) and C(4) protons could be assigned to the proton signals at 2.21 and 2.52 ppm.

Unfortunately, the yield of pure **12** from the first experiment was only 16%, significantly lower than that reported by Leysen and Van Daele (39%).<sup>1,2</sup> UV spectral analysis of this product revealed low absorption of light at 254 nm, the wavelength of light used for compound detection on T.L.C. Therefore, a reverse phase HPLC method was developed using an absorbance detection for light at 280 nm to monitor preliminary, and further reactions. Isolated coupled product **12**, identified structurally by NMR analysis, eluted on the HPLC system with a retention time of 6 min, compared with 21 min for fluorobenzene **11**. Acetamide **10** did not absorb light at this, or any other wavelength and could not be monitored by HPLC. HPLC analysis of the earlier reactions revealed 688 mg (63%) of unconverted fluorobenzene **11**, indicating the reported reaction conditions were sub-optimal. In addition, a broad band of impure fractions from the flash column purification contained the desired product **12** with either a yellow oil impurity that was formed in conjunction with the desired product or acetamide **10**. HPLC analysis of impure fractions containing the yellow oil revealed a second peak with high absorbance at 280 nm eluting at 6.5 min. The close retention times for the desired product (6 min) and the unidentified impurity (6.5 min) indicated that further purification of **12** after initial flash column chromatography would be difficult. Starting material **10** was recovered when the column was eluted with 100% methanol. However, fractions containing acetamide **10** also contained

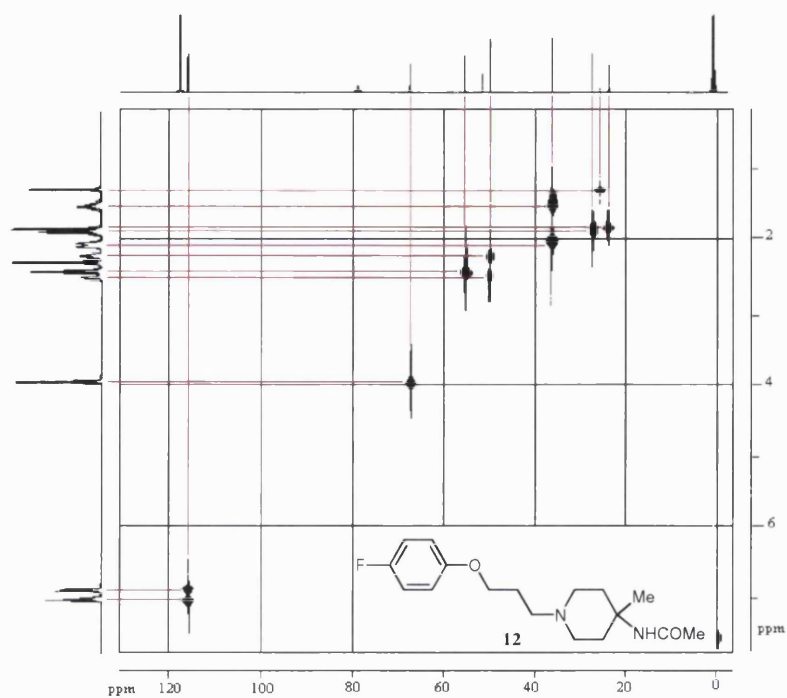


**Figure 4.17:** NMR spectra obtained from a  $^1\text{H}$ - $^{13}\text{C}$  COSY experiment on pure **12**.

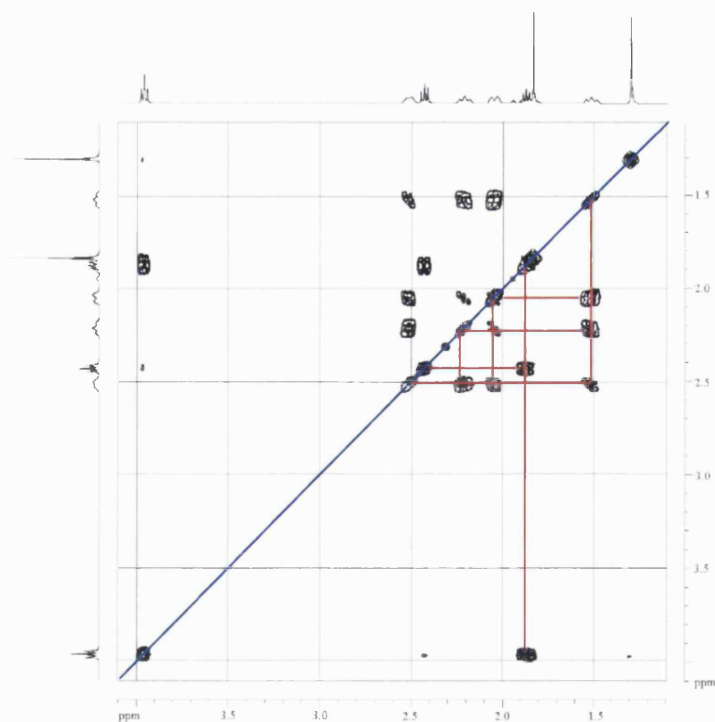


**Figure 4.18:** NMR spectra obtained from a  $^1\text{H}$ - $^{13}\text{C}$  COSY experiment on pure **12**.

Base	10: base equivalents	Temp.	Reaction time (h)	Product 12: Impurity: fluorobenzene 11: other peaks
Et <sub>3</sub> N/DMF	6	160°C	1	1: 0.02: 0.0045: 0.94
			1.5	1: 0.01: 0.016 : 0.81
NaOH/MeOH	2.4	RT	16	1: 0.07: 3.70 : 0.42
NaH/DMF	1.2	RT	16	1: 0.11: 5.60 : 1.63
KH/DMF	2.4	RT	16	1: 1.10: 13.20 : 5.20
Pyridine		RT	70	1: 3.50: 428 : 50.2
Hunig's base	2.4	RT	70	1: 0.10: >>9 : 1.58

**Table 4.2:** Experiments investigating possible bases for the coupling to form **12**. The ratios represent the relative integrated areas for the respective HPLC peaks.

the desired product **12** indicating that, in addition to sub-optimal reaction conditions, the method for purification reported by Leysen and Van Daele<sup>1,2</sup> using only 5% methanol is unsatisfactory.

Different reaction conditions were investigated to try and eliminate the formation of the unidentified impurity and maximise the consumption of the fluorobenzene **11** (Table 4.2). Unfortunately, it was not possible to eliminate completely the formation of the previously observed impurity. However, increasing the molar ratio of triethylamine to acetamide **10** from 2.4 to 4 and 6 for reactions carried out at 90°C increased the amount of desired product **12** to 26 and 28%, respectively. In one experiment with 6 equivalents of triethylamine, a further increase in reaction temperature completely converted the fluorobenzene **11**. Unfortunately, this was also associated with an increase in the number and amount of impurities and could not be repeated. None of the other bases investigated were as successful as triethylamine in forming the desired product. Both potassium and sodium hydride were too basic resulting in decomposition of **11**. The other bases investigated namely, sodium hydroxide, pyridine and Hunig's base formed amine **12** but provided considerably lower yields than observed when triethylamine was employed.

Initially alternative purification methods were investigated, such as recrystallisation since the unidentified impurity was insoluble in di-isopropyl ether. The aim was to establish reaction conditions that lead to a total conversion of 1-(3-chloropropoxy)-4-fluorobenzene **11** since its high solubility meant that its removal from the crude reaction by recrystallisation was not an option.

Unfortunately, consistent results for any given reaction condition were not obtained. HPLC profiles suggests that the purchased 1-(3-chloropropoxy)-4-fluorobenzene **11** was decomposing. With a new batch of fluorobenzene **11**, a reduction in the formation of the unidentified impurity was observed. However, complete conversion of the new batch of fluorobenzene **11** was not seen, even under conditions that had previously been successful in this respect. The inconsistencies observed

with this reaction suggested that yield optimisation was going to be time consuming. Since this reaction was not the primary focus of this thesis, a stock of acetamide **12** was obtained using conditions that gave the most consistent yield irrespective of the batch of fluorobenzene **11**. Therefore, six equivalents of triethylamine were used with the reaction mixture heated to 90°C for 1.5 h followed by flash column purification using chloroform and methanol as eluent. The percentage of methanol in the column eluent was increased in a gradient from 5 % to 100% to ensure full recovery of the desired product **12** off the column. Loss of product due to impure fractions was considered acceptable for the purposes of this work. Under these reaction conditions the overall yield of pure product **12** was 26%. It should be noted that the 39% yield reported by Leysen & Van Daele<sup>1,2</sup> was never obtained.

#### 4.2.3.6 1-[3-(4-Fluorophenoxy)propyl]4-methyl-4-piperidinamine **13**

Keith *et al.*<sup>17</sup> reported acetamide deprotection in good yield following treatment with hydrazine hydrate. These basic conditions failed to hydrolyse acetamide **12** with 100% of the starting material recovered. One possible explanation is the lower concentration of hydrazine hydrate available (55% compared with 85%).

The published method for hydrolysis of acetamide **12** used *c.* HCl which afforded amine **13** in only 19% yield.<sup>1,2</sup> Reducing the concentration of hydrochloric acid to 2M with a longer reaction time was not only successful in deprotecting acetamide **12**, but lead to 100% yield, eliminating undesirable side reactions, and the need for purification. Total conversion was only possible when fresh hydrochloric acid was used. This was a significant improvement on the literature procedure, which afforded 29% of amine **13**, and has turned an unacceptably low yielding reaction into a highly viable one.

#### 4.2.3.7 Model Coupling Reactions

Conditions for the final coupling of amine **13** with 4-amino salicylic acid were explored using a model system. The readily available 1-methyl cyclohexylamine **25** (Figure 4.19) and 4-amino salicylic acid **18** were utilised to test the conditions reported by Leysen and Van Daele<sup>1,2</sup> for coupling 4-amino salicylic acid with amine **13** to form the target precursor **2**. Reactions conditions identical to those published by Leysen and Van Daele<sup>1,2</sup> could not be used for 4-amino salicylic acid due to its insolubility in dichloromethane. Therefore, the solvent was changed to tetrahydrofuran, and finally to dimethylformamide. A solution of 4-amino salicylic acid in dimethylformamide was treated with triethylamine at a low temperature for 15 min, after which, ethyl chloroformate was added and stirred for a further hour. The reaction temperature was allowed to reach 10°C during the addition of 1-methyl cyclohexylamine in dimethylformamide and the reaction mixture was stirred at ambient temperature overnight. Coupling of salicylic acid **18** with amine **25** was unsuccessful in all solvents investigated, with 1-methyl cyclohexyl acetamide **26** formed as the main product (Figure 4.19). There are two possible ways in which this unwanted product may have been formed. Successful coupling under these reaction conditions would normally proceed via acid activation to an ethyl formate

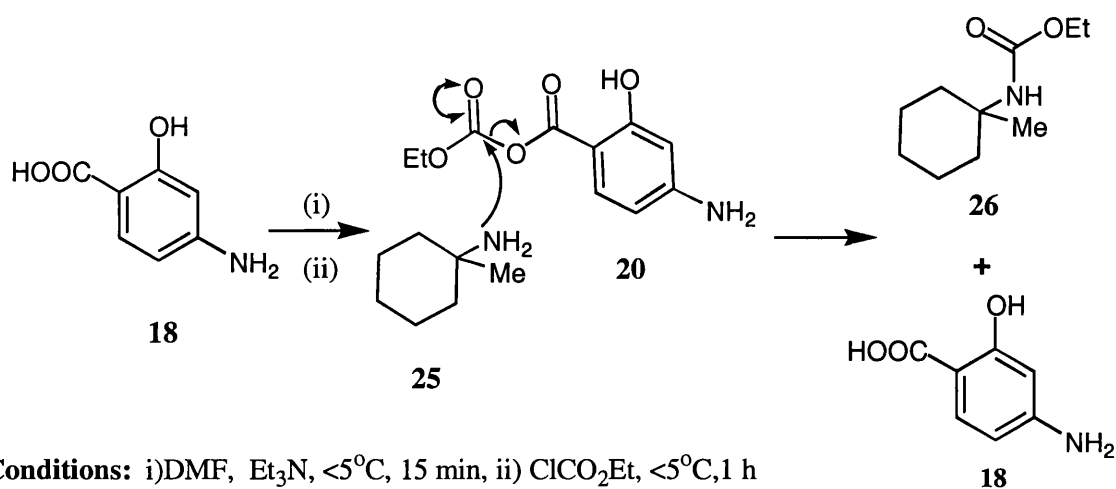


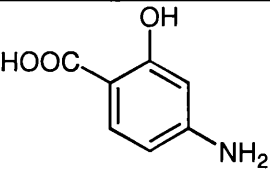
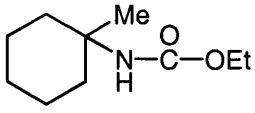
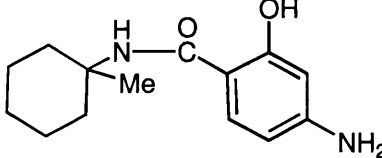
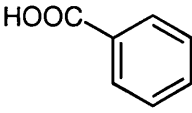
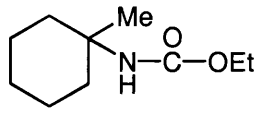
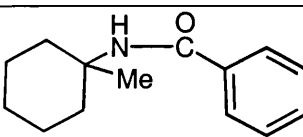
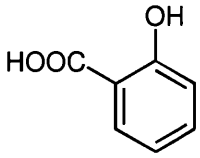
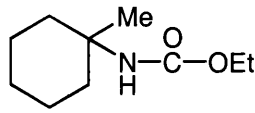
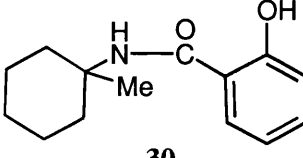
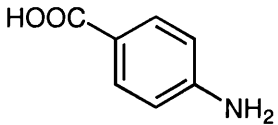
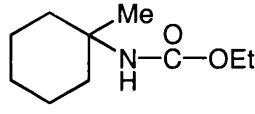
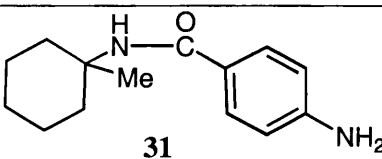
**Figure 4.19:** Possible mechanism leading to the production of the side product **26** from the coupling of acid **18** with model amine **25**.

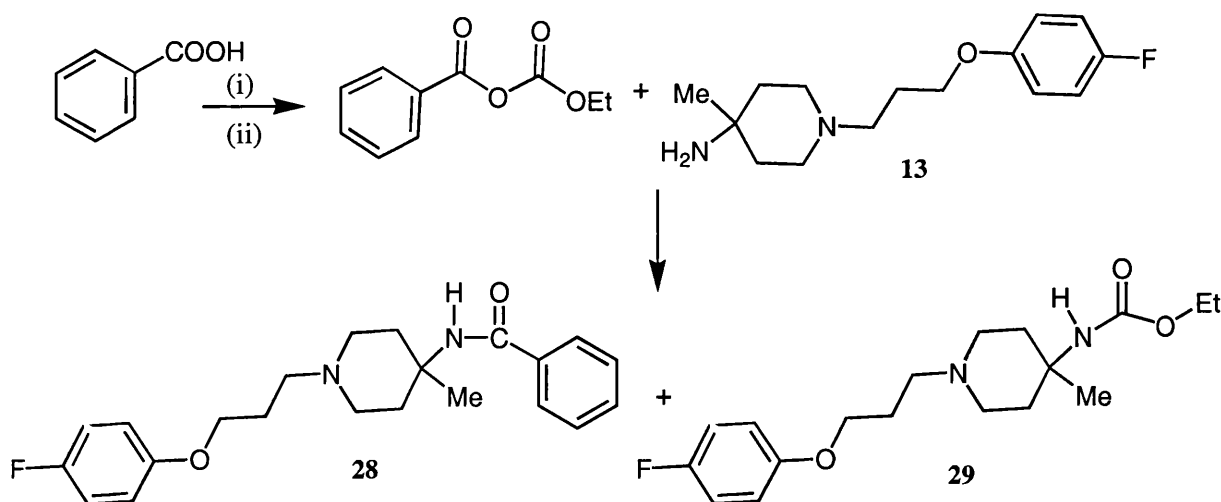
intermediate such as **20** (Figure 4.19). The slightly positive charge associated with both carbonyl carbons allows nucleophilic attack by compounds such as amines. When coupling is successful nucleophilic attack occurs at either carbon at a given ratio. Attack at the first carbonyl carbon results in the desired product (Figure 4.10). It is possible that with 4-amino salicylic acid the presence of the electron-rich ring has an inductive effect making the first carbonyl carbon more electron-rich than normal, thereby altering the ratio of nucleophilic attack. An increase in nucleophilic attack at the carbonyl furthest from the arene ring would lead to the formation of acetamide **26** (Figure 4.19). Alternatively, if the ethyl chloroformate intermediate **20** was not formed *in situ*, then direct attack on ethyl chloroformate by amine **25** could result in the observed product. Treating amine **25** with ethyl chloroformate did in fact lead to the formation of acetamide **26** in 43% yield. Both of these processes could be occurring and confirmation of the formation of the ethyl formate intermediate would be required to determine if coupling would be possible using these reaction conditions. Despite choosing the most suitable model for this coupling reaction, it is still not a direct representation of the behaviour of the actual system. It was possible that the key intermediate **13** would behave differently to the model. Given the failed attempts at coupling 4-amino salicylic acid **18** with the model amine **25**, a small scale reaction was performed with amine **13**. HPLC analysis of the reaction before amine **13** addition gave little indication that an ethyl formate activated intermediate was present. Addition of the amine had no immediate or long-term (16 h) effect on the HPLC profile. There was also no MS evidence that the desired coupling had occurred. This provided further evidence that direct coupling of 4-amino salicylic acid **18** with amine **13** was not a feasible strategy for the synthesis of precursor **2**. The reasoning for this was thought to be the number, and relative positions of the reactive, electron-rich substituents in acid **18** preventing coupling. These results indicate that protection of the phenol and/or amine group of 4-amino salicylic acid would be required to promote nucleophilic attack at the carbonyl carbon appropriate for the formation of the target precursor **2**. Protective groups may also improve the solubility of the acid allowing the use of the reported coupling conditions *i.e.* the use of dichloromethane.

Since 1-methyl cyclohexylamine appears to be an appropriate model for amine **13**, a series of reactions were carried out with amine **25** and model benzoic acids to determine the impact each of the reactive groups of 4-amino salicylic acid had on the coupling. This provided some indication of the level of protection required. The results are shown in Table 4.3.

When a solution of benzoic acid in dichloromethane was treated with triethylamine, followed by ethyl chloroformate a visible change in the reaction mixture occurred. The observed white solid disappeared on amine **25** addition and after 16 h stirring afforded the desired product, *N*-(1-methyl-cyclohexyl)-benzamide **27** (Table 4.3) in 50% yield. This result indicates that with the appropriate carboxylic acid the ethyl formate-activated intermediate was formed and that amine **25** attacked the appropriate carbonyl carbon, allowing fruitful coupling. The other product from this reaction was acetamide **26** in about 50% yield. While it has been shown that ethyl chloroformate reacts directly with amine **25** to form acetamide **26**, the amine was added to the reaction 1 h after ethyl chloroformate. It is unlikely that only a fraction of the starting material was converted to the activated intermediate in the absence of a competing reaction. Therefore, this result indicates that with benzoic acid, 1-methyl cyclohexylamine attacks both carbonyl carbons at approximately the same ratio.

**Table 4.3** The main products formed from model coupling reactions with a series of benzoic acid analogues and 1-methyl cyclohexylamine.

Acid	Main Product	Desired product (% yield)
 <p><b>18</b></p>	 <p><b>26</b></p>	 <p><b>27</b></p>
	 <p><b>26</b></p>	 <p><b>27</b> (49.5%)</p>
	 <p><b>26</b></p>	 <p><b>30</b> (&lt;10%)</p>
	 <p><b>26</b></p>	 <p><b>31</b> 10.7%</p>



**Conditions:** i)DMF, Et<sub>3</sub>N, <5°C, 15 min, ii) ClCO<sub>2</sub>Et, <5°C, 1 h

**Figure 4.20:** Products formed following the coupling of benzoic acid with the key intermediate, amine13.

A small scale coupling reaction was carried out with benzoic acid and the key intermediate **13** (Figure 4.20) to obtain proof that coupling was possible with both the model, and key amine. The desired product *N*-[1-3-(4-fluorophenoxy)propyl]-4-methyl-4-piperidiny]-benzamide **28** was formed in association with the analogous acetamide, [1-3-(4-fluorophenoxy)propyl]-4-methyl-4-piperidiny]-carbamic acid ethyl ester **29** (Figure 4.20). However, the yield for both of these products was lower than observed with 1-methyl cyclohexylamine (less than 17% and 34%, respectively).

Salicylic acid was partially soluble in dichloromethane but became totally soluble on addition of triethylamine. Therefore, the reaction was preformed using dichloromethane in order to mimic the reported coupling conditions as closely as possible. Coupling of salicylic acid with amine **25** under these reaction conditions had limited success. While the desired product, 2-hydroxy-*N*-(1-methyl-cyclohexyl)-benzamide **30** was formed, the yield was very low (<10%). The fact that the major product was acetamide **26** suggested that protection of the phenol group was a requirement for the desired coupling.

Coupling of 4-amino benzoic acid to amine **25** was tested with one modification to the standard reaction conditions *i.e.* dimethylformamide was used as the solvent. This was because the acid was insoluble in dichloromethane. The presence of the amino group was sufficient to severely hinder coupling with amine **25** to form the desired product 4-amino-*N*-(1-methyl-cyclohexyl)-benzamide **31**. As with salicylic acid the yield was very low (10.8%) with acetamide **26** being the main product. In addition, two other unidentified products were formed. These results indicate that protection of the amino group should be added to the list of requirements for coupling to be achieved in acceptable yields.

Investigation into the coupling benzoic acid with amine **13** revealed lower yields than those obtained with the model amine **25**. Therefore, it can be expected that the yield obtained from coupling either salicylic acid or 4-amino benzoic acid with the key amine **13** would be even lower than those

reported with 1-methyl cyclohexylamine. Thus, protection of the reactive, electron-rich substituents of 4-amino salicylic acid is necessary for coupling to occur.

#### 4.2.3.8 Interpretation of NMR experiments

The  $^1\text{H}$ -NMR spectra obtained at ambient temperature ( $\sim 300$  K) for *N*-(1-methyl-cyclohexyl)-benzamide **27**, 4-amino-*N*-(1-methyl-cyclohexyl)-benzamide **31** and 2-hydroxy-*N*-(1-methyl-cyclohexyl)-benzamide **30** showed pairs of resonances corresponding to two possible conformers about the amide bond. The assignment of the proton spectra was based on analysis of signal intensities and on consideration of information obtained from the  $^1\text{H}$ - $^{13}\text{C}$  correlations for benzamide **27**.

For *N*-(1-methyl-cyclohexyl)-benzamide **27**, the  $^1\text{H}$ -NMR spectra included multiple aromatic proton signals, two distinct signals for the methyl protons (2.82 and 2.96 ppm), and two clusters of broad signals for the cyclohexyl ring protons (Figure 4.21A). Two additional broad signals, assigned to the NH proton of the amide bond, were detected resonating with chemical shifts of 3.45 and 4.41 ppm. Spectra from an experiment run at a higher field (400 MHz) was identical to that obtained at 300 MHz. Integration of the proton signals indicated that while the number of protons did not correspond to that expected for compound **27**, the relative ratio of aromatic to cyclohexyl ring signals was correct *i.e.* 1 to 2. The intensities of the multitude of proton signals detected between 0.82 and 1.96 ppm suggested that proton signals resonating between 0.82–1.3 ppm arose from 2 protons, possibly the C(4) protons, and the other signals (1.32–1.96 ppm) from the remaining 8 cyclohexyl protons. A  $^1\text{H}$ - $^{13}\text{C}$  COSY experiment showed this was not the case (Figures 4.22 and 4.23). Protons from two different groups were responsible for the downfield proton signals (0.82–1.3 ppm) while all of the cyclohexyl protons contributed to the proton signals detected between 1.32 and 1.96 ppm. The chemical shifts for the methyl protons were further downfield than would be predicted; in fact ChemDraw Ultra estimates a chemical shift of 1.4 ppm. The assignment of the signals at 2.82 and 2.96 ppm to the methyl protons was substantiated by the  $^1\text{H}$ - $^{13}\text{C}$  COSY spectra.

In the  $^{13}\text{C}$ -NMR spectra the four aromatic carbon signals were as predicted. However, the presence of a resonance pair was observed for the methyl carbon as identified from DEPT and  $^1\text{H}$ - $^{13}\text{C}$  correlation experiments (Figures 4.22 and 4.23). Both of the carbon signals at 28.0 and 32.8 ppm were identified as methyl carbons and were coupled to the singlets in the  $^1\text{H}$ -NMR spectra resonating at 2.82 and 2.96 ppm. Seven other  $\text{CH}_2$  carbon signals were observed representing the cyclohexyl ring region of the compound. The quaternary carbon of the cyclohexyl ring was assigned to two carbon signals resonating at 55.07 and 60.19 ppm. Interestingly, both of these signals were identified as CH carbons in the DEPT-135 ( $\text{CH}_2$  carbons appear as negative signals, CH and  $\text{CH}_3$  carbon are positive) and DEPT-90 spectrum (CH carbons only). This is possibly due to the observed coupling to the proton signals assigned to the NH proton ( $^1\text{H}$ - $^{13}\text{C}$  COSY, Figures 4.22 and 4.23). The remaining five signals were all coupled to protons. This is contrary to the 3 signals corresponding to  $\text{CH}_2$  carbons that would be predicted. This could be due to carbon-2 and carbon-6 having a different magnetic



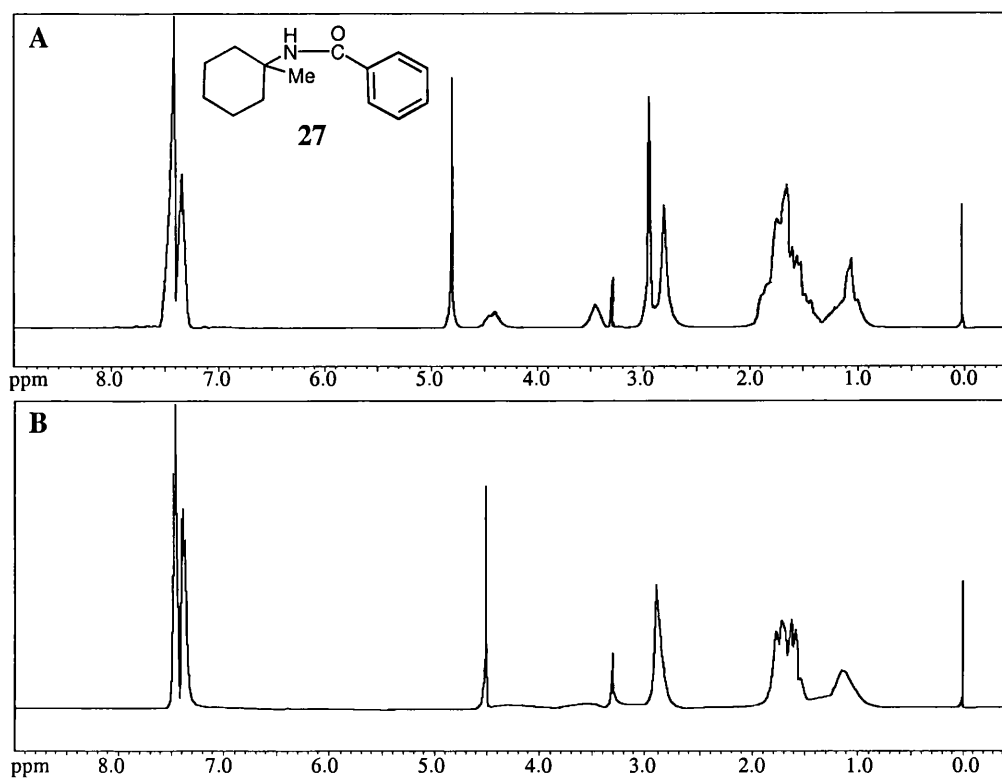


**Figure 4.21:**  $^1\text{H}$ -NMR spectra of *N*-(1-methyl-cyclohexyl)-benzamide **27** run at 300 K (A) and 330 K (B).

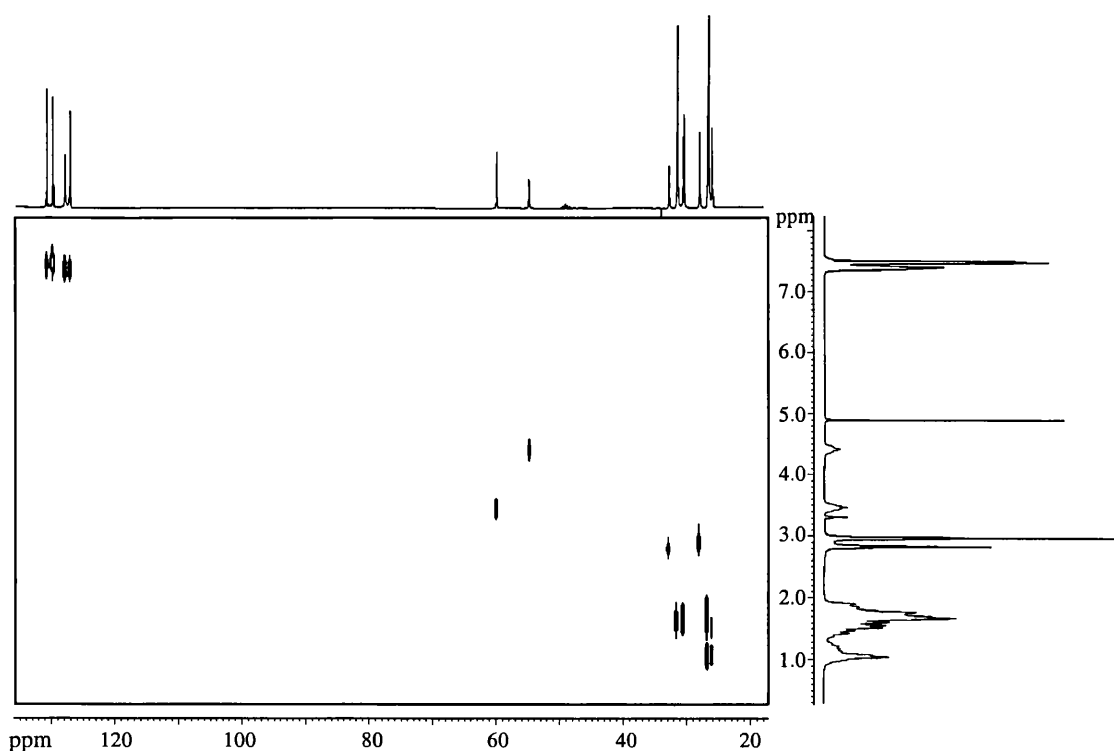


**Figure 4.22:** NMR spectrum obtained from the  $^1\text{H}$ - $^{13}\text{C}$  COSY experiment performed on benzamide **27** at ambient temperature.

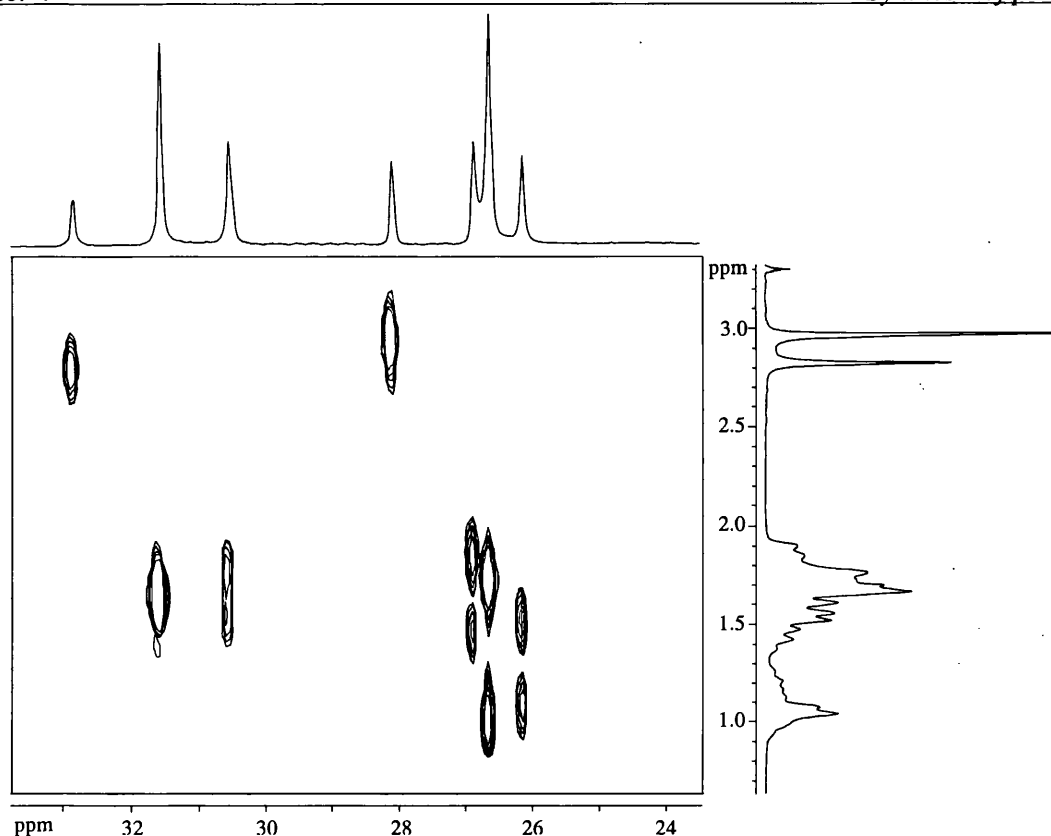


**Figure 4.23:** Enlargement of cyclohexyl ring region of the NMR spectrum obtained from the  $^1\text{H}$ - $^{13}\text{C}$  COSY experiment performed on benzamide **27**.

environment leading to a different chemical shift or the detection of different conformers for only some of the carbons in the cyclohexyl ring. The lack of resolution in the cyclohexyl ring region of the proton spectrum meant that the  $^1\text{H}$ - $^{13}\text{C}$  correlation experiment provided little additional information to help in the assignment of these signals to their respective carbon(s).  $^1\text{H}$ -NMR experiments were performed at 310, 320 and 330 K. This incremental increase in temperature was associated with a reduction in the size of the methyl proton signal at 2.82 ppm until the two signals observed at 300 K coalesced into a relatively broad peak with a chemical shift of 2.90 ppm at 330 K (Figure 4.21B). The proton signals resonating at 3.45 and 4.41 ppm broadened significantly with an increase in temperature until they were undetectable at 330 K. The pattern and intensity of the aromatic signals was not influenced by temperature. The cyclohexyl region of the spectrum did sharpen but not to the extent where only one conformation of the product was detected by NMR.

In theory the  $^1\text{H}$ -NMR spectrum for 2-hydroxy-*N*-(1-methyl-cyclohexyl)-benzamide **30** should include four aromatic proton signals. However, a multiplet (7.22 and 7.43 ppm) was observed (Figure 4.24A). The three methyl protons were detected as two distinct resonant pairs while the protons of the cyclohexyl ring appeared as two clusters of signals (0.91–1.18 ppm and 1.42–1.93 ppm) with a relative intensity of 1 and 4 protons, respectively. However, the information obtained from the COSY experiment performed on benzamide **27** would suggest that all of the cyclohexyl protons contribute to the downfield cluster of signals while two groups of protons resonate between 0.91 and 1.18 ppm.

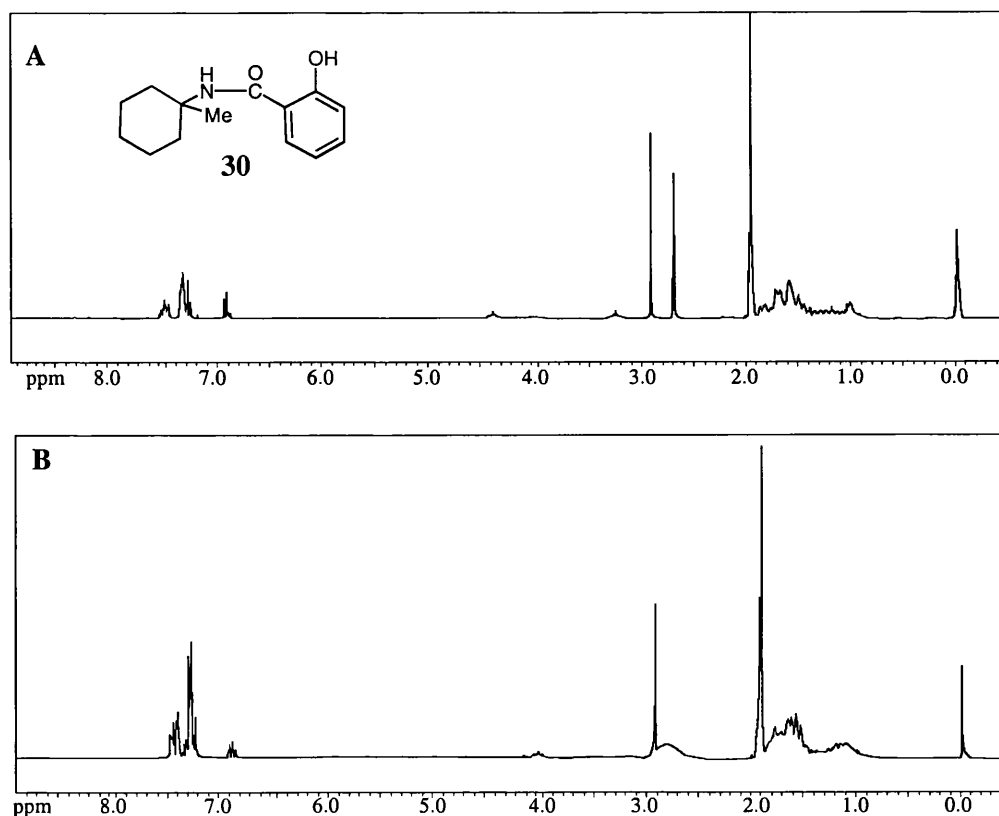


**Figure 4.24:** Ambient (300K, **A**) and high temperature (355 K, **B**)  $^1\text{H}$ -NMR spectra of 2-hydroxy-*N*-(1-methyl-cyclohexyl)-benzamide **30**.

Even though the NMR spectrum run at 300 K was not as expected, the relative number of aromatic to cyclohexyl ring protons was correct (4 to 5, respectively).

Incremental increases in temperature (320, 330, 350 and 355 K) only had a significant effect on the signal for the methyl protons. The signal resonating at 2.66 ppm at 300 K broadened until it was detected as a broad shoulder to the sharp singlet at 2.90 ppm at 355 K (Figure 4.24B). For the other proton(s) the change in temperature had little effect on the pattern or intensity of the signals detected thereby providing no additional information for compound signal assignment or identification.

The  $^{13}\text{C}$  spectra for 2-hydroxy-*N*-(1-methyl-cyclohexyl)-benzamide **30** differed from benzamide **27** with all of the carbons being detected as resonance pairs. This was true for both the cyclohexyl ring and aromatic regions. The two signals resonating with a chemical shift of 53.78 and 59.13 ppm were assigned to the quaternary carbon of the cyclohexyl ring even though they were detected as a CH carbon in DEPT experiments. This assignment was supported by the  $^1\text{H}$ - $^{13}\text{C}$  COSY data obtained for benzamide **27** where similar observations were made.

Four aromatic doublets were observed for 4-amino-*N*-(1-methyl-cyclohexyl)-benzamide **31** when only two signals were expected (Figure 4.25A). Resonance pairs were also detected for the methyl protons (2.79 and 3.42 ppm) and the NH proton (7.73 and 7.82 ppm). As with the other coupled products the cyclohexyl ring protons were represented as two broad multiplets. As with the two previous products, the relative ratio of the different proton(s) was correct for benzamide **31** e.g. 2

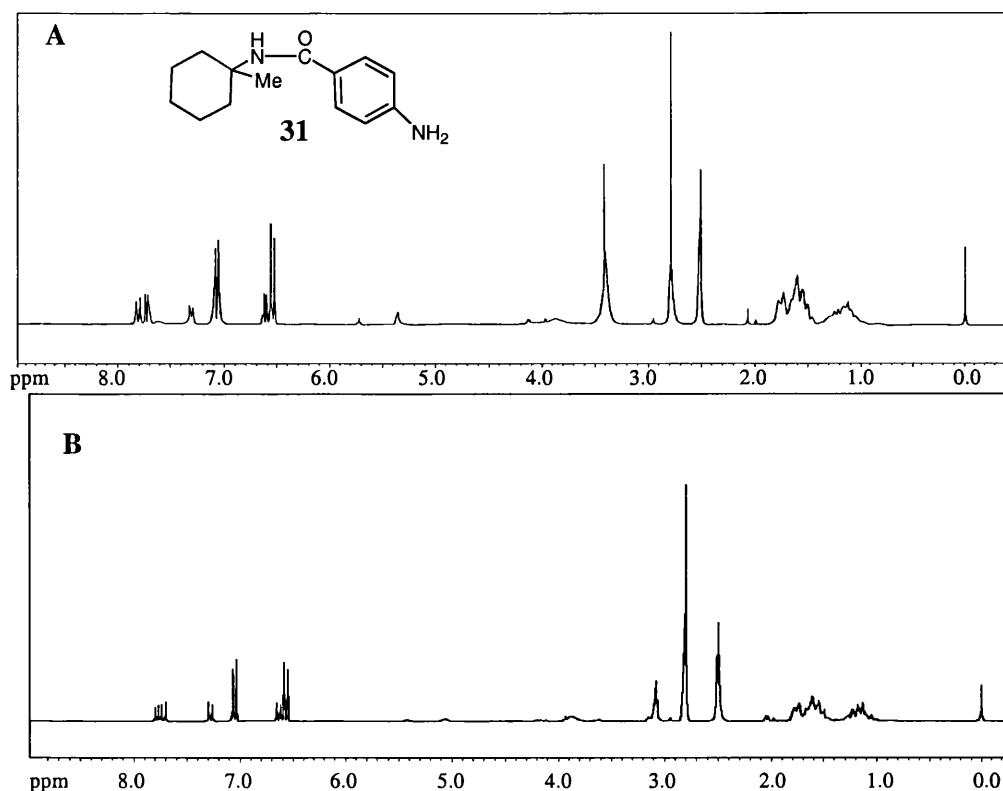


**Figure 4.25:** <sup>1</sup>H-NMR spectra obtained for 4-amino-*N*-(1-methyl-cyclohexyl)-benzamide **31** measured at 300 K (A) and 355 K (B).

aromatic to 5 cyclohexyl ring signals, respectively even though the integration of the proton signals did not correspond to the number of protons in the desired product. <sup>1</sup>H-NMR experiments were performed at 320, 330, 350 and 360 K. The intensity and pattern of the resonance pairs for the different conformers for all protons was consistent for all temperatures. The only proton signals that showed any temperature effect were the pair assigned to the methyl protons. For benzamide **31** the downfield peak at 3.07 ppm broadened but not to the extent seen for the other coupled products. The signal resonating at 2.82 ppm remained as a sharp singlet (Figure 4.25B). The relative intensity of the two methyl proton signals remained unchanged.

In NMR spectroscopy, the broadening or doubling of signals, as observed in these compounds, may be due to dynamic processes; a different resonance for the same proton or carbon nucleus may arise as a result of a particular compound interconverting between two distinct forms that have significant life-times and give two different magnetic environments for the detected nucleus. For the products from the model coupling reactions the C<sub>CO</sub>-N bond displays partial double-bond characteristics. This is because the formal lone pair of electrons on the nitrogen atom partially delocalises into the  $\pi$ -system of the carbonyl group, thereby generating a conjugated 1,3-dipole. The two canonical forms that contribute to such a delocalised structure are illustrated for *N*-(1-methyl-cyclohexyl)-benzamide **27** in Figure 4.26. Rotation about the C<sub>CO</sub>-N bond is restricted because of its partial double bond character. Two conformers of the product, the *syn*- and *anti*- version, are possible as a result of the lone pair delocalisation (Figure 4.27). NMR can detect the distinct chemical shifts associated with these two forms if interconversion is low. When the two forms of the amide bond

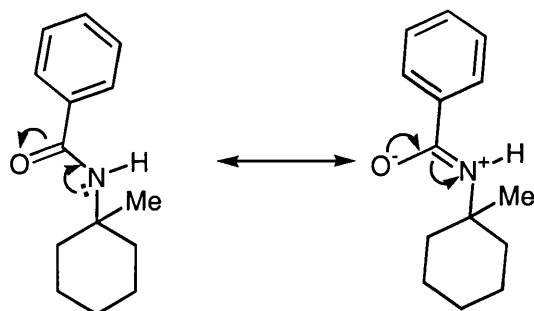


**Figure 4.26:** The two canonical forms present for *N*(1-(methyl(cyclohexyl)-benzamide **27** leading to the partial delocalisation of the C<sub>CO</sub>-N bond.

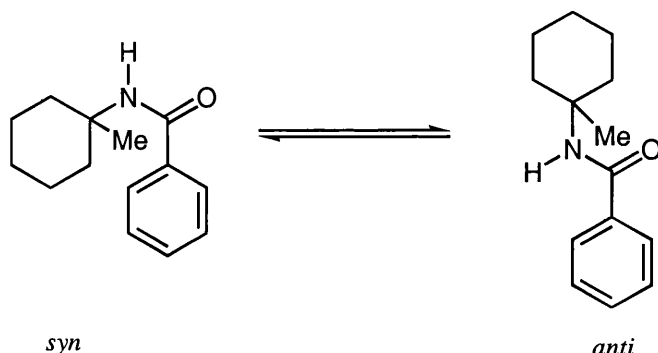


**Figure 4.27:** The two conformations of of the coupled product **27** detected by NMR.

readily and rapidly interconvert, then a single NMR signal is registered which has the average chemical shift of the two isomers. Increasing the temperature will increase the rate of interconversion, thereby enabling an average chemical shift and single NMR peaks to be observed.

<sup>1</sup>H-NMR experiments at higher temperatures showed little change the spectrum for the three coupled products discussed above. The rate of conversion between the two conformers was not increased to the point where only one sharp signal was registered for a particular proton(s). The methyl proton signal was most influenced by an increase in temperature. While coalescence was only observed for benzamide **27**, a single peak may have been observed for compound **30** with a temperature slightly higher than 350 K. A large body of work has been carried out on the <sup>1</sup>H-NMR and <sup>13</sup>C-NMR spectroscopy of *N,N*-dimethylbenzamides. Jones & Wilkins found that for a series of para-substituted *N,N*-dimethylbenzamides the electrical effects of para-substitutents through the benzene ring to the carbonyl carbon is heavily dominated by field effects which induce changes in the polarisation of the amido group  $\pi$  electrons.<sup>20</sup> This results in an increased contribution of the polar ( $\text{>}\overset{+}{\text{N}}\text{--}\overset{-}{\text{O}}$ ) form of the carbonyl group and it possibly one reason why an increase in temperature had no effect on the <sup>1</sup>H-NMR spectrum for the *para* amine substituted benzamide **31**.

The NH proton signal detected in compound **27** was also influenced by temperature. At 300K a broad pair of signals was detected (Figure 4.21A). An increase in temperature lead to exchange broadening to the point where no signals were detected at 330 K. A further increase in temperature might have resulted in the detection of a single signal for this proton. This effect has been observed for 18-annulene.<sup>21</sup> At room temperature the exchange rate between 'inside' and 'outside' protons was

close to the coalescence temperature at the field at which the  $^1\text{H}$ -NMR was obtained. The result was massive broadening to the point where no proton signal was detected.<sup>21</sup> An increase in temperature resulted in a single sharp proton signal.

The fact that the other proton signals were almost identical at all temperatures indicates that the restricted rotation around the  $\text{C}_{\text{CO}}\text{-N}$  bond has a strong influence on the aliphatic and aromatic regions of these compounds.

$^1\text{H}$ -NMR spectroscopic data of benzamide **27** has been reported by Koziara *et al.* (Table 4.4).<sup>22</sup> There are two interesting discrepancies between this data and that reported in this thesis. Firstly, there was no mention of the detection of resonance pairs for any of the proton signals. Secondly, the chemical shift for the methyl protons observed in deuterated water (*i.e.* 1.28 ppm) was more inline with what would be expected for this group. Solvent effect is one possible explanation for these observed differences. A change from methanol to water might be sufficient to increase the rate of conversion between the two resonant forms of the compound leading to coalescence and the registration of only one proton signal for each group of proton(s). However, this would go against the trend reported for solvent effects on the rotational barrier for *N,N*-dimethylbenzamide where barriers were higher in more polar solvents.<sup>23</sup> This data suggests that rotation would be more restricted in water than methanol. It is possible that replacing the two methyl groups with a hydrogen and the cyclohexyl ring significantly changes the system preventing hydrogen bonding, the proposed reason for the solvent effect in dimethylbenzamide.

$^1\text{H}$ -NMR ( $\text{D}_2\text{O}$ , $\text{TMS}_{\text{ext}}$ , 80mHz)	1.28	(s, 3H)
	1.05-2.20	(m, 10H)
	5.85	(s, 1H)
	7.00-7.70	(m, 5H)

Table 4.4: Spectroscopic data of benzamide **27** as reported by Koziara *et al.*<sup>22</sup>

The chemical shift observed for the methyl protons in methanol could be explained by the anisotropic effect of the amide group where large diamagnetism (shielding) occurs in cone regions extending above and below the plane of the amide group. Regions in the plane of the amide group are paramagnetic (deshielding). The presence of the methyl protons in this region of the molecule might explain the difference between the expected and observed chemical shift. However, both of the signals for the conformers resonate further downfield than the 1.28 ppm reported by Koziara *et al.*<sup>22</sup> Solvent effect may not fully explain this difference since a similar chemical shift was observed for all of the compounds in this series.  $^1\text{H}$ -NMR was obtained in a different solvent for all three of the coupled compounds ( $\text{CD}_3\text{OD}$ , DMSO and  $\text{CD}_3\text{CN}$ ). A similar chemical shift was also observed for the methyl protons in the by-product from these reactions, 1-methyl cyclohexyl acetamide **26** (2.72 ppm). It is possible that dissolving benzamide **27** in water alters the partial double bond characteristics of the  $\text{C}_{\text{CO}}\text{-N}$  bond leading to the reported NMR data. Repeating the  $^1\text{H}$ -NMR experiment in deuterated water would be the only way to determine if this was in fact true.

The observation that resonance pairs were not observed for all of the carbon signals in benzamide **27** is an interesting point. While the aromatic carbons were detected as single signals the quaternary carbon of the cyclohexyl ring was detected resonating at two chemical shifts. It is possible that this was also the case for two other carbons in the cyclohexyl ring. One explanation is that the effect of the C<sub>CO</sub>-N bond decreases with distance and the effect is stronger either for aryl carbons or those closest to the nitrogen. This situation changed with hydroxy substitution of the aromatic ring with all carbons detected in the two conformations of benzamide **30**. One possible explanation for this effect is an increase in hydrogen bonding for benzamide **30**. This would lead to an increase in the rotational barrier.

No attempt has been made to assign the different signals to the different isomers. The NMR data obtained for this thesis was not sufficient to permit complete assignment of the different signals to their respective proton(s) or carbon(s). This could only be achieved following NMR decoupling experiments where different regions of the spectrum are irradiated, something that was not within the scope of this thesis. However information reported on the chemical shifts for the *syn* and *anti* methyl carbon of *N,N*-dimethylamide could provide some useful information that could be applied to this data. Rae<sup>24</sup> found that the *syn* methyl carbon was always found 3-5 ppm to high field of the *anti* carbon. This range of separation was observed for the methyl carbon in both benzamide **27** and **30**. Therefore, it could be speculated that the *syn* conformation of benzamide **27** was detected as the carbon signal at 28.05 ppm while the *anti* conformation resonated at 32.82 ppm. Similarly, for the carbon spectra of benzamide **30**, the *syn* and *anti* conformations would be responsible for the signals at 27.43 and 31.70 ppm, respectively.

Restricted rotation about the C<sub>CO</sub>-N bond is likely to occur in compounds that are coupled with the key intermediate **13**. These NMR experiments have provided a basis for the analysis of any further amide products and highlighted the possible approach that is required to enable full characterisation from the NMR data. In the future it would also be interesting to investigate whether the proton coupling detected in DEPT and COSY experiments between the quaternary carbon of the cyclohexyl ring and the NH proton was a true phenomenon.

#### 4.2.3.9 Protection of 4-amino salicylic acid

Protection of 4-amino salicylic acid was investigated from two perspectives. The first was concerned with achieving acid activation in the presence of ethyl chloroformate and base to give an intermediate that would be attacked by the amine at the appropriate carbonyl carbon. The nature of the protective groups was not restricted except in terms of the deprotection conditions following coupling with the key intermediate, amine **13**. The ultimate aim of this approach was to synthesise precursor **2**. The second approach required protection of the phenol group by methylation to form 4-amino-2-methoxybenzoic acid **19**. This would provide a pathway to both **2** and **1** as proposed in Figure 4.11.

Experiments using basic conditions (5 and 1.2 molar equivalents of potassium carbonate and sodium hydride, respectively) and 1.1 molar equivalents of iodomethane did not lead to the selective methylation of the phenol group. A complex mixture of products was formed which included

compounds with both the phenol and/or the acid group methylated. It was decided that the number of products formed could be reduced if reaction conditions were altered to force methylation of both the acid and the phenol. Selective deprotection of the methyl ester would give the desired benzoic acid **19**. This strategy proved to be unsuccessful due to the failure to form the dimethylated amine in an acceptable yield.

Synthesis of the benzyloxymethyl ether (Bom-ether) was investigated as an alternative protective group for the phenol, and as a possible route to the formation of precursor **2**. Given that Bom deprotection occurs with 95% yield following treatment with thiophenol and boron trifluoride etherate at  $-78^{\circ}\text{C}$ ,<sup>25</sup> the Bom group could be removed with minimal decomposition of **2**. Since there was a major concern about being able to maintain the integrity of **2** in the harsh deprotection conditions required for demethylation, protection as the Bom-ether was favoured over the methoxy for the synthesis of the phenol precursor **2**. However, this alternative route proved futile since the benzyloxymethyl ether was not formed when the salicylic acid **18** was treated with sodium hydride and benzyloxymethylchloride.

One approach for selective benzylation of the phenol group is to block reactive groups as their sodium salts by employing an excess of sodium hydroxide as the base.<sup>26</sup> With 4-amino salicylic acid **18**, four equivalents of sodium hydroxide was thought to be sufficient to inactivate both the acid and amino groups *in situ*, allowing formation of the benzyl ether. This approach did not work for 4-amino salicylic acid, possibly due to strong hydrogen bonding between the acid and the phenol functionalities.

In conclusion, initial attempts at protecting the phenol group of salicylic acid **18** were fruitless. There was little indication of preferential protection of the phenol group over the acid and dual protection seemed to be strongly influenced by the presence of the reactive amino group preventing acceptable yields of the desired product. Protection of the amino group would improve the solubility of the salicylic acid and allow a larger variety of solvents and conditions to be employed, presumably resulting in improved yields from either the selective phenol protection approach or dual protection of the acid and phenol groups with subsequent acid deprotection. Deprotection of the amino group could be performed either before the key coupling step or after the coupling reaction. However, there may be benefits to keeping the amino group protected for coupling with intermediate **13**, especially if it is expedient to use mild conditions for the removal of the protective group.

Protection of the amine with *t*-butyl carbamate was investigated since the literature indicated that cleavage is typically achievable in high yield following treatment with a 3M hydrochloric acid in ethyl acetate for 30 min at ambient temperature.<sup>27</sup> Under these reaction conditions the amide and ether linkages in the molecule should remain intact to yield the phenol precursor **2**. A two-phase system of *tert*-butanol and sodium hydroxide in the presence of di-*tert*-butyl dicarbonate was used to protect the amino group of salicylic acid **16** (Figure 4.28). The crude product contained the desired product 4-*tert*-butoxycarbonylamino-2-hydroxy-benzoic acid **32** plus an unidentified impurity. The ratio of product to impurity by NMR was 65: 35. Purification by flash column chromatography resulted in



cleavage of the Boc group due to the slightly acid conditions associated with this procedure. Therefore, coupling of the crude Boc-protected salicylic acid **32** with 1-methyl cyclohexylamine **25** was investigated to determine whether further protection was required. Unfortunately, coupling was unsuccessful, producing acetamide **26** as the main product. While the unidentified impurity present in the starting material could be complicating the results, this corroborates the earlier finding indicating that phenol protection might also be required. The crude product from the above reaction was carried through to investigate the feasibility of both methyl and benzyl protection of the phenol and acid groups. The products formed from small-scale reactions using conditions promoting double methylation, included both the respective *t*-butyl carbamate **33** and amino products **34** (Figure 4.28). Since the principal purpose of protecting the amino group was to achieve phenol protection, the cleavage of the Boc group during methylation was not a primary concern, as this would have had to be undertaken at some stage in the strategy. The results from a scaled up reaction were less conclusive with an increase in the number of products making purification and characterisation difficult. Reactions involving the Boc-protected salicylic acid and benzyl bromide showed some evidence of successful benzylation of the phenol and acid functions. However, a complex mixture of products was formed preventing any isolation, identification and characterisation. In order to obtain further information on possible benzylated products, preliminary investigations into amine and selective acid deprotection were performed. When the crude product from the benzylation reaction was treated with a solution of 3 M hydrochloric acid in ethyl acetate at ambient temperature for 16 h a hydrochloric salt formed. Unfortunately, this solid proved to be the benzyl ester **35** (Figure 4.29) substantiating that dual benzylation to the benzyl ether and ester was not achieved.

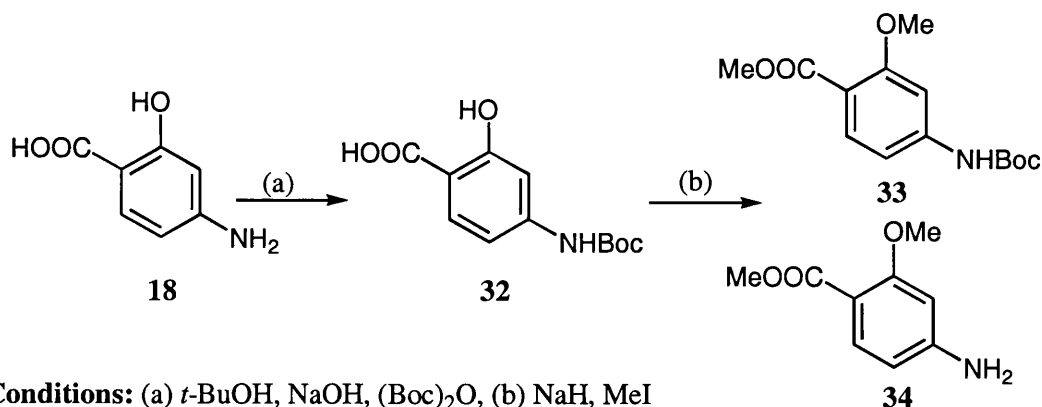


**Figure 4.28:** Products identified following protection of the amino, phenol and acid groups of 4-amino salicylic acid.

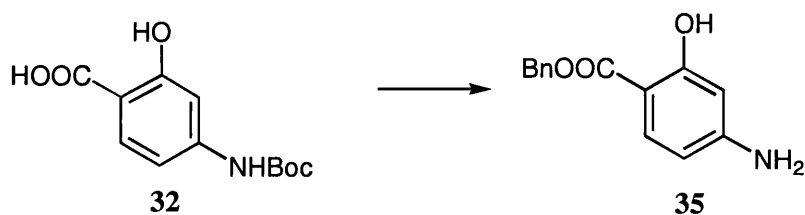


**Figure 4.29:** Isolated products following benzylation and deprotection of the crude Boc protected acid.

## 4.2.3.10 Palladium-Catalysed carbonylation and coupling of aromatic halides and amines

The limited success in synthesising an analogue of 4-amino salicylic acid that contained an acid group that could be activated by ethyl chloroformate lead to the investigation of other reaction conditions for the final coupling with the key intermediate, amine **13**. Palladium-catalyzed carbonylation of aromatic halides is a common pathway for the preparation of aromatic carbonyl compounds<sup>28-30</sup> which could be used to form both precursors **1** and **2**. Paul *et al.*<sup>16</sup> investigated regioselective bromination of a series of activated aromatics including 3-aminophenol. However, the specific reaction conditions for the synthesis of 2-bromo-5-aminophenol were not included. The standard reaction conditions indicated the need for heating. However, when 3-aminophenol was heated to reflux with one equivalent of *N*-bromosuccinimide undesirable di- and tri-bromination occurred. Tri-bromination was still observed when the reaction temperature was reduced to 20°C and after 20 min at an even lower temperature (-8°C). The problem was that the monobrominated product is more reactive than the starting material so the reaction needs to be stopped before further attack. Given these results, it is difficult to determine how the reported yield of 84%<sup>16</sup> was obtained.

These results were disappointing especially since recent developments in PET radiochemistry have resulted in methods that increase the efficiency of [<sup>11</sup>C]carbon monoxide trapping. [<sup>11</sup>C]Carbon monoxide is readily prepared from cyclotron-produced no-carrier added [<sup>11</sup>C]carbon dioxide.<sup>31</sup> However, its low solubility in organic solvents limits the efficiency of trapping by a single pass into a reagent solution (~10%). Rapid recirculation of untrapped [<sup>11</sup>C]carbon monoxide through the reagent solution<sup>32</sup> and the use of a high pressure microautoclave to confine the [<sup>11</sup>C]carbon monoxide with reactants<sup>33</sup> are two techniques that have successfully solved this problem. [<sup>11</sup>C]Carbon monoxide has since been used in the palladium-mediated synthesis of [<sup>11</sup>C]ketones,<sup>32</sup> aryl[<sup>11</sup>C]ketones,<sup>34</sup> and [<sup>11</sup>C]esters.<sup>35</sup> Of most interest to this work is the palladium-mediated carbonylation of amides with aryl halides and [<sup>11</sup>C]carbon monoxide in nearly quantitative yields.<sup>36</sup> Phenyl and benzyl halides were carbonylated and reacted with primary and secondary amines as shown in Figure 4.30. This method could be applied to analogues of R91150 to obtain a new series of potential PET radioligands (Figure 4.31). Initial discussions with the Uppsala group that pioneered the resurgence of [<sup>11</sup>C]carbon monoxide chemistry suggest that this is a worthwhile strategy to investigate.

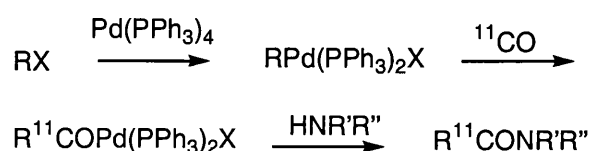


**Figure 4.30:** The published scheme for the synthesis of <sup>11</sup>C-labelled amides.<sup>36</sup>

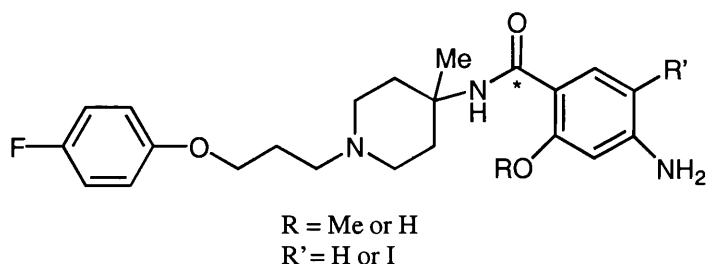


**Figure 4.31:** Analogues of R91150 that could be formed via palladium-mediated carbonylation. \* denotes the site of the  $^{11}\text{C}$  label.

### 4.3 Conclusions

The key intermediate, amine **13** has been synthesised using a modification of a reported strategy.<sup>1,2</sup> For some reactions the yields reported by Leysen and Van Daele<sup>1,2</sup> were never repeated while altering the reaction conditions in others (*e.g.* hydrolysis of acetamide **12** to amine **13**) resulted in a significant improvement in the recovered yield (>95% compared with 29%<sup>1,2</sup>). Reaction conditions were optimised for the Grignard alkylation of 1-benzyl-4-piperidone **23** which afforded 100% conversion to 4-methyl-1-(phenylmethyl)-4-piperidinol **8**. The overall yield of amine **13** from this product was 7%, compared with 5% for the original strategy.<sup>1,2</sup>

The initial strategy for the formation of the phenol precursor **2** involved direct coupling of 4-amino salicylic acid to the key intermediate **13** (Figure 4.9). This was not achieved. Model reactions revealed that the unprotected phenol and amine groups were having a negative influence on either the activation of the acid by ethyl chloroformate or the nature of the nucleophilic attack by the amine. Boc protection of the amino group was achieved in acceptable yields. However, further protection was required as indicated by the failed coupling of the Boc protected salicylic acid **30** with the model amine **25**. Further protection has met with limited success possibly due to the presence of the unidentified impurity in the starting material. The lack of success in obtaining any analogue with the phenol protected as a methoxy also meant that the proposed strategy for the synthesis of R91150 (Figure 4.9) was not feasible.

An alternative strategy was also investigated that should bypass the need for acid activation during coupling with amine **13** (Figure 4.12). Monobromination of the commercially available 3-aminophenol and 3-methoxyaniline would have provided compounds that might be coupled with amine **13** to synthesise both of my target compounds. However, bromination of 3 aminophenol could not be restricted to one substitution with both the di- and tri-bromo compounds formed.

Initial research into the application of palladium-mediated carbonylation suggests that this could be an alternative strategy for the radiosynthesis of potential PET radioligand for imaging the 5-HT<sub>2A</sub> receptor. For this to be successful further work is required on the synthesis of phenyl halides that could be employed in these reactions.

While the ultimate goal of this work was not achieved, a strong body of information has been obtained about the behaviour of 4-amino salicylic acid. This information will be useful in the future when other reaction conditions are scrutinised as possible alternatives for the final coupling step. One possibility that is being investigated is the use of the thiol reagent, 2,2'-dipyridyl disulfide, which has been used with triphenylphosphine as a condensing agent in the amidation of carboxylic acids.<sup>37</sup> This approach has been used to couple aromatic amines with aryl acids.<sup>37,38</sup>

## 4.4 Experimental

### Materials and Methods

For general methods refer to Chapter 2.

4-Amino salicylic acid **18**, and 1-benzyl-4-piperidone **15** were purchased from Lancaster Synthesis Ltd. (UK). 1-(3-Chloropropoxy)-4-fluorobenzene **11** was purchased from Acrōs Organics, Fisher Scientific (UK). All other materials were analytical grade and purchased from Aldrich Chemical Co. Ltd. (UK).

### 4-Methyl-1-benzyl-4-piperidinol **8**

A solution of 1-benzyl-4-piperidone **23** (10.37 ml, 0.053 mol) in anhydrous tetrahydrofuran (50 ml) was added dropwise to a 3M solution of methylmagnesium bromide in diethyl ether (28 ml, 0.106 mol), under a positive pressure of nitrogen and stirred at room temperature for 5 min. The reaction mixture was quenched with water (30 ml) and then extracted with ethyl acetate (3 x 40 ml). The organic layers were combined, dried over magnesium sulphate, filtered and concentrated *in vacuo* to give 10.82 g (98%) of dark yellow oil. This oil was shown to be the desired product by the appearance of the single peak resonating at 1.14 ppm in <sup>1</sup>H NMR and the absence of a carbonyl carbon in <sup>13</sup>C NMR.

$\delta_{\text{H}}$  (400 MHz; CD<sub>3</sub>CN; Me<sub>4</sub>Si) 1.14 (3 H, s, CH<sub>3</sub>), 1.49–4.53 (4 H, m, C(3)H, C(5)H), 2.32–2.44 (4 H, m, C(2)H, C(6)H), 3.47 (2 H, s, Ph-CH<sub>2</sub>), 7.34–7.23 (5 H, m Ph);

$\delta_{\text{C}}$  (100 MHz; CD<sub>3</sub>CN; Me<sub>4</sub>Si) 29.47 (CH<sub>3</sub>), 39.06 (C(3), C(5)), 49.97 (C(2), C(6)), 62.98 (C(1')), 67.17 (C(4)), 127.19 (C(5')), 128.52 (C(3'), C(7')), 129.33 (C(4'), C(6')), 129.68 (C(2'));

HRMS: obsd (MH<sup>+</sup>) 206.1542. Calcd for C<sub>13</sub>H<sub>19</sub>NO, 205.1467.

### Dimer **24**

To a solution of methylmagnesium bromide (3M; 30 mmol) in diethyl ether (10.0 ml) was added a solution of ketone **23** (4.8 ml; 26.4 mmol) in diethyl ether (60 ml) under an inert atmosphere of nitrogen. The reaction was heated at reflux for 2 h, cooled to ambient temperature and quenched with water (30 ml). The white solid that formed was dissolved by addition of 1M sulphuric acid (80 ml). The resultant reaction mixture was neutralised with sodium hydrogen carbonate powder and then extracted with ethyl acetate (3 x 40 ml). The combined organic phases were dried over magnesium sulphate, filtered and concentrated under reduced pressure to afford a yellow oil which was purified by

column chromatography [silica; dichloromethane - methanol (95: 5 v/v)] to provide 400 mg (7%) of the desired alcohol **8** as a yellow oil and 1.25 g of dimer **24**:

$\delta_C$  (100 MHz;  $CD_3CN$ ;  $Me_4Si$ ) 36.29 C(2'), 36.69 C(4'), 49.03 C(5'), 49.38 C(1'), 61.69  $CH_2$ , 62.93  $CH_2$ , 70.30 C(3'), 127.94 C(4), 128.53 C(5), 128.84 C(3), 129.33 C(6), 129.67 C(2) 138.16 C(1).

#### *N*-[1-benzyl-4-methyl-4-piperidinyl]acetamide hydrochloride **9**

Concentrated sulphuric acid was added dropwise to a well-stirred mixture of piperidinol **8** (5.14 g, 25.07 mmol) in acetonitrile (6.5 ml). The temperature was maintained at 70°C throughout the addition by cooling of the reaction with an ice bath. Following complete addition of the concentrated sulphuric acid, the reaction was allowed to cool to ambient temperature and stirred. After 20 h, the crude reaction was added to crushed ice (50 g) and neutralised with potassium carbonate powder, then strongly alkalinised (pH = 14) with a 15% aqueous potassium hydroxide solution. The reaction was extracted with ethyl acetate (3 x 100 ml) and the aqueous layer saturated with potassium hydroxide pellets and extracted again with ethyl acetate. (3 x 100 ml). The organic phases were combined, dried over magnesium sulphate, and concentrated *in vacuo* affording a semi-solid residue. This residue was triturated with diethyl ether and the resulting cream solid was filter off giving a slightly cloudy filtrate. Sufficient acetone was added until the filtrate turned into a clear solution. The solution was subsequently saturated with gaseous hydrogen chloride and evaporated to give a white solid that was recrystallised from iso-propanol to afford 2.12 g (30%) of the desired salt **9**. The product was structurally identified by the appearance of a second methyl group with protons resonating at 2.0 ppm and the carbonyl carbon (173 ppm) in the  $^{13}C$  NMR.

mp 286°C (from iso-propanol) (lit.,<sup>1,2</sup> 288-289°C);

$\delta_H$  (400 MHz;  $CD_3OD$ ;  $Me_4Si$ ) 1.38 (3 H, s,  $CH_3$ ), 1.82 (2 H, dt,  $J = 14.1$  C(2) $H$  or C(6) $H$ ), 2.0 (3 H, s,  $OCH_3$ ), 2.54 (2 H, d,  $J = 7.1$ , C(2) $H$  or C(6) $H$ ), 3.16 (2 H, t,  $J = 12.3$ , C(5) $H$  or C(3) $H$ ), 3.32 (2 H, t,  $J = 2.5$ , C(5) $H$  or C(3) $H$ ), 4.84 (2 H, s,  $NCH_2$ ), 7.47-7.48 (3 H, m, C(4') $H$ , C(6') $H$  and C(5') $H$ ), 7.57-5.60 (2 H, m, C(3') $H$  and C(7') $H$ );

$\delta_C$  (100 MHz;  $CD_3OD$ ;  $Me_4Si$ ) 29.83 ( $OCH_3$ ), 26.54 ( $CH_3$ ), 33.44 (C(2) and C(6)), 49.30 (C(3) and C(5)), 50.81 (C(4)), 61.20 (C(1')), 130.0 (C(4') and C(6')), 131.0 (C(5')), 132.0 (C(3') and C(7')), 173.61 (C=O);

HRMS: obsd ( $MH^+$ ) 247.1803. Calcd for  $C_{15}H_{22}N_2O$  246.1732.

#### *N*-[4-Methyl-4-piperidinyl]acetamide hydrochloride **10**

Anhydrous methanol (10 ml) as added to a mixture of **9** (0.5 mg, 1.77 mmol) and palladium-on-carbon catalyst 10% (131mg) in an inert atmosphere of nitrogen. Hydrogen gas was bubbled through the solution at room temperature, and the reaction monitored by T.L.C. (eluent:  $H_2O - AcOH - n-BuOH$  1: 1: 0.4 by vol.), visualising the formation of product **10** with ninhydrin spray. Once consumption of **9** was complete as indicated by T.L.C, the palladium was filtered off over a pad of celite. The resulting

filtrate was concentrated *in vacuo* to afford 335 mg (99% yield) of the desired compound **10** as a cream salt:

mp 235°C (from methanol) (lit.,<sup>1,2</sup> 230-233°C);

$\delta_{\text{H}}$  (400 MHz; CD<sub>3</sub>OH; Me<sub>4</sub>Si) 1.40 (3 H, s, CH<sub>3</sub>), 1.71 – 1.79 (2 H, m, C(4)H), 1.98 (3 H, s, COCH<sub>3</sub>), 2.47 (2 H, d,  $J$  = 14.2, C(2)H), 3.12 – 3.35 (4 H, m, C(1)H and C(5)H);

$\delta_{\text{C}}$  (100 MHz; CD<sub>3</sub>OH; Me<sub>4</sub>Si) 23.73 (OCH<sub>3</sub>), 26.28 (CH<sub>3</sub>), 33.20 (C(2) and C(4)), 41.36 (C(1) and C(6)), 51.22 (C(3)), 173.70 (CO).

#### *N*-[1-[3-(4-Fluorophenoxy)propyl-4-methyl-4-piperidinyl]acetamide **12**

To a solution of **10** (1 g, 5.2 mmol) in anhydrous DMF (28 ml) was added freshly distilled triethylamine (1.72 ml; 1.25 mmol), followed by 1-(3-chloropropoxy)-4-fluorobenzene **11** (1.06 ml; 0.573 mmol) and a spatula tip of potassium iodide. After heating the reaction mixture at 90°C for 1.5 h, the reaction was cooled to ambient temperature and the DMF removed under high pressure vacuum to give a dark brown residue. This residue was dissolved in 1M aqueous sodium carbonate solution (20 ml) and extracted with dichloromethane (3 x 30 ml). The combined extracts were washed with water (2 x 80 ml), 1M sodium carbonate (1 x 80 ml) and again with water (1 x 80 ml). Drying over magnesium sulphate, then filtration and concentration *in vacuo* gave a yellow oil (1.38 g). Purification was performed via column chromatography employing a gradient elution of methanol and chloroform, starting with 5% methanol, increasing to 10, 20, 50, and finally 100%. The pure fractions as indicated by T.L.C (eluent: chloroform - methanol, 95: 5) were combined, concentrated and the residue was recrystallised from di-isopropylether affording 213 mg (16%) of pure product **12**.

mp 104-106°C (from di-isopropylether) (lit.,<sup>1,2</sup> 103.4°C);

Found: C, 66.18; H, 7.92; N, 8.83 C<sub>17</sub>H<sub>25</sub>FN<sub>2</sub>O<sub>2</sub> requires C, 66.21; H, 8.17; N, 9.08;

$\lambda_{\text{max}}$  (EtOH)/nm 224 and 279.8 ( $\epsilon/\text{dm}^3 \text{ mol}^{-1} \text{ cm}^{-1}$  0.711, 0.815);

$\delta_{\text{H}}$  (400 MHz; CD<sub>3</sub>CN; Me<sub>4</sub>Si) 1.30 (3 H, s, CH<sub>3</sub>), 1.52 (2 H, t,  $J$  = 10.0 C(2)H or C(5)H), 1.83 (3 H, s, OCH<sub>3</sub>), 1.87 (2 H, t,  $J$  = 6.95, C(7)H<sub>2</sub>), 2.05 (2 H, d,  $J$  = 6.8, C(2)H or C(5)H), 2.21 (2 H, t,  $J$  = 10.45, C(3)H or C(4)H), 2.43 (2 H, t,  $J$  = 7.15, C(6)H<sub>2</sub>), 2.52 (2 H, d,  $J$  = 7.3, C(3)H or C(4)H), 3.96 (2 H, t,  $J$  = 6.40, C(8)OCH<sub>2</sub>), 5.97 (1 H, bs, NH), 6.85 – 7.03 (4 H, m, Ph);

$\delta_{\text{C}}$  (100 MHz; CD<sub>3</sub>CN; Me<sub>4</sub>Si) 23.8 (CO-CH<sub>3</sub>), 25.82 (CH<sub>3</sub>) 27.16 (C(7)), 36.25 (C(2), C(5)), 49.72 (C(3), C(4)), 51.46 (Cq), 55.09 (C(6)), 67.15 (C(8)), 115.91 (C(2')), 115.94 (C(6')), 116.01 (C(3')), 116.14 (C(5')), 155.80 (C(4')), 156.18 (C(1')), 169.93 (CO);

HRMS: obsd (MH<sup>+</sup>) 309.1978. Calcd for C<sub>17</sub>H<sub>25</sub>FN<sub>2</sub>O<sub>2</sub>, 308.1900.

#### *Using NaH as the base*

A suspension of 60% sodium hydride in oil (27 mg, 0.40 mmol) was washed with hexane, dried *in vacuo* and dissolved in dimethylformamide (2 ml). A solution of amine **10** (100 mg, 0.52 mmol) in dimethylformamide (5 ml), was added and the resultant reaction mixture stirred for 15 min at ambient temperature before fluorobenzene **11** (90  $\mu$ l; 0.57 mmol) was added. The reaction was left to stir for

48 h after which, an aliquot was taken for HPLC analysis (Bondapak C<sub>18</sub> 7.5 x 300 mm; MeCN - H<sub>2</sub>O - AcOH, 50: 50: 1 by vol.; 3 ml/min flow rate, **12** retention time = 6 min).

#### *Using KH as the base*

To a solution of **10** (11.3 mg, 0.06 mmol) in anhydrous DMF (2 ml) as added 35% potassium hydride in a suspension of oil (120 mg, 1.05 mmol). The reaction was stirred for 15 min at ambient temperature before the fluorobenzene **11** (13 µl; 0.065 mmol) was added. Regular aliquots of the crude reaction were removed for analysis by HPLC (Bondapak C<sub>18</sub> 7.5 x 300 mm; MeCN - H<sub>2</sub>O - AcOH, 50: 50: 1 by vol.; 3 ml/min flow rate).

#### *Using aqueous sodium hydroxide as the base*

An aqueous solution of sodium hydroxide (6M; 312 µl; 1.88 mmol) was added to a solution of amine **10** (150 mg, 0.78 mmol) in methanol (5 ml) and stirred at room temperature for 30 min before the fluorobenzene **11** (160 µl, 1.88 mmol) was added. The reaction was stirred at ambient temperature for 30 min, then heated to reflux for 16 h and monitored by HPLC (Bondapak C<sub>18</sub> 7.5 x 300 mm; MeCN - H<sub>2</sub>O - AcOH, 50: 50: 1 by vol.; 3 ml/min flow rate).

#### *Pyridine as base*

Amine **10** (10.5 mg, 0.06 mmol) and the fluorobenzene **11** (11 µl; 13.20 mg, 0.07 mmol) was stirred in 2 ml of pyridine at ambient temperature, overnight. The reaction was initially heated with an air gun to improve the solubility of **10** in pyridine. An aliquot of the crude reaction was taken after 16 h for analysis by HPLC (Bondapak C<sub>18</sub> 7.5 x 300 mm; MeCN - H<sub>2</sub>O - AcOH, 50: 50: 1 by vol.; 3 ml/min flow rate).

#### *Hinig's base*

To a solution of amine **10** (10 mg, 0.05 mmol) in dimethylformamide was added *N,N*-diisopropyl ethylamine (20 µl; 14.84 mg; 0.11 mmol) and the fluorobenzene **11** and stirred at room temperature for 16 h and then an aliquot of the reaction mixture was analysed by HPLC (Bondapak C<sub>18</sub> 7.5 x 300 mm; MeCN - H<sub>2</sub>O - AcOH, 50: 50: 1 by vol.; 3 ml/min flow rate).

### **1-[3-(4-Fluorophenoxy)propyl]4-methyl-4-piperidinamine 13**

#### *Method 1:*

Acetamide **12** (50 mg, 0.17 mmol) was dissolved in 55% hydrazine hydrate (2 ml, 1.2 mmol) and heated to 90°C (oil bath temperature). The reaction was monitored by HPLC (µ Bondapak C<sub>18</sub> 7.5 x 300 mm; MeCN - H<sub>2</sub>O - AcOH, 50: 50: 1 by vol.; 3 ml/min flow rate). After 16 h the reaction mixture was concentrated *in vacuo* yielding a white solid (51 mg) which on HPLC was shown to be unconverted acetamide **12**.

*Method 2:*

Acetamide **12** (200 mg, 0.66 mmol) was heated in freshly prepared aqueous 2M HCl (2.77 ml) at reflux for 48 h. The reaction was monitored by HPLC ( $\mu$  Bondapak C<sub>18</sub> 7.5 x 300 mm; MeCN - H<sub>2</sub>O - AcOH, 50: 50: 1 by vol.; 3 ml/min flow rate). The pH of the reaction mixture was increased to 14 with an aqueous solution of 6M NaOH and extracted with dichloromethane (3 x 5ml). The combined organic phases were dried over magnesium sulphate, filtered and concentrated *in vacuo* to give 177 mg of the desired product, 1-[3-(4-fluorophenoxy)propyl]4-methyl-4-piperidinamine, as a brown oil:

$\delta_{\text{H}}$  (400 MHz; CD<sub>3</sub>OH; Me<sub>4</sub>Si) 1.08 (3 H, s, CH<sub>3</sub>), 1.42 – 1.58 (4 H, m, C(2)H and C(6)H), 1.84 – 1.97 (2 H, m, C(7)H<sub>2</sub>), 2.47 (6 H, t,  $J = 7.1$  C(4)H<sub>2</sub>, C(3)H<sub>2</sub>, C(6)H<sub>2</sub>), 3.97 (2 H, t,  $J = 6.4$ , C(8)O-CH<sub>2</sub>), 6.86 – 7.04 (4 H, m, Ph);

$\delta_{\text{C}}$  (100 MHz; CD<sub>3</sub>OH) 28.15 (C(7)), 28.77 (CH<sub>3</sub>), 40.30 (C(2), C(5)), 51.43 (C(3), C(4)), 55.62 (C(6)), 68.3 (C(8)), 116.9 (C(2')), 117.03 (C(6')), 117.11 (C(3')), 117.9 (C(5')), 157.05 (C(4')), 157.84 (C(1'));

HPLC r.t = 4.18 min;

HRMS: obsd (MH<sup>+</sup>) 267.1863. Calcd for C<sub>15</sub>H<sub>23</sub>FN<sub>2</sub>O, 266.1794.

*Standard procedure for model coupling reactions*

Triethylamine (1.8 ml, 12.8 mmol) was added to a solution of salicylic acid **18** (1.86 g, 11.9 mmol) in anhydrous dimethylformamide (40 ml) at -5°C and stirred for 15 min before ethyl chloroformate (1.2 ml, 12.0 mmol) was added. Following a further one hour stirring, the reaction temperature was increased to 10°C and a solution of 1-methyl cyclohexylamine (1.3 ml, 10 mmol) in dimethylformamide (35 ml) was added and the reaction stirred overnight at room temperature. The dimethylformamide was removed under positive pressure and the residue dissolved in dichloromethane, washed with water, then 5% aqueous sodium hydroxide solution and finally once more with water. The organic phase was dried over magnesium sulphate, filtered and concentrated under reduced pressure to provide a yellow oil (1.02 g) which by T.L.C (eluent: ether) was shown to be a mixture of compounds.

*Cyclohexyl methylacetamide 26*

1-Methyl cyclohexylamine **25** (2 ml, 17.7 mmol) in dichloromethane (10 ml) was added to a solution of ethyl chloroformate (1.8 ml, 18.3 mol) in dichloromethane (10 ml) at a temperature of 10°C. After stirring overnight at ambient temperature the reaction was washed with water (50 ml), NaOH (5%, 50 ml) and again with water (50 ml), dried over magnesium sulphate, filtered and concentrated *in vacuo* to give 1.52 mg of a yellow liquid that was shown to be cyclohexy methylacetamide **26**.

$\delta_{\text{H}}$  (250 MHz; CD<sub>3</sub>CN; Me<sub>4</sub>Si) 1.20 (3 H, t,  $J = 7.0$ , CH<sub>2</sub>CH<sub>3</sub>), 1.29 – 1.47 (6 H, m, C(3)H<sub>2</sub>, C(4) H<sub>2</sub> and C(5) H<sub>2</sub>), 1.55 (2 H, bd,  $J = 16.6$ , C(6)H<sub>2</sub>), 1.78 (2 H, bd,  $J = 12$  C(2)H<sub>2</sub>), 2.72 (3 H, s, CH<sub>3</sub>), 4.05 (2 H, q,  $J = 7.0$ , OCH<sub>2</sub>);



$\delta_{\text{C}}$  (62.9 MHz;  $\text{CD}_3\text{CN}$ ;  $\text{Me}_4\text{Si}$ ) 15.16 ( $\text{CH}_2\text{CH}_3$ ), 26.67 (C(4)), 26.27 (C(3), C(5)), 28.72 ( $\text{CH}_3$ ), 30.90 (C(2), C(6)), 55.78 (C(1)), 61.65 ( $\text{OCH}_2$ ), 156.98 (CO);

HRMS: obsd ( $\text{MH}^+$ ) 186.1493. Calcd for  $\text{C}_{10}\text{H}_{19}\text{NO}_2$ , 185.1416.

#### *N*-(1-methyl-cyclohexyl)-benzamide 27

Triethylamine (1.79 ml, 12.8 mmol) was added dropwise to a solution of benzoic acid (1.46 g, 11.9 mmol) at a temperature of  $-5^\circ\text{C}$  and stirred for 15 min before to the addition of ethylchloroformate (1.18 ml, 12 mmol). After stirring for 1 hour the reaction temperature was increased to  $10^\circ\text{C}$  for the addition of a solution of 1-methyl cyclohexylamine (1.3 ml, 10 mmol) in dichloromethane (35 ml). After stirring overnight at room temperature the reaction mixture was washed with water (50 ml), NaOH (5%, 50 ml) and again with water (50 ml), dried over magnesium sulphate, filtered and concentrated *in vacuo* to give a yellow liquid which by T.L.C (eluent: diethyl ether: hexane, 80:20) was shown to be a mixture of two compounds. Flash column chromatography employing 80% diethyl ether - 20% hexane as the eluent gave 1.04 g of cyclohexyl methylacetamide **26** as a yellow liquid and the desired product, *N*-(1-methyl-cyclohexyl)-benzamide **27** which was recrystallised as a white solid from diethyl ether (1.25 g, 49.5%):

mp (from diethyl ether)  $85^\circ\text{C}$ ;

Found: C, 77.46; H, 8.79; N, 6.51  $\text{C}_{14}\text{H}_{19}\text{NO}$  requires C, 77.38; H, 8.81; N, 6.45;

$\delta_{\text{H}}$  (250 MHz;  $\text{CD}_3\text{OD}$ ;  $\text{Me}_4\text{Si}$ ; 300K) 0.82 – 1.3 (4 H, m, (hexyl)*H*), 1.32 – 1.96 (16 H, m, (hexyl)*H*), 2.82 (2.4 H, s  $\text{CH}_3$ ), 2.96 (3.6 H, s,  $\text{CH}_3$ ), 7.32 – 7.58 (10 H, m, aromatic H);

$\delta_{\text{H}}$  (250 MHz;  $\text{CD}_3\text{OH}$ ;  $\text{Me}_4\text{Si}$ ; 330K) 1.13 (2 H, bs, (hexyl)*H*), 1.54 – 1.82 (8 H, m, (hexyl)*H*), 2.90 (3 H, bs  $\text{CH}_3$ ), 7.32 – 7.35 (5 H, m, aromatic H);

$\delta_{\text{C}}$  (62.9 MHz;  $\text{CD}_3\text{OD}$ ;  $\text{Me}_4\text{Si}$ ) 26.12 (C(2), C(3), C(4), C(5)) or C(6)), 26.62 (C(2), C(3), C(4), C(5)) or C(6)), 26.82 (C(2), C(3), C(4), C(5)) or C(6)), 28.05 ( $\text{CH}_3$ ), 30.55 (C(2), C(3), C(4), C(5)) or C(6)), 31.58 (C(2), C(3), C(4), C(5)) or C(6)), 32.82 ( $\text{CH}_3$ ), 55.07 (C(1)), 60.19 (C(1)), 127.08 (C(2')) and C(6')), 127.76 (C(3')) and C(5')), 129.75 (C(4')), 130.67 (C(1')), 138.15 (CO).

HRMS: obsd ( $\text{MH}^+$ ) 218.1540. Calcd for  $\text{C}_{14}\text{H}_{19}\text{NO}$ , 217.1467.

#### *N*-[1-3-(4-fluorophenoxy)propyl]-4-methyl-4-piperidinyl-benzamide 28

Following the standard reaction conditions triethylamine (0.42 ml, 0.42 mmol) was added dropwise to a solution of benzoic acid (48 mg, 0.39 mmol) followed by ethylchloroformate (0.39 ml, 0.40 mmol) and 1-[3-(4-fluorophenoxy)propyl]-4-methyl-4-piperidinamine **13** (88.1 mg, 0.33 mmol) in dichloromethane. After stirring overnight at room temperature the reaction mixture was worked up as for the coupling with the model amine **25** to give a yellow oil (67.6 mg). This crude mixture was purified by flash column chromatography employing a gradient of diethyl ether and hexane as the eluent. The percentage of hexane was increased from 0 to 20 and finally 50%. Two major fractions (38 mg and 24 mg, respectively) were recovered off the column. MS (CI +ve mode) of the first fraction included a peak at  $m/z = 338$  ( $\text{MH}^+$ , 75%) indicating the presence of [1-3-(4-

fluorophenoxy)propyl)-4-methyl-4-piperidinyl]-carbamic acid ethyl ester **29**. The second fraction contained the desired product, *N*-[1-3-(4-fluorophenoxy)propyl)-4-methyl-4-piperidinyl]-benzamide **29**. MS (CI +ve mode) revealed a peak at  $m/z = 371$  ( $MH^+$ , 68%). The presence of impurities in these fractions prevented the assignment of  $^1H$ -NMR.

#### 2-Hydroxy- *N*-(1-methyl-cyclohexyl)-benzamide **30**

The standard procedure was followed for salicylic acid (822 mg, 5.95 mmol) in dichloromethane (20 ml). The reaction mixture was stirring overnight at ambient temperature and then worked up as for the coupling of benzoic acid to yield 768 mg of a yellow liquid. Flash column chromatography employing 50% diethyl ether: 50% hexane as the eluent gave 440 mg of cyclohexyl methylacetamide **26** as a yellow liquid, 49 mg of an unidentified compound and 141 mg of 2-hydroxy- *N*-(1-methyl-cyclohexyl)-benzamide **30** (10.1%).

$\delta_H$  (250 MHz;  $CD_3CN$ ;  $Me_4Si$ ; 300K) 0.91 – 1.18 (2 H, m, (cyclohexyl)*H*), 1.42 – 1.93 (8 H, m, (cyclohexyl)*H*), 2.66 (1 H, s  $CH_3$ ), 2.89 (2 H, s,  $CH_3$ ), 3.45 (1 H, bs, *NH*), 4.41 (1 H, bs, *NH*) 7.22 – 7.43 (4 H, m, aromatic *H*);

$\delta_H$  (250 MHz;  $CD_3CN$ ;  $Me_4Si$ ; 355K) 1.04 – 1.23 (2 H, m, C(11)*H*), 1.48 – 1.76 (8 H, m, (cyclohexyl)*H*), 2.90 (3 H, s + broad shoulder  $CH_3$ ), 7.22 – 7.43 (4 H, m, aromatic *H*);

$\delta_C$  (62.9 MHz;  $CD_3CN$ ;  $Me_4Si$ ) 25.84 (C(2), C(3), C(4), C(5)) or C(6)), 26.17 (C(2), C(3), C(4), C(5)) or C(6)), 26.37 (C(2), C(3), C(4), C(5)) or C(6)), 26.55 (C(2), C(3), C(4), C(5)) or C(6)), 26.59 (C(2), C(3), C(4), C(5)) or C(6)), 27.43 ( $CH_3$ ), 30.20 (C(2), C(3), C(4), C(5)) or C(6)), 30.86 (C(2), C(3), C(4), C(5)) or C(6)), 31.40 (C(2), C(3), C(4), C(5)) or C(6)), 31.70 ( $CH_3$ ), 53.78 (C(1)), 59.19 (C(1)), 117.5 (C(3'), C(4'), C(5') or C(6')), 123.59 (C(3'), C(4'), C(5') or C(6')), 123.77 (C(3'), C(4'), C(5') or C(6')), 127.41 (C(3'), C(4'), C(5') or C(6')), 128.21 (C(3'), C(4'), C(5') or C(6')), 128.65 (C(3'), C(4'), C(5') or C(6')), 129.03 (C(1')), 130.82 (C(3'), C(4'), C(5') or C(6')), 130.96 (C(3'), C(4'), C(5') or C(6')), 131.75 (C(1')), 154.22 (C(2')), 154.11 (C(2')), 167.59 (CO), 167.73 (CO).

HRMS: obsd ( $MH^+$ ) 234.1490. Calcd for  $C_{14}H_{19}NO_2$ , 233.1467.

#### 4-amino-*N*-(1-methyl-cyclohexyl)-benzamide **31**

A solution of 4-amino benzoic acid (500 mg, 3.61 mmol) in dimethylformamide (10 ml) was treated with triethylamine (0.54 ml, 3.89 mmol) and ethyl chloroformate (360  $\mu$ l, 3.66 mmol) following the standard procedure before the addition of 1-methyl cyclohexylamine. After stirring overnight at ambient temperature the reaction was worked up as for the coupling of 4-amino salicylic acid to yield a yellow liquid (456 mg). Flash column chromatography employing a gradient of diethyl ether and ethanol (0, 10, 20, 50%) gave 4 products: 175 mg of cyclohexyl methylacetamide **26** as a yellow liquid, two unidentified product (93 mg, T.L.C eluent: diethyl ether,  $r_f$  0.44 and 42 mg, T.L.C eluent: diethyl ether,  $r_f$  0.07), and the desired product 4-amino-*N*-(1-methyl-cyclohexyl)-benzamide **31** as a white solid (89 mg, 10.7%):

$\delta_{\text{H}}$  (250 MHz;  $(\text{CD}_3)_2\text{SO}$ ;  $\text{Me}_4\text{Si}$ ; 300K) 1.05 – 1.78 (14.5 H, m, (cyclohexyl) $H$ ), 2.79 (4.2 H, s  $\text{CH}_3$ ), 3.19 (3 H, s,  $\text{CH}_3$ ), 6.55 (2 H, d,  $J = 8.5$ , C(2) $H$ , C(6) $H$ ), 6.62 (0.68 H, d,  $J = 8.5$ , C(2) $H$ , C(6) $H$ ), 7.07 (2 H, d,  $J = 8.3$ , C(3) $H$ , C(5) $H$ ), 7.34 (0.77 H, d,  $J = 8.3$ , C(3) $H$ , C(5) $H$ ), 7.71-7.83 (1.40 H, dd,  $J = 8.5$ ,  $\text{NH}_2$ );

$\delta_{\text{H}}$  (250 MHz;  $(\text{CD}_3)_2\text{SO}$ ;  $\text{Me}_4\text{Si}$ ; 360K) 1.05 – 1.78 (15 H, m, (cyclohexyl) $H$ ), 2.82 (4.2 H, s  $\text{CH}_3$ ), 3.07 (3 H, bs,  $\text{CH}_3$ ), 6.57 (2 H, d,  $J = 8.5$ , C(2) $H$ , C(6) $H$ ), 6.64 (0.75 H, d,  $J = 8.5$ , C(2) $H$ , C(6) $H$ ), 7.06 (2 H, d,  $J = 8.5$ , C(3) $H$ , C(5) $H$ ), 7.28 (0.79 H, d,  $J = 8.5$ , C(3) $H$ , C(5) $H$ ), 7.72-7.78 (1 H, dd,  $J = 8.5$ ,  $\text{NH}_2$ );

HRMS: obsd ( $\text{MH}^+$ ) 233.120. Calcd for  $\text{C}_{14}\text{H}_{20}\text{N}_2\text{O}$ , 232.160.

#### 4-*tert*-Butoxycarbonylamino-2-hydroxy-benzoic acid 32

A two-phase system of *t*-butanol (9.9 ml) and aqueous sodium hydroxide (600mg, 15 mmol in 14 ml water) was added to salicylic acid **18** (2.00 g, 13 mmol), followed by di-*tert*-butyl dicarbonate (2.85 ml, 2.86 mg, 12.2 mmol). The reaction was stirred at room temperature for 70 h and subsequently quenched with water (10 ml), then extracted with ethyl acetate (15 ml). The aqueous layer was acidified (pH 2) with 1M hydrochloric acid and further extracted with ethyl acetate (3 x 30 ml). The organic phases were combined, dried over magnesium sulphate and concentrated *in vacuo* to afford a brown foam (3.15 mg) that was identified as the Boc-protected product **32** (65% pure by NMR).

$\delta_{\text{H}}$  (400 MHz;  $(\text{CD}_3)_2\text{CO}$ ;  $\text{Me}_4\text{Si}$ ) 1.49 (9 H, s,  $(\text{CH}_3)_3$ ), 7.31 (1 H, d,  $J = 2.02$ , Ar  $H$ ), 7.79 (2 H, d,  $J = 8.79$ , Ar  $H$ ), 8.76 (1 H, bs,  $\text{NH}$ );

$\delta_{\text{C}}$  (100MHz;  $(\text{CD}_3)_2\text{CO}$ ;  $\text{Me}_4\text{Si}$ ) 28.39 ( $\text{C}(\text{CH}_3)_3$ ), 60.61 ( $\text{C}(\text{CH}_3)_3$ ), 107.12 C(3), 110.08 C(5), 131.95 C(6), 147.53 C(4), 164.16 C(2), 172.4 ( $\text{CO}_2\text{H}$ ), 206.41 ( $\text{CO}_2\text{Boc}$ ).

#### 4-amino-2-hydroxybenzoic acid benzyl ester 33

A suspension of 60% sodium hydride in oil (995 mg, 24.88 mmol) was washed with hexane, dried *in vacuo* and dissolved in dimethylformamide (5 ml). A solution of crude Boc-protected salicylic acid **32** (3.146 g, 8.08 mmol) in dimethylformamide (7 ml), was added and the resultant reaction mixture stirred for 15 min at ambient temperature before the benzylbromide (3 ml, 24.88 mmol) was added. The reaction was left to stir for 60 h after which, water (5 ml) was added to quench the sodium hydride. The dimethylformamide was removed under positive pressure, then the residue was diluted in water (15 ml) and extracted with ethyl acetate (3 x 20 ml). The combined ethyl acetate phases were dried over magnesium sulphate, filtered and concentrated under reduced pressure to give a yellow oil (5.482 mg). A fraction of this crude product (2 g) was treated with 3M hydrochloric acid in ethyl acetate (3 ml) until a white solid formed (16 h). The reaction mixture was concentrated *in vacuo* and 4-amino-2-hydroxybenzoic acid benzyl ester **33** was recrystallised from ethanol and diethyl ether (382 mg, 1.54 mmol).

$\delta_{\text{H}}$  (400 MHz;  $\text{CD}_3\text{OD}$ ;  $\text{Me}_4\text{Si}$ ) 5.41 (2 H, s,  $\text{CH}_2$ ), 6.93 (2 H, dd,  $J = 9.57, 7.5$ , C(5) $H$ ), 7.01 (2 H, d,  $J = 2.07$ , C(3) $H$ ), 7.33-7.47 (5 H, m, Ar $H$ ), 7.99 (2 H, d,  $J = 8.48$ , C(6) $H$ );

$\delta_c$  (100 MHz; CD<sub>3</sub>OD; Me<sub>4</sub>Si) 69.02 CH<sub>2</sub>, 113.27 C(4), 114.39 C(2), 115.32 C(6), 130.01 C(2'), C(6'), 130.14 C(4'), 130.2 C(3'), C(5'), 133.74 C(1), 137.06 C(1'), 139.54 C(5), 164.13 C(3), 170.57 CO<sub>2</sub>H

### 2,4,6-Tribromo-5-aminophenol

A mixture of 3-aminophenol (168 mg, 1.5 mmol) and *N*-bromosuccinimide (275 mg, 1.5 mmol) in carbon tetrachloride was heated to reflux. After 5 h succinimide was filtered off and washed with carbon tetrachloride and the filtrate was concentrated *in vacuo*. The resulting brown crystals were purified by column chromatography [silica; diethyl ether – hexane, 50/50 v/v] to provide 68.1 mg of 2,4,6-tribromo-5-aminophenol as green crystals:

$\delta_H$  (400 MHz; CD<sub>3</sub>OD; Me<sub>4</sub>Si) 7.473 (1 H, s, C(6)H);

HRMS: obsd ( $M^+$ ) 242.784 233 (33, 3 x <sup>79</sup>Br), 344.782 (100, 2 x <sup>79</sup>Br, 1 x <sup>81</sup>Br), 346.780 (98.1, 2 x <sup>81</sup>Br, 1 x <sup>79</sup>Br), 348.779 (32.1, 3 x <sup>81</sup>Br). Calcd for C<sub>6</sub>H<sub>4</sub>Br<sub>3</sub>NO, 342.784

and 5 mg of 2-bromo-5-aminophenol (0.03 mmol, 0.2%) as a yellow solid:

$\delta_H$  (400 MHz; CD<sub>3</sub>OD; Me<sub>4</sub>Si) 7.09 (1 H, d,  $J$  = 8.55, C(3)H), 6.30 (1 H, d,  $J$  = 2.53, C(6)H), 6.15 (1 H, dd,  $J^1$  = 10.88,  $J^2$  = 2.53, C(4)H).

The other two products were shown by MS to be the di-brominated compounds.

## 4.5 References

1. Leysen J & Van Daele G. 4-Amino-N-(4-methyl-4-piperidiny)-2-methoxybenzamide for treating smooth muscle contraction disorders. Patent US-0549818 1996
2. Leysen J & Van Daele G. 4-Amino-N-(4-methyl-4-piperidiny)-2-methoxybenzamide. Patent WO-09402462 1995
3. Mertens J, Terriere D, Sipido V, Gommeren W, Janssen PMF, Leysen JE. Radiosynthesis of a new radioligand for serotonin-5-HT<sub>2</sub>-receptor, a promising tracer for gamma-emission tomography. *J Label Compd Radiopharm.* 1995; **34**: 795-806.
4. Terriere D, Janssen PMF, Gommeren W, Gysemans M, Mertens JJR, Leysen JE. Evaluation of radioiodo-4-amino-N-[1-[3-(4-fluorophenoxy)-propyl]-4-methyl-4-piperidiny]-5-iodo-2-methoxybenzamide as a potential 5-HT<sub>2</sub> receptor tracer for SPECT. *Nucl Med Biol.* 1995; **22**: 1005-1010.
5. Abi-Dargham A, Zea-Pounce Y, Terriere D, Al-Tikriti M, Baldwin RM, Hoffer P, Charney D, Leyen JE, Laurelle M, Mertens J, Innis RB. Preclinical evaluation of [<sup>123</sup>I]R93274 as a SPET radiotracer for imaging 5-HT<sub>2A</sub> receptors. *Eur J Pharmacol.* 1997; **321**: 285-293.
6. Busatto GF, Pilowsky LS, Costa DC, Mertens J, Terriere D, Ell PJ, Mulligan R, Travis MJ, Leysen JE, Lui D, Gacinovic S, Waddington W, Lingford-Hughes A, Kerwin RW. Initial evaluation of 123-I-5-R91150, a selective 5-HT<sub>2A</sub> ligand for single photon emission tomography (SPET), in healthy human subjects. *Eur J Nucl Med.* 1997; **24**: 119-124.
7. Travis MJ, Busatto GF, Pilowsky LS, Mulligan R, Acton PD, Gacinovic S, Mertens J, Terriere D, Costa DC, Ell PJ, Kerwin RW. 5-HT<sub>2A</sub> receptor blockade in patients with schizophrenia treated with risperidone or clozapine. A SPET study using the novel 5-HT<sub>2A</sub> ligand <sup>123</sup>I-5-I-R-91150. *Br J Psychiatry.* 1998; **173**: 236-241.
8. Travis MJ, Visvikis D, Erlandsson K, Mulligan RS, Waddington WA, Matthiasson P, Pilowsky LS, Costa DC, Ell PJ, Kerwin RW. Dynamic displacement of the selective 5-HT<sub>2A</sub> receptor ligand I-123-5-I-R91150 by unlabelled ketanserin. *J Nucl Med.* 2000; **41**: 935.
9. Mulligan RS, Osman S, Travis MJ, Eersels JLH, Pilowsky LS, Ell PJ, Pike VW. [123I]5-Iodo-R91150, a radioligand for 5-HT<sub>2A</sub> receptors – Radiochemical stability and metabolism. *J Label Cpd Radiopharm.* 1999; **42**: S669-S671.
10. Kessler RM, Ansari MS, de Paulis T, Schmidt DE, Clanton JA, Smith HE, Manning RG, Gillespie D, Ebert MH. High affinity dopamine D<sub>2</sub> receptor radioligands. 1. Regional rat brain distribution of iodinated benzamides. *J Nucl Med.* 1991; **32**: 1593-1600.
11. Lundkvist C, Halldin C, Ginovart N, Nyberg S, Swahn CG, Carr AA, Brunner F, Farde L. [C-11]MDL 100907, a radioligand for selective imaging of 5-HT<sub>2A</sub> receptors with positron emission tomography. *Life Sciences.* 1996; **58**: PL187-PL192.

12. Price J, Lopresti, B, Mathis C, Simpson N, Mahmood K, Huang Y, Smith G, Mintum M. Kinetic analyses of [C-11]MDL 100907 in baboons: evaluation of its suitability as a serotonin (5-HT<sub>2A</sub>) radiotracer. *J Nuc Med.* 1996; **37**: 45P.
13. Ito H, Nyberg S, Halldin C, Lundkvist C, Farde L. PET imaging of central 5-HT<sub>2A</sub> receptors with carbon-11-MDL 100,907. *J Nucl Med.* 1998; **39**: 208-214.
14. Niwa H, Hida T, Jamad K. A new method for cleavage of aliphatic methylethers. *Tetrahedron Lett.* 1981; **22**: 4239-4240.
15. March J. *Advanced Organic Chemistry. Reactions, mechanisms and structure.* 4<sup>th</sup> Ed. John Wiley & Sons New York. p 531-532.
16. Paul V, Sudalai A, Daniel T, Srinivasan. Regioselective bromination of activated aromatic substrates with N-bromosuccinimide over HZSM-5<sup>#</sup>. *Tetrahedron Lett.* 1994; **35**: 7055-6056.
17. Keith DD, Tortora JA, Yang R. Synthesis of L-2-amino-4-(methoxy)-*trans*-but-3-enoic acid. *J Org Chem.* 1978; **43**: 3711-3713.
18. Dilbeck GA, Field L, Gallo AA, Gargiulo RJ. Biologically Oriented Organic Sulfur Chemistry. 19. Synthesis and properties of 4-amino-5-mercapto-5-methylhexanoic acid, a bishomologue of penicillamine. Use of boron trifluoride etherate for catalysing Markownikoff addition of a thiol to an olefin. *J Org Chem.* 1978; **43**: 4593-4596.
19. Kharasch MS. *Grignard Reactions of Nonmetallic Substances.* Prentice-Hall, Englewood Cliffs, NJ. 138-528.
20. Jones RG & Wilkins JM. Carbon-13 NMR spectra of a series of *para*-substituted *N,N*-dimethylbenzamide. Comparisons of linear free energy relationships for carbon-13 and nitrogen-15 chemical shifts and rotation barriers. *Org Mag Resonance.* 1978; **11**: 20-26.
21. Sanders JKM & Hunter BK. *Modern NMR spectroscopy. A guide for Chemists.* 2<sup>nd</sup> Ed. Oxford University Press, Oxford. 1993.
22. Koziara A, Osowska-Pacewicz K, Zawadzki S, Zwierzak A. A simple one-pot transformation of *t*-alkyl chloride into (*t*-alkyl)amines. *Synthesis.* 1987; **5**: 487-489.
23. Jackman LM, Kavanagh TE, Haddon RC. Studies in nuclear magnetic resonance – IX: Rotational barriers in substituted *N,N*-dimethylbenzamide. *Org Mag Resonance.* 1969; **1**: 109-123.
24. Rae ID. Carbon-13 NMR spectra of some amides and lactams and their thio and seleno analogues. *Aust J Chem.* 1979; **32**: 567-573.
25. Suzuki K, Tomooka K, Katayama E, Matsumoto T, Tsuchihashi G. Stereocontrolled asymmetric total synthesis of photomycinolide-IV. *J Am Chem Soc.* 1986; **108**: 5221-5229.
26. Dr Robin Allan, The Adrien Albert Laboratory of Medicinal Chemistry, Department of Pharmacology, The University of Sydney, New South Wales 2006, Australia; personal communication.

27. Stahl GL, Walter R, Smith CW. General procedure of the synthesis of mono-*N*-acylated 1,6-diaminohexanes. *J Org Chem.* 1978; **43**: 2285-2286.
28. Perry RJ, Turner SR. Preparation of *N*-substituted phthalimides by the palladium-catalyzed carbonylation and coupling of *o*-dihalo aromatics and primary amines. *J Org Chem.* 1991; **56**: 6573-6579.
29. Cai M-Z, Song C-S, Huang X. Amidation of aryl halides catalyzed by silica-supported bidentate phosphine palladium complex. *Syn Comm.* 1997; **27**: 367-373.
30. Schoenberg A, Heck RF. Palladium-catalyzed amidation of aryl, heterocyclic, and vinylic halides. *J Org Chem.* 1974; **39**: 3327-3331.
31. Zeisler SK, Nader M, Theobald A, Oberdorfer F. Conversion of no-carrier-added [<sup>11</sup>C]carbon dioxide to [<sup>11</sup>C]carbon monoxide on molybdenum for the synthesis of C-11-labelled aromatic ketones. *Appl Radiat Isot.* 1997; **48**:1091-1095.
32. Lidström P, Kihlberg T, Långstöm B. [<sup>11</sup>C]Carbon monoxide in the palladium-mediated synthesis of <sup>11</sup>C-labelled ketones. *J Chem Soc, Perk Trans 1.* 1997;2701-2706.
33. Kihlberg T, Lidström P, Långstöm B. Palladium mediated carbonylation reactions using [<sup>11</sup>C]carbon monoxide in a high pressure microautoclave. *J Labelled Compd Radiopharm.* 1997; **40**: 781-782.
34. Al-Qahtani MH, Pike VW. Palladium(II)-mediated <sup>11</sup>C-carbonylative coupling of diaryliodonium salts with organostannanes – a new, mild and rapid synthesis of aryl [<sup>11</sup>C]ketones. *J Chem Soc, Perk Trans 1.* 2000; **5**: 1033-1036.
35. Kihlberg T, Långstöm B. [<sup>11</sup>C]Carbon monoxide in synthesis of <sup>11</sup>C-labeled esters using palladium –mediated reaction with organo halides. *J Labelled Compd Radiopharm.* 2001; **44**: S990-S992.
36. Kihlberg T, Långstöm B. Biologically active <sup>11</sup>C-labeled amides using palladium-mediated reactions with aryl halides and [<sup>11</sup>C]carbon monoxide. *J Org Chem.* 1999; **64**: 9201-9205.
37. Special reagents for thiol groups. In *Aldrichimica Acta*. Aldrich Chemical Company, Inc., Wisconsin. 1971; **4**: 33-48.
38. Di Fabio R, Capelli AM, Conti N, Cugola A, Donati D, Feriani , Gastaldi P, Gaviraghi G, Hewkin CT, Micheli F, Missio A, Mugnaini M, Pecunioso A, Quaglia AM, Ratti E, Rossi L, Tedesco G, Trist DG, Reggiani A. Substituted Indole-2-carboxyates as *in vivo* potent antagonists acting as the strychnine-insensitive glycine binding site. *J Med Chem.* 1997; **40**: 841-850.

## ***Chapter 5:***

***Radiolabelling of [ $^{123}\text{I}$ ]epidepride with alkyl-stannyl precursors***



## 5.1 Introduction

### 5.1.1 Dopamine role in the brain

Dopamine is a monoamine neurotransmitter that is widely distributed in the human brain. Most dopaminergic neurons are mesencephalic with cell bodies located in the dorsal portion of the substantia nigra and the medially adjacent ventral tegmental area.<sup>1</sup> Three partially overlapping fiber bundles project from these cell bodies. The nigrostriatal fibers project from the substantia nigra to the caudate nucleus and putamen (*i.e.* the striatum). The mesocortical fibers, arising primarily from the ventral tegmental area lead to extensive, but not uniform, cerebral cortical innervation with localisation in motor and limbic areas. The third group of dopaminergic neurons, the mesolimbic fibers, innervate limbic structures such as the amygdala. The localisation of dopaminergic neurons throughout the brain suggests an involvement in movement initiation, motivation, cognition, affect and neuroendocrine secretion.<sup>2</sup> More specifically, nigrostriatal neurons appear to be involved in the control of movement; the mesolimbic neurons in emotion and memory and neurons of the mesocortical pathway in motivation and planning, temporal organization of attention and social behaviour.<sup>1</sup> These functions are often disrupted in neurological and psychiatric disorders suggesting a direct or indirect involvement of altered dopaminergic transmission in several brain dysfunctions. For example, dopaminergic deficiency is critical to Parkinson's disease while over activity is implicated in schizophrenia. *In vivo* imaging of the dopaminergic system has become a useful tool for studying these putative functional imbalances.

### 5.1.2 Dopamine receptors

Two subtypes of dopamine receptors were originally classified with respect to pharmacological and biochemical criteria.<sup>3</sup> The D<sub>1</sub> dopaminergic receptor subtype activated G-protein linked adenylate cyclase while D<sub>2</sub> receptors inhibit this enzyme and the subsequent generation of the second messenger, cAMP. The introduction of molecular cloning has revealed this classification to be an oversimplification, with several novel subtypes being identified. These can be classified as D<sub>1</sub>-like or D<sub>2</sub>-like depending on their structural and pharmacological similarities to the original dopamine receptor nomenclature.<sup>4,6</sup> The D<sub>1</sub>-like receptors all stimulate cAMP accumulation and utilise this second messenger as its major signalling pathway. To date, this family includes the D<sub>1</sub> and the D<sub>5</sub> subtypes. The D<sub>2</sub>, D<sub>3</sub> and D<sub>4</sub> receptors are members of the D<sub>2</sub>-like receptor family and are all capable of inhibiting adenylate cyclase, leading to an inhibition of cAMP accumulation. However, like other G<sub>i</sub>-coupled receptors, this family is capable of modulating a number of second messengers such as ion channels, Na<sup>+</sup>/H<sup>+</sup>exchanger, arachidonic acid release and phosphoinositol hydrolysis.<sup>2</sup> The diversity in dopaminergic receptors allows the whole family to respond to the same signal, but at the same time provides variations in both their affinity for dopamine and signal transduction pathways. The result is a mechanism for providing complex signals to a single cell.

The most abundant and widely spread dopamine receptor subtype in human brain is the D<sub>1</sub> (B<sub>max</sub> ~ 50 pmol/g striatal tissue) followed by D<sub>2</sub> (B<sub>max</sub> ~ 20 pmol/g striatal tissue).<sup>7</sup> The region with the highest density for both D<sub>2</sub> and D<sub>1</sub> receptors is the striatum. However, both are also located at significantly lower concentrations in extrastriatal regions (B<sub>max</sub> ~ 0.5–3.0 pmol/g tissue for D<sub>2</sub>).<sup>7,8</sup> The D<sub>3</sub> receptor is specifically expressed in discrete areas of the limbic system at low concentrations (~ 1 pmol/g tissue).<sup>9</sup> The D<sub>4</sub> receptor is another subtype present at low concentrations (~ 1 pmol/g tissue) in several limbic regions.<sup>10</sup> Unlike the D<sub>1</sub> and D<sub>2</sub> receptors, the density of D<sub>3</sub> and D<sub>4</sub> in the striatum is low compared to other regions. The low levels and relative distributions of the different populations of dopaminergic receptors have meant that visualisation of one subtype *in vivo* requires a very selective ligand with very high affinity.

### 5.1.3 Relevance of the dopaminergic system to psychiatry

Abnormalities in dopaminergic transmission are implicated in many neuropsychiatric disorders. The work of this chapter has arisen from a collaboration between the Institute of Nuclear Medicine and the Institute of Psychiatry, Kings College London which focuses on the action of antipsychotic drugs at extrastriatal D<sub>2</sub>/D<sub>3</sub> receptors. Two dominant hypotheses in schizophrenia research are i) maldevelopment of the cerebral cortex, and ii) malfunction of the dopaminergic system in the brain.<sup>11</sup> The classical dopamine hypothesis proposes that the positive symptoms of schizophrenia are the result of hyperactive dopamine transmission.<sup>12</sup> Support for this hypothesis came from two key findings. Neuroleptics used successfully to manage some symptoms of schizophrenia selectively block D<sub>2</sub> receptors. There is also a correlation between the effective clinical dose and the potency of the antipsychotic at the D<sub>2</sub> receptor.<sup>13,14</sup> Secondly, dopamine enhancing drugs, such as amphetamine, induce psychotic symptoms (such as paranoid delusions) which closely resemble, and at times are from, the positive symptoms of schizophrenia.<sup>15</sup>

*In vivo* imaging of the selective D<sub>2</sub> receptor radioligand, [<sup>123</sup>I](S)-(+)-3-iodo-2-hydroxy-6-methoxy-*N*-[(1-ethyl-2-pyrrolidiny)methyl]benzamide ([<sup>123</sup>I]IBZM), in unmedicated schizophrenic patients revealed a hyperdopaminergic state in response to amphetamine challenge during the initial episode and subsequent relapse of the disease.<sup>16</sup> This same study found that during periods of remission dopamine transmission is “apparently” normal. The general perception today is that the antipsychotic effects of neuroleptics are due to their action on mesolimbic dopamine receptors. The extreme movement disorder, known as extrapyramidal side effects, suffered in 90% of medicated patients is thought to be the result of high striatal D<sub>2</sub> receptor blockade.

In addition to pharmacological evidence suggesting an extrastriatal site for the antipsychotic action of neuroleptic drugs, findings from post-mortem, neuropsychological and neuroimaging studies implicate a developmental dysconnection of temporolimbic-prefrontal cortices.<sup>11</sup> The therapeutic mechanism of antipsychotic drugs is possibly an indirect compensation of dysfunctional communication in a region of the nucleus accumbens that receives converging inputs from both the prefrontal and temporolimbic regions of the brain.<sup>11</sup>

The capacity to visualise dopaminergic transmission in highly relevant extrastriatal (thalamic and temporal cortical) regions *in vivo* has become a major direction in schizophrenia research. The lower receptor density and the presence of multiple subtypes in these regions means that radiolabelled antagonists with high affinity and selectivity are required to image these receptor sites.

#### 5.1.4 Radioligand for imaging $D_2$ receptors

Most radioligands for the  $D_2$  receptor belong to one of two groups. The first radioligands were developed from analogues of butyrophenone neuroleptics, especially spiperone (Figure 5.1). However, this group of compounds, which includes [ $^{11}\text{C}$ ]N-methylspiperone (Figure 5.1), suffer from irreversible binding and a lack of selectivity for  $D_2$  over  $5\text{-HT}_2$  receptors.<sup>17</sup> The second group are the substituted benzamides which are derived from the atypical antipsychotic, sulpiride (Figure 5.1). Because of their high selectivity, a number of substituted benzamides have been developed as

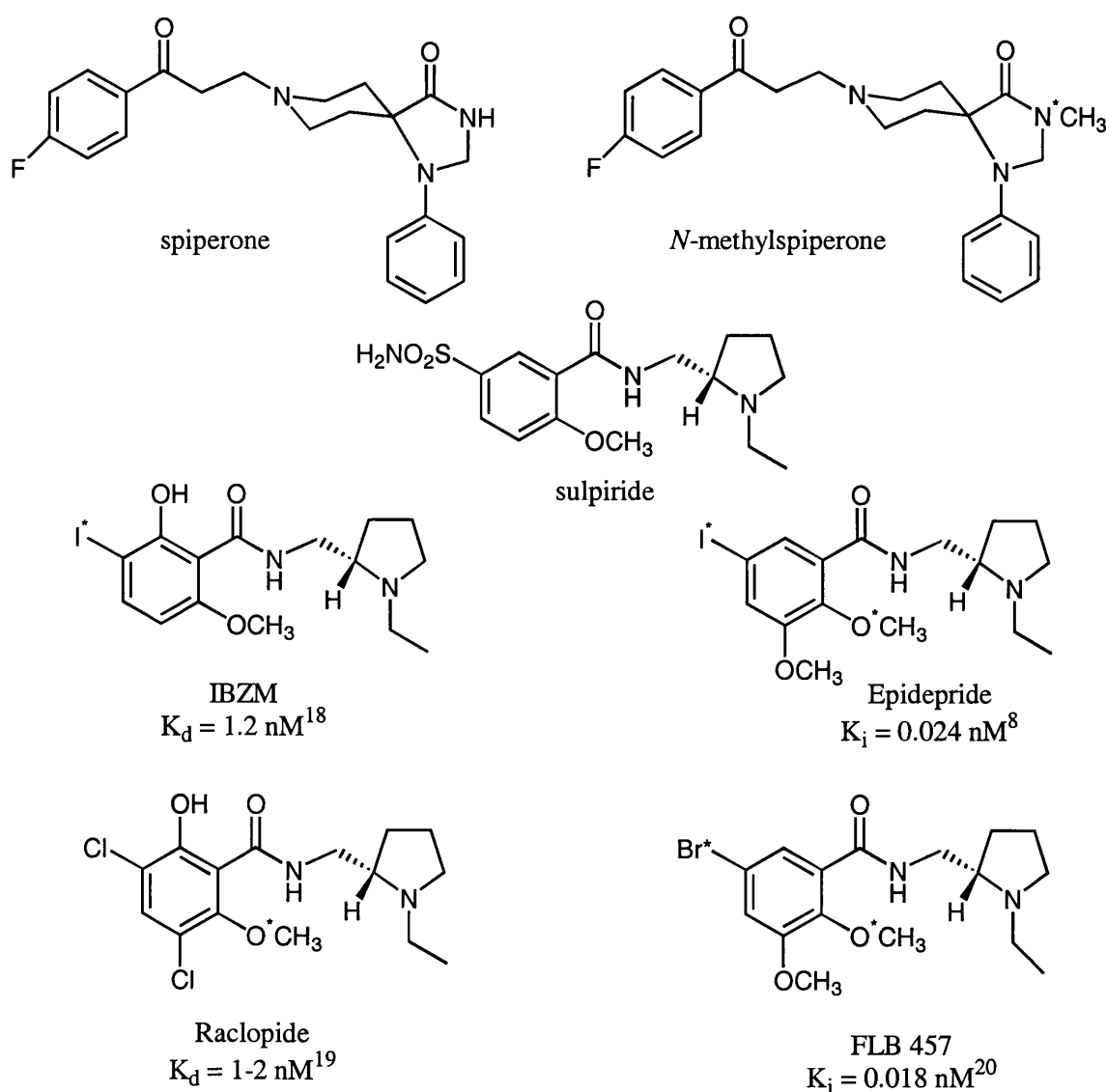


**Figure 5.1:** Structure and affinity of two classes of  $D_2$  antagonists.

\* indicates the preferred sites for radiolabelling in those that have been developed for *in vivo* visualisation of  $D_2$  receptors in human brain.

radioligands for both SPET and PET. Those that have successfully imaged human D<sub>2</sub> receptors are illustrated in Figure 5.1. The most routinely used radioligands for SPET and PET are (<sup>123</sup>I-IBZM) and [<sup>11</sup>C]raclopride (([<sup>11</sup>C](-)-(S)-3,5-dichloro-*N*(1-ethyl-2-pyrrolidinyl)methyl)-6-methoxy-salicylamide). Both have high selectivity and equilibrium dissociation constants in the nanomolar range (*i.e.* high affinity) for the D<sub>2</sub>-like dopamine receptor;<sup>18-20</sup> they are the ‘gold standards’ in their respective disciplines for the visualisation of striatal D<sub>2</sub> receptors *in vivo*. Studies employing these radioligands have greatly improved our understanding of the role of dopamine in schizophrenia<sup>16,21</sup> and the action of neuroleptics at striatal D<sub>2</sub> receptors.<sup>22-25</sup> However, for [<sup>123</sup>I]IBZM and [<sup>11</sup>C]raclopride, the low signal to noise ratio in areas of low receptor density has prevented imaging of extrastriatal receptor populations. The concentration of D<sub>2</sub> receptors in the cortex is 10–100 times lower than in the striatum.<sup>8</sup> For this reason, substituted bezamides with lower dissociation constants for the D<sub>2</sub> receptor have been developed as radioligands for visualising these receptors *in vivo*. Iodine-123 labelled epidepride ([(*S*)-*N*-((ethyl-2-pyrrolidinyl)methyl)-5-iodo-2,3-dimethoxybenzamide]) was the first effective radioligand for imaging low densities of D<sub>2</sub> receptors in man (Figure 5.2). Its high affinity ( $K_d = 0.024$  nM<sup>8</sup>) and favourable lipophilicity (apparent lipophilicity at pH 7.5 was measured as  $\log k_w = 2.05$ ;  $k_w$  the capacity factor at various concentrations of methanol extrapolated to 0%<sup>26</sup>) meant that acceptable ratios of radioactivity in striatal and extrastriatal regions, to that in the receptor-devoid cerebellum (7.8 and 2.4, respectively) were obtained in healthy volunteers.<sup>26</sup> While [<sup>123</sup>I]epidepride has been used effectively to investigate the limbic selectivity of various antipsychotic drugs,<sup>27-29</sup> the quantitative modelling of this radioligand is complicated by the occurrence of a radioactive, lipophilic metabolite that is able to enter the brain,<sup>30</sup> and its very slow kinetics in receptor-rich regions such as the striatum.

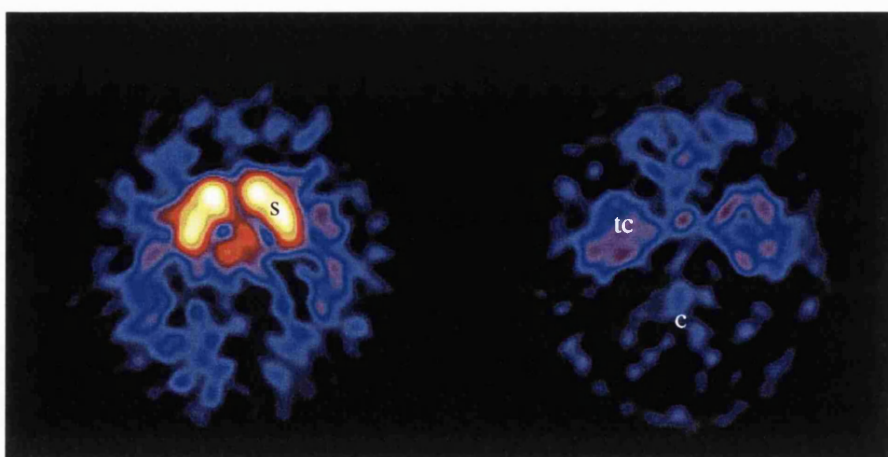
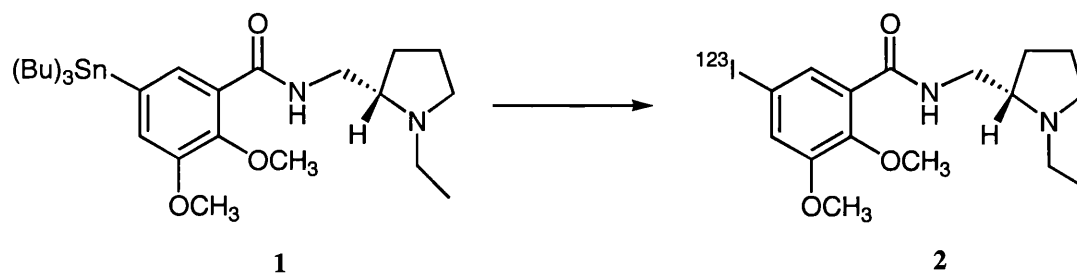


**Figure 5.2:** Human SPET images following injection of [<sup>123</sup>I]epidepride illustrating the differentiation that is possible between the cerebellum (c), temporal cortex (tc) and striatum (s) with a high affinity radioligand.

PET radioligands that enable the visualisation of extrastriatal dopamine D<sub>2</sub> receptors include [<sup>11</sup>C]epidepride,<sup>31</sup> [<sup>11</sup>C]FLB 457<sup>32</sup> and [<sup>76</sup>Br]FLB 457.<sup>33</sup> A bromo analogue of epidepride, FLB 457, has a similar affinity for D<sub>2</sub> receptors as epidepride ( $K_i = 0.018\text{nM}^{20}$ ) and the kinetics in regions of high receptor density are similarly very slow. The short half-life of carbon-11 means that an equilibrium state in the striatum cannot be reached within a PET scan for either [<sup>11</sup>C]epidepride<sup>31</sup> or [<sup>11</sup>C]FLB 457,<sup>32</sup> thereby preventing true measurement of receptor density in this region. In comparison, an equilibrium state is achieved in the low-density extrastriatal regions allowing quantification of receptor density. Since the relationship between extrastriatal and striatal regions is of key importance to the investigation of neuroleptic action in schizophrenia treatment, these <sup>11</sup>C-labelled ligands have a limited use. The limbic selectivity of various antipsychotics has been studied with carbon-11 PET.<sup>34</sup> However, the level of antipsychotic occupancy in the striatal and extrastriatal regions were determined with two radioligands, [<sup>11</sup>C]raclopride and [<sup>11</sup>C]FLB 457, respectively. To enable quantification of both extrastriatal and striatal D<sub>2</sub> receptors in the one PET scan FLB 457 has been labelled with the longer-lived positron emitter, <sup>76</sup>Br.<sup>35</sup>

In the majority of work performed with [<sup>123</sup>I]epidepride the radiosynthesis involves the radioiododestannylation of a *tri*-butylstannylated precursor using chloramine T as the oxidising agent (Figure 5.3). This work investigates the efficiency of radiolabelling two *tri*-alkylstannyl precursors of epidepride, the *tri*-methyl and *tri*-butyl, and the effect different alkyl groups can have on the results obtained. The implications of these results for alkyl-destannylation reactions in general will be discussed. The *in vivo* metabolism of radiochemically pure [<sup>123</sup>I]epidepride was also investigated employing isocratic, reverse phase HPLC.



Conditions: Na<sup>123</sup>I, HCl, chloramine-T

Figure 5.3: Radioiododestannylation of *tri*-butylstannyl precursor 1.

## 5.2 Discussion

### 5.2.1 Synthesis of the *tri*-butyltin precursor 1

The *tri*-butylstannyl precursor was a gift from Nycomed Amersham. However, no information was available on the method of synthesis or characterisation. The reported strategies for the synthesis of the *tri*-butylstannyl precursor are via bromo-metal<sup>36</sup> or iodo-metal<sup>37</sup> interchange. Treatment of (S)-N-[(1-ethyl-2-pyrrolidinyl)methyl]-5-iodo-2,3-dimethoxybenzamide with an equal amount of bis(tributyltin) in refluxing triethylamine and catalytic amounts of tetrakis(triphenylphosphine) for 3.5

h afforded the *tri*-butylstannyl precursor in 79% yield.<sup>36</sup> Flash column purification was required to remove the very lipophilic *tri-n*-butyltin iodide. Preparation from the bromo analogue, FLB 457 used the same reactions conditions but required 16 h reflux and achieved 82% yields.<sup>37</sup>

### 5.2.2 Radioiododestannylation of tributyltin precursor 1

This work used the reaction conditions developed by Clanton *et al.*<sup>36</sup> and de Paulis & Smith<sup>37</sup> for radioiododestannylation of the *tri*-butylstannyl precursor **1** (Amersham, UK) to prepare [<sup>123</sup>I]epidepride. Modifications were made in the work-up, with HPLC purification of the crude reaction mixture being carried out using the eluent reported by Hall *et al.*<sup>38</sup> (System A, see Section 5.3.2). The use of solid-phase extraction enabled dose formulation from the collected radioactive fraction without the need for a rotary evaporator. [<sup>123</sup>I]Epidepride was retained on the Sep-pak and recovered in an acceptable yield by elution with ethanol, and diluted in saline for injection.

Initial HPLC separation, following radioiododestannylation of the *tri*-butylstannyl precursor, in the presence of chloramine-T and acid, suggested 80% incorporation of <sup>123</sup>I into [<sup>123</sup>I]epidepride (Figure 5.6A). HPLC analysis of the resulting dose using System A indicated 98% radiochemical purity. However, development of a slower reverse phase HPLC system (System B, see Section 5.3.3) revealed a very broad radioactive peak (Figure 5.7A) eluting with a retention time of 26 min. This was significantly slower than expected since reference epidepride had a retention time of 18.5 min on the same HPLC system. Addition of carrier epidepride to the analyte remarkably altered the elution profile and revealed a significantly lower level of radiochemical purity (Figure 5.7B). Only 40–45% of radioactivity of the formulated dose could be credited to [<sup>123</sup>I]epidepride (r.t. = 18.5 min). The remaining 55–60% of the total radioactivity was an unidentified impurity with a longer retention time (22 min; peak c). This undesired radioactive product was also found in similar analysis of another 8 preparations from the *tri*-butylstannyl precursor. Under some HPLC conditions the radioactive impurity behaved in a very similar manner to epidepride *e.g.* System A and System B without added reference epidepride. Separation from [<sup>123</sup>I]epidepride was only observed when the formulated dose was analysed on System B, in the presence of carrier epidepride (Figure 5.7).

To determine if two different products were in fact formed during iododestannylation of the *tri*-butylstannyl precursor the two radioactive peaks were collected and separately analysed by HPLC (System B) in the presence of reference compound (Figure 5.8). The different elution behaviour of the two radioactive peaks was conserved on re-injection. The 18.5 min radioactive peak co-eluted with reference epidepride while the impurity maintained its slower retention time of 22 min. These results showed that previous observations were not an artefact of the HPLC method and that radiolabelling of our original supply of precursor **1** resulted in the formation of two radioactive products that were undistinguishable under certain HPLC conditions.

### 5.2.3 Radioiododestannylation of tri-methylstannyl precursor

The formation of the radioactive by-product was unique to reactions employing the *tri*-butylstannyl precursor. Radiolabelling with the *tri*-methylstannyl precursor (MAP Medical Oy) proceeded in good

radiochemical yield (>95%) (Figure 5.6B) and showed [ $^{123}$ I]epidepride at a high radiochemical purity when analysed on both System A and B (Figure 5.9). In comparison to the findings with reactions performed with the *tri*-butylstannyl precursor, the radiochemical purity of the formulated dose from the *tri*-methylstannyl precursor was >98% irrespective of whether reference epidepride was added to the analyte or not (System B). These results indicate that the pathway to the radioactive impurity was one that occurred at a consistent ratio to that forming [ $^{123}$ I]epidepride, but only when the *tri*-alkylstannyl group contained a butyl as opposed to a methyl group.

#### 5.2.4 Analysis of the *tri*-butylstannyl precursor

One possible explanation for the formation of the undesired radioactive byproduct, might have been the presence of an impurity in the *tri*-butylstannyl precursor. Nycomed Amersham provided no information on the original stock of *tri*-butyltin precursor. However, MS and HPLC analysis (System C, see Section 5.3.4) of the original *tri*-butylstannyl precursor indicated only traces of impurity (Figure 5.10 and 5.11). MS revealed a number of other molecular ions at significantly lower abundance than the desired compound. The most abundant had a molecular mass of 292.1 corresponding to the destannylated precursor (18% abundance). This molecular ion could be the result of fragmentation of the *tri*-butylstannyl compound during MS (see below) or due to the presence of destannylated derivative. If destannylated precursor was present as an impurity, direct iodination would be possible due to activation of the arene ring by the methoxy groups. In theory this could lead to electrophilic iodination at three possible sites (carbons 4, 5 and 6). However, Clanton *et al.*<sup>36</sup> reported that direct iodination of the desiodo derivative produced only the 6-iodobenzamide. Two factors suggest that reduced purity of the *tri*-butylstannyl precursor due to the presence of a destannylated analogue can be excluded as an explanation for the production of the radiolabelled byproduct. Thus, the radioactive impurity was formed in similar yields to [ $^{123}$ I]epidepride (ratio of 1: 0.8 respectively). If a destannylated analogue was acting as a precursor for the radiolabelled byproduct it would have to be present at least in a amount comparative to the stannylated precursor. MS revealed that the abundance of the destannylated analogue was only 18% compared with 100% for the stannylated precursor. Secondly, organostannanes are among the most reactive organometallic reagents for radioiodinations making the *tri*-butylstannyl group significantly more susceptible to displacement by radioiodine than hydrogen. Therefore, the destannylated compound would need to be present in significantly higher amounts for direct iodination to be a competitive reaction.

HPLC and MS may not have distinguished between different isomers or compounds with the same molecular weight. To eliminate this possibility, the reverse phase HPLC system developed for precursor analysis was used to purify our supply of precursor 1. This afforded sufficient sample to carry out structural identification. The yellow oil recovered was identified as a pure sample of the desired tin precursor by MS and NMR analysis (Figure 5.12, 5.13 and 5.14). Only one significant molecular ion was observed in the MS. The absence of the second most abundant ion ( $MH^+$  293) observed in the crude precursor indicates that HPLC was an appropriate method of purification, and

that its presence in the mass spectrum of the crude precursor was due to a destannylated impurity and not fragmentation of the *tri*-butylstannyl precursor. Two NMR findings support the absence of the destannylated precursor, and the presence of only one isomer of precursor **1** with the *tri*-butylstannyl group on carbon 5 of the aromatic ring. Firstly, the proton NMR of the purified precursor showed only two aromatic protons. Both resonated with stannyl satellites indicating the presence of two isotopomers. The aromatic protons adjacent to the stannyl group will have different coupling interactions depending on the tin isotope present in the compound. The result is different chemical shifts and tin satellites. The presence of a compound stannylated at carbon 4 or 6 would have resulted in an increase in the number of aromatic signals and the absence of stannyl satellites for at least one of the these signals, since there would be no interaction with the tin atom. The presence of the destannylated compound in the purified oil would result in at least one other aromatic proton and the absence of stannyl satellites for any extra peaks. Secondly, only six aromatic carbons were observed in the  $^{13}\text{C}$  NMR (Figure 5.14). The presence of any of the impurities mentioned above would have resulted in additional aromatic carbon signals.

The proton NMR data published by Clanton *et al.*<sup>36</sup> and de Paulis & Smith<sup>37</sup> is illustrated in Figure 5.4. A direct comparison of this data with the NMR obtained from the purified precursor revealed inconsistencies in the chemical shifts assigned for the protons within the *tri*-butyl group. The reported analysis assigned the protons on carbons 2 and 3 of the butylstannyl groups to a double-triplet at 1.29 ppm. However, these protons were not equivalent in the NMR spectrum obtained from purified precursor **1** which showed each group of protons resonating with a different chemical shift (Figure 5.13). This disparity could be due to nuclear interactions between the butyl protons and other parts of the molecule. The mechanism for inducing such an interaction in one preparation and not another is unclear. Despite these discrepancies, this NMR data, in combination with the MS data defines the purified oil as being the *tri*-butylstannyl precursor in high purity.

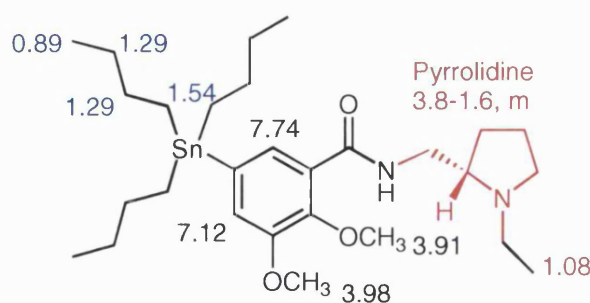


**Figure 5.4:** Assignment of proton NMR spectrum for the *tri*-butylstannyl precursor **1** as reported by Clanton *et al.*<sup>35</sup>

### 5.2.5 Radioiododestannylation of purified tributyltin precursor **1**

Radiolabelling with the purified *tri*-butylstannyl precursor was carried out on 2 separate occasions using identical reaction conditions as in Section 5.2.1. The radioactive impurity was still formed during these radioiododestannylation. The slower eluting radioactive by-product was still observed when the formulated dose was analysed on HPLC System B in the presence of reference epidepride



(data not shown). The radioactivity in the slower eluting peak was 55-60% of the total radioactivity of the formulated dose. This level was identical to that observed with the crude *tri*-butylstannyl precursor. Therefore, purification of the precursor failed to eliminate or even reduce formation of the radioactive impurity.

These results failed to provide any rationale, based on the quality of the precursor, for the consistently high proportion of radioactive by-product in [ $^{123}$ I]epidepride preparations with both the original and purified stock of precursor 1. Therefore, the formation of the impurity was not solely a function of the quality of the *tri*-butylstannyl precursor.

#### 5.2.6 Organic reactions with *tri*-butylstannyl precursor

In radioiodination chemistry oxidising agents are commonly used to convert radioiodide into effective electrophiles. *N*-Chloro-4-toluene sulfonamide sodium monohydrate (chloramine T) is the most widely used oxidising agent for rapid and simple iodinations, yielding products with high specific radioactivity. However, reactions that use chloramine-T are known to generate harsh oxidising conditions that can lead to side reactions. These can include cleavage of peptide bonds, oxidation of thiols and chlorination.<sup>39</sup> In addition to the harsh conditions generated by chloramine-T, the radioiodination of the *tri*-butylstannyl precursor proceeded at a pH of approximately 1. It is possible that the *tri*-butylstannyl precursor is affected by these reaction conditions, while [ $^{123}$ I]epidepride and the *tri*-methylstannyl precursor are not.

The involvement of chloramine-T and the subsequent reaction conditions in the production of the radioactive co-product is supported by HPLC analysis of small-scale cold reactions employing the *tri*-butylstannyl precursor. Following treatment of the *tri*-butylstannyl precursor with sodium iodide in the presence of chloramine-T, the HPLC profile was similar to that of the radioactive dose. Two major products with a high extinction coefficient at 254 nm were observed with only slightly different retention times (24.4 and 25.4 min, Figure 5.15). The products were not readily identifiable from their retention times since they differed from those obtained from radioiodinations (18.5 and 22 min). However, HPLC analysis of the crude reaction spiked with reference epidepride resulted in an increase in magnitude of the first peak (Figure 5.15, peak a). The second, more retained peak (Figure 5.15, peak b) was unaffected. These results verified that small-scale reactions that mimic the conditions of radioiodinations lead to the formation of epidepride and another unidentified product with a slightly slower elution profile.

In comparison, the treatment of the *tri*-butylstannyl precursor with excess iodine was unable to mimic the results observed with [ $^{123}$ I]sodium iodide in the presence of chloramine-T. The addition of iodine is the normal strategy for iodinating compounds in larger scale reactions where no-carrier-added conditions are irrelevant. That a single product peak, with a high absorbance at 254 nm was obtained from these reaction conditions indicated that the special conditions of radioiododestannylation contributed to the formation of a major  $^{123}$ I-labelled by-product.

Unfortunately, it has not been possible to synthesise a sufficient amount of the by-product for characterisation. Radiolabelling reactions are designed for use with trace amounts of compounds. Since the formation of the by-product is specific to the reaction conditions and the *tri*-butyl precursor, scaling up the quantities to maximise the yield was unsuccessful. The supply of precursor was also a limiting factor in achieving this goal.

Generally, it may be possible to speculate on the mechanism behind the formation of a side-product at a fixed ratio that is attributed to reaction conditions. However, the mechanism here would also need to be specific to the *tri*-butylstannyl precursor.

Zea-Ponce *et al.*<sup>40</sup> have identified a volatile  $^{123}\text{I}$  labelled byproduct that is associated with the preparation of [ $^{123}\text{I}$ ]iomazenil from its *tri*-butyltin precursor as [ $^{123}\text{I}$ ]1-iodobutane. Formation of [ $^{123}\text{I}$ ]1-iodobutane was dependent of the stannyl precursor but was not due to impurities in the precursor. The mechanism proposed for the formation of [ $^{123}\text{I}$ ]1-iodobutane is aliphatic substitution, which becomes a significant reaction pathway in the presence of electron-withdrawing groups *ortho* or *para* to the tin atom.<sup>40,41</sup> [ $^{123}\text{I}$ ]1-Iodobutane can be eliminated as a candidate for the observed radioactive impurity in the [ $^{123}\text{I}$ ]epidepride preparations reported here. Firstly, the methoxy groups of the *tri*-butylstannyl derivative of epidepride are not electron-withdrawing. This is supported by findings from radioiododestannylations of *tri*-butylstannyl derivatives of IBF,  $\beta$ -CIT and significantly epidepride where less-than-or-equal-to 2% of the total radioactivity was incorporated into [ $^{123}\text{I}$ ]1-iodobutane.<sup>40</sup> Secondly, the mechanism for the formation of [ $^{123}\text{I}$ ]1-iodobutane is not restricted to *tri*-butylstannyl precursors. [ $^{123}\text{I}$ ]Iodomethane was formed during iododestannylation of the *tri*-methylstannyl derivative of  $\beta$ -CIT,<sup>40</sup> and the *N*-*t*-Boc-5-*tri*-methylstannyl precursor of 5-iodo-6-nitroquipazine.<sup>41</sup>

The *tri*-butyltin derivative of epidepride is stable under basic conditions.<sup>36</sup> However, stannyl compounds are among the most reactive organometallic agents. It is possible that hydrolysis of the precursor occurs when exposed to the acidic conditions of radioiododestannylation. The destannylated precursor could then undergo direct iodination as discussed in Section 5.2.3 to produce the 6-iodobezamide. While the specific reaction conditions and yields for the synthesis of the 6-iodobenzamide were not reported, it is possible that the radioactive by-product observed following radioiododestannylation of the *tri*-butylstannyl precursor could be this isomer of [ $^{123}\text{I}$ ]epidepride. Therefore, the ratio at which the radioactive by-product was formed relative to [ $^{123}\text{I}$ ]epidepride would indicate the extent of precursor hydrolysis. It is possible that the *tri*-methylstannyl precursor is not as reactive as the *tri*-butyl compound preventing hydrolysis and the formation of the 6-iodo analogue under the same reaction conditions. Monitoring the stability of the *tri*-butylstannyl precursor during treatment with chloramine-T under acidic conditions could be one technique to investigate this possible mechanism for the formation of the radioactive by-product. Since the 6-iodobenzamide has been synthesised by direct iodination of the desiodo derivative and identified by NMR and HPLC<sup>36</sup> this isomer could be used as a reference to verify if this is the mechanism behind the formation of the radiolabelled by-product.

Liquid chromatography–mass spectrometry (LC/MS) enables quick characterisation of different components as they elute off an HPLC column. This technique has the potential to overcome some of the problems of product identification usually associated with radiolabelling reactions that are performed at trace levels. However, if the radiolabelled by-product was in fact the 6-iodo analogue of epidepride then LC/MS would provide minimal additional information since both products would have the same molecular mass. Other potential problems with this particular situation includes the need for reference epidepride to be added to the analyte to achieve separation of the radioactive by-product from [ $^{123}\text{I}$ ]epidepride and the tailing of the epidepride peak.

Irrespective of the mechanism behind the formation of the radioactive impurity, these observations raise a general concern associated with chloramine-T mediated radioiododestannylation of *tri*-butylstannylated compounds and highlights the need for very careful analysis of radioiodinated products and possibly, further investigations into the mechanism of radioiodinations. The trace levels employed with radiolabelling means that standard methods for quality control are not viable options. The example presented here highlights the need for a distinction between the HPLC methods or conditions employed for purification and the determination of radiochemical purity. For fluorine-18 and carbon-11 labelled PET radioligands time is a primary concern and rapid HPLC methods for both purification and quality control are essential. However, with I-123 labelled radioligands the 13.2 h half-life provides a wider time window that should be utilised if analysis under a number of HPLC conditions indicates the need for a slower HPLC system.

As a result of these findings [ $^{123}\text{I}$ ]epidepride is now prepared from the *tri*-methylstannyl precursor in the presence of chloramine-T and acid. HPLC purification is performed using System A. Since the exact mechanism behind the formation of the radioactive side product of the *tri*-butylstannyl preparations is still unknown, its possible formation with the *tri*-methylstannyl analogue is monitored using the slower, reverse phase system (System B) as part of quality control of the formulated dose. However, the addition of reference epidepride to enable separation of [ $^{123}\text{I}$ ]epidepride from the unidentified radioactive impurity prevents the use of HPLC System B for the dual purpose of determining the specific radioactivity and the radiochemical purity of the prepared doses. Initially, the increased flexibility associated with the 13.2 h half-life of 123-iodine was exploited with both HPLC systems used to assess the formulated doses of [ $^{123}\text{I}$ ]epidepride. System A was used to calculate the specific radioactivity, while System B was used to monitor the possible formation of the radioactivity impurity. To date the radioactive impurity has never been observed from these preparations so the quality control protocol has been simplified so that analysis on System B is not performed on every preparation. Occasionally full analysis with both HPLC systems is performed in order to affirm that the formation of the radioactive by-product is specific to the *tri*-butyl precursor.

### 5.2.7 Pharmacokinetics

#### 5.2.7.1 Plasma clearance

Relatively slow sampling of venous blood as opposed to rapid sampling of arterial blood meant that the initial peak in plasma radioactivity following injection of radiochemically pure [ $^{123}$ I]epidepride was either underestimated or in some individuals missed completely (Figure 5.16). As a result, it was difficult to determine the relative clearance rate of total radioactivity and unchanged radioligand and whether the final level of radioactivity in plasma was low. This type of information clearly demonstrates the need for arterial samples if an accurate measure of radioactivity in plasma is required as an input function for biomathematical models. The fact that the blood to plasma radioactivity ratio remained constant throughout the sampling period shows an absence of binding to red blood cells. The measured plasma free fraction of [ $^{123}$ I]epidepride ( $12.9\% \pm 0.5\%$ ;  $n = 4$ ) was comparable to the mean value of  $12.0\% \pm 2.6\%$  ( $n = 6$ ) reported by Ichise *et al.*<sup>42</sup> The high level of binding to plasma proteins (87%) does not prevent [ $^{123}$ I]epidepride from penetrating the blood-brain barrier and reaching brain D<sub>2</sub> receptors *in vivo*. Due to the high affinity of epidepride for its target site, non-specific binding to plasma proteins is not a significant factor especially when imaging areas of high receptor density. Potentially, plasma protein binding could have a greater impact in areas of lower density. The volume of distribution for [ $^{123}$ I]epidepride in temporal cortex ( $4.20 \pm 1.36$ )<sup>43</sup> suggests that this is not the case.

#### 5.2.7.2 Metabolism

The implementation of quantitative methods of analysis requires an investment into analytical equipment that enables the measurement of unchanged parent fractions in plasma. While gradient HPLC systems have increased flexibility, the initial cost associated with such setups may be beyond the budget of some SPET centres. A cheaper option is to purchase a single pump system and use isocratic HPLC conditions. This was the main rationale behind the development of an isocratic reverse phase HPLC system for analysis of [ $^{123}$ I]epidepride metabolism in human plasma.

Acetonitrile pretreatment of human plasma samples taken at various times after injection of [ $^{123}$ I]epidepride proved to be an effective method for precipitating plasma proteins with >95% of the total plasma radioactivity being recovered. The absence of any temporal relationship with the percentage of radioactivity recovered indicated that no radioactive metabolites were formed that could not be separated from plasma proteins by this procedure. Elution of the column for 20 min was sufficient for at least 90% of the injected radioactivity to be recovered. Any variation in this value between samples was possibly due to different rates of iodine-123 attenuation with different volumes, low count rates or minor errors in volume measurements. The recovery of radioactivity at the different steps of metabolite analysis was consistent with that obtained when [ $^{123}$ I]epidepride was incubated in plasma *in vitro*. The HPLC analysis of such samples revealed no metabolism or degradation of [ $^{123}$ I]epidepride *in vitro*.

The isocratic reverse phase HPLC system developed for studying the *in vivo* metabolism of [ $^{123}$ I]epidepride showed good resolution and separation of the parent compound from its five radioactive metabolites (Figure 5.17). This degree of separation was only possible when reference epidepride was added to the plasma sample before injection onto the HPLC column. Metabolites A, B and C were all more polar than [ $^{123}$ I]epidepride, eluting before the parent compound. Two radioactive metabolites, fractions D and F were more lipophilic than metabolites A, B and C, eluting with retention times of 11.2 and 18 min. Fraction F was even more lipophilic than parent radioligand which had a retention time of 14.2 min. [ $^{123}$ I]epidepride is rapidly cleared from the plasma over time. However, a high degree of variability in the measured fraction of unchanged parent was observed between individuals ( $31.2\% \pm 8.0\%$ , 60 min after injection; mean  $\pm$  SD). The main reason for this was the unpredictable nature of the lipophilic metabolite, F. In some individuals this metabolite represented a significant fraction of the total plasma radioactive (10 – 20%). In other subjects metabolism of [ $^{123}$ I]epidepride to compound F was an insignificant pathway with less than 5% of the total plasma radioactivity measured in fraction F.

The isocratic HPLC system developed for the analysis of [ $^{123}$ I]epidepride was only effective as a method for accurately measuring the fraction of unchanged radioligand when reference compound was added to the analyte. In the absence of authentic epidepride separation of [ $^{123}$ I]epidepride from the more lipophilic metabolite F was not possible (Figure 5.18). Samples analysed under these conditions could attribute a significantly higher fraction of the total plasma radioactivity to unchanged parent. The accurate measure of the true fraction of unchanged radioligand has more importance for radioligands such as [ $^{123}$ I]epidepride, since it is likely that a lipophilic metabolite like F could penetrate the blood-brain barrier. Depending on the nature of the compound it could bind to specific sites such as D<sub>2</sub>-like receptors, other receptor populations, or non-specific binding sites. Since SPET cameras are unable to distinguish between different chemical forms of radioactivity all of these scenarios can influence the quantification of D<sub>2</sub> binding. Binding to non-specific sites such as plasma proteins would lead to an increase in the general background radioactivity in the brain. If the radioactive metabolite had affinity for a specific target site a second equilibrium could occur which would have major implications for kinetic modelling of the SPET measurements. The fast clearance rate of [ $^{123}$ I]epidepride by peripheral metabolism does not preclude it as a useful radioligand. However, the high variability in the metabolic pathway, especially with respect to the formation of radioactive metabolite F, does complicate the quantification of any results.

The rapid and variable metabolism of [ $^{123}$ I]epidepride observed here using an isocratic HPLC system agrees strongly with those reported by Kuikka *et al*<sup>44</sup> and Bergström *et al*.<sup>45</sup> Using acetonitrile precipitation of plasma proteins followed by gradient HPLC analysis with acetonitrile and phosphoric acid (0.01M) as the eluent, both groups revealed a radioactive metabolite that was more lipophilic than [ $^{123}$ I]epidepride. The relative percentage of this metabolite was highly variable between individuals, as confirmed by the high standard deviation in the relative percentage attributed to this metabolite 60 min after injection of [ $^{123}$ I]epidepride. Using a gradient HPLC system the percentage of total plasma

radioactivity attributed to the radioactive, lipophilic metabolite was  $9.3\% \pm 7.5\%$  ( $n = 14$ ).<sup>45</sup> This is comparable to  $8\% \pm 9.7\%$  ( $n = 6$ ) obtained in this work using an isocratic HPLC system.

Analysis of [<sup>123</sup>I]epidepride metabolism required a 15 min gradient program as opposed to the 20 min required for the isocratic system developed here. The major difference between the HPLC profiles of the two systems was the resolution of the polar radioactive metabolites. Using gradient elution one polar radioactive peak was observed. Radioactive metabolites A, B and C observed with isocratic HPLC conditions eluted together on the gradient system. While, time is not a prime consideration for iodine-123 labelled compounds the resolution observed with the isocratic system is not an essential requirement for the quantification of SPET measures. What is most important is to obtain good resolution between the parent radioligand and lipophilic, labelled metabolites. This has been achieved, thus enabling metabolite analysis of plasma samples following injection of [<sup>123</sup>I]epidepride using an HPLC system that requires significantly less financial outlay.

Analysis of the *in vivo* metabolism of substitute benzamides, such as epidepride, [<sup>11</sup>C]raclopride and [<sup>11</sup>C]FLB 457, has been compared with the close structural analogue, remoxipride. In rodent species, remoxipride is metabolised primarily at the aromatic moiety<sup>46</sup> leading to metabolites that exhibited relatively high affinity for dopamine D<sub>2</sub> and D<sub>3</sub> receptors.<sup>47</sup> In comparison, the predominant pathways of metabolism in human are oxidations at  $\alpha$ -carbons of the pyrrolidine moiety leading to *N*-deethylated and/or pyrrolidone and hydroxypyrrolidone products (Figure 5.5).<sup>46</sup> None of the primary human metabolites showed any significant affinity to rat striatal membranes or membranes from cells expressing cloned human dopamine D<sub>2</sub> and D<sub>3</sub> receptors.<sup>47</sup> Following the analogy that [<sup>123</sup>I]epidepride, [<sup>11</sup>C]FLB 457 and [<sup>11</sup>C]raclopride are metabolised in a

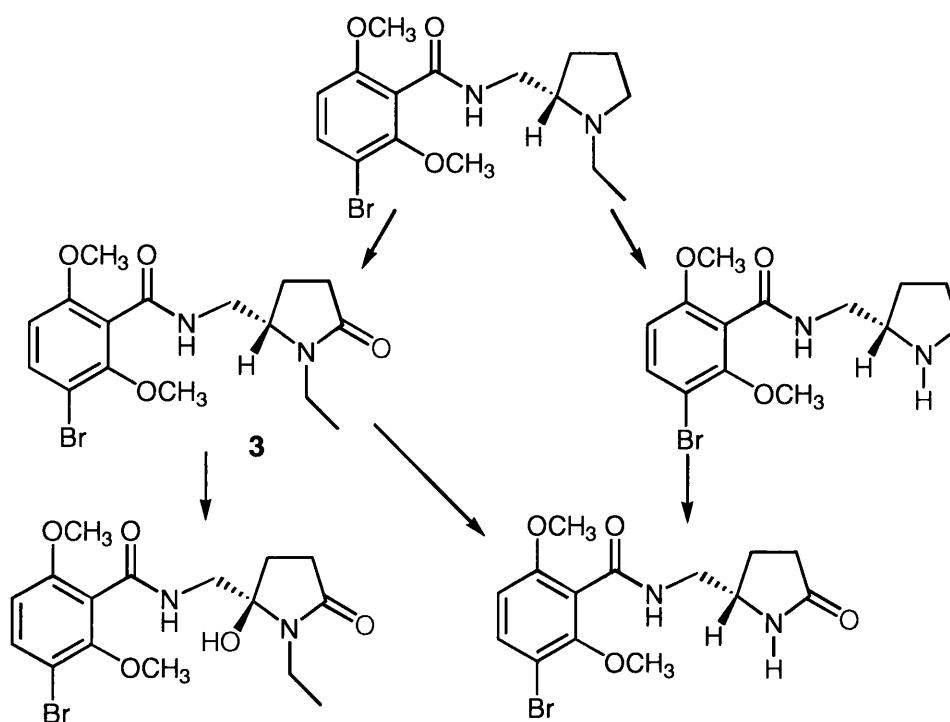


Figure 5.5: Proposed metabolic routes of remoxipride in humans.

similar manner to remoxipride, it is expected that their metabolites would have negligible affinity for the dopamine receptor. [ $^{11}\text{C}$ ]Raclopride is more slowly metabolised than epidepride and FLB 457, with unchanged parent representing 70–80% of the total radioactivity in plasma 42 min after injection.<sup>48</sup> However, one major lipophilic metabolite of [ $^{11}\text{C}$ ]raclopride was observed which co-eluted with the  $\alpha$ -lactam analogous to compound **3** (Figure 5.5). While the lipophilic non-parent fraction resulting from *in vivo* metabolism of [ $^{123}\text{I}$ ]epidepride has not been conclusively identified, it can be assumed that its contribution to brain radioactivity during the SPET scan will be non-specific in nature. The large inter-individual variation observed in the relative fraction of this metabolite and the impact this has on the non-displaceable distribution volume suggests that semi-quantitative measures of receptor density by the semi-quantitative ratio method is unreliable.<sup>44</sup> This is supported by the negative correlation between the fraction of lipophilic metabolite and the measure of receptor density obtained from a simple ratio of radioactivity in the striatum relative to the receptor-devoid cerebellum.<sup>30</sup> The accuracy of [ $^{123}\text{I}$ ]epidepride SPET binding parameters has been investigated using both the fraction of unchanged parent and lipophilic metabolite as input functions for kinetic models. The results were compared with those obtained from equilibrium studies. The standard 1 or 2 compartment models ignore radioactive metabolites that could contribute to brain radioactivity. However, Fujita *et al.*<sup>43</sup> found that the specific volume of distribution in both the striatum and temporal cortex obtained from a one-input function model was consistent with those obtained from the equilibrium paradigm. Consideration of the lipophilic metabolite as an input function provided consistent values only in the striatum. The accuracy of the values obtained when only the input of the parent fraction is considered provides further support to the lack of affinity of the lipophilic metabolite to specific target sites in the brain. Further investigation into the accuracy of the specific volume of distribution for [ $^{123}\text{I}$ ]epidepride obtained from simplified methodology has shown that any correlation with “true” values from full kinetic models is only moderate for analysis that do not account for the lipophilic radioactive metabolite.<sup>42</sup> This is the result of the high inter-subject variability in the fraction of this metabolite.

[ $^{123}\text{I}$ ]Epidepride illustrates some of the key problems that are associated with quantification of receptor parameters when a radioligand is metabolised to a lipophilic compound that is likely to cross the blood-brain barrier and contribute to brain radioactivity. The high variability in the metabolic process in different subjects also prevents the simplification of data analysis to a method that allows accurate measures of receptor density that could be applied to a routine, clinical situation. Hence, accurate determination of the extent of metabolism of a radiochemically pure radioligand is a vital contribution to the understanding of radioligand behaviour and the quantification of targeted receptors.

## 5.3 Methods

### 5.3.1 Materials and Methods

For general methods refer to Chapter 2.

(*S*)-5-(*Tri-n*-butyltin)-*N*-[(1-ethyl-2-pyrrolidinyl)methyl]-2,3-dimethoxybenzamide was a gift from Nycomed Amersham (UK). (*S*)-5-(*Tri-n*-methyltin)-*N*-[(1-ethyl-2-pyrrolidinyl)methyl]-2,3-dimethoxybenzamide was donated from two different sources, MAP Medical Oy (Tukio, Finland) and Research Biochemicals International (RBI, Natick MA, U.S.A.). Reference [(*S*)-*N*-((ethyl-2-pyrrolidinyl)methyl)-5-iodo-2,3-dimethoxybenzamide was also a gift from RBI. No-carrier-added sodium [ $^{123}$ I]iodide in 0.01M sodium hydroxide solution was purchased from MDS Nordion International Ltd. (S.A., Belgium). All other materials were analytical grade and purchased from Aldrich Chemical Co. Ltd (UK).

### 5.3.2 Standard procedure for radioiododestannylation of tri-alkylstannyl precursors

An aqueous solution of *N*-chloro-4-toluenesulfonamide sodium monohydrate (chloramine T) (10  $\mu$ l, 0.5 mg/ml water) was added to a vial containing [ $^{123}$ I]sodium iodide (1 GBq in *ca* 20  $\mu$ l 0.01M NaOH), aqueous [ $^{127}$ I]sodium iodide (10  $\mu$ l, 0.1mM), 0.1M hydrochloric acid (*ca* 20  $\mu$ l), and (*S*)-5-(*tri-n*-butyltin)-*N*-[(1-ethyl-2-pyrrolidinyl)methyl]-2,3-dimethoxybenzamide (**1**, 10  $\mu$ l, 5 mg/ml ethanol). The reaction was allowed to proceed for 3 min at room temperature after which 0.1M sodium metabisulfate solution (10  $\mu$ l) was added. The crude reaction mixture was purified by reverse phase HPLC using a  $\mu$ -Bondapak C18 column (100 x 7.8 mm, 10  $\mu$ m particle size; Waters, UK) plus guard column eluted with acetonitrile - 0.01M phosphoric acid (2: 3 v/v) at 4 ml/min (System A). The major radioactive peak eluted at 6 min, the same retention time as reference epidepride (from RBI). This fraction was collected (volume *ca* 4 ml), diluted with sterile water (*ca* 12 ml) and adjusted to pH 10 with aqueous 2M sodium hydroxide. This fraction was loaded onto a Sep-pak column (Adsorbex RP-18 (100 mg), Merk, Germany) that had previously been activated with ethanol (5 ml) and washed with water (10 ml). The radioactivity retained on the Sep-pak was recovered by eluting with ethanol (0.5 ml) and formulated for injection by dilution with saline for injection. The final concentration of ethanol was less than 5%.

Radiolabelling reactions were also performed with (*S*)-5-(*tri-n*-methyltin)-*N*-[(1-ethyl-2-pyrrolidinyl)methyl]-2,3-dimethoxybenzamide (10  $\mu$ l, 5 mg/ml ethanol) using identical conditions. Radioiodination of two sources of *tri*-methyl precursor were investigated; MAP Medical and RBI.

### 5.3.3 Determination of radiochemical purity

The radiochemical purity of [ $^{123}$ I]epidepride was assessed by reverse phase HPLC on System A and System B [a  $\mu$ -Bondapak C18 column (100 x 7.8 mm, 10  $\mu$ m particle size; Waters, UK) eluted isocratically with methanol - 0.1M ammonium formate (1: 1 v/v) at 3 ml/min]. The product was analysed on System B twice. In the second analysis reference epidepride was added to the analyte.



### 5.3.4 Analysis and purification of the tri-butylstannyl precursor

To obtain more information on our supply of tri-butylstannyl precursor, analysis and purification by HPLC was performed on a  $\mu$ -Bondapak C18 column (100 x 7.8 mm, 10  $\mu$ m particle size; Waters) eluted with methanol - water - triethylamine (90: 10: 0.05 by vol.) at 4 ml/min (System C). Pure tri-butylstannyl precursor was obtained by collecting fractions from repeated HPLC injections and concentrating these *in vacuo*. MS, proton and carbon NMR were used to analyse and characterise the purified product.

### 5.3.5 Cold reactions with tri-butylstannyl precursor

In separate experiments, the purified tri-butylstannyl precursor was treated with either an excess of iodine or sodium iodide in the presence of chloramine-T. In the first reaction (S)-5-(tri-n-butyltin)-N-[(1-ethyl-2-pyrrolidinyl)methyl]-2,3-dimethoxybenzamide (**1**, 200  $\mu$ l 5 mg/ml ethanol) was treated with a crystal of iodine for 3 min at room temperature. The reaction was quenched by adding sufficient sodium metabisulfate solution (0.1M) for the colour to disappear. The reaction was purified by HPLC (System A) and analysed using reverse phase HPLC (System B).

The second reaction involved treating purified (S)-5-(tri-n-butyltin)-N-[(1-ethyl-2-pyrrolidinyl)methyl]-2,3-dimethoxybenzamide (**1**, 20  $\mu$ l, 5 mg/ml ethanol) with sodium iodide (10  $\mu$ l, 0.1M solution in 0.01 M NaOH) in the presence of hydrochloric acid (20  $\mu$ l, 0.1 M) and chloramine-T (20  $\mu$ l, 0.5 mg/ml water). After 3 min at room temperature the reaction was quenched with sodium metabisulfate (20  $\mu$ l; 0.1 M). Again the reaction products were separated by HPLC on System A and the collected peak (r.t. = 6 min) was analysed on System B.

### 5.3.6 Pharmacokinetics of pure [ $^{123}$ I]epidepride

#### 5.3.6.1 Plasma clearance

Six healthy volunteers were injected intravenously with [ $^{123}$ I]epidepride prepared from the tri-methylstannyl precursor (185 MBq, >98 % radiochemically pure). Venous blood samples (2.5 ml) were collected into heparinised containers at regular intervals for the first 60 min of the scanning period, followed by 30 min intervals out to 120 min after intravenous injection for measurement of the level of radioactivity in blood and plasma. An aliquot of blood (0.5 ml) was taken before centrifugation at 3000 rpm for 5 min at room temperature. A plasma sample of equal volume (0.5 ml) was taken and the  $^{123}$ I radioactivity in both blood and plasma was obtained by counting in an automatic gamma counter (LKB 1282, Wallac).

#### 5.3.6.2 Metabolite Analysis

Larger blood samples (5 ml) were also taken at 5, 30, 60, 90 and 120 after injection for metabolite analysis of plasma. Cell-free plasma was prepared by mixing plasma (1 ml) with acetonitrile (9 ml). Following centrifugation (3000 rpm, 10 min, 4°C) the supernatant was concentrated *in vacuo* and the residue reconstituted in mobile phase [MeOH - 0.1M HCOONH<sub>4</sub> (50: 50 v/v)]; 1.5 ml. Reference

epidepride (50  $\mu$ l, 0.1 mmol/ ml) was added to reconstituted sample before filtering through a Millipore MV syringe filter. The resulting sample was analysed by HPLC on a Waters  $\mu$ -Bondapak C18 column (300 x 7.8 mm; 10  $\mu$ m particle size) eluted with 0.1M ammonium formate - methanol (50: 50 v/v) at 3 ml/min. The HPLC eluate was monitored sequentially for absorbance at 254 nm and radioactivity. The fraction of unchanged [ $^{123}$ I]epidepride was determined by integrating the areas under the radioactive curve for each sample.

#### 5.3.6.3 Plasma protein binding

Ultrafiltration was used to determine plasma protein binding *in vitro*. Human plasma was incubated with [ $^{123}$ I]epidepride (30 min, 37°C) and then centrifuged in ultrafiltration units with YMT membranes that have a 10000 molecular weight cut off (MPS micropartition device No. 4010, Amicon, Beery, MA, USA). *In vitro* incubation of [ $^{123}$ I]epidepride diluted in 0.9% NaCl was run concurrently to control for non-specific binding to the unit. Aliquots of equal volume were taken from both the ultrafiltrate and total sample (plasma or saline) and counted. The degree of plasma protein binding was determined by expressing the radioactivity in the ultrafiltrate as a percentage of the total radioactivity in the plasma, corrected for the degree of non-specific binding.

### 5.4 Results

#### 5.4.1 Radiiododestannylation of tri-alkylstannyl precursors

Preparations were performed under identical conditions using a number of different precursors. Initial radioiodinations employed a gift of *tri*-butylstannyl precursor from Nycomed Amersham (UK) on which no analytical data was available. Two further reactions were carried out with the same *tri*-butylstannyl precursor following purification by HPLC (see Section 5.2.3). Radiolabelling of the corresponding *tri*-methylstannyl precursor was performed using two supplies, ex MAP and RBI ( $n = 8$  and  $n = 1$ , respectively).

For all of the radioiodinations carried out one major radioactive product was observed in HPLC profiles with System A. This eluted with the same retention time (~6 min) and shape as reference epidepride. This result was obtained irrespective of the batch of precursor used. Figure 5.6A illustrates a typical HPLC elution profile obtained following radioiododestannylation of the *tri*-butylstannyl precursor. Eighty percent of the original radioactivity was accounted for in the collected major radioactive fraction (Figure 5.6A; d). This apparent level of  $^{123}$ I incorporation was obtained both before and after purification of the *tri*-butyl precursor. The other radioactive peak eluting with the column void volume (a) was most probably unreacted iodide. Radioiodination of the two sources of *tri*-methylstannyl precursor gave varying yields. The RBI compound gave a poor yield of only 25% ( $n = 1$ ). However, more than 95% of the radioactivity was incorporated into the major fraction with the MAP precursor ( $n = 5$ , Figure 5.6B). Any reference made to the radiolabelling of the *tri*-methyl precursor refers to the supply from MAP Medical Oy. The difference between the apparent efficiency of radioiododestannylation of the *tri*-methylstannyl (>95%) and *tri*-butylstannyl (80%) precursor was

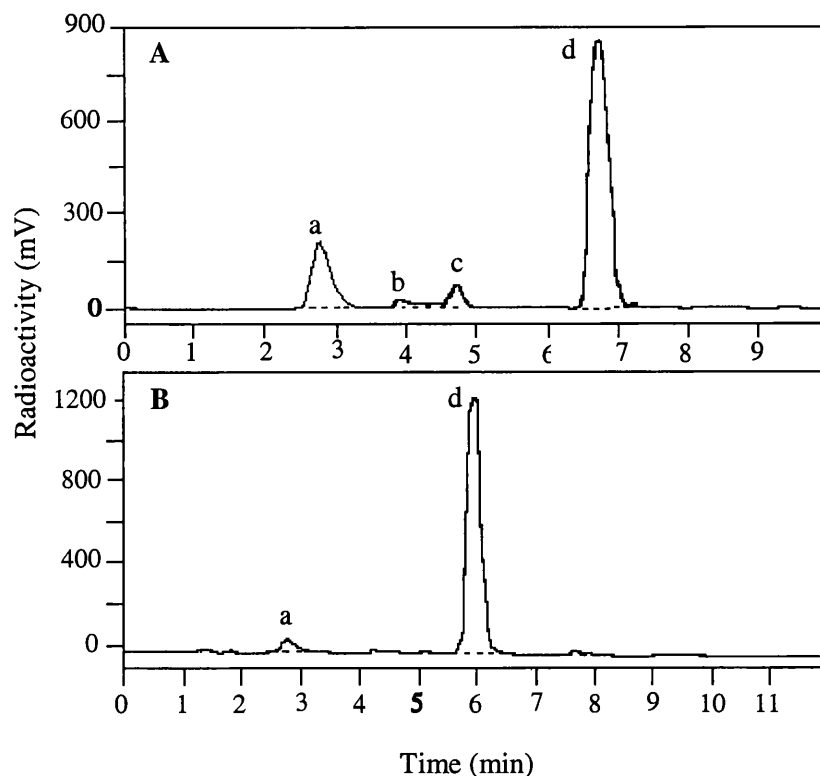


**Figure 5.6:** HPLC profile of crude radioiodination reactions employing the *tri*-butyl (Panel A) or *tri*-methylstannyl (Panel B) precursor. The peak eluting around 6–6.8 min (d) has the same retention time as authentic unlabelled epidepride (d). The peak eluting with the column void volume (a) was most probably unreacted iodine, while peaks b and c were unidentified side products.

the level of unreacted [ $^{123}\text{I}$ ]iodide (a) and the presence of two other radioactive products (b and c) in the radioiodination of the *tri*-butylstannyl (r.t. 3.9 and 4.7 min, respectively).

#### 5.4.2 Assessment of radiochemical purity

Analysis of the formulated dose following HPLC purification of the crude reaction with the *tri*-butylstannyl precursor gave a single peak on System A, indicating an apparent radiochemical purity of 98%. On System B one broad radioactive peak was observed with a retention time of 26 min (Figure 5.7A; peak a). However, when reference epidepride was added to the same analyte and reanalysed, two radioactive peaks were observed (Figure 5.7 B). The first co-eluted with reference epidepride (r.t. 18.5 min; b and d) while the second peak was more retained, eluting at 22 min (Figure 5.7B; peak c).

Both of these radioactive fractions were collected separately and re-analysed in the presence of reference epidepride (Figure 5.8). The different elution behaviours were retained on re-injection with the 18 min fraction co-eluting with reference epidepride (Figure 5.8A) and the second, more retarded peak eluting at 22 min (Figure 5.8B).

Analysis of the product from eight radioiodinations of the *tri*-butylstannyl precursor by reverse phase HPLC (System B) indicated a consistent ratio of [ $^{123}\text{I}$ ]epidepride to  $^{123}\text{I}$ -labelled co-product (40–45% : 55–60%). The main radioactive fraction isolated following iododestannylation of

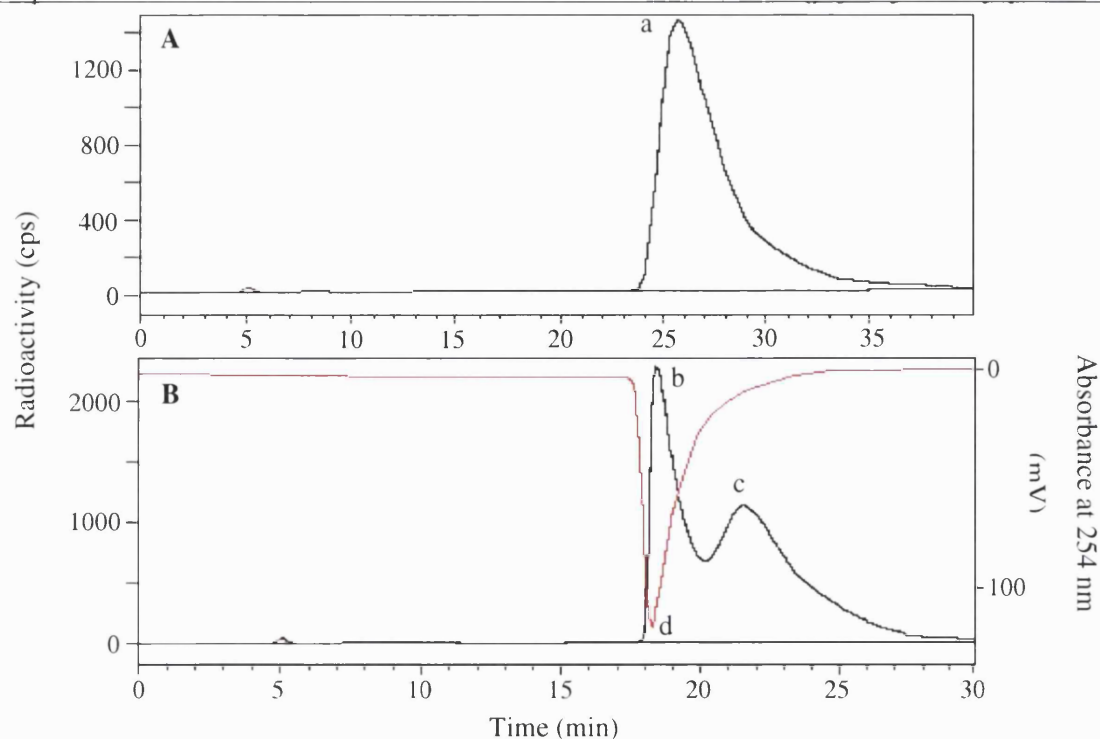


**Figure 5.7:** HPLC analysis (System B) of the main radioactive product from the radioiodination of the *tri*-butylstannyl precursor in the presence of chloramine-T. Panel **A**, without reference epidepride and Panel **B**, with reference epidepride (d) added.

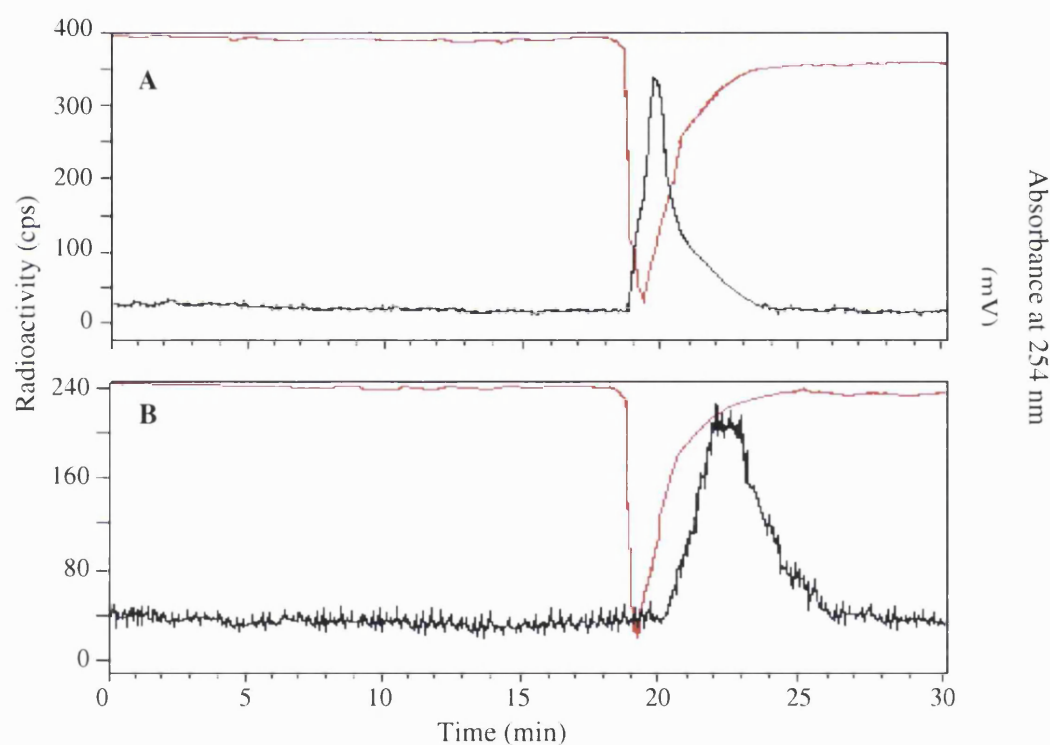


**Figure 5.8:** HPLC chromatograms following re-injection of the two radioactive products identified during analysis of [ $^{123}\text{I}$ ]epidepride prepared from *tri*-butyl tin precursor when co-injected with reference epidepride (System B). **A**, the radioactive peak with a retention time of 18.5 min (b in Figure 5.7) and **B**, the 22 min peak (c in Figure 5.7). Both analytes were injected with reference epidepride (red).

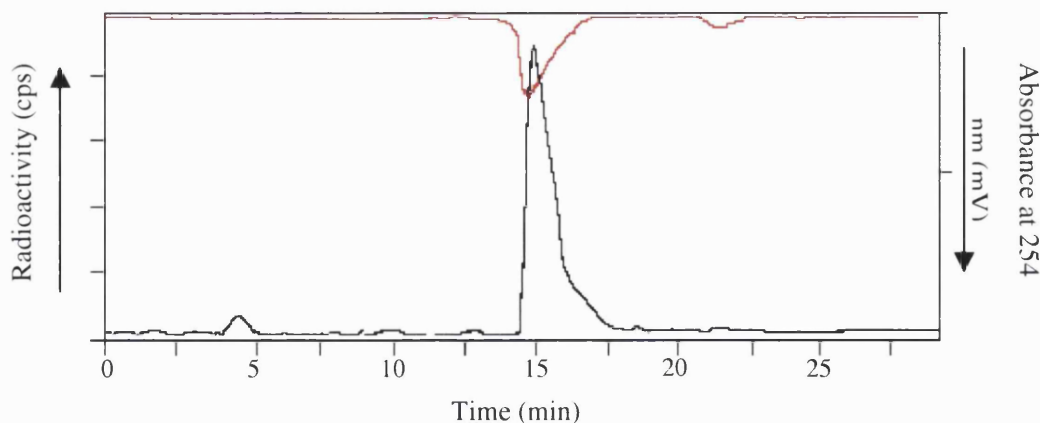


**Figure 5.9:** HPLC analysis (System B) of the main radioactive product from the radioiodination of the *tri*-methylstannyl precursor with reference epidepride added. The radioactive peak (black) eluted with a retention time of 15.5 min and co-eluted with authentic unlabelled epidepride (red).

the purified *tri*-butylstannyl precursor exhibited identical behaviour on HPLC (System B) to the product from the reaction with the unpurified precursor. Two radioactive products in a 40: 60 ratio were observed but only when analysed in the presence of reference standard.

In contrast, the formulated doses from radioiododestannylation of (*S*)-5-(*tri*-*n*-methyltin)-*N*-[(1-ethyl-2-pyrrolidinyl)methyl]-2,3-dimethoxybenzamide (ex MAP, *n* = 5) were found to be 98% radiochemically pure by HPLC when analysed on both System A and B. On System B the HPLC profile was identical with and without added epidepride (Figure 5.9).

#### 5.4.3 Analysis of the *tri*-butylstannyl precursor

With HPLC System C (see Section 5.3.4) the *tri*-butylstannyl precursor **1** eluted with a retention time of 16 min. HPLC analysis of the crude stock of precursor showed only traces of impurities with strong absorbance at 254 nm (Figure 5.10). Integration showed 86% of the area above background was the *tri*-butylstannyl precursor peak. Electrospray MS showed a base peak at  $m/z$  = 583.5 (MH<sup>+</sup>, 100%), 293 (18), 871.3 (1.6), 1185 (0.5) (Figure 5.11).

Following HPLC purification and concentration *in vacuo* 34 mg of the *tri*-butylstannyl precursor was obtained as a yellow oil.  $\delta_{\text{H}}$  (400 Hz, CDCl<sub>3</sub>, Me<sub>4</sub>Si) 8.38 (broad s, 1H, NH), 7.78 (s, 1H, C(6)H), 7.10 (s, 1H, C(4)H), 3.91 (s, 6H, OCH<sub>3</sub>), 3.8-1.75 (m, 11H, pyrrolidinyl ring H plus N-CH<sub>2</sub>), 1.55 (dt, 6H, Sn-(CH<sub>2</sub>CH<sub>2</sub>CH<sub>2</sub>CH<sub>3</sub>)<sub>3</sub>), 1.33 (dt, 6H, Sn-(CH<sub>2</sub>CH<sub>2</sub>CH<sub>2</sub>CH<sub>3</sub>)<sub>3</sub>), 1.13 (t, 3H, J = 7.22, N-CH<sub>2</sub>CH<sub>3</sub>), 1.07 (t, 6H, J = 2.63, Sn-(CH<sub>2</sub>CH<sub>2</sub>CH<sub>2</sub>CH<sub>3</sub>)<sub>3</sub>), 0.85 (t, 9H, J = 7.30, Sn-(CH<sub>2</sub>CH<sub>2</sub>CH<sub>2</sub>CH<sub>3</sub>)<sub>3</sub>) (Figure 5.12 and 5.13).

Expected  $\delta_{\text{H}}$  8.62 (b, NH), 7.74 (d, 1H, J=0.9, C(6)H), 7.12 (d, 1H, J=0.9, C(4)H), 3.98 (s, 3H, OCH<sub>3</sub>), 3.91 (s, 3H, OCH<sub>3</sub>), 3.8-1.6 (m, 11H, pyrrolidine-H), 1.54 (t, 6H, 1-Bu), 1.29 (dt, 12H, OCH<sub>3</sub>), 3.91 (s, 3H, OCH<sub>3</sub>), 3.8-1.6 (m, 11H, pyrrolidine-H), 1.54 (t, 6H, 1-Bu), 1.29 (dt, 12H, 2+3-Bu), 1.08 (t, 3H, N-Et), 0.89 (t, 9H, 4-Bu).<sup>35, 36</sup>

$\delta_C$  (100 Hz,  $CDCl_3$ ,  $Me_4Si$ ) 10.16 ( $Sn-CH_2$ ), 14.13 ( $Bu-CH_3$ ), 14.30 ( $N-CH_3$ ), 22.99 ( $C3'$ ), 27.77 ( $Sn-C3$ ), 28.80 ( $C2'$ ), 29.47 ( $Sn-C2$ ), 41.54 ( $N-CH_2$ ), 48.43 ( $N-CH_2-CH_3$ ), 53.95 ( $C4$ ), 56.46 ( $OCH_3$ ), 61.66 ( $OCH_3$ ), 62.95 ( $C1'$ ), 122.95 ( $C4$ ), 126.43 ( $C1$ ), 131.12 ( $C6$ ), 138.25 ( $C5$ ), 148.07 ( $C2$ ), 152.36 ( $C3$ ), 166.37 ( $CO$ ) (Figure 5.14).

$m/z$  (EI) 583.1 ( $M^+ - C_{28}H_{50}N_2O_3Sn$  requires 583.28).

The purified precursor was also found to be chromatographically homogeneous on System C with only one peak showing strong absorbance at 254 nm (r.t. = 16 min).

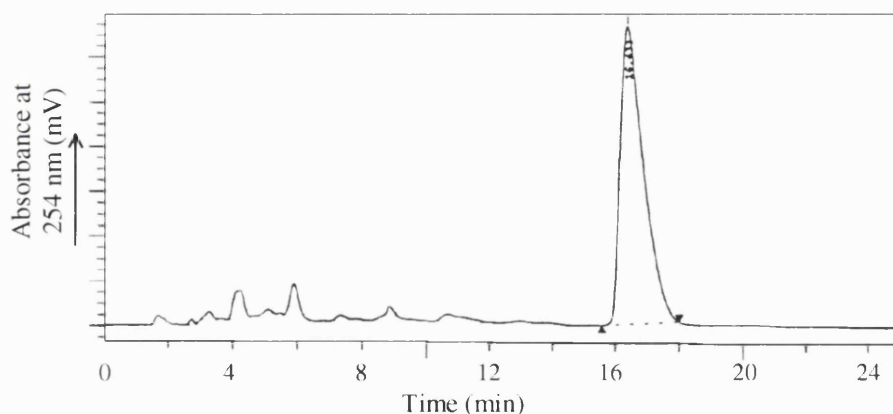


**Figure 5.10:** HPLC analysis (System C) of the crude supply of *tri*-butylstannyl precursor.

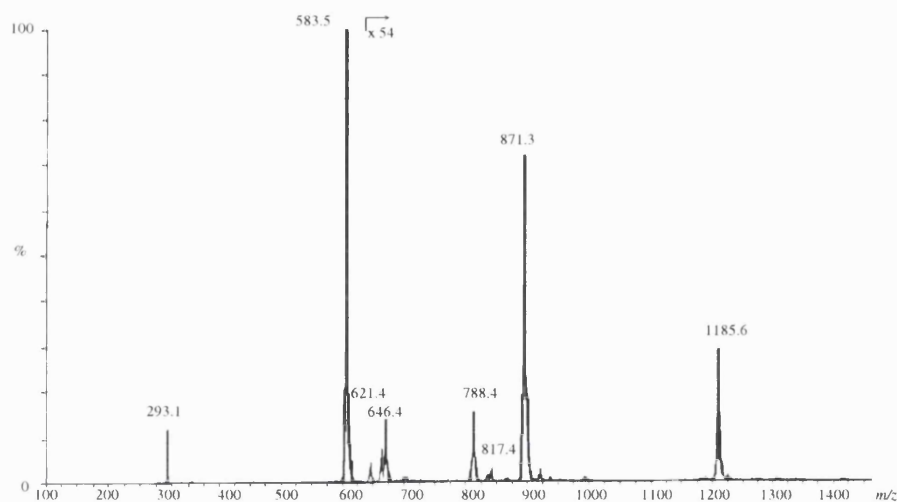


**Figure 5.11:** Electrospray MS of the crude *tri*-butylstannyl precursor.

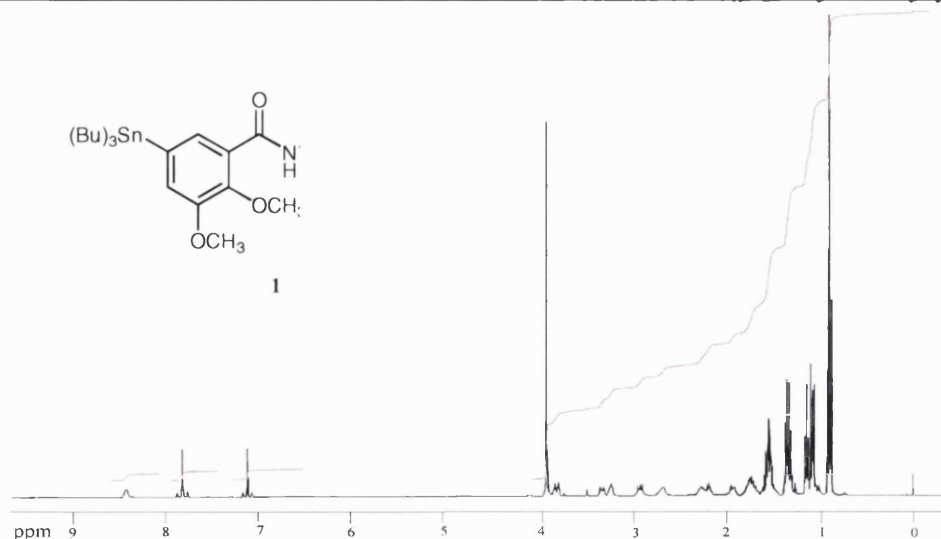


Figure 5.12:  $^1\text{H}$ -NMR spectra of purified *tri*-butylstannyl precursor.

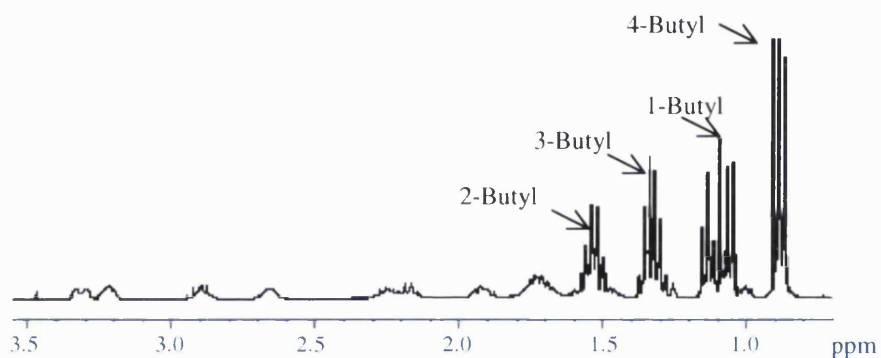


Figure 5.13: Enlargement of the aliphatic region of the  $^1\text{H}$ -NMR spectrum, including the assignment of the butyl protons.

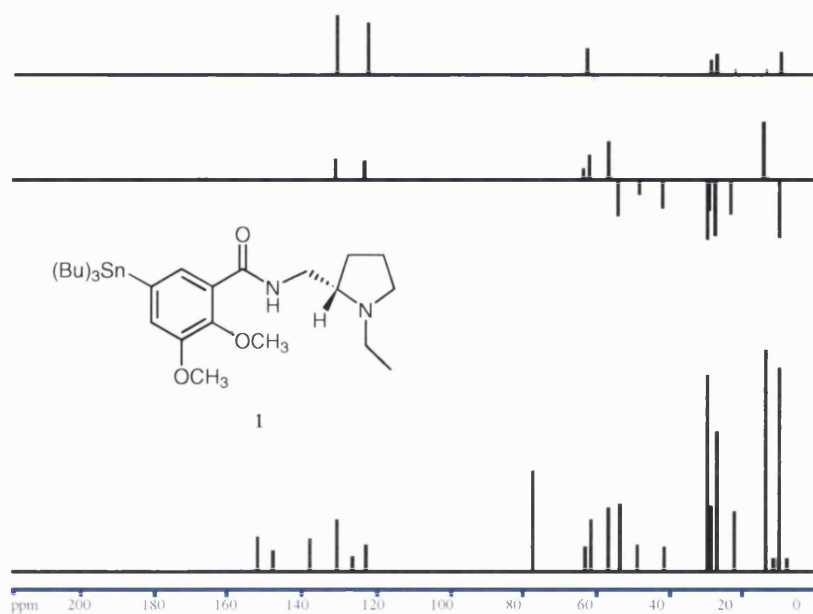
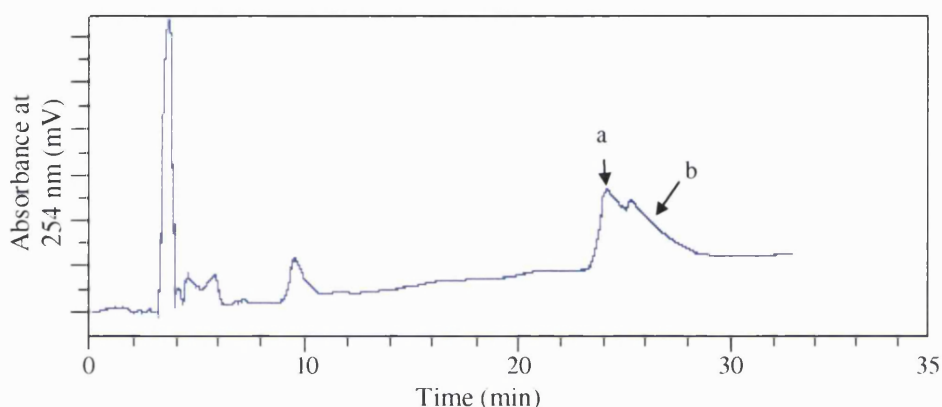


Figure 5.14:  $^{13}\text{C}$ -NMR spectrum of purified *tri*-butylstannyl precursor.

#### 5.4.4 Cold reactions with tri-butylstannyl precursor

Treatment of the purified tri-butylstannyl precursor with iodine produced only one peak with high extinction coefficient at 254 nm. This peak eluted at 6 and 18 min on System A and B, respectively. In comparison, iododestannylation of the purified precursor with sodium iodide in the presence of chloramine-T resulted in two products with strong absorbance at 254 nm. When analysed by reverse phase HPLC (System B) two peaks were observed (Figure 5.15; a and b). The first peak had a retention time of 24.4 min and increased in magnitude when reference epidepride was added. The second peak had slower mobility eluting at 25.5 min.



**Figure 5.15:** Analysis of crude reaction of tri-butylstannyl precursor with sodium iodide in the presence of chloramine-T using HPLC System B. Peak a increased in size with co-injection with authentic unlabelled epidepride. Peak b was an unidentified product.

#### 5.4.5 Pharmacokinetics

##### 5.4.5.1 Plasma clearance

The total radioactivity in human plasma peaked within the first 5 min after injection of [ $^{123}$ I]epidepride (Figure 5.16). An initial reduction in counts was followed by an increase in total radioactivity to an almost constant level. The slope of the rebound in total radioactivity depended on the radioactive metabolite profile (see Section 5.4.7). The fraction of plasma radioactivity attributed to parent compound dropped at a steady rate throughout the scan (Figure 5.16). The relative level of clearance is unclear since it is not certain that the initial peak is a true representation of the input function due to the slow sampling rate of venous blood. The ratio of radioactivity in blood to that in plasma was approximately 0.60 and showed no appreciable change during the scanning period. *In vitro* plasma protein binding of [ $^{123}$ I]epidepride, corrected for non-specific binding was  $87.1\% \pm 0.5\%$  ( $n = 4$ ).



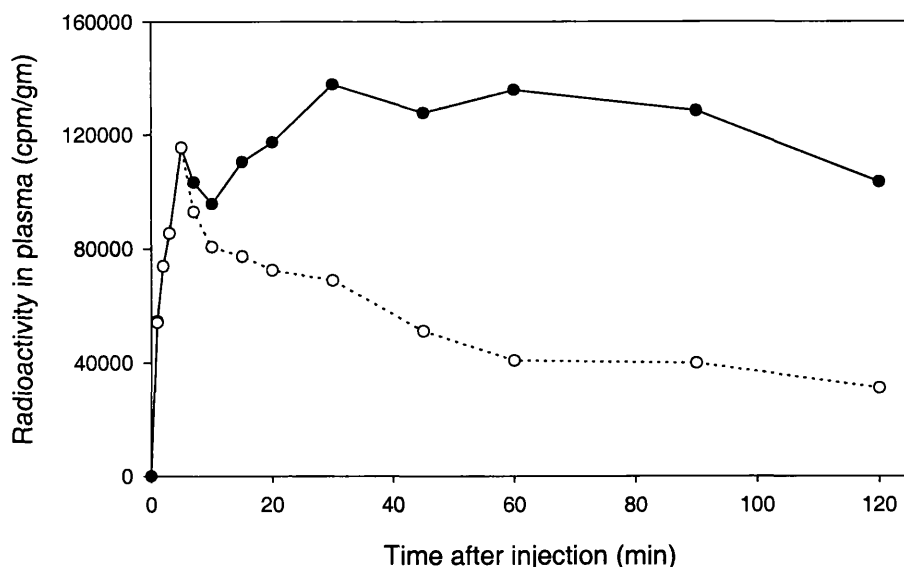


**Figure 5.16:** Clearance of total radioactivity (●) and unchanged parent compound (○) from venous plasma for one subject.

#### 5.4.5.2 Metabolism

Deproteinisation of plasma with 9 equivalents of acetonitrile before HPLC analysis recovered greater than 95% of the radioactivity in plasma. The percentage of radioactivity that precipitated with proteins showed no relationship with sampling time. On the isocratic HPLC system developed for metabolite analysis of [ $^{123}$ I]epidepride reference epidepride eluted with a retention time of 14.5 min. Eluting the HPLC column for 20 min recovered 90–100 % of the injected radioactivity.

[ $^{123}$ I]Epidepride was rapidly metabolised *in vivo* with only  $31.2\% \pm 8.0\%$  (mean  $\pm$  SD) of the total plasma radioactivity attributed to unchanged radioligand 60 min after injection of radiochemically pure [ $^{123}$ I]epidepride. In the presence of reference epidepride five possible radioactive metabolites were separated from [ $^{123}$ I]epidepride (r.t. 14.2 min) on reverse phase HPLC (Figure 5.17). The radioactive metabolites A, B, C and D all eluted before [ $^{123}$ I]epidepride. One of these metabolites, D, was more lipophilic than A, B and C. The other radioactive metabolite (F) was more lipophilic than fractions A, B, C and D and eluted after the parent compound with a retention time of 18 min. However, its separation from [ $^{123}$ I]epidepride was only possible under isocratic conditions when reference epidepride was added to the analyte (Figure 5.18). The mean percentage of the plasma total radioactivity attributed to this lipophilic metabolite was  $8\% \pm 9.7\%$  at 60 min after injection. Figure 5.19 illustrates the relative composition of the radioactivity in plasma over time as values for each subject and the overall mean  $\pm$  SD. The relative amount, and the time course of the lipophilic metabolite F was unpredictable. In some individuals metabolite F was observed within the first 30 min after injection of [ $^{123}$ I]epidepride while in others, it was observed only in later plasma samples. For some individuals the relative percentage of total plasma radioactivity attributed to this metabolite was minimal (less than 5%), in others this value was between 10 – 25%.

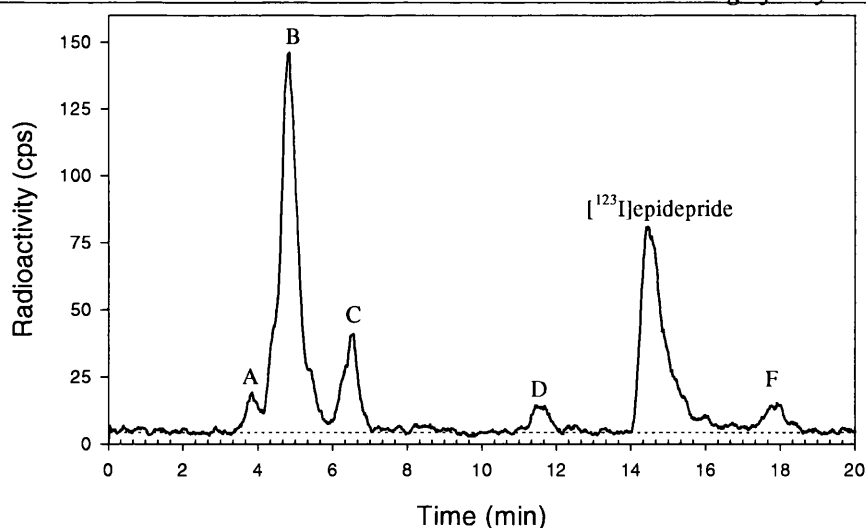


**Figure 5.17:** HPLC chromatogram of a 60 min plasma sample. (A) polar fraction eluting at 4 min; (B) eluted at 5.5 min; (C) eluted at 6.5 min; (D) fraction eluting at 11.5 min; (E) unchanged [<sup>123</sup>I]epidepride; (F) more lipophilic metabolite (r.t 18 min).

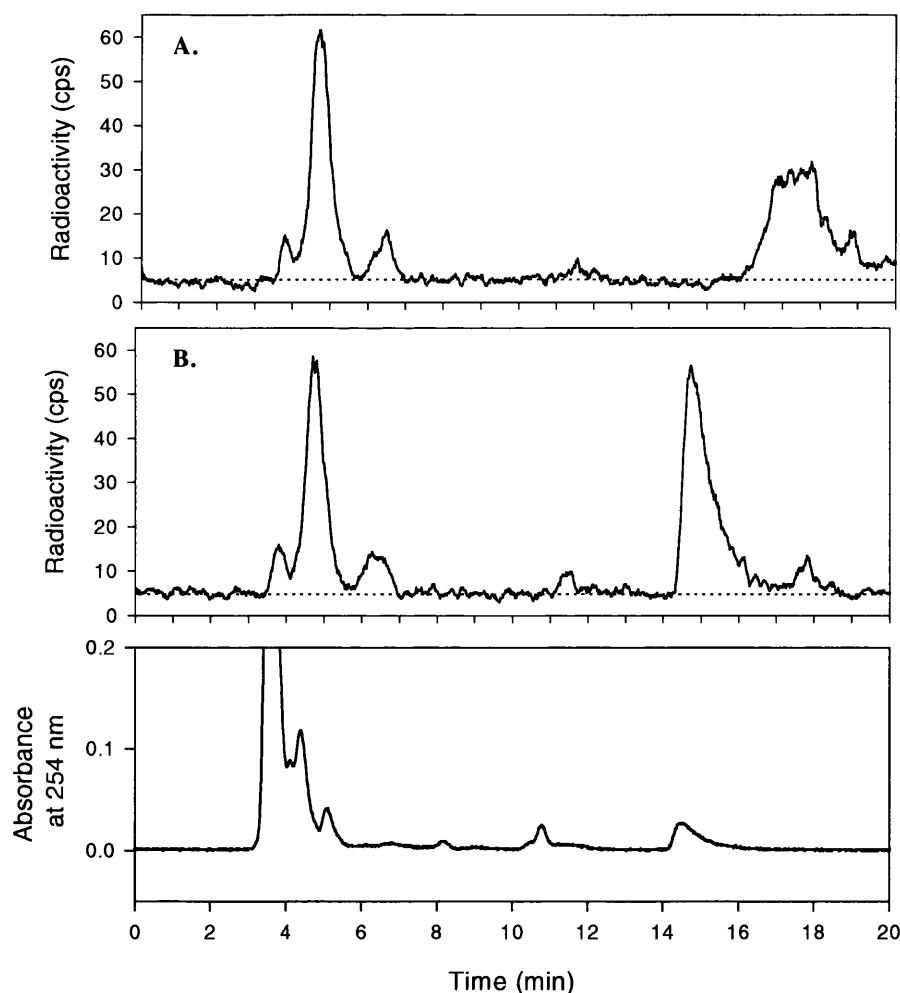


**Figure 5.18:** Panel A is the chromatogram from a plasma sample 30 min after injection of [<sup>123</sup>I]epidepride analysed in the absence of reference epidepride. The same sample analysed in the presence of reference epidepride is shown in panel B. The bottom panel is the corresponding profile of absorbance at 254 nm. The peak at 14.5 min is authentic unlabelled epidepride.

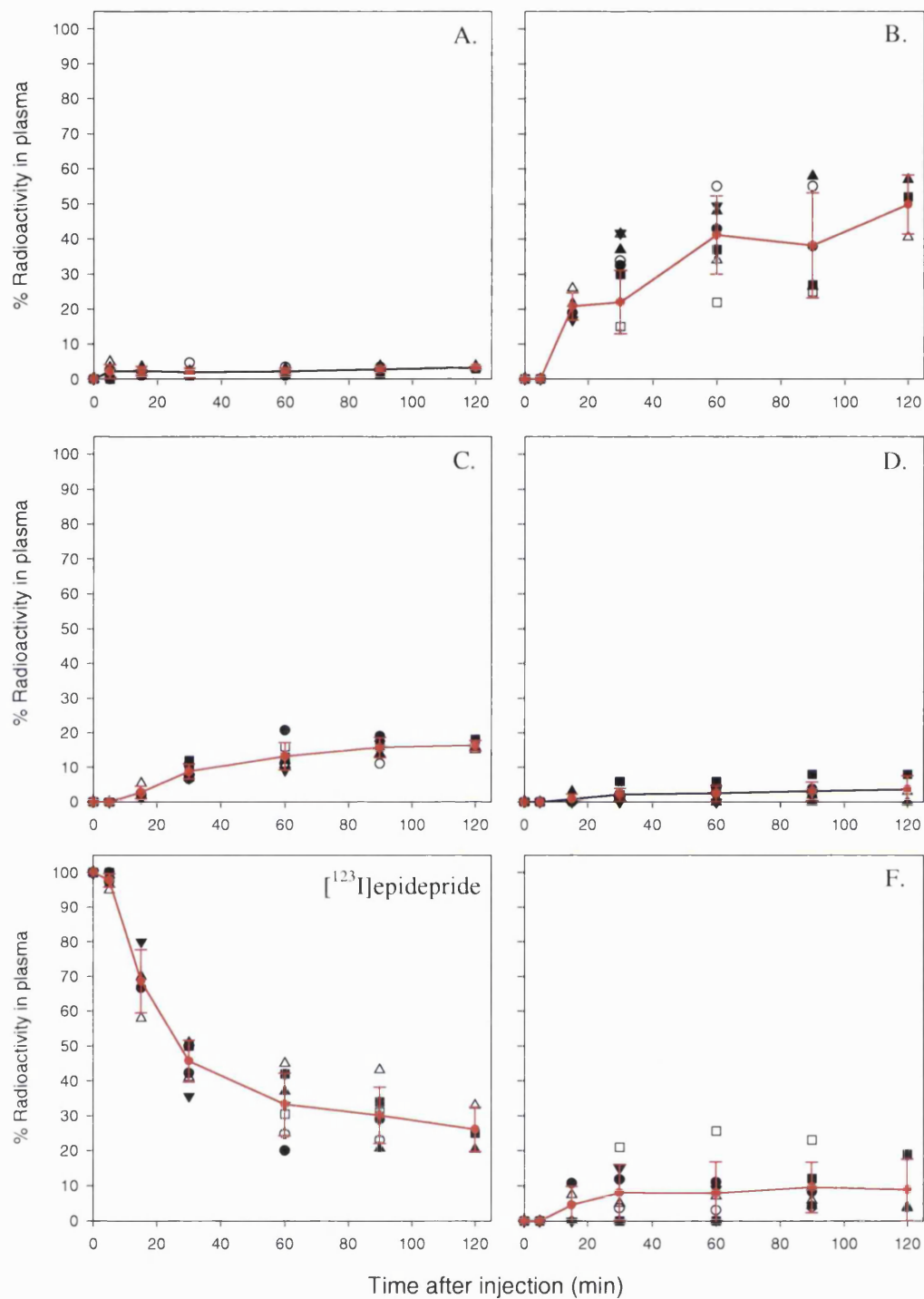


**Figure 5.19:** The time course of radioactive metabolites observed in human plasma after injection of  $[^{123}\text{I}]$ epidepride. (A), (B) and (C) are the polar fractions eluting with retention times of 4, 5.5 and 6.5 min respectively; (D) fraction eluting at 11.5 min; (E) unchanged  $[^{123}\text{I}]$ epidepride; (F) the more lipophilic metabolite (r.t. = 18 min). The black symbols are the values for each individual ( $n = 6$ , except for 120 min when  $n = 4$ ) while the red curve is the combined data (symbols = mean  $\pm$  SD).

## 5.5 References

1. Nolte J. *The Human Brain. An introduction to its functional anatomy* 4<sup>th</sup> Ed. Mosby, St Louis. 1999.
2. Jaber M, Robinson SW, Missale C, Caron MG. Dopamine receptors and brain function. *Neuropharmacology*. 1996; **35**: 1503-1519.
3. Keabedian JW & Calne DB. Multiple receptors for dopamine. *Nature*. 1979; **277**: 93-96.
4. Sokoloff P, Giros B, Martres M-P, Bouthenet M-L, Schwart J-C. Molecular cloning and characterization of a novel dopamine receptor (D<sub>3</sub>) as a target for neuroleptics. *Nature*. 1990; **347**: 146-151.
5. Van Tol HHM, Bunzow JR, Guan H-C, Sunahara RK, Seeman P, Niznik HB, Civelli O. Cloning of the gene for a human dopamine D<sub>4</sub> receptor with high affinity for the antipsychotic clozapine. *Nature*. 1991; **350**: 610-614.
6. Sunahara RK, Guan H-C, O'Dowd BF, Seemna N, Laurier LG, Ng G, George SR, Torchia J, Van Tol HM, Niznik HB. Cloning of a gene for a human dopamine D<sub>5</sub> receptor with higher affinity for dopamine than D<sub>1</sub>. *Nature*. 1991; **350**: 615-619.
7. Hall H, Sedvall G, Magnusson O, Kopp J, Halldin C, Farde L. Distribution of D<sub>1</sub>- and D<sub>2</sub>-dopamine receptors, and dopamine and its metabolites in the human brain. *Neuropsychopharmacology*. 1994; **11**: 245-256.
8. Kessler RM, Whetsell WO, Ansari MS, Votaw JR, de Paulis T, Clanton JA, Schmidt DE, Mason NS, Manning RG. Identification of extrastriatal dopamine D<sub>2</sub> receptors in post-mortem human brain with [<sup>125</sup>I]epidepride. *Brain Res*. 1993; **609**: 237-243.
9. Lévesque D, Diaz J, Pilon C, Martres MP, Giros B, Souil E, Schott D, Morgat JL, Schwartz JC, Sokoloff P. Identification, characterization, and localization of the dopamine D<sub>3</sub> receptor in rat brain using 7-[<sup>3</sup>H]hydroxy-N-N-di-n-propyl-2-aminotetralin. *Proc Natl Acad Sci USA*. 1992; **89**: 8155-8159.
10. Primus R, Thurkauf A, Xu J, Yevich E, Mcinerney S, Shaw K, Tallman JF, Gallager DW. Localization and characterization of dopamine D<sub>4</sub> binding sites in rat and human brain by use of the novel, D<sub>4</sub> receptor-sensitive ligand [<sup>3</sup>H]NGD 94-1. *J Pharmacol Exp ther*. 1997; **282**:1020-1027.
11. Weinberg DR & Lipska BK. Cortical maldevelopment, antipsychotic drugs, and schizophrenia: a search for common ground. *Schizophr Res*. 1995; **16**: 87-110.
12. Carlsson A & Lindquist M. Effect of chlorpromazine or haloperidol on formation of 3-methoxytyramine and normetanephrine in mouse brain. *Acta Pharmacol Toxicol*. 1963; **20**: 140-144.
13. Creese I, Burt DR, Snyder SH. Dopamine receptor binding predicts clinical and pharmacological potencies of antischizophrenic drugs. *Science*. 1976; **19**: 481-483.

14. Seeman P & Lee T. Antipsychotic drugs: Direct correlation between clinical potency and presynaptic action on dopamine neurons. *Science*. 1975; **188**: 1217-1219.
15. Angrist B & van Kammen DP. CNS stimulants as a tool in the study of schizophrenia. *Trends Neurosci*. 1984; **7**: 388-390.
16. Laruelle M, Abi-Dargham A, Gil R, Kegeles L, Innis R. Increased dopamine transmission in schizophrenia: relationship to illness phases. *Biol Psychiatry*. 1999; **46**: 56-72.
17. Wong DF, Wagner HN, Dannals RF, Links JM, Frost JJ, Ravert HT, Wilson AA, Rosenbaum AE, Gjedde A, Douglas KH, Petronis JD, Folsterin MF, Toung JK, Burns HD, Kuhar MJ. Effects of age on dopamine and serotonin receptors measured by positron emission tomography in the living brain. *Science*. 1984; **226**: 1393-1396.
18. Kung HF, Pan S, Kung MP, Billings J, Kasliwal R, Reilly J, Alavi A. In vitro and in vivo evaluation of [I-123]IBZM – a potential CNS D-2 dopamine receptor imaging agent. *J Nucl Med*. 1989; **30**: 88-92.
19. Köhler C, Hall H, Ogren SO, Gawell L. Specific in vitro binding of [H-3]-raclopride – a potent substituted benzamide drug with high-affinity for dopamine D-2 receptors in the rat brain. *Biochem Pharmacol*. 1985; **34**: 2251-2259.
20. Halldin C. Dopamine receptor radioligands. *Med Chem Res*. 1994; **4**: 217-249.
21. Breier A, Su TP, Saunders R, Carson RE, Kolachana BS, deBartolomeis A, Weinberger DR, Weisenfeld N, Malhotra AK, Eckelman WC, Pickar D. Schizophrenia is associated with elevated amphetamine-induced synaptic dopamine concentrations: Evidence from a novel positron emission tomography method. *Proc Natl Acad Sci USA*. 1997; **94**: 2569-2574.
22. Pilowsky LS, Costa DC, Ell PJ, Murray RM, Verhoeff NPLG, Kerwin RW. Clozapine, single photon emission tomography and the D<sub>2</sub> dopamine receptor blockade hypothesis of schizophrenia. *Lancet*. 1992; **340**: 199-202.
23. Pilowsky LS, Costa DC, Ell PJ, Murray RM, Verhoeff NPLG, Kerwin RW. Antipsychotic medication, D<sub>2</sub> dopamine receptor blockade and clinical response: a <sup>123</sup>I IBZM SPET (single photon emission tomography) study. *Psychol Med*. 1993; **23**: 791-797.
24. Farde L, Wiesel FA, Nordström A-L, Sedvall G. D<sub>1</sub> and D<sub>2</sub> receptor occupancy during treatment with conventional and atypical neuroleptics. *Psychopharmacology*. 1989; **99**: S28-S31.
25. Farde L, Nordström A-L, Wiesel FA, Pauli S, Halldin C, Sedvall G. Positron emission tomography analysis of central D<sub>1</sub> and D<sub>2</sub> dopamine receptor occupancy in patients treated with classical neuroleptics and clozapine: relation to extrapyramidal side-effects. *Arch Gen Psychiatry*. 1992; **499**: 538-543.
26. Kessler RM, Mason NS, Votaw JR, de Paulis T, Clanton JA, Ansari MS, Schmidt DE, Manning RG, Bell RL. Visualization of extrastriatal dopamine D<sub>2</sub> receptors in human brain. *Eur J Pharmacol*. 1992; **223**: 105-107.

27. Pilowsky LS, Mulligan RS, Acton PD, Ell PJ, Costa DC, Kerwin RW. Limbic selectivity of clozapine. *Lancet*. 1997; **350**: 490-491.
28. Bigliani V, Mulligan RS, Acton PD, Visvikis D, Ell PJ, Stephenson C, Kerwin RW, Pilowsky LS. *In vivo* occupancy of striatal and temporal cortical D<sub>2</sub>/D<sub>3</sub> dopamine receptors by typical antipsychotic drugs. *Brit J Psychiatry*. 1999; **175**: 231-238.
29. Bigliani V, Mulligan RS, Acton PD, Ohlsen RI, Pike VW, Ell PJ, Gacinovic S, Kerwin RW, Pilowsky LS. Striatal and temporal cortical D<sub>2</sub>/D<sub>3</sub> dopamine receptors by olanzapine and sertindole in vivo: a [<sup>123</sup>I]epidepride single photon emission tomography (SPET) study. *Pharmacology*. 2000; **150**: 132-140.
30. Bergström K, Yu M, Kuikka J, Åkerman KK, Hiltunen J, Lehtonen J, Halldin C, Tiihonen J. Metabolism of [<sup>123</sup>I]epidepride may affect brain dopamine receptor imaging with single photon emission tomography. *Eur J Nucl Med*. 2000; **27**: 206-208.
31. Langer O, Halldin C, Dollé F, Swahn C-G, Olsson H, Karlsson P, Hall H, Sandell J, Lundkvist C, Vaufrey F, Loc'h C, Crouzel C, Mazière B, Farde L. Carbon-11 epidepride: a suitable radioligand for PET investigation of striatal and extrastriatal dopamine D<sub>2</sub> receptors. *Nucl Med Biol*. 1999; **26**: 509-518.
32. Olsson H, Halldin C, Swahn CG, Farde L. Quantification of [<sup>11</sup>C]FLB 457 binding to extrastriatal dopamine receptors in the human brain. *J Cereb Blood Flow Metab*. 1999; **19**: 1164-1173.
33. Mazière B, Halldin C, Loc'h C, Moresco RM, DelForge J, Bottlaender M, Fuseau C, Syrota A, Farde L, Mazière M. Evaluation in baboon and human of Br-76 FLB 457, a high affinity PET ligand for studying dopamine D-2 receptors. *J Nucl Med*. 1993; **34**: P102-P102.
34. Farde L, Suh ET, Nyberg S, Karlsson P, Nakashima Y, Hietala J, Halldin C. A PET-study of [<sup>11</sup>C]FLB 457 binding to extrastriatal D<sub>2</sub>-dopamine receptors in healthy subjects and antipsychotic drug-treated patients. *Psychopharmacology*. 1997; **133**: 396-404.
35. Delforge J, Bottlaender M, Loc'h C, Guenter I, Fuseau, Bendriem B, Syrota A, Mazière B. Quantitation of extrastriatal D2 receptors using a very high-affinity ligand (FLB 457) in the multi-injection approach. *J Cereb Blood Flow Metab*. 1999; **19**: 533-546.
36. Clanton JA, De Paulis T, Schmidt DE, Ansari MS, Manning RG, Baldwin RM, Kessler RM. Preparation of [<sup>123</sup>I]- and [<sup>125</sup>I]epidepride: a dopamine D-2 receptor antagonist radioligand. *J Label Compd Radiopharm*. 1991; **29**: 745-751.
37. de Paulis T & Smith HE. Facile preparation of (S)-N-[(1-ethyl-2-pyrrolidinyl)methyl]-2,3-dimethoxy-5-(tributyl)benzamide from isoremixipride: The precursor of [<sup>125</sup>I]- and [<sup>123</sup>I]epidepride. *Synth Communications*. 1991; **21**: 1091-1095.
38. Hall H, Farde L, Halldin C, Hurd YL, Pauli S, Sedvall G. Autoradiographic localization of extrastriatal D<sub>2</sub>-dopamine receptors in the human brain using [<sup>125</sup>I]epidepride. *Synapse*. 1996; **23**: 115-123.

39. Seevers RH & Counsell RE. Radioiodination techniques for small organic molecules. *Chem Rev.* 1982; **82**: 575-590.
40. Zea-Ponce Y, Baldwin RM, Zoghbi SS, Innis RB. Formation of 1-[I-123]iodobutane in labelling [I-123]iomazenil by iododestannylation – implications for the reaction-mechanism. *Appl Radiat Isot.* 1994; **45**: 63-68.
41. Zea-Ponce Y, Baldwin RM, Milius RA, Bakthavachalam W, Innis RB. [<sup>123</sup>I]Iodomethane, a main product in the synthesis of 5-[<sup>123</sup>I]iodo-6-nitroquipazine by iododestannylation. *J Label Compd Radiopharm.* 1995; **36**: 331-337
42. Ichise M, Fujita M, Seibyl JP, Verhoeff NPLG, Baldwin RM, Zoghbi SS, Rajeevan N, Charney DS, Innis RB. Graphical analysis and simplified quantification of striatal and extrastriatal dopamine D<sub>2</sub> receptor binding with [<sup>123</sup>I]epidepride. *J Nucl Med.* 1999; **40**: 1902-1912.
43. Fujita M, Seibyl JP, Verheff PLG, Ichise M, Baldwin RM, Zoghbi SS, Burger C, Staley JK, Rajeevan N, Charney DS, Innis RB. Kinetic and equilibrium analyses of [<sup>123</sup>I]epidepride binding to striatal and extrastriatal dopamine D<sub>2</sub> receptors. *Synapse.* 1999; **34**: 290-304.
44. Kuikka JT, Åkerman KK, Hiltunen J, Bergström KA, Räsänen P, Vanninen E, Halldin C, Tiihonen J. Striatal and extrastriatal imaging of dopamine D<sub>2</sub> receptors in the living brain with [<sup>123</sup>I]epidepride single-photon emission tomography. *Eur J Nucl Med.* 1997; **24**: 483-487.
45. Bergström KA, Halldin C, Yu MX, Swahn C-G, Åkerman KK, Hiltunen J, Tiihonen J, Kuikka JT, Lassen N, Widebeck C, Farde L. The metabolite pattern of [<sup>123</sup>I]epidepride in human plasma determined with a gradient HPLC method. *J Label Compd Radiopharm.* 1997; **40**: 151-153.
46. Widman M, Nilsson LB, Bryske B, Lundström J. Disposition of remoxipride in different species – species-differences in metabolism. *Drug Res.* 1993; **41**: 287-297.
47. Mohell N, Sällemark M, Rosqvist S, Malmberg Å, Högberg T, Jackson DM. Binding characteristics of remoxipride and its metabolites to dopamine D<sub>2</sub> and D<sub>3</sub> receptors. *Eur J Pharmacol.* 1993; **238**: 121-125.
48. Swahn C-G, Halldin C, Lundström J, Erixon E, Farde L. A rapid and efficient HPLC-method for determination of ligand metabolism during PET-studies – exemplified with [<sup>11</sup>C]raclopride. *J Label Compd Radiopharm.* 1993; **32**: 284-285.

***Chapter 6:***  
***General Overview***



## 6.1 Radioligand Development

PET and SPET radioligands are intended for the *in vivo* investigation of biochemical, physiological and pharmacological processes in man. Understanding the pharmacology, structure, function and relative concentration of target binding sites is a prerequisite for radioligand development. This information can then be related to the criteria that generally need to be satisfied for a radioligand to measure its target binding site *in vivo* (see Section 1.4.2 for discussion).

### 6.1.1 Selection of a lead compound

Promising candidates for radioligand development are generally chosen from analogues of a lead compound that exhibit antagonism for the site of interest. Pharmacokinetic data obtained from *in vivo* validation studies in man and animals can be utilised to try and obtain a radioligand with far superior efficacy.

There are radioligands that *in vivo* afford a specific radioactive signal for its target site that is not within the general limits associated with effective radioligands (ratio of 3-10<sup>1</sup>). [<sup>123</sup>I]5-Iodo-R91150 is one such compound. SPET scans in healthy human volunteers injected intravenously with [<sup>123</sup>I]5-iodo-R91150 show a ratio of radioactivity in the receptor-rich frontal cortex to that in the receptor-devoid cerebellum of 1.4 2 h after injection.<sup>2</sup> While useful data on neuroleptic drug action has been obtained from imaging with [<sup>123</sup>I]5-iodo-R91150,<sup>3</sup> compounds with such a low specific signal have limited sensitivity with respect to measuring changes in available binding sites.

Part of the work described in this thesis (Chapter 4) was directed at the synthesis of two precursors that could be used for the radiosynthesis of a number of potential radioligands with the aim of improving the specific signal obtained when imaging 5-HT<sub>2A</sub> receptors. One possible explanation for the low signal obtained with [<sup>123</sup>I]5-iodo-R91150 is a high level of binding to non-specific sites such as plasma proteins, vasculature or white matter leading to a high level of background radioactivity in the brain. Since plasma protein binding is related to lipophilicity it is possible that reducing lipophilicity could lead to an improved signal *in vivo*. This could be achieved by changing substituents in certain parts of the molecule that have minimal impact on receptor affinity. Removing iodine and labelling R91150 with carbon-11 should lower the lipophilicity of the compound without significantly altering affinity and selectivity for the target site. However, brain uptake for [<sup>123</sup>I]5-iodo-R91150 is 2% of the injected dose.<sup>2</sup> A reduction in lipophilicity could have an opposite effect to that desired by preventing acceptable penetration of the blood-brain barrier. The two target precursors have the potential to provide five novel PET radioligands for imaging 5HT<sub>2A</sub> receptors with varying lipophilicity. It is possible that one of these compounds might have improved *in vivo* characteristics for the imaging of 5-HT<sub>2A</sub> receptors.

### 6.1.2 Precursor synthesis

Once potential compounds have been selected, an appropriate radionuclide, labelling method and strategy for precursor synthesis needs to be investigated. In this work the four compounds selected as possible new candidates for imaging 5-HT<sub>2A</sub> receptors could be radiolabelled from two precursors. While the syntheses of 4-amino-*N*-[1-3-(4-fluorophenoxy)propyl]-4-methyl-4-piperidinyl]-2-methoxybenzamide and its hydroxy analogue were not accomplished within the time frame of this work, a key intermediate has been synthesised and a large body of information has been gathered that will be useful in the future when alternative synthetic strategies are being scrutinised. In future this intermediate could also be used in palladium catalysed carbonylation with [<sup>11</sup>C]carbon monoxide.

#### 6.1.2.1 Radiolabelling

Radiolabelling conditions need to maximise the radiochemical yield and the specific radioactivity of a radiopharmaceutical preparation. For radioiodinations, the reactions generally follow standard radiolabelling conditions *e.g.* the use of either chloramine-T or peracetic acid to generate a radioiodinating agent that will participate in electrophilic substitution of a *tri*-alkylstannyl precursor. Identification of the exact nature of the radioiodinating agent generated with various oxidising agents is often only a matter of speculation. Since our understanding of the exact mechanism of radioiodination is not clear, rigorous analysis of the radioactive products is required. Chapter 5 describes the radiolabelling of [<sup>123</sup>I]epidepride from the corresponding *tri*-butylstannyl and *tri*-methylstannyl precursors. The radioactive impurity observed in [<sup>123</sup>I]epidepride preparations from the *tri*-butylstannyl precursor illustrates a potential problem with radioiododestannylation reactions. More specifically, very similar organostannane precursors, reacting by notionally identical processes (*i.e.* iododemetalation) give very different product distributions under certain circumstances (reaction with radioiodide and oxidising agents). Organostannanes are often chosen over other reagents for radioiodination because of their ease of production and high reactivity towards radioiodine. However, there appears to be a question surrounding the stability of the *tri*-butylstannyl precursor under the reaction conditions for radiolabelling [<sup>123</sup>I]epidepride. The low mass of iodine associated with radioiodinations limits the characterisation techniques that can be applied to the radioactive product. Performing an equivalent non-radioactive reaction with [<sup>127</sup>I]iodine or iodide on a macroscale will enable molecular characterisation by all the conventional methods. However, the products from a non-radioactive, macro reaction may not always match identically with those from radioiodinations performed at trace levels. Such factors need to be taken into consideration during the characterisation process of radioligand development.

This work also indicated that further investigation into the exact mechanisms by which radioiodinations proceed *i.e.* the oxidative species involved and the radioiodination agent generated, would help to identify the source of potential problems. The scale at which radioiodinations are performed has placed limitations on this type of work. However, the use of liquid-chromatography/mass spectroscopy could play a role in increasing our understanding of iodinations in the presence of oxidising agents. It would also be of use to have a bank of information indicating the

reactivity of different precursors under various radiolabelling conditions *e.g.* different oxidising agents and pH's. In future this knowledge could be utilised during the selection of precursors for novel radioligands.

### 6.1.3 Radioligand analysis

The direct analysis of a radioiodinated compound involves the use of radiochromatographic techniques that detect radioactive components. Radio-HPLC is the preferred method due to its superior resolution over radio-TLC. However, the work in this thesis (Chapter 5) illustrates that HPLC as an analytical technique has limitations that need to be considered. The impurity in [ $^{123}\text{I}$ ]epidepride preparations from the *tri*-butylstannyl precursor was only visible by HPLC with slow elution and in the presence of reference epidepride. Without such rigorous analysis a true measure of radiochemical purity for these preparations would not have been achieved. The 13.25 h half-life of iodine-123 means that time is not the prime consideration during the preparation and analysis of iodinated radioligands. Therefore, the quickest HPLC system may not always be the most appropriate.

One of the benefits of single photon emission radionuclides is their longer half-lives which, in the case of 123-iodine has eliminated the need for on-site radiolabelling facilities. A number of 123-iodine labelled radioligands can be purchased commercially. For imaging centres in the United Kingdom this usually means that they are prepared in another country and shipped to the imaging centre for use the following day. The presence of a radioactive impurity, no matter how small may have a significant impact on the plasma-input function during the scanning period especially if a false representation of the fraction of unchanged radioligand is obtained as a result of less than optimal radiochemical purity. This could reduce the accuracy of any binding parameters obtained from biomathematical modelling. This type of effect was observed with [ $^{123}\text{I}$ ]5-iodo-R91150 (Chapter 3) where the radiochemical purity on release of the dose in Amsterdam was >95% but on arrival in London was only 93%. This level of radiochemical purity was less than the value obtained from stability tests performed at the production site and the values measured at two centres in Holland and Belgium where transportation took only a few hours. The percentage of radioactivity in the plasma attributed to the radioactive impurity at 180 min after injection of 93% pure doses of [ $^{123}\text{I}$ ]5-iodo-R91150 was significantly higher than predicted from metabolite analysis of plasma following injection of the same radioligand with high radiochemical purity (>98%). On the basis of this work the Free University of Amsterdam has changed the method of dose formulation to include a radical-scavenger that is non-toxic, stable during autoclaving and prevents radiolysis during transportation. As a general comment, this work has highlighted the fact that standard stability tests *e.g.* constant shaking of the vial at room temperature, do not necessarily mimic the conditions of transportation especially from Europe to the United Kingdom. Radiopharmaceutical companies that are commercially supplying doses need to determine the exact conditions of transportation and measure stability under these conditions or formulate a dose that has minimal radiolysis even under the harshest of conditions.

In a move from semi-quantitative to quantitative methods of analysis, the success of any mathematical interpretation of the data could be compromised along with scan quality for doses with

lower than optimal radiochemical purity. Therefore, quantification of SPET measurements may be jeopardised by one of the benefits usually associated with SPET as an imaging technique *i.e.* accessibility without the need for investment in radiochemistry.

#### 6.1.4 Metabolite analysis in plasma

The pharmacokinetics of radioligands can have implications for quantification of neuroimaging data. Ideally, a radioligand for neuroimaging should clear quite rapidly from plasma and should not form radioactive metabolites that are able to penetrate the blood-brain barrier. Radio-HPLC of plasma samples is the technique of choice for such studies and was used in this thesis to investigate the *in vivo* metabolism of two SPET radioligands, [ $^{123}\text{I}$ ]5-iodo-R91150 (Chapter 3) and [ $^{123}\text{I}$ ]epidepride (Chapter 5). [ $^{123}\text{I}$ ]5-iodo-R91150 has favourable pharmacokinetics for quantitative SPET. In humans, the four radioactive metabolites were measured at low levels and all were more polar than the parent compound suggesting peripheral localisation. In comparison, [ $^{123}\text{I}$ ]epidepride was rapidly metabolised to a number of radioactive metabolites that included a compound that was more lipophilic than the parent radioligand. Quantitative analysis of imaging data by kinetic modelling assumes that the radioactivity measured in the brain is unchanged radioligand. The presence of a lipophilic metabolite that could penetrate the blood-brain barrier invalidates this assumption. Comparative quantitative analysis of [ $^{123}\text{I}$ ]epidepride data, ignoring or including the lipophilic metabolite as an input function, showed that this lipophilic metabolite is not at equilibrium with a specific binding site but influences the non-specific/free compartment of the model.<sup>4</sup> The presence of lipophilic metabolites requires complex validation of quantitative analytical methods and even then, misrepresentation of physiological parameters is possible. If the identity of any radioactive lipophilic metabolite is known, its formation *in vivo* may be prevented by modification of the radioligand. The flexibility associated with isotopic labelling with carbon-11 means that this approach is often a viable option for PET radioligands. Unfortunately, this is not always the case for iodine-123 labelled radioligands.

The resolution of HPLC systems used to investigate *in vivo* metabolism is critical for radioligands such as [ $^{123}\text{I}$ ]epidepride, that have less than ideal metabolite profiles. Lipophilic metabolites may have similar retention times to the unchanged parent under certain HPLC conditions. Without resolution of the two fractions, an inaccurate measure of unchanged radioligand would be obtained. On an isocratic HPLC system (Chapter 5), separation of [ $^{123}\text{I}$ ]epidepride from its lipophilic metabolite was only possible with the relatively slow system (20 min per run compared with the 10 min gradient HPLC run reported by Bergström *et al.*<sup>5</sup>), and in the presence of reference epidepride. The 13.25 h half-life of iodine-123 enabled this system to be used without the logistical problems that would be present due to low count rates for radioligands labelled with carbon-11. Here is another example of where the benefits of using a longer-lived SPET radionuclide can come into play to ensure accurate measures of unchanged parent compound in plasma.

## 6.2 Conclusion

The short half-life of the important positron-emitters has meant that a high degree of radiochemical support has always been a necessity for PET. The increased application of quantitative SPET and full validation of a number of novel radioligands has led to an increase in the number of centres with radiochemistry facilities. This work has explored many of the facets of radioligand development. More specifically, rigorous methods of analysis have been applied to ensure precursor purity, radioligand purity and stability, and quantitatively true measures of metabolism *in vivo*. As a result of this work, a number of potential problems and areas of limited understanding have been highlighted with respect to SPET radiochemistry. In order to maximise the benefits of quantitative neuroimaging with SPET and increase the power of this technique for objectively and quantitatively evaluating specific target sites there needs to be an increase in our understanding of  $^{123}\text{I}$  and  $^{99\text{m}}\text{Tc}$  radiochemistry, and the analytical procedures that are routinely used in PET. The vast knowledge that has been accumulated in the field of PET radioligand development and evaluation should be appraised and modified when appropriate to incorporate the benefits of using longer-lived radionuclides with SPET.

### 6.3 References

1. Pike VW. Positron-emitting radioligands for studies *in vivo* – probes for human psychopharmacology. *J Psychopharmacol*. 1993; **37**: 139-158.
2. Busatto GF, Pilowsky LS, Costa DC, Mertens J, Terriere D, Ell PJ, Mulligan R, Travis MJ, Leysen JE, Lui D, Gacinovic S, Waddington W, Lingford-Hughes A, Kerwin RW. Initial evaluation of 123-I-5-R91150, a selective 5-HT<sub>2A</sub> ligand for single photon emission tomography (SPET), in healthy human subjects. *Eur J Nucl Med*. 1997; **24**: 119-124.
3. Travis MJ, Busatto GF, Pilowsky LS, Mulligan R, Acton PD, Gacinovic S, Mertens J, Terriere D, Costa DC, Ell PJ, Kerwin RW. 5-HT<sub>2A</sub> receptor blockade in patients with schizophrenia treated with risperidone or clozapine. A SPET study using the novel 5-HT<sub>2A</sub> ligand <sup>123</sup>I-5-I-R-91150. *Br J Psychiatry*. 1998; **173**: 236-241.
4. Fujita M, Seibyl JP, Verheff PLG, Ichise M, Baldwin RM, Zoghbi SS, Burger C, Staley JK, Rajeevan N, Charney DS, Innis RB. Kinetic and equilibrium analyses of [<sup>123</sup>I]epidepride binding to striatal and extrastriatal dopamine D<sub>2</sub> receptors. *Synapse*. 1999; **34**: 290-304.
5. Bergström KA, Halldin C, Yu MX, Swahn C-G, Åkerman KK, Hiltunen J, Tiihonen J, Kuikka JT, Lassen N, Widebeck C, Farde L. The metabolite pattern of [<sup>123</sup>I]epidepride in human plasma determined with a gradient HPLC method. *J Label Compd Radiopharm*. 1997; **40**: 151-153.

## ***Appendix***

### ***Co-Authored Publications Arising Directly From The Work Described In This Thesis***

#### ***Meeting Abstracts***

Mulligan RS, Osman S, Travis MJ, Eersels JLH, Pilowsky LS, Ell PJ, Pike VW. [123I]5-Iodo-R91150, a radioligand for 5-HT<sub>2A</sub> receptors – Radiochemical stability and metabolism. *J Label Cpd Radiopharm.* 1999; 42: S669-S671.

Mulligan RS, Osman S, Pilowsky LS, Ell PJ, Pike VW. Preparation of [123I]epidepride from trialkylstannyl precursors in the presence of chloramine-T – some cautionary observations. *J Label Cpd Radiopharm.* 1999; 42: S774-S776.

### ***Co-Authored Publications Arising Out Of The Work Described In This Thesis***

Bigliani V, Mulligan RS, Acton PD, Ohlsen RI, Pike VW, Ell PJ, Gacinovic S, Kerwin RW, Pilowsky LS. Striatal and temporal cortical D<sub>2</sub>/D<sub>3</sub> dopamine receptors by olanzapine and sertindole in vivo: a [<sup>123</sup>I]epidepride single photon emission tomography (SPET) study. *Psychopharmacol.* 2000; **150**: 132-140.

Stephenson CME, Bigliani V, Jones HM, Mulligan RS, Acton PD, Visvikis D, Ell PJ, Kerwin RW, Pilowsky LS. Striatal and extra-striatal D-2/D-3 dopamine receptor occupancy by quetiapine in vivo - [I-123]-epidepride single photon emission tomography (SPET) study. *Br J Psychiatry.* 2000; **177**: 408-415.

Bigliani V, Mulligan RS, Acton PD, Visvikis D, Ell PJ, Stephenson C, Kerwin RW, Pilowsky LS. *In vivo* occupancy of striatal and temporal cortical D<sub>2</sub>/D<sub>3</sub> dopamine receptors by typical antipsychotic drugs. *Brit J Psych.* 1999; **175**: 231-238.